Real-time Monitoring of Scour and Sediment Deposition Evolution at Bridges and Offshore Wind Turbine Foundations based on Soil Electromagnetic Properties

Panagiotis A. Michalis

Thesis submitted to the Department of Civil and Environmental Engineering,
University of Strathclyde, Glasgow, in fulfilment of the requirements
for the degree of

Doctor of Philosophy

in

Civil and Environmental Engineering

December 21, 2014

Glasgow, UK

Keywords: Structural health monitoring; Geophysics; Electromagnetism; Scour; Sediment deposition; Offshore foundations; Sensor development.

Declaration of authenticity

This thesis is the result of the author's original research. It has been composed by the author and has not been previously submitted for examination which has led to the award of a degree.

The copyright of this thesis belongs to the author under the terms of the United Kingdom Copyright Acts as qualified by University of Strathclyde Regulation 3.50. Due acknowledgement must always be made of the use of any material contained in, or derived from, this thesis.

Signed:

Date: 21 January 2015

Panagiotis Michalis BEng (Hons), MSc, PhD

Real-time Monitoring of Scour and Sediment Deposition Evolution at Bridges and Offshore Wind Turbine Foundations based on Soil Electromagnetic Properties

Panagiotis A. Michalis

ABSTRACT

This doctoral thesis describes the development of a novel methodology for monitoring the evolution of scour and sediment re-deposition processes in the vicinity of foundation structures. The system employs two different devices in the Amplitude Domain (AD): an off-the-shelf and a new low-cost prototype sensor that yields an economical, accurate and robust structural health monitoring solution. Measurement principles are based on the Reflection (off-the-shelf ADR sensor) and Transmission (new ADT sensor) characteristics of propagating electromagnetic waves affected by impedance mismatches.

The study initially validated the capability of an off-the-shelf ADR sensor, with ring-shaped electrodes, to monitor scour and sediment re-deposition processes under various environmental media through experiments conducted under both 'static' scour and real-time flume conditions. A novel approach was developed that enabled discrimination between in-situ and re-deposited sediments at the foundation structure.

A new impedance-based sensor consisting of strip electrodes was then developed based on the ADT measuring principle and characterised in terms of its ability to detect bed level variations. The sensor design process included electromagnetic field modelling to optimise the electrode geometry within models that simulated various surrounding permittivity conditions. Principles of the sensor's operation were established through a theoretical analysis that provided further insight into the electrical behaviour of the instrument. Sensor optimisation and the assessment of the frequency that maximises its sensitivity were then investigated experimentally and its operation was validated using 'static' scour and open channel flume experiments under different environmental conditions (salinity, temperature and sediment) that will vary in a practical offshore installation environment.

Results indicate that both prototype sensors can accurately measure scour and re-deposited sediment processes, potentially offering an accurate and low-cost alternative to existing scour monitoring instruments. Validation of the newly developed ADT sensor in a representative operational environment enables the instrument to be classified at Technology Readiness Level (TRL) 6.

Παρακολούθηση του φαινομένου της υδραυλικής υποσκαφής και της εναπόθεσης φερτών υλικών σε θεμελιώσεις γεφυρών και υπεράκτιων αιολικών μηχανών με βάση τις ηλεκτρομαγνητικές ιδιότητες των εδαφών

Παναγιώτης Α. Μιχάλης

ΠΕΡΙΛΗΨΗ

Η σταδιακή αύξηση των βροχοπτώσεων έχει προκαλέσει σοβαρές και συχνές καταστροφικές πλημμύρες. Σαν αποτέλεσμα οι υδραυλικές κατασκευές διατρέχουν υψηλό κίνδυνο αστοχίας λόγω του φαινομένου της υδραυλικής υποσκαφής, με σοβαρές συνέπειες για τη δημόσια ασφάλεια και σημαντικές οικονομικές απώλειες. Η τοπική διάβρωση εδαφών στον περιβάλλοντα χώρο των θεμελιώσεων είναι η κύρια αιτία των αστοχιών γεφυρών και μία από τις σημαντικές επιπτώσεις της κλιματικής αλλαγής σε οδικές και σιδηροδρομικές υποδομές. Επίσης, θεωρείται ως σημαντική απειλή για τον σχεδιασμό και την λειτουργία των υπεράκτιων αιολικών κατασκευών, δεδομένου ότι οδηγεί σε υπερβολική διάβρωση του περιβάλλοντα θαλάσσιου βυθού.

Η στάθμη του εδάφους σε στοιχεία θεμελιώσεων είναι πολύ δύσκολο να αξιολογηθεί, λαμβάνοντας υπόψη ότι το υποσκαπτόμενο έδαφος συχνά αναπληρώνεται από φερτά υλικά που διαβρώνονται ευχερώς κατά τη διάρκεια πλημμυρών μικρότερης κλίμακας. Η συγκέντρωση πληροφοριών σχετικά με την εξέλιξη της υδραυλικής υποσκαφής θα επιτρέψει την αξιολόγηση των αναπτυγμένων εμπειρικών μοντέλων που προέρχονται από εργαστηριακές μελέτες και τον επανασχεδιασμό των θεμελιώσεων των κατασκευών. Πολλές ερευνητικές προσπάθειες έχουν επικεντρωθεί στην ανάπτυξη τεχνικών για παρακολούθηση της δραστηριότητας της υδραυλικής υποσκαφής σε θεμελιώσεις. Ωστόσο, δεν εφαρμόζονται λόγω των πολλών τεχνικών προβλημάτων και του υψηλού κόστους.

Ο στόχος της παρούσας διατριβής είναι να διερευνήσει δύο διαφορετικές γεωφυσικές μεθόδους βασισμένες στην αρχή μέτρησης Amplitude Domain (AD). Οι τεχνικές προτείνονται να χρησιμοποιηθούν για πρώτη φορά για τη παρακολούθηση της εξέλιξης του φαινομένου της υδραυλικής υποσκαφής και της εναπόθεσης φερτών υλικών στα θεμέλια των δομικών στοιχείων. Οι αρχές μέτρησης των αξιολογούμενων τεχνικών βασίζονται στις παραμέτρους της ανάκλασης (ADR) και μετάδοσης (ADT) των ηλεκτρομαγνητικών κυμάτων που προέρχονται λόγω αναντιστοιχίας των σύνθετων αντιστάσεων μεταξύ του συστήματος μέτρησης και αισθητήρα.

Η έρευνα αρχικά επικεντρώθηκε στην αξιολόγηση της απόδοσης ενός ADR αισθητήρα για την παρακολούθηση των διακυμάνσεων του επιπέδου του εδάφους σε διαφορετικές περιβαλλοντικές συνθήκες. Οι περιορισμοί του ADR αισθητήρα εντοπίστηκαν και καταγράφηκαν σε διαλυτικά μέσα με γνωστές διηλεκτρικές σταθερές. Ένα πρωτότυπο μοντέλο επίσης παρουσιάζεται το οποίο συνδέει την πυκνότητα του εδάφους με την απόκριση του οργάνου με σκοπό την διαφοροποίηση των συνθηκών μεταξύ επί τόπου εδαφών και εναπόθεσης φερτών υλικών. Η αξιολόγηση του μοντέλου και του αισθητήρα πραγματοποιήθηκε με πειραματική αναπαράσταση της υδραυλικής υποσκαφής με προσομοιώσεις σε υδραυλικό κανάλι.

Ένας νέος πρωτότυπος αισθητήρας βασισμένος στην ADT αρχή μέτρησης στη συνέχεια αναπτύχθηκε και αξιολογήθηκε για την ποσοτικοποίηση της ικανότητάς του να εντοπίζει δραστηριότητες υδραυλικής υποσκαφής και εναπόθεσης φερτών υλικών. Μοντελοποίηση μέσω της μεθόδου των πεπερασμένων στοιχείων χρησιμοποιήθηκε για να καθορίσει τα βέλτιστα γεωμετρικά χαρακτηριστικά του πρωτότυπου αισθητήρα βασιζόμενα σε μοντέλα με διάφορες διηλεκτρικές σταθερές. Η ανάπτυξη του αισθητήρα συνοδεύεται από μια θεωρητική ανάλυση με σκοπό να επεξηγήσει την ηλεκτρική συμπεριφορά του οργάνου. Η πειραματική ανάλυση διεξάγεται με προσομοιώσεις, σε πραγματικό χρόνο, ανοικτού υδραυλικού καναλιού χρησιμοποιώντας δύο τύπους αμμωδών εδαφών. Η γεωμετρική βελτιστοποίηση των ηλεκτροδίων του αισθητήρα και η πρόβλεψη της συχνότητας που ενισχύει την ευαισθησία του επίσης παρουσιάζεται σε αυτό το ερευνητικό έργο. Οι επιπτώσεις της θερμοκρασίας του ύδατος και των διαφορετικών συγκεντρώσεων άλατος στην απόκριση του οργάνου αξιολογούνται επίσης και αναφέρονται σε αυτήν την έρευνα.

Η ανάλυση των αποτελεσμάτων υποδεικνύει ότι ο αναπτυγμένος πρωτότυπος ADT αισθητήρας μπορεί να παρέχει μια αξιόπιστη, εναλλακτική και χαμηλού κόστους λύση συγκριτικά με τα υφιστάμενα μέσα παρακολούθησης. Επισημαίνεται επίσης η ικανότητα και των δύο ADT και ADR αισθητήρων να παρέχουν μετρήσεις των δραστηριοτήτων διάβρωσης και εναπόθεσης φερτών εδαφών. Έχουν επίσης σημαντικές δυνατότητες για την ενσωμάτωσή τους σε ένα σύστημα παρακολούθησης με σκοπό την εφαρμογή σε θεμελιώσεις, συμβάλλοντας στην βελτίωση της ανθεκτικότητας και κατά συνέπεια της βιωσιμότητας των υδραυλικών και υπεράκτιων κατασκευών.

Dedicated

To those who are struggling in this path of making this world a better place

and also

To my parents Andreas & Ifigeneia, who value education above all.

Acknowledgements

This Ph.D. thesis is the result of a challenging four year journey that was accomplished with the generous help and support of many people.

First and foremost, my greatest appreciation and gratitude goes to my supervisors Professor Alessandro Tarantino and Professor Martin D. Judd. Martin, thank you for advising and supporting me during all the phases of my Ph.D., I really appreciate all your contributions of ideas, time and your valuable guidance. Alessandro, the passion and enthusiasm you have for research was contagious and motivational for me, thank you for guiding this work and for your detailed and instructive comments. It was a pleasure and a great honour to work with both of you. I would also like to thank Dr Mohamed Saafi for his guidance at the beginning of this work.

I would like to thank my examiners Professor Guido Musso and Dr Phillippe Sentenac who provided encouraging and constructive feedback.

A special thanks goes to a number of people for their support and advice in difficult times during the past four years and especially to Dr Stella Pytharouli, Dr Elsa João, Professor Zoe Shipton, Professor Becky Lunn, Dr Vasilis Avdikos, Dr Christos Tachtatzis, Dr Manousos Valurakis and Dr Bruno Giordano.

I would also like to thank the team of technicians from the Department of Civil and Environmental Engineering for their support during my experimental work in the laboratories and especially John Carlin, Derek McNee and the computer officer Ron Baron. Thanks also goes to Francis Cox who provided technical support in the Department of Electronic and Electrical Engineering.

I gratefully acknowledge the funding source for my Ph.D. work which was provided by the Faculty of Engineering and the Department of Civil and Environmental Engineering of the University of Strathclyde, Glasgow.

I would like to thank a number of friends and colleagues in Glasgow, Brasilia and Athens for the support and the nice time we had the last years and especially Fabrizio, Matteo, Maduka, Rose, Francesco and Eirini.

Attribution

This doctoral thesis consists of self-contained chapters. Parts of the manuscripts of each chapter have been published or are currently under preparation or at submission stage in peer reviewed journals and international conference proceedings. This attribution page is for introducing the co-authors and clarifying their contribution to these chapters.

Chapter 3: Professor Alessandro Tarantino of the Civil and Environmental Engineering Department at University of Strathclyde, Glasgow, Professor Martin D. Judd[*] of the Electronic and Electrical Engineering Department at University of Strathclyde, Glasgow, Dr Christos Tachtatzis a Research Associate of the Electronic and Electrical Engineering Department at University of Strathclyde, Glasgow and Dr Mohammed Saafi a Senior Lecturer of the Civil and Environmental Engineering Department at University of Strathclyde, Glasgow. The experiments, analysis of the results and preparation of the article were conducted by Panagiotis Michalis. The work was carried out under the supervision of Professor Alessandro Tarantino and Professor Martin D. Judd[*] who reviewed and revised the manuscript. Dr Christos Tachtatzis provided assistance with regards to the wireless interface connections and reviewed the article. Dr Mohammed Saafi provided guidance in sections 3.2.3, 3.2.4, 3.2.5, 3.3.1 and 3.4.1.

Chapter 4: The experimental simulations, analysis of the results and preparation of the article were conducted by Panagiotis Michalis. The work was carried out under the supervision of Professor Martin D. Judd[*]. Professor Alessandro Tarantino reviewed and revised the manuscript.

Chapter 5: The experimental work, analysis of the results and preparation of the article were conducted by Panagiotis Michalis. The work was carried out under the supervision of Professor Martin D. Judd[*] and Professor Alessandro Tarantino who also reviewed and revised the manuscript.

---

[*] Now Technical Director at High Frequency Diagnostics and Engineering Ltd, Glasgow, UK.

Table of Contents

Table of Figures

List of Tables

Chapter 1

Introduction

1.1 Outline

This chapter introduces the problem of scour and sediment re-deposition focusing on their implications to the stability of foundations of hydraulic and marine structures. It briefly discusses the importance of real-time monitoring in contrast to the current visual inspection practice and finally presents the research goals and the organisation of the thesis.

1.2 Overview of the scour problem

The foundations of hydraulic and marine structures constitute one of the most vulnerable components of infrastructure systems. In recent years, severe and more frequent flood incidents across the globe have put bridges at high risk of failure due to scour. Scour is the result of the erosion of streamed around the foundation of a structure, leading to structural instability and ultimately catastrophic failures. Flood induced scour is the leading cause of bridge failures worldwide. Scour action is also considered one of the main challenges in the design and operation of offshore wind farms as it leads to excessive excavation of the surrounding seabed.

Over the past decades several efforts have focused on the development of instrumentation techniques to measure scour processes at foundations. However, they are not being used routinely due to numerous technical and cost issues, therefore, scour continues to be inspected visually in the majority of cases.

The difficulty of scour monitoring in the field is considered a major gap in the knowledge and general understanding of scour mechanism. Predictive models for scour depth and scour countermeasure techniques are essentially based on laboratory studies. These prediction models have not been validated in real field conditions and

cannot be directly applied to foundation elements. As a result important aspects of scour processes are not yet fully understood and therefore they are not incorporated into design methods.

The detection of scoured holes hidden by re-deposited soil is also of great importance for the assessment of stability conditions of the foundation. The current post-event visual inspection is not able to reveal the actual bed level conditions at foundations as re-deposited soil often re-fills the scoured holes. The re-filling material does not have the same resistance to hydrodynamic forces as the in-situ sediment and it is easily scoured again during small-scale floods compromising the integrity of the foundation structure. Continuous scour monitoring would enable early remedial maintenance and repair actions to be carried out, reducing costs and improving public safety. However, the majority of the existing monitoring techniques cannot detect sediments re-deposited in scour holes.

1.3 Description of the research goals

The aim of this work is to develop a new approach for monitoring underwater bed level variations in the vicinity of the foundation structure based on (i) an off-the-shelf instrument and (ii) a new prototype sensor. This research intends to provide an insight of the Amplitude Domain (AD) technique which appears to have been used for the first time for the purpose of measuring scour and re-deposited sediment processes. The evaluated instruments should deliver a low-cost, easy-to-use and accurate alternative to existing scour monitoring instruments. They should also be ready to be incorporated effectively into existing monitoring platforms offering an attractive solution to assess remotely bed level conditions around the foundation.

The study initially focuses on developing a methodology to measure scour and re-deposited sediment processes using an off-the-shelf sensor based on Amplitude Domain Reflectometry (ADR) technique. The sensor is evaluated in tests simulating the scour and sedimentation processes under 'static' conditions using sediments that represent common river/sea bed mediums. The influence on the sensor response to environmental variables such as salinity and temperature, which can fluctuate in seasonal patterns, is investigated. The work also aims to develop an approach to 'extract' soil density information from sensor signals that will allow discriminating

between in-situ and re-deposited sediment conditions. An offshore environment simulated in open channel flume experiments is finally used to validate the response of the ADR sensor to monitor scour and re-deposited sediment evolution in real-time.

The thesis then focuses on the development of a new impedance-based low-cost sensor for the purpose of measuring bed level variations. The objective is to identify optimum geometric and electronic configurations to enable accurate measurement of scour and sedimentation processes. The Amplitude Domain Transmissometry (ADT) technique is utilised in this work which appears to be the first application for monitoring soil-water mixtures. The development of the sensor is based on a combination of theoretical analysis and experimental validation. The initial design is supported by finite element modelling simulating various permittivity conditions that represented scour, in-situ and re-deposited sediment environments. The electrical behaviour of the sensor is then investigated with the development of an analogue analysed via transmission line theory. A primary investigation using a Network Analyser aims at identifying wave propagation variables that can provide accurate and easy-to-detect measurement of scour and re-deposited sediment conditions.

The capability of the developed ADT sensor is evaluated under various environments in 'static' scour experiments examining sediment types, salinity concentrations, and temperatures typically found in real field conditions. Finally, validation is achieved by simulating scour and re-deposited sediment processes in an open channel flume.

1.4 Structure of the thesis

The doctoral thesis is divided into four major chapters (Chapters 2 to 5), each of which is formatted to be an independent original manuscript. Each of the Chapters 2, 3, 4 and 5 has either been published, or is currently under submission or preparation stage to peer reviewed journals and international conference proceedings in the research fields of geophysics, geosciences, hydraulic and electrical engineering. The chapters are obviously presented with a slightly different format compared to the articles submitted or to be submitted for publication to enhance presentation of the thesis as a whole.

Chapter 2 provides a background of scour mechanisms and its implications caused to hydraulic and marine infrastructure. The problem of scour monitoring that arises from the lack of current inspection practice is then identified. Finally, a review of the up to date monitoring techniques and efforts to measure scour processes at foundations is presented.

Chapter 3 presents the investigation of an off-the-shelf sensor proposed to measure bed level variations around foundation elements based on the ADR technique. The sensor was equipped with a wireless interface and was evaluated to quantify its capability to detect scour and sediment re-deposition processes in various soil types, temperature and water conditions. The use of permittivity measurements to estimate the soil density around each sensor location to discriminate between in-situ and deposited sediment is also investigated and presented herein. The analysis is conducted using 'static' scour simulations and real-time open channel flume experiments.

In **Chapter 4**, the optimisation of the geometric characteristics of the electrodes of a new electromagnetic sensor is presented. Finite element modelling is performed to optimise the sensor components based on the computed capacitance and electric displacement field in various simulated media. The effect of the various inner cross sections of the sensor, electrode arc lengths and angular separation on the obtained results are investigated.

Chapter 5 introduces the development and the laboratory validation of a new prototype electromagnetic sensor. The investigation presents the ADT technique that utilises a through-Transmission configuration in the Amplitude Domain. The performance and optimisation of the newly developed sensor under different environmental conditions is presented and discussed in this section. The capability of the proposed instrument and technique to detect scour and deposited sediment was evaluated via 'static' scour simulations and real-time flume experiments.

Finally, **Chapter 6** summarises the major findings of this study and provides recommendations for future research and next stage developments.

Chapter 2

Background

2.1 Introduction

This chapter aims to provide a background of scour and re-deposited sediment processes investigating their consequences to hydraulic and marine infrastructure. The first section initially focuses on the threat to bridge foundations imposed by scour action. The different scour types that occur in river environment and the key variables affecting the bridge scour evolution are then presented followed by a review of the bridge scour risk management and the current inspection practice. The chapter then presents the scour mechanism in offshore environment investigating the impact of bed level variations in wind farm developments. Finally, the study focuses on the problem of current scour inspection methods and presents a review of the existing monitoring techniques that are employed to assess scour processes at the foundation structure.

2.2 Bridge scour

Nowadays the engineering industry should be aware that the possibility of extreme weather events is increasing as a result of the global changing climate. Unexpected flooding incidents are more likely to occur causing the severe damage and collapse of bridges due to scour action at their foundations.

2.2.1 Scour threat to infrastructure

Design engineers should have a good understanding of the weak points of a structure and the reasons that lead to failures. Infrastructure systems are also designed in a way so that in the case of an event the structure will give a visual warning before its actual collapse allowing for time to be examined. However, scour is considered as one of the

incidents that can cause catastrophic bridge failures without prior visual warning leading to destructive consequences for the infrastructure.

Bridge failures due to scour action

In the UK, the Glanrhyd (South Wales) railway bridge collapse in 1987 with four fatalities, the Ness Viaduct failure (Inverness) in 1989 during severe floods and the failure of a railway bridge over River May (Perth) are some cases of disasters due to scour process. During the last decade, scour was also the main cause for the Malahide viaduct failure (railway bridge linking Belfast to Dublin) in August 2009 [see Figure 2.1 (a)]; the collapse of several bridges during the Wales and Cumbria floods in summer 2007 and November 2009 respectively [see Figure 2.1 (b)]; and the failure of the Bridge RDG1 48 (West London) in November 2009.

Figure 2.1: (a) The collapsed Pier 4 of Malahide viaduct (Ireland), source: RAIU, (2010). **(b)** The Northside bridge in Workington (Cumbria) during the floods in 2009, source: Byrne, (2009).

In Europe scour has also been identified as the main cause of the collapsed pier on the A12 motorway linking Munich and Verona near Kufstein (Austria) in 1990 and the Hintze Ribeiro bridge failure (Portugal) in March 2001 with 59 fatalities [see Figure 2.2 (a)].

Major structural collapses due to scour action have also been reported in East-Asian countries such as Korea, Taiwan and Japan [see Figure 2.2 (b)]. Bridge failures are occurring as a result of typhoons and extreme flood events during the winter and fall seasons as witnessed by the collapse of several bridges in Taiwan during the 1996 floods (Lu et al., 2008).

Figure 2.2: (a) Hintze Ribeiro Bridge failure (Portugal) due to scour of a masonry bridge pier, source: Briaud, (2011). **(b)** The collapsed Houfeng Bridge in Central Twain, source: Chao-Yang, (2008).

In the United States, research was focused on scour processes after the Schoharie Creek road bridge failure in April 1987 with 10 fatalities [see Figure 2.3 (a)] and the collapse of Hatchie river road bridge in 1989 with 8 victims [see Figure 2.3 (b)]. After these structural failures every US state was required to classify all highway bridges over water ways in the different categories of low risk, scour susceptible and scour critical (Lasa et al., 1999).

Figure 2.3: (a) The Schoharie Creek Bridge collapse due to severe foundation scour with 10 fatalities, source: AP (1987 cited in UMKC, n.d.). **(b)** The impact of the Hatchie river road bridge with 8 victims, source: Briaud, (2011).

Public attention was again concentrated on scour action after the 1993 flooding of the Mississippi river which caused many bridge failures. Foundation scour was also identified as the main cause of bridge collapses during the 2005 and 2008 hurricanes Katrina and Ike respectively (Stearns and Padgett, 2012).

Scour impact on infrastructure

As presented in the aforementioned cases, scour poses a great threat to the transportation infrastructure across the globe. In the UK for example, there are more

than 9,000 major bridges over waterways (see Figure 2.4) and almost 95,000 bridge spans and culverts susceptible to scour processes (RSSB, 2004).
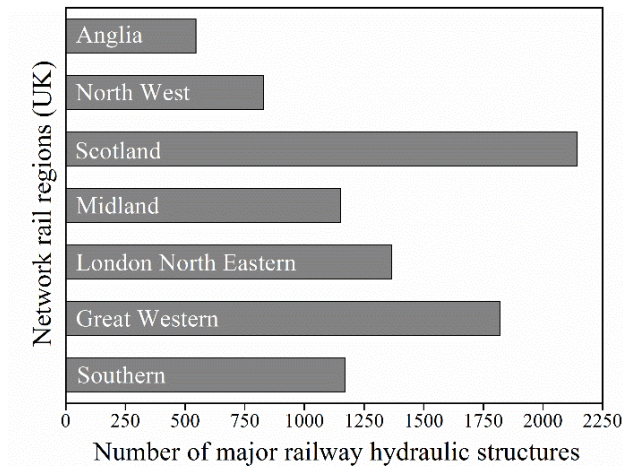
Figure 2.4: Number of major hydraulic structures in the UK rail network.

Up to 2003, abutment and pier scour had been identified as the most common cause of more than 130 railway bridge failures (see Figure 2.5) associated with fatalities (RSSB, 2004). The damage due to scour action at railway structures alone in the UK is estimated to be over £1 million per year on average (RSSB, 2005). It is estimated that over the past years there is an average of at least one structural failure in a flooded catchment every 2.5 years and a 40% chance that at least one rail structure will fail each year due to a flood event (RSSB, 2004). Future projections also indicate that the frequency of extreme flooding across Europe is anticipated to double by 2050 (Jongman et al., 2014) with major implications for highway and railway infrastructure.
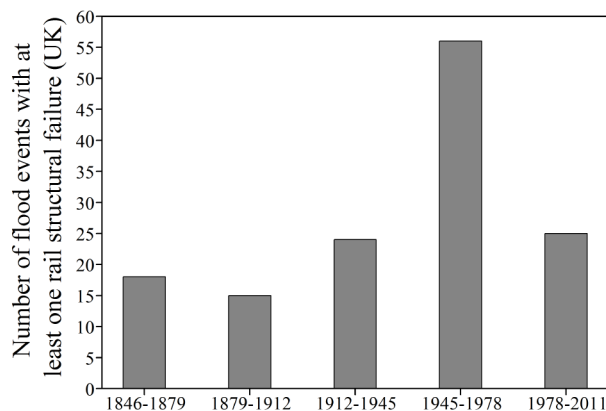
Figure 2.5: Rail structural failures in the UK, sources: RSSB, (2004) and Imhof, (2011).

In the United States, the 84% of the bridges have been constructed over waterways (Landers, 1992). Scour action is expected to occur at most of the hydraulic structures during their service life (Richardson and Davis, 2001). During the period

from 1961 to 1976 it was identified that more bridge failures were caused by scour action than by any other cause including earthquakes, wind, structural, corrosive, and accidental or during construction (Placzek and Haeni, 1995). Other reports also associated scour action with 95% of all seriously damaged and collapsed highway bridges over waterways (Richardson and Davis, 2001). The number of scour critical bridges in the US has also increased from 2% in 1997 to 5% in 2005 while for the same period of time the number of bridges over waterways that are susceptible to scour also rose from 29% to 40% (Chen et al., 2011). As a result, in 2009 more than 20,904 bridges in the US were categorised as scour critical (Hunt, 2009).

The high economic loss due to scour action at hydraulic structures has also been investigated by the US Federal Highway Administration (FHWA), which estimated that the indirect costs of structural failures suffered by the general public, business and industry are five times greater than the direct costs of bridge repair (Lagasse and Richardson, 2001). The total cost of a bridge failure was also estimated to be two or three times greater compared to the original cost of the bridge (FHWA, 1991).

Most recent UK reports on bridge scour

In the UK many reports have highlighted scour process as one of the potential challenges facing civil infrastructure systems due to the changing climate. RSSB (2004) pointed out the negative impact of scour at the 95,000 bridge spans and culverts, part of the UK railway network, taking into account the predicted high intensity precipitation which may result to increased period of unusual high floods. The impact of scour and flood risk at railway structures was the objective of the T112 project (RSSB, 2004) which revealed the lack of guidance for the up to that date standards regarding the underwater examination of the structures.

The need to adapt our infrastructure to deal with more frequent extreme weather events was underlined by the UK Bridges Board (2009). Highways Agency (2009) identified scour as highly disruptive and time critical vulnerability due to its destructive consequences on bridges and other hydraulic structures. Scour action was also considered by Transport Committee (2010) as a particularly important problem at railway structures, taking into account that can cause sudden loss to a structure without apparent signs and the long breaking distance required for trains. The Royal Academy

of Engineering (2011) also listed scour processes at structures as one of the ten effects with the biggest risks to highway networks.

The impact of the changing climate on infrastructure is considered as an 'important economic, environmental and social issue' as revealed by recent flooding and severe weather events (HM Government, 2011, p.4). Increased bridge scour due to intense flooding and rainfall is also identified as one of the main climate change impacts and as one of the big challenges in order to achieve a climate resilient infrastructure (HM Government, 2011; Defra, 2011; and Defra, 2012).

2.2.2 Bridge scour mechanism

Scour action causes a drastic reduction in the safe capacity and stability of structures and may occur in relatively low flow conditions before a general movement of the sediment. Scour is defined as the erosion or removal of streambed or bank material from the foundation structure due to the flowing water (Kattell and Eriksson, 1998). The initial scour process where no sediment is transported is referred as 'clear-water' scour. 'Live-bed' scour occurs when the flow increases and sediment is been transported from the upstream location of the structure (Melville and Coleman, 2000). During scouring the rate of erosion of the sediment around a location exceeds the rate of the replacement sediment that is supplied from upstream. The erosion and sediment transport of a river depends on the flow conditions and is becoming greater as the flow velocity increases. This relation is not linear considering that a double increase of the flow rate may result to an increase of sediment transport ten times greater (Highways Agency, 2006).

Scour process is developed as the water flow increases during a flood event while the eroded holes start to be re-filled again as the flow reduces (May et al., 2002). However, scour continues to develop after the peak of a flood as it is a time-dependent process. The presence of an obstacle (i.e. bridge pier-abutment) may also result to increased velocities sufficient to cause scouring around the foundations of a structure. Several types of scour exist and according to the Construction Industry Research and Information Association (CIRIA) 551 manual are classified into the following categories (May et al., 2002).

Local scour

Local scour is considered one of the most complex and challenging water flow and boundary erosion phenomenon as a result of complexities derived from the shape of the pier and the site conditions (Ettema et al., 2011). This type of scour occurs at the foundations due to the removal of sediment around the structural elements caused by the flow. In bridge piers and abutments the deepest scour is usually recorded around the upstream location of the structure due to the formation of the vortices (see Figures 2.6 and 2.7).
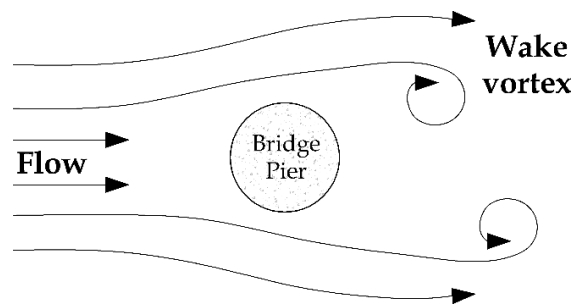
Figure 2.6: Vortices created by flow conditions at a bridge pier (adapted from May et al., 2002, p. 35).

The horseshoe vortex is created as the flow approaches the structure and is deflected downwards to the bed level, rolling up around the bridge pier (see Figure 2.7). The excavated material is deposited downstream of the foundation, forming a level above that of the surrounding bed.
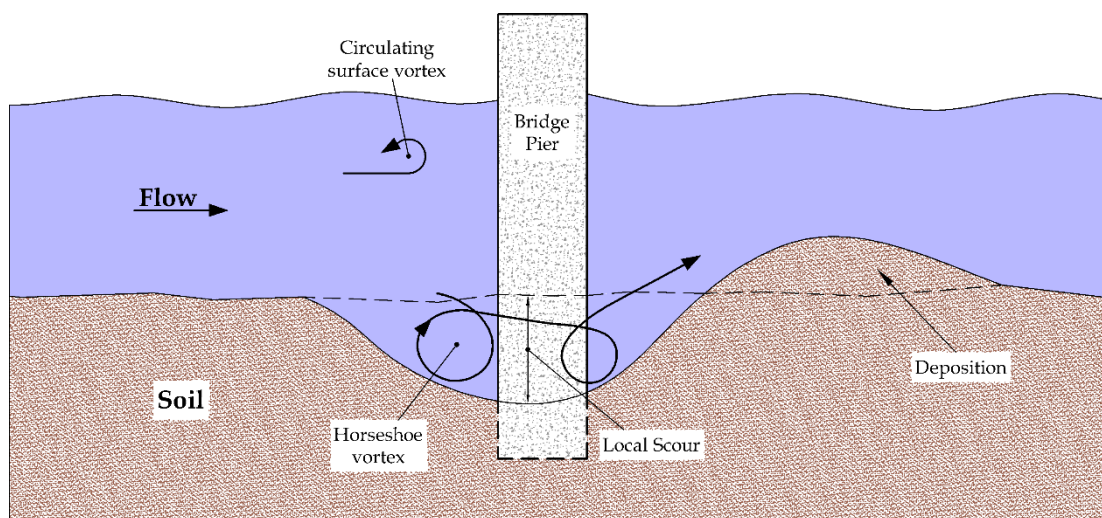
Figure 2.7: Horseshoe Vortex and local scour caused by flow at a circular pier (adapted from May et al., 2002, p. 35)

Contraction, natural and total scour

Contraction scour is caused by higher velocities due to narrowing of the channel and affect all or most of the channel bed in the general area of the hydraulic structure (May et al., 2002). Natural scour includes bed degradation, lateral channel movement and any other scouring processes that are not defined by local and contraction scour. Finally, the total scour is categorised as the sum of local, contraction and natural scour.

The interaction of many factors leads to the creation of the aforementioned different scour types as presented in the following section.

2.2.3 Key variables affecting scour evolution

The assessment of scour action requires a multi-disciplinary approach including the integration of geotechnical and hydraulic engineers, hydrologists as well as geomorphologists for a detailed design, construction and operation planning (May et al., 2002). The advice note BA 74/06 categorises the following key variables that affect the development of scour action at hydraulic structures (Highways Agency, 2010, p. I 2/3):

- ❖ **Flow parameters:**
    - Magnitude of the flood peak being considered.
    - Increased rate of flow during flood.
    - Duration of the flood and its duration after a certain critical discharge.
    - Average flood water depths and velocities at the site.
    - Three dimensional variations of velocities at the site.
- ❖ **Geometrical parameters of the site and the structure:**
    - Plan geometry of the river.
    - Angle of the bridge to the approach flow.
    - Alignment and position of the abutments and piers.
    - Shape and width of abutments and piers.
- ❖ **Bed and bank materials parameters:**
    - Particle size distribution.
    - Shape of the particles.
    - Density of the particles.

- Chemical and electrostatic interactions of cohesive materials.

- Variability of these materials across the site and within the riverbed.

The development of scouring is affected by all the aforementioned factors but mainly from the sediment type of the bed material.

Scour behaviour in various sediment types

Scour is a natural phenomenon that involves the interaction between the hydraulic conditions and mobile erodible bed materials. The bed may consist of cohesive (silt and clay) and non-cohesive (gravel and sand) materials. Non-cohesive sediments typically have granular structure and specific separate particles may be eroded when the applied fluid forces are overcoming the stabilising forces of gravity and the contact of other particles (May et al., 2002). The particle movement depend on their size, density, shape in addition to the packing and orientation in the bed. The denser and larger the particles, the greater the resistance is expected to retain in high flow velocities. On the other hand, cohesive material requires large forces to separate and move particles but relatively small forces are considered sufficient to transport the sediment. With regards to the time effect scour can reach its maximum depth in (Richardson et al., 1993):

❖ sands and gravels in hours;

❖ clays and mudstones in days;

❖ shales and weak sandstones in months;

❖ good sandstones and limestones in years.

In rivers and streams, scour is most likely to occur when the riverbed is composed of granular alluvial and cohesive materials and in some cases even in deeply weathered rock (May et al., 2002). When the bed material consists of sand sediments, maximum scour depth can be reached in one only event while this soil type is also more likely to in-fill a scour hole after an event. In sand sediments greatest scour depth has also been reported to occur on the upstream face of the pier (Hunt, 2009).

In clay soil types, the maximum scour action may occur after numerous events while greater scour depths usually appear in the downstream area of the pier (Hunt, 2009). Based on laboratory experiments using clay bed material around a cylindrical pier, Briaud et al. (2004) also reported that scour process usually will not occur

upstream of the pier, as in sand sediments, but significant erosion is expected at the side of the pier due to high turbulence.

Many other considerations should also be taken into account for the estimation of the scour depth, as it is dependent of the bed material and can be directly affected by phenomena such as armouring of the scour hole. During the development of armouring on a river bed, the small particles are transported and washed away while the larger particles are settling down until they form the entire surface of the bed (May et al., 2002). In the case of a major flood event with high flow velocities the armour layer could be easily washed away resulting in increased scour depth at the foundation structure.

2.2.4 Bridge scour risk management

The majority of scour guidance used nowadays for the design, operation and maintenance of structures over waterways has been conducted in the UK and US. This section presents the bridge scour risk management and the current scour inspection practices that are utilised to evaluate underwater conditions at the foundations of hydraulic structures.

Scour guidance in the UK and US

Over the past decades many research programmes have provided guidance with regards to the assessment of scour processes. Most of the published efforts presented the current state of practice for bridge scour action and also evaluated monitoring techniques for scour detection.

In the UK the first manual to address issues associated with scour activity was published in 2002 by the CIRIA. The objective of the CIRIA 551 project was to produce guidance for engineers with regards to the design, construction, operation and maintenance of hydraulic structures that may be vulnerable to scour processes (May et al., 2002). A project currently carried out by the CIRIA intends to update the C551 manual taking into account high profile events such as the bridge collapses during the Cumbria floods in autumn 2009 and other bridge failures on the rail network (CIRIA, 2014).

One of the main industry standard documents on scour inspections in the UK was published by the Highways Agency (2006). The advice note BA 74/06 intended to evaluate the potential of scour to damage bridge structures. The assessment was proposed to be carried out following a two stage process; the first part contained the evaluation and inspection of the structures by collecting data to evaluate the potential of scour. The second part analysed aspects of scour (i.e. scour depth) and prioritised by ranking vulnerable structures. However, a recent document published by the Highways Agency (2010) highlighted a number of weaknesses in the BA 74/06 report that need to be addressed.

In the US, the first efforts to provide guidance on scour process were initiated by the FHWA and the US Department of transportation. In 1988, the FHWA issued a Technical Advisory revising the National Bridge Inspection Standards (NBIS) and required evaluation of scour susceptibility of all bridges. The FWHA and US Department of transportation published two more documents entitled 'Hydraulic Engineering Circulars' (HEC). The purpose of the HEC No.18 was to evaluate scour conditions at bridge sites (Richardson and Davis, 1995) while the HEC No.20 intended to provide guidelines for identifying stream instability problems due to scour activity at highway stream crossings (Lagasse et al., 1995).

Research conducted by the US Army Corps of Engineers focused on the development of real-time monitoring systems and the impact of ice force and scour activity on a bridge in the White river, Vermont (US) that was presented in the Special report 96-6 (Zabilansky, 1996). The Forest Service of the US Department of Agriculture also developed a scour evaluation program that was implemented in almost 7,650 bridges over waterways on the National Forest land (Kattell and Eriksson, 1998).

Scour research was again focused on the development of scour monitoring systems in 1998 with the document FHWA-RD-99-085 conducted by the US Geological Survey (USGS) and FWHA. This research effort examined the use of commercially available products that could be modified in order to provide a portable scour measurement system (Mueller and Landers, 1999). The National Cooperative Highway Research Program (NCHRP) 515 report also provided guidance with regards to the use of portable scour monitoring devices (Schall and Price, 2004).

The Synthesis 396 report (Hunt, 2009) presented the up to date state of practice for fixed monitoring of scour critical bridges taking into account almost 120 bridge sites where scour techniques were employed. The same period of time the document HEC No.23 (Lagasse et al., 2009) was published which represents the current state of practice for bridge scour and stream stability evaluation and design. The HEC No.23 also provides design guidelines regarding bridge scour instabilities and countermeasures that have been deployed in the US.

Finally, the Document 175 (Ettema et al., 2011) evaluated the current knowledge with regards to the bridge pier scour processes and proposed new practices in order to predict scour depth. The report highlighted that further research is required for better understanding of the scour processes to address the design issues. This can be achieved with the development of real-time monitoring techniques to evaluate pier foundation conditions, as the existing established methods cannot provide reliable estimation of scour depth (Ettema et al., 2011).

Current bridge scour inspection practice

In the UK the current practice requires general inspections at hydraulic structures to be carried out on biennial basis (UK Bridges Board, 2009). General inspections include the visual evaluation of the parts of a structure that can be assessed without the need for special equipment. Special inspections requiring an underwater examination of the structural elements at a close range take place at time intervals of six years or after specific events (i.e. floods, struck incidents) (UK Bridges Board, 2009). In Ireland special inspections (scour included) at foundations are also proposed to be carried out at maximum time intervals of six years (Iarnród Éireann, 2009). Similarly, in the US scour at hydraulic structures is being evaluated with visual inspections at time intervals of five years (Chen et al., 2011).

The lack of available monitoring techniques to evaluate underwater foundations pose a major threat to bridge structures. Likewise, scour processes in offshore environment cause severe consequences to the foundations of marine and offshore renewable infrastructure.

2.3 Offshore scour

Offshore wind energy has become one of the major domestic renewable energy sources in the UK. Many technical challenges need to be addressed for the development of mature and reliable offshore installations. One of the main complications in the design and operation of offshore wind turbines arises from the uncertainty about maximum scour depth around their foundations.

2.3.1 Scour impact in offshore environment

Scour action can lead to excessive excavation of the surrounding seabed and undercut the foundations of offshore structures. The main types of scour in the offshore environment are caused by the influence of the foundation structure on the flow pattern and the overall seabed movement, where loose material of upper soil of the bed is transported by sea currents. Scour activity at offshore wind turbines occurs when a steady current approaches and reaches the intersection of the seabed with the cylindrical pile (Den Boon et al., 2004). As the flow increases, a highly turbulent horseshoe vortex is produced in the region of the turbine foundation. The combination of these effects washes away the sediment around the foot of the pile leading to a scour hole in the area of the foundation structure. In addition to the scour holes around the foundations, a more general influence of erosion is observed in the region of the individual structural elements, known as global scour (Whitehouse, 1998). Scour activity around offshore wind turbine foundations poses many technical challenges that arise from the following issues (Zaaijer and van der Tempel, 2004):

❖ reduction of the structure's stability,

❖ increased hydraulic loading on the vertical face of the structure,

❖ increased maximum moments at the foundation structure,

❖ decrease and variation in the natural frequency of the turbine,

❖ need for more complicated foundation design requirements,

❖ increased bending stresses on cables, which may exceed the design limits.

Up to now, offshore wind farms have been constructed in relatively shallow waters due to limited options with regard to their foundations (Musial et al., 2006). Their near-shore locations indicate that they have been founded on particularly mobile

coastal sediments (Black, 2008). The movement of these sediments is associated with scouring issues; therefore they are significantly susceptible to the development of scour holes around their foundations. In addition, re-deposited soil often fills the scour holes, making them difficult to detect and locate. This in-filling material is loose and does not have the same resilience as the original soil; consequently, the in-filled holes are easily scoured again, reducing the integrity of the structure.

The monopile is currently the most preferred foundation type and is commonly used in the offshore industry (Zaaijer and van der Tempel, 2004). Issues arising from the complexity of other foundation types, such as the tripod, have delayed their consideration as an option for offshore wind farms (Stahlmann and Schlurmann, 2011). In fact, there is a significant lack of knowledge regarding the scour processes for all types of foundations. This has led to increased dimensions of the foundation; increased pile length for the monopile type; and a more complex dynamic response of the structure. Consequently, current offshore wind farm developments are considered to be designed on a security-based but cost-ineffective strategy (Stahlmann and Schlurmann, 2011).

2.3.2 Report on scour action at offshore sites

In recent years, the rapid increase in the development of the offshore industry has led to a number of reports dealing with scour activity. Scour monitoring data from existing offshore sites as well as from laboratory-based studies are discussed in this section.

The diameter of the monopile foundation type has been designed based on the estimated depth and horizontal extent of scour activity. Experience showed that scour holes in offshore environment can reach a depth of 1.5 times the pile diameter (Zaaijer and van der Tempel, 2004). Data obtained from the Arklow Bank wind farm (Ireland) also revealed that the presence of the monopile foundation type led to an increase in scour holes influenced by strong currents and the wave heights (Whitehouse et al., 2006). In addition, during the foundation construction and before the installation of scour protection, symmetrical scour holes of 4.0 m depth were reported. Laboratory models also showed that scour holes up to 7.0 m deep were possible with 80% - 90% of equilibrium scour occurring in the first six hours (Whitehouse et al., 2006). Moreover, initial scouring following the foundation installation appeared to be in the

order of a few tens of centimetres at more than half the wind turbines at Burbo wind farm located at Liverpool Bay (Carroll et al., 2010). Extended bathymetric surveys conducted at the Robin Rigg wind farm site (Scotland) also revealed scour depths that reached the upper limit of values reported so far, varying from 4.0 to 7.7 m (Carroll et al., 2010).

The offshore industry has also focused on the evaluation of new foundation types and the implications caused by scour activity. A comparison of in-situ and laboratory measurements of a tripod foundation installed at the Alpha Ventus offshore site (Germany) revealed scour depths lower than the real sea conditions (Stahlmann and Schlurmann, 2011). Large-scale physical models also indicated scour depths greater than expected, which were found to be influenced by wave parameters and the orientation of the tripod foundation. Data obtained from offshore wind farms located in the UK and Europe also highlighted the uncertainty and the lack of specific guidance with respect to scour action at sites with complex soil types and during severe weather conditions (Carroll et al., 2010).

The difficulty to evaluate bed level conditions at the foundation structure and to develop reliable scour prediction formulas arise from the lack of available monitoring techniques. The following section aims to identify the importance of real-time assessment of erosion processes and to provide an overview of the scour monitoring problem in both hydraulic and marine structures.

2.4 Scour monitoring

Monitoring is an important tool that enables the evaluation of the scour conditions around the foundation structure. Although it will not offer a solution to problems associated with scour at hydraulic and marine structures, monitoring can provide advanced warning for the public safety and collect data from the field necessary to understand the scour mechanism. This, in return will help develop scour countermeasures strategies and improved scour design tools. Real-time data will also help engineers better understand the impacts of climate change on the scour process. Advanced scour monitoring systems will also prevent structural failures thus reducing energy consumption and CO_2 emissions associated with replacement and re-construction of structures.

2.4.1 The problem of bridge scour monitoring

The lack of reliability of the methods that are currently used to identify scour at structures is highlighted by the case of Malahide viaduct failure. On the 21st August 2009 the Pier 4 of the viaduct collapsed minutes after a passenger train had crossed it. The investigation report conducted by the Irish Railway Accident Investigation Unit (RAIU, 2010) identified scour as the cause of collapse. The report also highlighted that an inspection carried out three days before the collapse, did not detect scouring effects at the foundation of the pier. In the year 2006, a special scour inspection did not also categorise the Malahide viaduct as a high risk structure due to the effects of scour (RAIU, 2010).

Failure of bridges due to scour is attributed to several issues associated with the present visual inspection procedure which often relies on specialist divers. This method is very expensive and time consuming, therefore bridges are inspected at intervals of several years. Severe scour usually occurs during a flood peak discharge with a high velocity, preventing concurrent diving inspections from being carried out because of safety considerations. After scouring loose re-deposited soil transported from upstream of the structure often re-fills the scoured holes resulting in difficulties to detect and locate them by visual inspection. The in-filling material is less dense and does not have the same resistance to scour as the original soil (Hunt, 2009). As a consequence, during smaller-scale flood events the in-filled holes are easily scoured again, compromising the integrity of the foundation structure. Furthermore, the 'as built' information for many scour critical structures is not available and as a result they are classified as having unknown foundation status (Arjwech et al., 2013), making scour risk assessment a particularly challenging issue.

As a result, most of the data used to develop predictions of scour depth and scour countermeasure techniques has been obtained from the laboratory. The evaluation of scour is also becoming a critical topic taking into account the deterioration of infrastructure as well as the cost and technical issues arising from the rehabilitation of bridges. The lack of instrumentation techniques to asses scour conditions has resulted in catastrophic structural failures without prior warning.

2.4.2 Importance of offshore scour monitoring

Sediment transport at the seabed presents a range of risks to offshore activities. At the same time, the evaluation of scour processes is considered to be very difficult as bed level changes are variable. The collection of information on the natural sediment and local processes is of great importance as most of the data used to predict offshore scour activity are derived from laboratory-based studies using wave and current flumes. Due to lack of field data the validation of these models has rarely been possible (Stahlmann and Schlurmann, 2011). As a result, different values regarding the depth and extent of scour around the foundation structure have been observed between the prototype models and real sea conditions.

In the UK, the round 1 and round 2 wind farms have been constructed in relatively shallow waters (up to 30 m deep). The round 3 wind farm sites are proposed to be constructed in deeper waters (30 m - 60 m) where different options of foundations will be required such as gravity bases, jacket and multi-leg structures (Carroll et al., 2010). The tidal currents on these sites may be of lower magnitude but wave exposure is expected to be more significant, which may lead to increased scour (Carroll et al., 2010). Scour monitoring information is therefore a key issue that will allow the evaluation of new foundation types that differ from the monopile option. In addition, the need for scour field data immediately after the construction is considered to be a very important issue, required to expand the scientific understanding of scour development around offshore wind turbine foundations during their lifetime (Carroll et al., 2010). The rate of scouring is also of particular interest, especially during the installation phase of the foundation, as it determines the time at which scour can be expected to reach its critical depth.

The difficulty of field measurements is considered a major gap in the knowledge and general understanding of scour mechanism. However, the offshore industry is not collecting scour information on a routine basis due to lack of available techniques (Black, 2008). An ability to gather information concerning the evolution of scouring is of great importance as it will enable the validation of models derived from laboratory-based studies, the investigation of the site-specific driving forces, and the evaluation of the structure performance under extreme hydrodynamic events.

Monitoring of scour action at offshore sites will also allow the assessment of different engineering designs and the development of improved scour countermeasures.

During the last decades many research efforts concentrated on the development of monitoring techniques to provide a real-time assessment of scour conditions around the foundation elements. The following sections aim to provide an up to date insight of the techniques that have been employed to evaluate and develop monitoring methods to measure scour activity at hydraulic and marine structures.

2.4.3 Scour monitoring methods

Numerous efforts focused on the development of monitoring techniques to evaluate bed level variations at foundation elements. The HEC No.23 categorises the methods that are currently being used in order to assess scour conditions at hydraulic structures in the following three categories (see Table 2.1):

Table 2.1: Instrumentation summary by category (adapted from Lagasse et al., 2009, p. 9.25)

Category	Advantages	Limitations
Visual	Forensic investigations	Specialised training required, labor intensive
Fixed	Continuous monitoring, remote surveillance, easy-to-use, low operational cost	Loss of equipment, maintenance, maximum scour not at instrument location
Portable	Point measurement or complete mapping, use at many bridges	Labor intensive, special platforms often required

Visual monitoring involves the regular examination of the structure at specific periods of time. The drawbacks of the visual inspections are many as discussed in the section 2.4.1.

Fixed instrumentation refers to monitoring devices that are attached to the structure in order to monitor scour at specific locations. The location and number of these devices are defined according to site and structure conditions. Some of the fixed instrumentation techniques are able to provide real-time evaluation of scour critical structures and remote safety surveillance. The drawback of fixed instrumentation techniques relies on the high maintenance and operation cost (see Table 2.2) as well as the impact of debris and ice on the instrumentation.

Table 2.2: Estimated cost information (in US Dollars) for fixed instrumentation (adapted: Lagasse et al., 2009, p. 9.29).

Type of Instrumentation	Instrument Cost with Remote technology ($)	Installation Cost	Maintenance/ Operation cost
Sonar	12,000-18,000	Medium to high;5 to 10 person days to install	Medium to high
Magnetic Sliding Collar	13,000-15,500	Medium, minimum 5 days to install	Medium
Tilt Sensors	10,000-11,000	Low	Low
Float-out Device	10,100-10,600	Medium; varies with number installed	Low
Sounding Rods	7,500-10,000	Medium; minimum 5 person days to install	High
Time Domain Reflectometers	5,500-21,700	Low	Medium

Portable instrumentation includes devices that can be transported and implemented in different structures. The use of portable devices is considered a cost effective method compared to fixed instrumentation (see Table 2.3). However, portable instruments are not able to provide continuous real-time field data of the structure site. Trained personnel is also required for their operation which increases the limitations of this method due to cost and safety considerations.

Table 2.3: Estimated cost information (in US Dollars) for portable instrumentation (adapted from: Lagasse et al., 2009, p. 9.26)

Type of Instrumentation	Instrument Cost	Installation Cost	Operation Cost
Physical Probes	<$500	varies by use	Varies, minimum 2 person crew for safety
Portable Sonar	fish finder: $500 survey grade: +/- $15,000	varies by use	Varies, minimum 2 person crew for safety
Traditional Land Survey	+/-$10,000	varies	2-3 person crew
GPS	$5,000 for submeter and $20,000 for centimetre accuracy	varies	1-2 person crew

Most of the existing scour measurement techniques cannot reveal the magnitude of the problem as they are not able to provide real-time data during major floods. They are also not able to detect re-deposited sediment which re-fills the scour holes and is easily scoured again leading to catastrophic structural failures. The high cost of existing monitoring techniques is also identified as the most common reason for the limited use and application of these devices for scour monitoring at hydraulic structures (Hunt, 2009). Other factors are associated with the complexity of the equipment, the capability of providing repeatable and reliable information, the harsh

environmental conditions, the processing and interpretation of data and the debris impact. An overview of the advantages and limitations of the existing scour monitoring technologies is presented in Table 2.4.

Table 2.4: Advantages and limitations of existing scour monitoring instruments.

Instrument	Advantages	Limitations
Physical probes	Effective in fast and shallow water	Limited use by depth, velocity – Debris/Ice impact – Personnel required
Sonar devices	Continuous scour monitoring	Debris/Ice impact – Transducer frequency - Beam width
Ground Penetrating Radar (GPR)	Continuous record of riverbed	Issues with clays /saltwater conditions – High cost/complex equipment – Trained personnel
MEMS sensors	Real-time monitoring of scour and deposition height.	Not yet tested in the field (Results based on laboratory environment)
Magnetic Collar	Easy to operate - Low-cost	High maintenance cost – Not able to detect deposition - Excavation of riverbed
Steel Rod	Easy to operate - Low-cost	Not real-time application – High maintenance cost – Excavation of riverbed
Numbered Brick Column	Commercially available – Applicable during high floods	Not able to detect deposition – Not real-time application – Excavation of riverbed
Buried Orientation Sensors	Low-cost - Automatic transmission of wireless signals	No continuous field data – Sensor battery life – Debris impact when floating – Excavation of riverbed
Optical-Fibre based Sensors	Real-time monitoring – Resistance to environmental corrosion	Installation issues – More field tests required
Time Domain Reflectometry (TDR)	Real-time application – Continuous data during high floods	Sensor battery life – Cable length –Limited application in conductive mediums
Wireless Smart Rocks	Cost effective and robust method – Can be deployed easily to structures	Reduction of the signal over distance – Sensor battery life - Not field tested yet
Diving	N/A	Not reliable method – Safety considerations
Offshore Cameras	N/A	Debris/Ice impact – Difficulty to detect scour in turbulent conditions
Passive Scour Chain System	No maintenance required	Cannot provide continuous data – Excavation of riverbed – Not reliable method
Brisco System	Commercially available	Not able to detect deposition – Need to attach the device on the structure
Tell-Tail System	Commercially available – Continuous monitoring of scour and deposition	Difficult to be installed at existing structures – Issues with durability of the sensors
Seismic Survey (PSS, RPSS)	Determination of both scour and foundation depth – Low-cost	Not real-time monitoring – Cannot be used during flood events – Trained personnel
Pneumatic Detection System	Can be implemented under extreme flood events-Real-time application	Not yet tested in the field
Piezoelectric Film devices	Cost effective	Debris/Ice impact – Unreliable measurements due to sensor sensitivity

The following sections aim to provide an outline of the up to date monitoring methods and their working principles used to detect scour activity at the foundation structure. Major findings from the application of current scour monitoring techniques in the field and laboratory environments are presented.

Geophysical instruments

Over recent decades, many techniques have been developed to measure scour action at hydraulic structures. Early research efforts focused on the use of geophysical methods such as seismic-reflection profiling systems and ground penetration radar (GPR) to detect scour at bridge piers and abutments (Gorin and Haeni, 1989; Placzek and Haeni, 1995; Forde et al., 1999). The same basic principle of wave propagation and reflection is used in both techniques. The seismic profiling systems transmit pulsed acoustic signals at low frequency (in the range of kHz) that propagate through the water to the riverbed. The reflected energy is recorded by a receiver transducer and scour is detected based on the magnitude and the arrival time of the reflected signal (Placzek and Haeni, 1995). The GPR technique also transmits electromagnetic pulses into the ground (typically in the MHz frequency range) and scour is identified based on the electrical properties of the materials by measuring the reflected signals (Forde et al., 1999).

These methods do not provide real-time evaluation of scour as in the majority of the cases they cannot be used during flood events for safety reasons. Debris, sediment transport and salinity in water greatly affect their signal, requiring expensive and time consuming data processing and interpretation. The scour inspection challenge using these instruments is even greater when considering the need for highly specialised and heavy equipment demanding skilled personnel (Placzek and Haeni, 1995).

Placzek and Haeni (1995) tested a series of techniques including fixed and swept frequency continuous seismic-reflection profiling (CPS) systems and ground penetration radar (GPR). The data were collected for a period of four years at six bridges in Connecticut, US. The authors indicated that the evaluated geophysical instruments detected scour holes, riverbed deposition and exposed pier footings. However, all the techniques did not provide real-time monitoring as use of boats and trained personnel of 2-3 people was required. Moreover they cannot be implemented during flood events for safety considerations (Placzek and Haeni, 1995).

Ford et al. (1999) also investigated the use of the GPR technique to detect scour at bridge foundations. In most sites, boats were used in order to move the operator and the GPR system over the survey area. The authors concluded that in shallow fresh water the GPR was able to determine the riverbed profile up to a depth of six meters

below the riverbed. GPR technique was also able to determine re-filled from deposited sediment scour holes and measure the maximum scour depth (Ford et al., 1999), but it also required high cost and use of complex equipment.

Mercado and O'Neill (2003) also proposed two methods for the quantification of scour depth at bridge structures. The Parallel Seismic Survey (PSS) method is based on the analysis of the seismic refraction waves that are generated in a drilled shaft and are recorded by hydrophones. The hydrophones were placed in a cased hole that is inserted into the riverbed. The advantage of this method relies on its ability to determine the extent of a soft-clay or loose sand-filled scour zone and the foundation depth of the structure. The Reverse Parallel Seismic Survey (RPSS) method switches the positions of the source and receiver as described in PSS technique (Mercado and O'Neill, 2003). The RPSS method was found capable of detecting scour in a zone filled with mud and of providing the depth of the toe of pile groups. However, both techniques cannot be used during flood events and can only be implemented between major floods.

Sonar instruments

Sonar instruments including fathometers, echo sounders and acoustic depth sounders have also been used to evaluate underwater bed level conditions around bridge piers and abutments (Mueller and Landers, 1999; Lasa et al., 1999; Nassif et al., 2002; Schall and Price, 2004; and Walker and Hughes, 2005). Sonar technology, similar to the one being used to evaluate bridge scour, is also employed for the assessment of scour conditions at marine structures (Browne, 2010). These techniques use the properties of the transmitted and reflected underwater acoustic waves to detect and locate scour holes. However, issues regarding the transducer frequency and debris impact are the major problems for the use of these devices (Schall and Price, 2004). High sediment concentrations or air entrainment has often negative effects on their readings (Hunt, 2009).

Mueller and Landers (1999) evaluated portable systems in order to monitor scour developing a limited and a detailed-data collection system to allow for different types of measurements under different flow conditions. Both systems used a chart recording echo sounder which was able to produce a permanent graphic record of the

streambed. The limited data collection system consisted of a floating knee board which was deployed from the bridge deck and provided velocity, channel geometry and sediment data under the bridge and along the sides of piers and abutments. The detailed data collection system provided velocity and channel geometry data in a wider upstream and downstream the structure area using a digital output echo-sounder attached to an un-manned remote-control boat. Mueller and Landers (1999) concluded that the systems successfully collected data during six major floods. However, these methods cannot be used for continuous real-time monitoring of scour processes.

Lasa et al. (1999) developed a scour monitoring unit using Echo Sounding Technology. The system used a fathometer to measure the distance from a fixed point to the bottom of the riverbed. It was also capable to monitor water temperature, flow velocity and tide elevation. The system was deployed in a scour critical bridge and satisfactorily detected erosion activity near the bridge piers. However, detailed engineering and installation of fixed support for the sensors were considered necessary (Lasa et al., 1999).

A portable scour monitoring device was developed during the NCHRP research program in the US based on existing deployment methods. The outcome of this research was a fully instrumented articulated arm truck (Schall and Price, 2004). This device consisted of a wireless sonar that could be positioned almost 9.1 m below the bridge deck in order to collect underwater data and assess scour conditions at bridge sites. Other methods were also developed using a wireless sonar in a sounding weight and in a kneeboard deployment to allow for monitoring of different bridge geometries (Schall and Price, 2004).

Walker and Hughes (2005) evaluated ultrasonic ranging transducers, mounted upstream and downstream of the bridge pier for scour monitoring at three sites in Wisconsin, US. The authors indicated that this automated method can be deployed to provide real-time monitoring during flood events but its application is limited due to the high cost derived from the installation and operation procedures.

TDR instruments

In an attempt to address the shortcomings associated with the portable instrumentation, several monitoring methods were developed to detect scour with sensors permanently installed around foundation elements. For example, the Time Domain Reflectometry (TDR) (Yankielun and Zabilansky, 1999; and Yu and Yu, 2009) was investigated at piers and abutments. In TDR technology, an electromagnetic pulse is generated and sent through a transmission line which is installed into the riverbed. The measure of scour is based on the reflection time required from the pulse to propagate through the line.

Yankielun and Zabilansky (1999) investigated the use of a TDR system to monitor bed level variations in laboratory environments. The authors concluded that TDR sensor accurately measured scour and sediment transport data and has the potential to provide a continuous monitoring system. However, the major challenges with TDR sensors are related to the high cost, the battery life, the maximum practical probe length, their applicability in conductive mediums and the debris impact (Yankielun and Zabilansky, 1999).

FBG sensors

Fibre Bragg Grating (FBG) sensors were also used as fixed scour monitoring systems and their application has been tested in both laboratory and field environments (Lin et al., 2006; and Huang et al., 2007).

In the FBG method a rod is embedded into the sediment and is instrumented with a number of FBG sensors. Scour activity is identified according to the exhibited strain signal of each sensor when exposed to water flow conditions (Lin et al., 2006). Another approach of the same technique uses a single FBG sensor for transduction of the vibration frequency. The scour depth is detected based on the inverse relationship between the fundamental frequency and the cantilevered length of the rod which increases as scour occurs (Zarafshan et al., 2012). However, for the use of FBG sensors, installation design and improved fabrication techniques are still required to withstand field conditions (Lin et al., 2006).

Lin et al. (2006) investigated the use of FBG sensors for scour detection in the Dadu bridge (Taiwan). The distance between each sensor was one meter while the top

sensor was installed one meter above the riverbed. The signal from the top sensor represented the water flow impact while the signal from the second sensor showed the scour action when the sensor became unburied. It was concluded that the FBG system successfully monitored scour depth, deposition height and water level variation at the bridge site. Lin et al. (2006) also indicated the need for installation procedures and careful design of the sensor, arising from the impact of debris and high velocities that can damage the system.

A new type of Optical FBG sensor was developed and tested in laboratory environment by Huang et al. (2007). The sensor could be anchored in the riverbed or it could be fixed on the pier in order to monitor scour action around the foundation of the structure. The sensors were installed orthogonal to the longitudinal axis into a cantilever beam. The FBG sensor was embedded in Fibre Reinforced Polymer (FRP) to increase the durability of the system and effectively measured scour depth (Huang et al., 2007). However, it was highlighted that the sensor fabrication technique needs to be improved for future field applications.

Traditional and commercially available methods

Other studies evaluated traditional methods at bridge sites using the passive scour chain, the Brisco system (Zabilansky, 1996) and columns of numbered bricks (Lu et al., 2008). Commercially available systems such as the sliding magnetic collar (SMC) and the 'tell-tail' system (May et al., 2002) were also used for monitoring scour conditions at hydraulic structures.

Zabilansky (1996) evaluated traditional methods such as the Brisco system and Passive scour chains. In Brisco system, scour monitoring is achieved by dropping a foot that rests on the bed adjacent to the pier and is able to measure the elevation of the riverbed. The passive scour chain system uses chains that lie on the bottom of the riverbed and are re-buried during deposition process. The scour hole and the amount of deposited soil are defined when the chain is recovered during low water. Erosion and re-deposition actions were monitored using the aforementioned techniques, however many disadvantages exist as these methods cannot provide reliable and real-time monitoring of bed level processes.

A scour monitoring system that can be attached at the nose of the pier was developed by HRL Wallingford (May et al., 2002). The 'tell-tail' system consists of sensors mounted on a vertical rod and buried into the riverbed at different depths. The sensors are activated and oscillate when they are exposed to flow conditions. Data loggers connected with the system can provide continuous monitoring of scour and deposition processes. The main limitations of this system are considered the long-term durability of the sensors and the difficulty to be installed at existing structures.

A Sliding Magnetic Collar (SMC) which measures the downward movement of the magnetic collar around a stainless steel support structure was also tested by Nassif et al. (2002). The results obtained indicated that the SMC successfully monitored scour action at bridge sites. However, the SMC does not detect river re-deposition and is not capable of providing real-time data of scour evolution while other limitations also arise from the debris and ice impact.

Another technique was also tested using a column of numbered bricks that were placed upstream of a bridge in Central Taiwan to provide measurement of general scour (Lu et al., 2008). The top surface of the brick was numbered with white paint and the location of the brick column was accurately measured. After flood events, the position of the column was surveyed to define its accurate position. The deposited sediment was then removed carefully using an excavator. The general scour depth was obtained based on the number of bricks that they were washed away during the flood, however this method cannot provide a real-time monitoring solution.

Physical probes and piezoelectric sensors

Monitoring techniques such as physical probes (Schall and Price, 2004) and piezoelectric film sensors (Lueker et al., 2010) have also been proposed for evaluation of scour at hydraulic structures.

Physical probes refer to devices that extend the reach of an inspector and the most common are physical weights and sounding poles (Schall and Price, 2004). Sounding poles are long poles used to probe the bottom while sounding weight devices use a torpedo-shaped weight suspended by a measurement cable. Physical probes can be deployed from a bridge, a boat or by an engineer diver. This monitoring method in some cases may be effective to measure scour at bridge sites, however its use is limited

by depth and velocity conditions. Moreover, physical probes do not provide continuous monitoring of bed level conditions.

Piezoelectric film sensors have also been used to evaluate scour activity at bridge sites. This type of device uses an array of film sensors which are buried into the riverbed. When the sensor becomes unburied is moved by the flow and exhibits a small current, thus scour and deposition can be detected (Lueker et al., 2010). However, limitations regarding the sensitivity of the sensor were also identified which can lead to false measurements.

Recent research monitoring efforts

Latest research efforts focused on the use of wireless Micro-Electro-Mechanical Systems (MEMS) sensors (Lin et al., 2010), buried orientation sensors (McCane et al., 2011), wireless smart rocks placed around the foundations of structures (Chen et al., 2011 and Chen et al., 2013) and accelerometers (Prendergast et al., 2013).

Lin et al. (2010) conducted laboratory tests using a wireless MEMS sensor network in order to measure the bed and water level variations. The system consists of MEMS pressure sensors mounted on the pier placed in the flume at interval of 10 cm. The sensors were connected to a Zigbee sensor network for real-time measurement of scour. It was concluded that the system detected scour process however it has not been applied yet in the field.

A new system to detect foundation scour was also proposed by McCane et al. (2011) which consists of orientation sensors that are buried into the riverbed around the location of the structure. When scour occurs, the un-buried sensor will float and its position will change from vertical to horizontal. The unit is able to detect this orientation change and to transmit a wireless signal to a receiver unit in order to identify the location of the device (McCane et al., 2011). However, the use of the orientation sensors is limited due to the difficulty to be installed at existing structures. Moreover, the method is not able to provide continuous field data with regards to the evolution of scouring.

Chen et al. (2013) proposed a new method of scour monitoring which uses wireless smart rocks placed around the foundation of the structure serving at the same time as rip-rap protection. This technique involves sensors embedded in rocks or

reinforced concrete blocks (smart rocks). The smart rocks use magneto-inductive and acoustic communications for real-time evaluation of scour conditions. They are placed distributed around the perimeter of a bridge footing and when scour occurs the smart rock will be positioned at the bottom of the scour hole. Another smart rock can be used for reference purposes and placed on the top of the footing with the purpose of collecting and transmitting data regarding changes in the positions of other rocks (Chen et al., 2013). The advantages of this technique are the cost effectiveness, robustness and that it can be deployed easily to structures. The authors also pointed out the challenges that need to overcome arising from the reduction of the signal over distance and the power supply of the sensors embedded in the rock.

Finally, Prendergast et al. (2013) examined the effect of various bed levels on the response of accelerometers using a driven pile in laboratory and 'static' field conditions. 'Static' scour depth was detected based on changes in the natural frequency of the pile, however further research is still required for the real-field application due to complexities that arise from flood conditions in river environment.

2.5 Summary

Scour action causes drastic reduction in the safe capacity and stability of structures. Foundation scour is the leading cause of bridge failures and one of the main climate change impacts on highway and railway infrastructure. Scour hazard in the offshore industry is also associated with different types of structures. From the foundations of offshore wind turbines, the cabling necessary for in-situ transmission and power export to pipelines and seawall structures, scour is considered a challenging issue affecting many types of infrastructure. Unlike the numerous studies that have focused on bridge scour activity the last decades, research efforts and findings regarding offshore scour processes are considered to be at an early stage.

The high economic losses and the severe consequences imposed by scour action at hydraulic and marine infrastructure have been highlighted by numerous reports presented in this chapter. During the recent decades many research efforts concentrated on the development of monitoring techniques to provide a real-time assessment of scour conditions around the foundations of structures. The monitoring of re-deposited soil is also of great importance for the evaluation of underwater conditions to determine actual load bearing characteristics of foundations. However, most of the existing monitoring techniques cannot provide complete data of both scour and sediment deposition processes due to technical and cost issues.

The objective of this work was to develop a new approach for monitoring scour and re-deposited sediment evolution in the vicinity of the foundation structure. This is based on two different devices in the Amplitude Domain (AD), using an off-the-shelf and developing a new prototype sensor that can offer an economical, accurate and robust monitoring solution compared to the existing methods.

References

Arjwech, R., Everett, M.E., Briaud, J.-L., Hurlebaus, S., Medina-Cetina, Z., Tucker, S., and Yousefpour, N. (2013). Electrical resistivity imaging of unknown bridge foundations. *Near Surface Geophysics,* 11(6), pp. 591-598.

Black, K. (2008). Offshore Wind Farm Developments and Scouring Effects. *Hydro International*, [online] Available at: <http://www.hydro-international.com/issues/articles/id972Offshore_Wind_Farm_Developments_and_Scouring_Effects.html> [Accessed 01/03/2011].

Briaud, J.-L. (2011). Bridge Scour and Levee Overtopping. *1ˢᵗ Webinar of International Society for Soil Mechanics and Geotechnical Engineering,* [online] Available at: https://ceprofs.civil.tamu.edu/briaud/Webinar%20Lecture-23Aug2011.pdf [Accessed 23/08/2011].

Briaud, J.-L., Chen, H.-C., Li, Y., Nurtjahyo, P., and Wang J. (2004). *Pier and Contraction Scour in Cohesive Soils*. NCHRP Report 516, Transportation Research Board, National Academy of Science, Washington, D.C.

Browne, T. (2010). Underwater Acoustic Imaging Devices for Portable Scour Monitoring. *Proceedings of the 5th International Conference on Scour and Erosion*, San Francisco, California, US., pp. 931-940.

Byrne, P. (2009). *The destroyed Northside bridge in Workington, Cumbria*. [online], Available at: <http://www.guardian.co.uk> [Accessed 02/07/2011].

Carroll, B., Cooper, B., Dewey, N., Whitehead, P., Dolphin, T., Rees, J., Judd, A., Whitehouse, R., and Harris, J. (2010). *A Further Review of Sediment Monitoring Data*. Cowrie Ltd, London, UK, Report ScourSed-09, pp.1-106.

Chao-Yang, Chan. (2008). *The collapsed Houfeng Bridge connecting Houli and Fengyuan in Taichung County*. [online] Available at: <http://taiwantt.org.tw/taipeitimes/2008/images/09/0916-4.jpg>[Accessed 05/12/2011].

Chen, G., Pommerenke, D. and Zheng R. (2011). Wireless Smart Rocks for Real Time Scour Monitoring. *International Society for Structural Health Monitoring of Intelligent Infrastructure (ISHMII) Monitor Magazine*, [online] Available at: <http://web.mst.edu/~mhszqd/Short%20Writeup%20for%20ISHMII%20Monitor%20Magazine%20on%20Bridge%20Scour%20Monitoring%20-%20October%2025%202011.docx> [Accessed 10/11/2012].

Chen, G., Pommerenke, D., Zhou, Z., Huang, Y., and Radchenko, A. (2013). *Sensors for integrated monitoring and mitigation of erosion*. US Patent 2013/0091939 A1.

CIRIA (Construction Industry Research and Information Association). (2014). *Update of manual on scour at bridges and other hydraulic structures (RP987)*. [online].Available at: http://www.ciria.org/Research/Projects_underway2/scour_at_bridges.aspx [Accessed 10/10/2014].

Defra. (2011). *Climate Resilient Infrastructure: Preparing Infrastructure for a Changing Climate*. UK, London: The Stationery Office Limited.

Defra. (2012). *UK Climate Change Risk Assessment: Government Report*. London: The Stationery Office Limited.

Den Boon, J.H., Sutherland, J., Whitehouse, R., Soulsby, S., Stam, C.J.M., Verhoeven, K., Høgedal, M., Hald, T. (2004). Scour behaviour and scour protection for monopile foundations of offshore windfarms. *European Wind Energy Conference*, London, UK. EWEA, Brussels, Belgium. 14 pp, CD-ROM.

Ettema, R., Constantinescu, G., and Melville, B. (2011). *Evaluation of Bridge Scour Research: Pier Scour Processes and Predictions*. [Online], US Transportation Research Board, Available at: <http://onlinepubs.trb.org/onlinepubs/nchrp/nchrp_w175.pdf>, [Accessed 02 January 2012].

FHWA (Federal Highway Administration). (1991). *Evaluating Scour at Bridges*. Technical advisory T5140.23, US Department of Transportation, Washington, D.C.

Forde, M.C., McCann, D.M., Clark, M.R., Broughton, K. J., Fenning, P. J., and Brown, A. (1999). Radar measurement of bridge scour. *NDT & E International,* 32(8), pp. 481–492.

Gorin, S. R., and Haeni, F. P. (1989). *Use of surface-geophysical methods to assess riverbed scour at bridge piers*. US Geological Survey Water-Resources Investigations Report No. 88-4212, Federal Highway Administration, Hartford, CT.

Highways Agency. (2006). *Design Manual for Roads and Bridges*. Highway structures: Inspection, Maintenance and Assessment, Advice note BA 74/06 [online] Available at: <https://www.gov.uk/standards-for-highways-online-resources> [Accessed 21/05/2011].

Highways Agency. (2009). *Climate Change Adaptation Strategy and Framework.* [online] Available at: <http://assets.highways.gov.uk/>, [Accessed 15/10/2012].

Highways Agency. (2010). *The Highway Agency's Interim Climate Change Risk Assessment*. [online] Available at: <http://assets.highways.gov.uk/>, [Accessed 20/08/2012].

HM Government. (2011). *Climate Resilient Infrastructure: Preparing for a Changing Climate*. London: The Stationery Office Limited.

Huang, L., Wang D., and Zhou Z. (2007). A New Type of Optical FBG-based Scour Monitoring sensor. *Pacific Science Review*, 9(1), pp. 101-109.

Hunt, B.E. (2009). *Monitoring scour critical bridges*. NCHRP synthesis 396, Transportation Research Board, Washington, DC.

Iarnród Éireann. (2009). Infrastructure Structures Standard – Structural Inspections Standard. *I-STR- 6510 Issue 3.0*, Iarnród Éireann, Dublin, Ireland.

Imhof, D. (2011). Bridge Collapse Database. [Online] Available at: <http://bridgeforum.org> [Accessed 20 July 2011].

Jongman, B., Hochrainer-Stigler, S., Feyen, L., Aerts, J.C.J.H., Mechler, R., Botzen, W.J.W., Bouwer, L.M., Pflug, G., Rojas, R., and Ward, P.J. (2014). Increasing stress on disaster risk finance due to large floods. *Nature Climate Change*, 4, pp. 264–268.

Kattell, J., and Eriksson, M. (1998). *Bridge Scour Evaluation: Screening, Analysis, & Countermeasures*. US Department of Agriculture Forest Service. San Dimas, California.

Lagasse, P.F., and Richardson, V.E. (2001). ASCE Compendium of Stream Stability and Bridge Scour Papers. *Journal of Hydraulic Engineering,* 127(7), pp. 531-533.

Lagasse, P.F., Clopper, P.E., Pagan-Ortiz, J.E., Zevenbergen, L.W., Arneson, L.A., Schall, J.D., Girard. L.D. (2009). *Bridge Scour and Stream Instabil-ity Countermeasures: Experience, Selection and Design Guidance*. Hydraulic Engineering Circular No. 23, Third Edition. Vol. 1. FHWA NHI-09-112, Federal Highway Administration, Washington, D.C.

Lagasse, P.F., Schall, J.D., Johnson, F., Richardson, E. V. and Chang, F. (1995). *Stream Stability at Highway Structures*. Hydraulic Engineering Circular No.20 Second Edition, Federal Highway Administration Publication No. FHWA-IP-90-014, Turner-Fairbank Highway Research Center, McLean, VA, pp. 1-204.

Landers, N.M. (1992). Bridge Scour Data Management. *Hydraulic Engineering: Saving a Threatened Resource - In Search of Solutions: Proceedings of the Hydraulic Engineering sessions at Water Forum*, American Society of Civil Engineers, Baltimore, Maryland, pp. 1094-1099.

Lasa, I.R., Hayes, G.H., and Parker, E.T. (1999). Remote Monitoring of Bridge Scour Using Echo Sounding Technology, TRB Transportation Research Board Circular 498, *Proceedings of the 8th International Bridge Management Conference*, Vol. 1, Denver, Colorado, pp. 1-9.

Lin, Y.B., Lai, J.S., Chang, K.C., and Li, L.S. (2006). Flood scour monitoring system using fibre bragg grating sensors. *Smart Material and Struct*ures, 15(6), pp. 1950–1959.

Lin, Y.B., Lai, J.S., Chang, K.C., Chang, W.Y., Lee, F.Z., and Tan, Y.C. (2010). Using mems sensors in the bridge scour monitoring system. *Journal of the Chinese Institute of Engineers,* 33(1), pp. 25-35.

Lu, J., Hong, J., Su, C., Wang, C., and Lai, J. (2008). Field Measurements and Simulation of Bridge Scour Depth Variations during Floods. *Journal of Hydraulic Engineering*, 134(6), pp. 810–821.

Lueker, M., Marr, J., Ellis, C., Winsted, V., and Akula S.R. (2010). *Bridge Scour Monitoring Technologies: Development of Evaluation and Selection Protocols for Application on River Bridges in Minnesota*. Publication MN/RC 2010-14, Minnesota Department of Transportation, St. Paul, Minnesota.

May, R.W.P., Ackers, J.C., and Kirby, A.M. (2002). *Manual of Scour at Bridges and Other Hydraulic Structures*. Construction Industry Research and Information Association (CIRIA) C551, London, UK.

McCane, K., Hawrylak, P., J., and Mickle, M., H. (2011). *Sensor and System to Detect Bridge Scour*. US Patent 2011/0012728 A1.

Melville, B.W. and Coleman, S.E. (2000). *Bridge scour*. Colorado: Water Resources Publications.

Mercado, E.J., and O'Neill, M.W. (2003). Methods to Measure Scour Depth and the Depth of Unknown Foundations. *Proceedings of the 3rd International Conference on Applied Geophysics*, Orlando, Florida, US.

Michalis, P., Saafi, M., and Judd, D.M. (2013). Capacitive Sensors for Offshore Scour Monitoring. *Proceedings of the ICE – Energy*, 166(4), pp. 189–196.

Mueller, D.S., and Landers N.M. (1999). *Portable Instrumentation for Real-time Measurement of Scour at Bridges*. Federal Highway Administration Report FHWA-RD-99-085, McLean, VA.

Musial, W., Butterfield, S., and Ram, B. (2006). Energy from offshore wind. *Proceedings of the 2006 Offshore Technology Conference*, Houston, Texas. [online] Available at: <http://www.nrel.gov/docs/fy06osti/39450.pdf> [Accessed 15/02/2012].

Nassif, H., Ertekin, A.O., and Davis, J. (2002). *Evaluation of bridge scour monitoring methods*. US Department of Transportation, Federal Highway Administration, Trenton.

Placzek, G., and Haeni, F.P. (1995). *Surface-geophysical techniques used to detect existing and infilled scour holes near bridge piers*. Water Resources Investigations Report 95-4009, US Geological Survey, Storrs, CT.

Prendergast, L.J., Hester, D., Gavin, K., and O'Sullivan, J.J. (2013). An investigation of the changes in the natural frequency of a pile affected by scour. *Journal of Sound and Vibration*, 332(25), pp. 6685-6702.

RSSB (Rail Safety and Standards Board). (2004). *Impact of scour and flood risk on railway structures*. Rail Safety & Standards Board Infrastructure Integrity Research Project Number T112, London.

RSSB (Rail Safety and Standards Board). (2005). *Safe Management of Railway Structures Flooding & Scour Risk*. Rail Safety & Standards Board Research Programme Engineering, London.

RAIU (Railway Accident Investigation Unit). (2010). *Investigation Report No. R2010 – 004: Malahide Viaduct Collapse on the Dublin to Belfast Line, on the 21st August 2009*. [online] Available at: <http://www.raiu.ie>, [Accessed 05/05/2011].

Richardson, E.V., and Davis, S.R. (1995). *Evaluating Scour at Bridges*. FHWA-IP-90-017: Hydraulic Engineering Circular No. 18, 3rd Ed., US Department of Transportation, Washington, D.C.

Richardson, E.V., and Davis, S.R. (2001). *Evaluating scour at bridges*. FHWA NHI 01-001: Hydraulic Engineering Circular No. 18, 4th Ed., US Department of Transportation, Washington, D.C.

Richardson, E.V., Harrison, L.J., Richardson, J.R., and Davis, S.R. (1993). *Evaluating scour at bridges.* Hydraulic Engineering Circular No. 18 2nd Ed., Publication FHWA-IP-90-017, Federal Highway Administration, US.

Royal Academy of Engineering (2011). Infrastructure, engineering and climate change adaptation: ensuring services in an uncertain future. [online] Available at: <http://www.raeng.org.uk/publications/reports/engineering-the-future> [Accessed 03/09/2012].

Schall, J.D., and Price, G.R. (2004). *Portable Scour Monitoring Equipment*. NCHRP Report 515, Transportation Research Board, Washington, DC.

Stahlmann, A., and Schlurmann, T. (2011). Physical Modeling of scour around tripod foundation structures for offshore wind energy converters. *Coastal Engineering Proceedings* (Smith, M.J., and Lynnet, P. (eds)). ASCE, North America, Reston, VA, USA.

Stearns, M., and Padgett, J. (2012). Impact of 2008 Hurricane Ike on Bridge Infrastructure in the Houston/Galveston Region. *Journal of Performance of Constructed Facilities*, 26(4), pp. 441–452.

Transport Committee. (2010). *The impact of flooding on bridges and other transport infrastructure in Cumbria* [pdf], The Stationary Office, Available at: <http://www.publications.parliament.uk/pa/cm200910/cmselect/cmtran/473/473.pdf> [Accessed 04 March 2011].

UK Bridges Board. (2009). *Background Briefing on Highway Bridges* [pdf]. UK Bridges Board. Available at: <www.ukroadsliaisongroup.org> [Accessed 15 May 2011].

UMKC (University of Missouri Kansas City), (n.d). *Scoured Bridge Systems Performance Assessment* [online] Available at: <http://laser.umkc.edu/~chen/tmp/remote-sensing-1/Schoharie_Creek_brdige_AP_press.jpg> [12/03/2011].

Walker, J.F., and Hughes, P.E. (2005). *Bridge scour monitoring at three sites in Wisconsin.* US Geological Survey Open-File Report 2005-1374.

Whitehouse, R.J.S. (1998). *Scour at Marine Structures*. Thomas Telford, London, UK.

Whitehouse, R.J.S., Sutherland, J., and O'Brien, D. (2006). Seabed scour assessment for offshore wind farm. *Proceedings of the 3rd International Conference on Scour and Erosion*, CURNET, Gouda, The Netherlands [online] Available at: <http://eprints. hrwallingford.co.uk/58> [Accessed 05/03/2012].

Yankielun, N., and Zabilansky, L. (1999). Laboratory Investigation of Time-Domain Reflectometry System for Monitoring Bridge Scour. *Journal of Hydraulic Engineering,* 125(12), pp. 1279–1284.

Yu, X., and Yu, X. (2009). Time Domain Reflectometry Automatic Bridge Scour Measurement System: Principles and Potentials. *Structural Health Monitoring*, 8(6), pp. 463-476.

Zaaijer, M.B., and van der Tempel, J. (2004). Scour protection: a necessity or a waste of money?. *Proceedings of the 43rd IEA Topical Expert Meeting - Critical Issues regarding Offshore Technology and Deployment, Skaerbaek, Denmark.* FOI, Stockholm, Sweden, pp. 43–51.

Zabilansky, L. (1996). Ice force and scour instrumentation for the White River, Vermont. *Special Report 96-6*, US Army Cold Regions Research and Engineering Laboratory, Hanover, NH.

Zarafshan, A., Iranmanesh, A., and Ansari, F. (2012). Vibration-Based Method and Sensor for Monitoring of Bridge Scour. *Journal of Bridge Engineering,* 17(6), pp. 829–838.

Chapter 3

Characterisation of a New ADR Sensor for Remote Monitoring of Re-deposited Sediment Processes

3.1 Introduction

This chapter introduces a new monitoring concept aimed to measure scour and re-deposited sediment depth variations in the vicinity of the foundation and to underpin systems for early warning of impending structural failure. An off-the-shelf sensor is used that employs the Amplitude Domain Reflectometry (ADR) technique which appears to have been proposed for the first time for measuring bed level variations at bridges and offshore wind turbine foundations. A novel methodology is also developed and presented in this study that enables discrimination between in-situ and re-deposited soil delivering critical information about the actual bearing load capacity of the foundation. The proposed sensor should deliver a more economical and attractive solution compared to other scour instruments as it can easily be incorporated to existing monitoring platforms to provide real-time remote surveillance.

This study initially introduces the monitoring concept and the operating principle of the ADR sensor. The integration of the sensor to a conceptual monitoring system and the protocols for remote monitoring are presented. A series of experimental procedures are carried out to quantify the sensor capability to measure scour and sedimentation processes. Feasibility tests are conducted to evaluate the sensor response in various bed level conditions using different soil types, temperature and salinity conditions commonly found in offshore environment. The calibration of the instrument is then evaluated and its limitations are identified. 'Static' scour experiments aimed to validate the sensor response in various environmental conditions. A novel model to obtain soil density information based on the sensor signals is also developed and presented. The capability of the sensor to measure in real-time scour depth variation and to differentiate between pre-scour and post-sediment deposition conditions is also validated in a representative offshore environment using the open channel flume. Finally, the main conclusions of the chapter are presented.

3.2 Monitoring concept

3.2.1 Soil dielectric properties

Several methods across a wide range of disciplines have employed the electromagnetic properties of materials to determine the moisture content of products that contain water. The major advantage of the electromagnetic measurements in soil samples originates from the sensitivity of the soil dielectric permittivity to its water content. This is due to the large difference between the permittivity value of water ($\varepsilon_w \approx 80$) when compared to dry solid particles ($\varepsilon_s = 3 \div 5$) and air ($\varepsilon_a \approx 1$). In the following text, the term 'permittivity' will refer to the dimensionless 'relative permittivity' (ε_r) unless otherwise stated.

In general, the permittivity is a frequency and temperature dependent complex variable, which describes the ability of a material to polarise when subjected to an alternating electric field. The complex permittivity is composed of the real part (ε_r'), which is a measure of the polarization property of a material, and the imaginary part (ε_r''), that represents the energy dissipation by polarization and ionic conduction losses. The apparent permittivity (ε_m) of a soil mixture is a function of the permittivity of the air, soil and water components and their volume fractions (Whalley et al., 1992). A three phase mixing model to describe a wet soil sample was also proposed by Roth et al. (1990):

$$\varepsilon_m^\alpha = \theta \times \varepsilon_w^\alpha + (1-\eta) \times \varepsilon_s^\alpha + (\eta - \theta) \times \varepsilon_a^\alpha \qquad \text{(eq. 3.1)}$$

where θ is the volumetric water content, η is the porosity of soil, 1-η and η-θ are the volume fractions that correspond to solid and air phases respectively. Several theoretical and experimental studies have been performed in order to determine the factor α, which describes the orientation of the electric field with respect to the geometry of the medium. The dimensionless factor α can theoretically range from $\alpha = +1$ for an electric field parallel to soil layers, and $\alpha = -1$ for an electric field perpendicular to soil layers. Birchak et al. (1974) found $\alpha = 0.50$ for an isotropic two-phase medium while Dobson et al. (1985) using a four phase model estimated $\alpha = 0.65$ by regression of data obtained from various soil types tested in different frequencies.

Roth et al. (1990) inferred from experiments $\alpha = 0.46$ by a weighted non-linear regression using a three phase mixing model (see equation 3.1) at thirteen soil samples.

For the case of a saturated soil sample ($\eta = \theta$), equation 3.1 reduces to a two phase mixing model:

$$\varepsilon_m^\alpha = \eta \times \varepsilon_w^\alpha + (1-\eta) \times \varepsilon_s^\alpha \qquad \text{(eq. 3.2)}$$

and can be used to infer the porosity η from the measurement of the soil permittivity (ε_m), once the parameter α is calibrated and the permittivity of the solids (ε_s) calibrated in dry soil or estimated:

$$\eta = \frac{\varepsilon_m^\alpha - \varepsilon_s^\alpha}{\varepsilon_w^\alpha - \varepsilon_s^\alpha} \qquad \text{(eq. 3.3)}$$

In turn, the porosity can be used to calculate the dry density of a soil sample based on the soil specific gravity (G_s) as follows:

$$\rho_d = (1-\eta) \times G_s \qquad \text{(eq. 3.4)}$$

When the permittivity becomes equal to the permittivity of water ($\varepsilon_m = \varepsilon_w$) then the porosity is calculated equal to 1 ($\eta = 1$) which corresponds to fully scoured conditions.

3.2.2 Scour probe operating principle

The large contrast in permittivity associated with water and soil having different densities is used to detect scour and sediment deposition processes around the bridge foundations. Figure 3.1 (a) presents an example of the permittivity values calculated from equation 3.2 assuming that $\alpha = 0.50$, $\varepsilon_s = 4$, and $\varepsilon_w = 80$. Let us also assume that the porosity of saturated soil forming the river bed varies in the range between 0.40 and 0.50. This results in permittivity values ranging from 23 to 30 [see Figure 3.1 (a)]. When the saturated soil is fully substituted by water, the porosity will become equal to 1 and the obtained permittivity will reach the value of 80. When soil is deposited and the scour hole is re-filled, the porosity of the soil will decrease. For example, porosity in the range from 0.5 to 0.6 will result in permittivity in the range 30-38. As depicted in Figure 3.1 (a), different permittivity values will correspond to pre-scour and post-scour conditions.

The probe is composed of a dielectric rod with multiple sensors along its length that is inserted into an access tube. Each sensor is formed by two electrodes which transmit an electromagnetic field that penetrates the external surrounding medium [see Figure 3.1 (b)]. Since the geometric characteristics of the instrument remain constant, the sensor output only depends on the dielectric properties of the sediment. The aforementioned principle is employed to develop a scour monitoring solution with wireless data transmission.
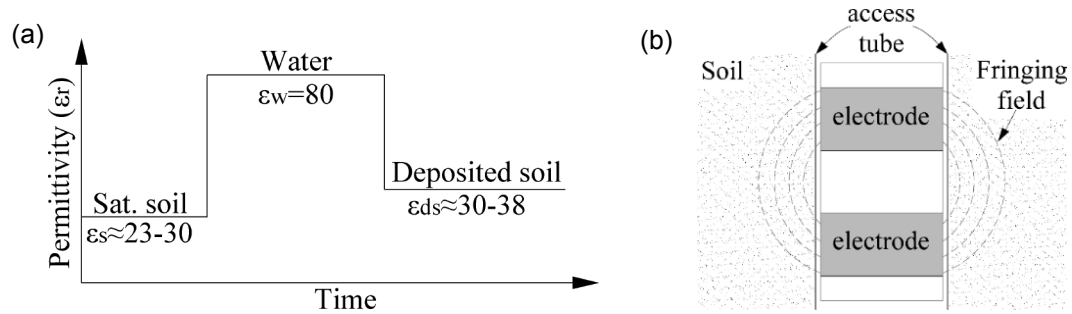
Figure 3.1: (a) Permittivity values obtained in various porosity conditions and **(b)** electromagnetic field generated between 2 electrodes penetrating the medium.

A Profile Probe PR2 (Delta-T Devices Ltd) is proposed for scour and sedimentation monitoring interfaced with an off-the shelf wireless device, as shown in Figure 3.2. The probe is composed of a 25 mm diameter hollow shaft equipped with several electromagnetic sensors placed along its length. The complete assembly is then inserted into a fibre glass access tube to protect it from water ingress.
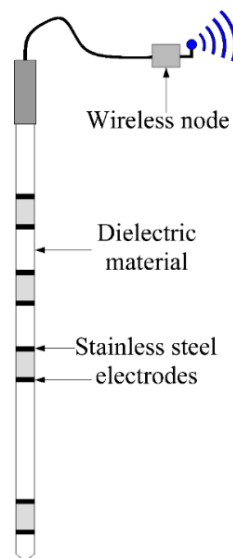
Figure 3.2: Small-scale off-the-shelf probe equipped with wireless interface.

The two stainless steel rings form the plates of a capacitor in an RLC circuit consisting of Resistive (R), Inductive (L) and Capacitive (C) elements, as shown in

Figure 3.3. The PR2 probe measuring principle is based on Amplitude Domain Reflectometry (ADR) method with the complex impedance mainly represented by the sediment or water-filled capacitor (Delta-T Devices Ltd, 2006). The signal detector is positioned between the signal source and the complex impedance.
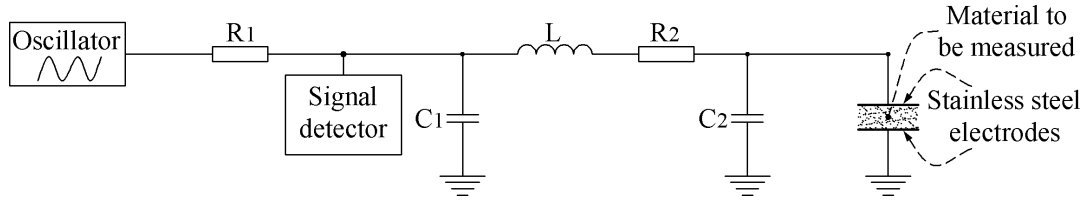
Figure 3.3: Sensing electronics placed at each sensor location (after Delta-T Devices Ltd, 2006).

The amplitude output of each sensor is based on the ratio of the incident signal that is generated by the oscillator and the reflected signal that is resulting from the impedance mismatch and is dependant of the medium permittivity. A 6th order polynomial is proposed by the manufacturer to relate the refractive index ($\sqrt{\varepsilon_r}$) of a soil sample to the voltage output of the sensor, as follows (Delta-T Devices Ltd, 2008):

$$\sqrt{\varepsilon_r} = 1.125 - 5.53 \times V + 67.17 \times V^2 - 234.42 \times V^3 + 413.56 \times V^4 - 356.68 \times V^5 + 121.53 \times V^6 \text{ (eq. 3.5)}$$

The sensor voltage can be therefore be used in order to infer the permittivity of the medium and provide an indication of underwater bed level processes.

The sensor and associated signal detector circuits are located in the shaft and near the sensor location to reduce interference and enhance the signal-to-noise ratio. The sensors are designed to operate with an input current of 20 mA and at the frequency of 100 MHz, generated by an oscillator. This frequency range is used to reduce the effect of the conductance of the medium and increase sensitivity to soil permittivity (Delta-T Devices Ltd, 2006).

The scour probe was interfaced with a low power AdvanticSys CM 5000 wireless sensor node (82 mm x 33 mm x 7 mm). The CM 5000 is equipped with an IEEE 802.15.4 compatible transceiver (CC2420) with maximum data rate of 250 kbps and a 16-bit MSP430F1611 microcontroller (see Figure 3.4). The microcontroller has an 8-channel and 12-bit Analogue-to-Digital Converter (ADC); the four sensor outputs are each attached to one channel leaving four channels spare for future use or for a longer probe with additional sensors. The device has an on-board antenna that provides a range of 35 m in free space.
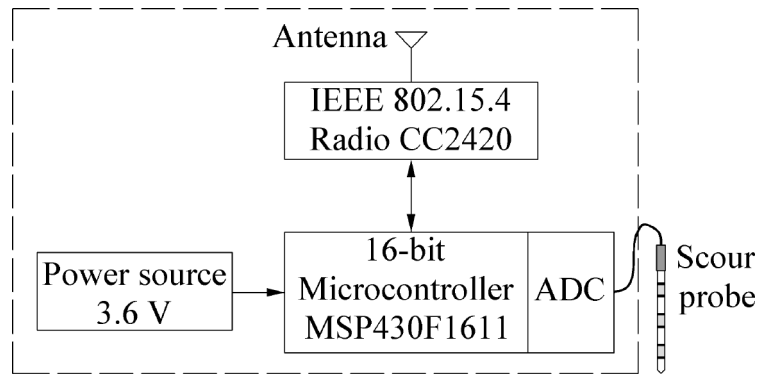
Figure 3.4: Wireless node components.

The wireless scour probe transmits readings at a configurable interval to an identical device connected to a laptop that acts as a base station. The complete probe assembly and the base station are shown in Figure 3.5.
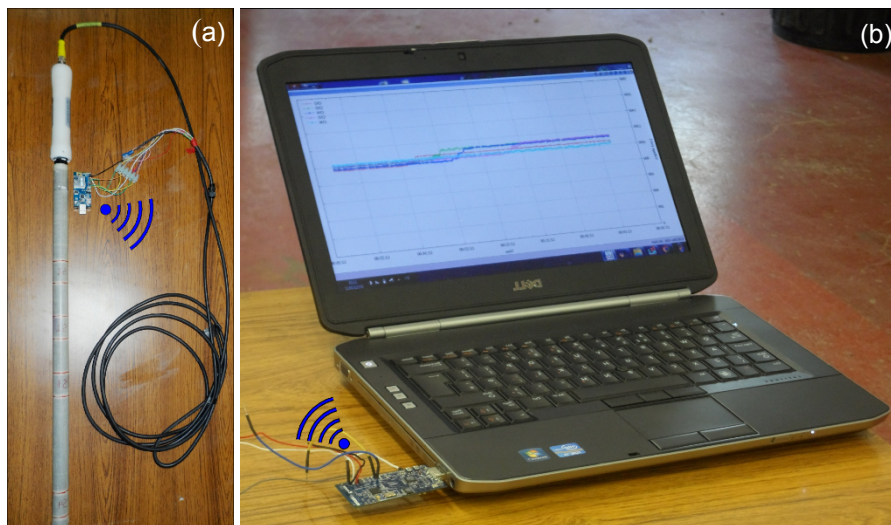
Figure 3.5: (a) Wireless probe used in the experimental scour tests and **(b)** real-time wireless data transmission to the base station.

3.2.3 Monitoring implementation

The concept of this scour monitoring solution is illustrated in Figure 3.6 where two probes are installed adjacent to a bridge pier. Each probe can be equipped with several sensors (in this example S1 to S6) placed at predetermined locations. In the example shown in Figure 3.6, sensor S1 is kept in the water above the bed level for reference purposes while the sensors S2 to S6 are embedded into the sediment next to the foundation structure. Figure 3.6 also shows the typical sensor responses expected when scour and sediment deposition conditions occur.

The sensor submerged in water (S1) is expected to experience higher permittivity and hence show a greater voltage when compared to the sensors that are embedded into the sediment. As scour occurs the composition of the material between the electrode rings is altered due to a change of the permittivity, which impacts the energy stored in the sensor capacitance. The output of the sensors S2, S3, and S4 is increased when the sediment surrounding the sensors is eroded and replaced by water. Sensors S5 and S6 are not affected by scour action and their signals remain constant. The amplitude change is an indication of erosion process around the bridge pier at a depth equal or greater than the location of S4, whose position gives an indication of the minimum scour depth. As depicted in Figure 3.6, during the sediment deposition process the scour hole is expected to be partially re-filled. Similarly to the conditions that corresponded to scouring, the sensors S1, S2 which are exposed to water, are anticipated to exhibit higher output due to water permittivity conditions. After deposition, the signals of S3 and S4 are anticipated to settle to values close to S5 and S6. In this scenario, the locations of the sensors S2 and S4 define the minimum range of sediment deposition depth.
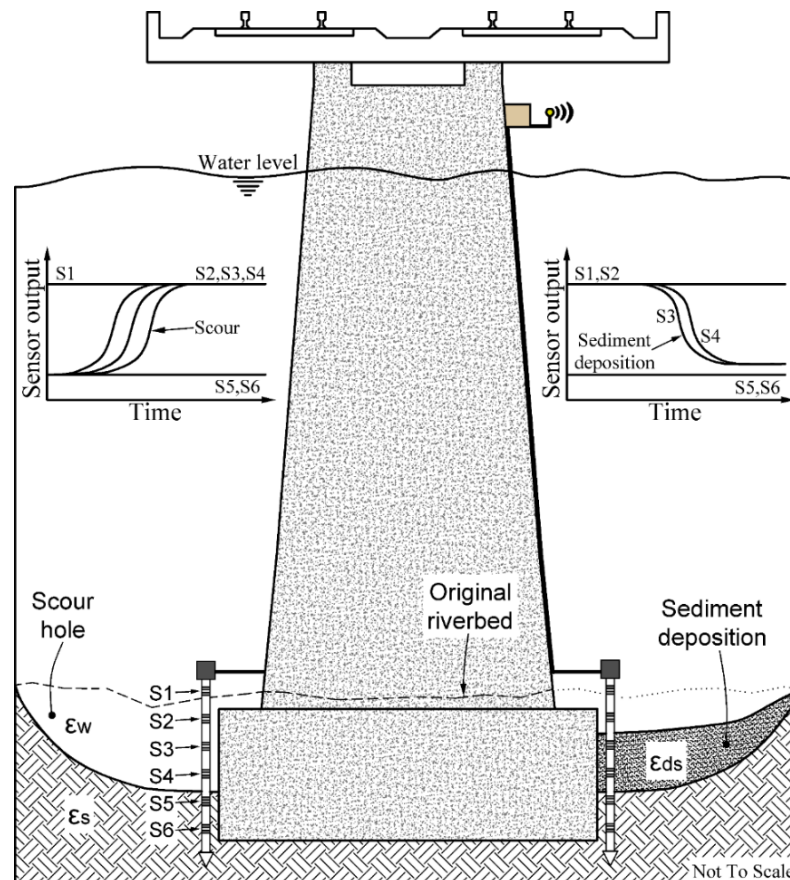
Figure 3.6: Anticipated amplitude response of the sensors during scour and sedimentation processes.

3.2.4 Conceptual monitoring system

The proposed monitoring system consists of probes installed at different locations around the foundation structure, in order to measure the scour depth variation and sediment deposition processes. As presented in Figures 3.7 and 3.8, the scour probe is driven into the river/sea bed and is completely submerged at a certain distance for the water surface so that is protected from the debris impact. The scour sensors transmit the obtained information via communication cable or an ultrasonic wireless network at pre-determined schedules or through a trigger mode when scour is detected. Processed data are transmitted to the Wireless Data Acquisition System (WDAS), which is attached to the structure.

The monitoring system could be powered by a rechargeable battery, which can be replenished from a solar panel or a small wind turbine installed at the structure for power harvesting (see Figure 3.7). The WDAS contains a memory for data storage; a transmitter/receiver antenna for remote data retrieval; a programmable timer unit for scheduled communication with a remote monitoring data collection system; and a trigger unit for emergency data retrieval when bed level variation is detected.
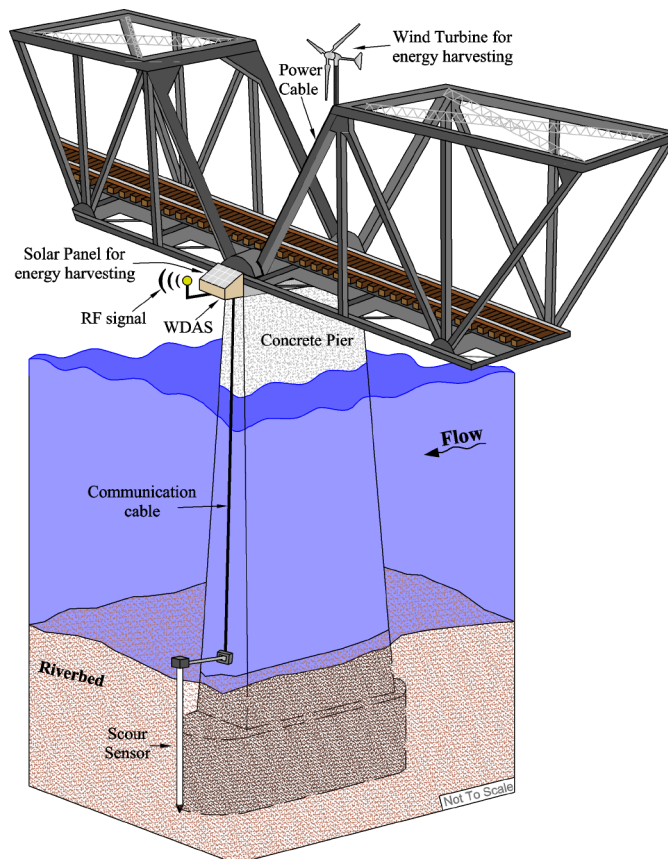
Figure 3.7: Conceptual remote monitoring system installed at a railway bridge pier.
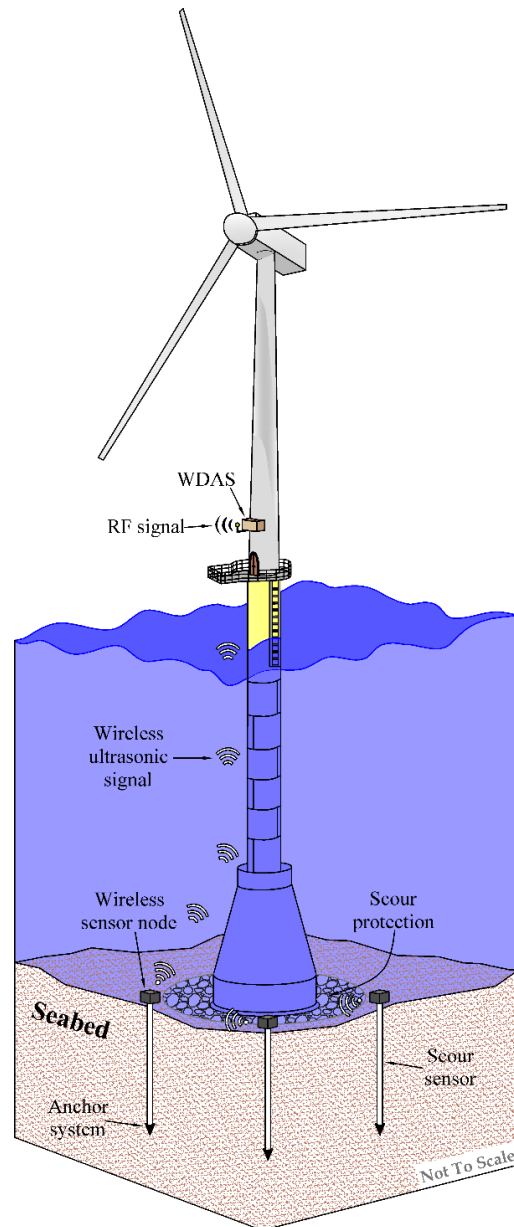
Figure 3.8: Conceptual monitoring system installed around an offshore wind turbine foundation.

3.2.5 Remote monitoring protocols

Surveillance and monitoring will be achieved through the protocols shown in Figures 3.9 and 3.10. When a probe detects scour or deposition action, signals are transmitted to the WDAS. The signal carries the sensor's identification location and the change in the operating amplitude of the sensor, where the scour is occurring. Immediately after, the WDAS sends a signal through a phone-bridge interaction process to the engineer in the form of SMS or email. The WDAS also transmits a warning signal through the train-bridge interaction process, allowing for precautionary action when a train is

approaching the structure (see Figure 3.9). On-site monitoring takes place through a human-bridge interaction mechanism where a bridge engineer equipped with a hand-held interrogation system will communicate with the WDAS and wirelessly download the data for analysis. The data are also remotely collected via internet and stored in a database for analysis and decision-making. The remote collection process is conducted through an inquiry-based scheme after a predetermined scheduling strategy.
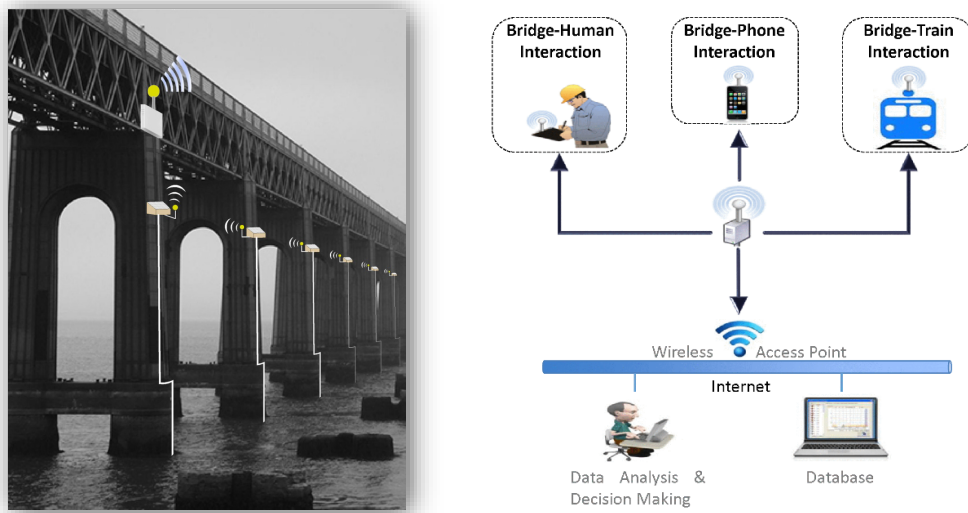
Figure 3.9: Protocols for remote surveillance and monitoring of bridge scour.

Figure 3.10 shows the protocols for offshore wind farm monitoring. The structures interact with each other forming a wireless sensor network in which selected turbines act as master nodes transmitting the information to a remote location through a radio link. Other wind turbines will relay their data to the nearest master nodes, to limit communications bandwidth and increase transmission energy efficiency.
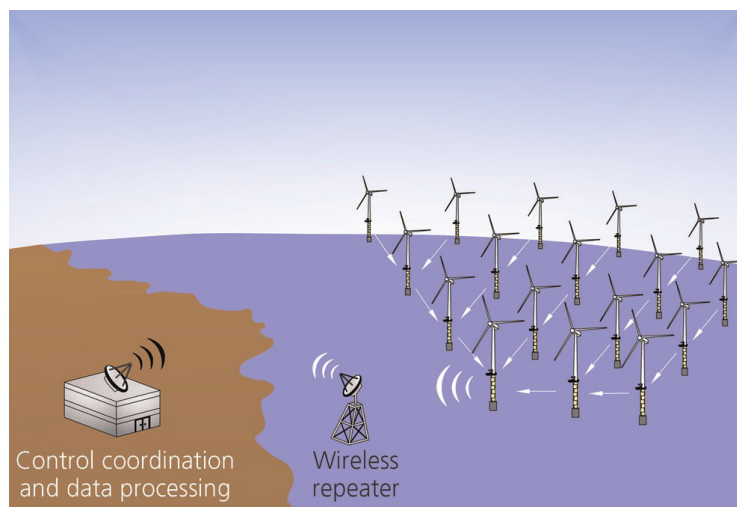
Figure 3.10: Concept for remote surveillance and monitoring of offshore wind farm.

As depicted in Figure 3.10, wireless repeaters placed at certain locations between the site and the control coordination room will ensure the quality of the transmitting data and will increase the wireless transferring distance to the control coordination room for condition monitoring and data processing. Other communications technologies including satellite and cellular services could also be implemented for real-time monitoring.

3.3 Experimental procedures

3.3.1 Feasibility study on the use of dielectric sensor to monitor scour and re-deposition under different environmental conditions

The probe was inserted at the centre of a clear acrylic cylindrical tank with diameter and height of 500 mm. The sensor close to the probe tip was placed at a distance of 3 cm above the tank base and covered by a soil layer, while the second sensor from the tip remained submerged in water for reference purposes. The small-scale probe was tested in saturated un-compacted soil conditions and at different water temperatures of 2 °C, 11 °C and 21 °C using fresh and saline water of 35 parts per thousand (ppt) of NaCl respectively. The tested materials consisted of gravel, sand, fine sand and a mixture of silt-clay sediments (see Figure 3.11).
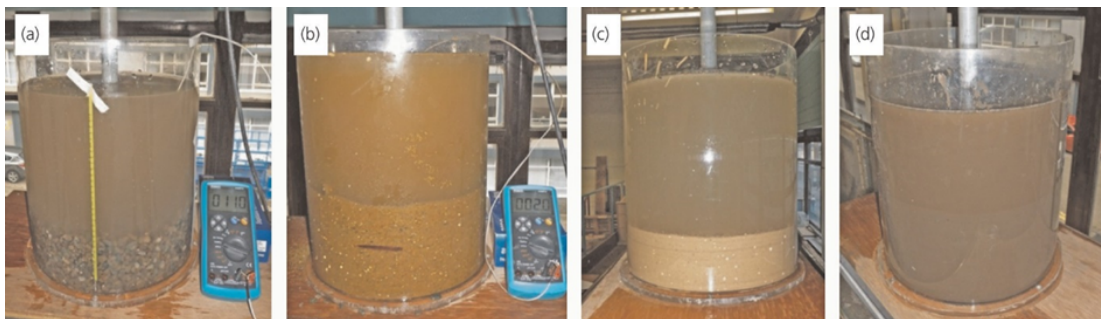
Figure 3.11: Simulations of scour and sediment deposition processes under different environmental conditions; evaluation of the sensor in **(a)** gravel soil type using saline water at a temperature of 11 °C; in **(b)** sand soil type using saline water at a temperature of 2 °C; in **(c)** fine sand soil type using saline water and in **(d)** silt-clay soil type using saline water.

The potential effect of long-term bed degradation on the sensor response was evaluated as follows. The tank was filled with fresh and saline water each time and the materials were added progressively in quantities of 600 g at 1 min intervals, until the embedded sensor was fully covered by soil. The readings started to be recorded when

the sensor amplitude was altered and each step of the soil mass added in the tank was calculated as % soil total weight.

The ability of the sensor to detect scour and sedimentation processes was also preliminary investigated. In this test, the probe was placed in the tank and covered with a soil layer. In turn, the soil layer was submerged with water so that the one sensor was embedded in the sediment and the second sensor remained submerged in fresh or saline water respectively. Sediment was first removed manually around the embedded sensor in order to simulate the scour process. Deposition was then simulated by adding 150 g of sediment at intervals of 30 sec to fill the scour hole. The aforementioned simulations were repeated for each soil type, different water and temperature conditions. The real-time response of the probe during the tests was recorded by a data logger (model: DL2e, Delta-T Devices Ltd).

3.3.2 Sensor calibration and sensitivity to water salinity and temperature

The response of the ADR probe and the calibration curve scaling the electrical signal to permittivity were initially evaluated by submerging the probe in solvents with known permittivity. The tests were performed with the probe placed at the centre of a clear acrylic cylindrical tank, with diameter and height of 300 and 600 mm respectively (see Figure 3.12).
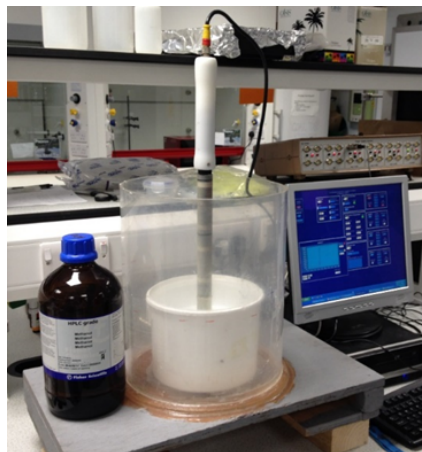
Figure 3.12: Evaluation of the probe in various solvents.

One sensor was immersed during each experiment and data recorded for the period of ten minutes with an average frequency of four readings per second, using the National Instrument data acquisition system (NI cDAQ-9178) interfaced to a computer via LabView programme. The sensor output was recorded in air ($\varepsilon_r = 1.00$) and fresh

water (ε_r = 78.54) conditions and then in various solvents with known dielectric constant values (Maryott and Smith, 1951) that consisted of acetic acid (ε_r = 6.15), acetone (ε_r = 20.70) and methanol (ε_r = 33.62).

Preliminary experiments revealed temperature and salinity effects on the signals of a sensor that was embedded into various sediment types (Michalis et al., 2013). Consequently, another set of experiments was carried out to investigate the sensor response in saline water environment at a temperature of 18 °C. Different salinity solutions were prepared by dissolving in fresh water for each test 0.085 moles (mol) NaCl per litre (L), 0.256 mol NaCl/L, 0.427 mol NaCl/L and 0.598 mol NaCl/L that corresponded to 5 ppt, 15 ppt, 25 ppt and 35 ppt of NaCl respectively. The temperature influence on submerged sensor response was also evaluated and reported herein using fresh water and saline water of 35 ppt at temperatures of 2 °C, 11 °C and 21 °C.

3.3.3 Calibration of the soil mixing model

The soil density influence on the probe output is of main importance in this study, as it will be used as a tool to differentiate between the pre-scour (in-situ saturated soil) and post-scour (deposited sediment) conditions. To assess the probe response to density changes one sensor was subjected to a series of experiments in soil samples with various density values. The aforementioned tank was used with the probe placed in the centre and one sensor at a distance of 3 cm from the tank base (see Figure 3.13).
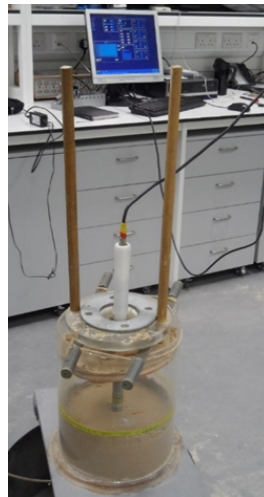
Figure 3.13: Experimental set up for soil density tests.

The sample consisted of medium sand with D_{50} of 0.375 mm and specific gravity of 2.83 that was experimentally determined according to the ASTM D 854-00

standard. The medium sand was first dried in a thermostatically controlled oven at the temperature of 110 $^{\circ}$C. The dry sample was weighed and then water was sprayed on the surface of a soil layer and mixed with the sediment in order to attain a target gravimetric moisture content of 10 %. A portion of the sample was also placed in the oven before each experiment in order to determine the actual achieved soil moisture content according to ASTM D2216 standard.

The wet sediment was then carefully positioned in layers into the tank and the sensor measurements were recorded. To compact the soil to various target densities, a plywood disk of 290 mm diameter was placed at the top of the sediment to allow distributing the force generated by a hammer dropped on the disk to compact the soil. The hammer consisted of a metal disk attached to Perspex acrylic with weight of 3016 g. Two wooden handles were fixed in the hammer that was dropped from a distance of 25 cm for 5, 15 and 25 blows in each experiment. The apparent permittivity for the different soil density conditions was measured from the sensor response using equation 3.5 and was then used to calibrate the parameter α in equation 3.3.

3.3.4 'Static' scour tests

The probe was subjected to a series of 'static' scour simulations in various water conditions using three different soil types. Figure 3.14 (a) shows the experimental setup used to quantify the effect of scour on the probe response. The probe was inserted at the centre of a clear acrylic cylindrical tank with diameter and height of 250 mm and 450 mm respectively [see Figure 3.14 (b)].
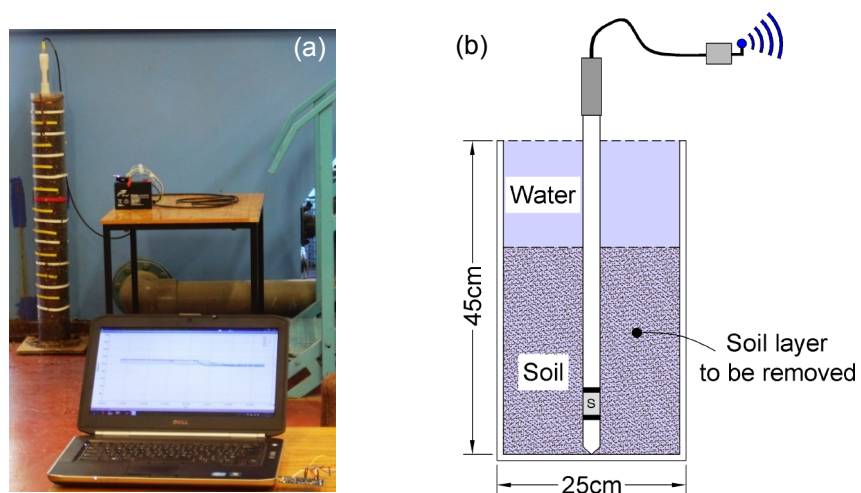
Figure 3.14: (a) Experimental setup and **(b)** sensor position during 'static' scour tests.

The tested soil types consisted of medium gravel, coarse sand and medium sand with median grain sizes D_{50} of 10 mm, 1.05 mm and 0.375 mm respectively. The probe was placed in the tank which was filled with water and then with un-compacted material. After recording the sensor response, the layer of sediment was removed around the embedded probe in order to mimic the scour process. The tests were performed for each soil type using fresh and saline water of 35 ppt at the temperature of 11 °C. The purpose of those experiments was to assess the effect of pore water salinity on the sensor output. Based on the soil porosity values estimated from equation 3.3 in fresh water, the tests in saline water also focused on the comparison between the measured and predicted by equation 3.2 permittivity values using the parameter α obtained from the previous calibration.

3.3.5 Flume experimental set up

Real-time scour experiments were conducted in the unidirectional current flume of the hydraulics laboratory located at the University of Strathclyde, Glasgow. The flume (see Figure 3.15) has bottom and sidewalls made of plexiglas supported by a metal frame with a rectangular cross-section of 0.90 m (height) x 0.40 m (width) and 12.0 m (length). A circulation system with a sump and a pump supplies water to the horizontally positioned flume and a valve is used to control the flow discharge and hence, the water depth. The riverbed segment consisted of 0.40 m width and 1.50 m length positioned 6.25 m downstream of the flume entrance and was confined by two smooth plywood plates level with the top surface of the test section. Ramps were used to accommodate the flow to and from the raised bed with slopes of 1/3.75 and 1/2.50 for the upstream and downstream ramps respectively, as shown in Figure 3.15.
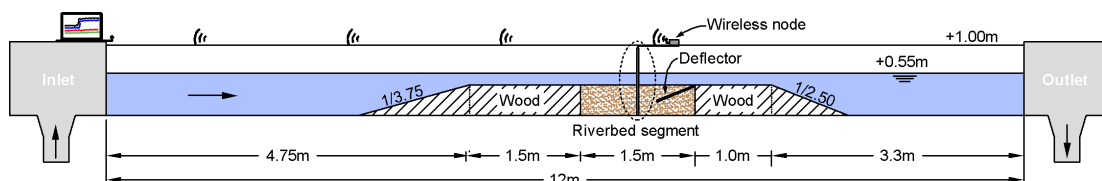
Figure 3.15: Flume experimental set up.

Preliminary experiments indicated scouring at the interface of the sediment and the plywood downstream plate. A deflector with a slope of 1/2.50 was therefore positioned within the downstream side of the test section to direct the flow away from

the interface. Sediment traps were also installed upstream and downstream of the ramps to decrease sediment transportation and re-deposition in the test section while water was re-circulating in the flume.

Separate flume experiments were conducted with two sand soil types; a non-uniform mixture of coarse sand sediments (Coefficient of gradation: C_c = 1.63) with median grain size D_{50} = 0.781 mm and specific gravity of 2.88 and a uniform medium sand (C_c = 1.19) with median grain size D_{50} = 0.375 mm and specific gravity of 2.83. The soil was placed un-compacted to achieve relatively low density values and to accentuate scouring process.

The scour probe was installed in the middle of the riverbed segment and fixed at the bottom of the flume. Although the probe is equipped with six sensors, only four were used in these experiments due to the limited depth of the flume. S1 was placed at 2.0 cm above the surface of the riverbed segment and it remained fully submerged in water during the experiments. S2, S3 and S4 were embedded into the sediment at depths of 2.5 cm, 12.5 cm and 32 cm below the riverbed segment surface as shown in Figure 3.16 (a). The wireless interface was placed 0.5 m downstream of the scour probe and attached to the flume frame while the base station was positioned 7.5 m away, on top of the flume inlet [see Figure 3.16 (b)].
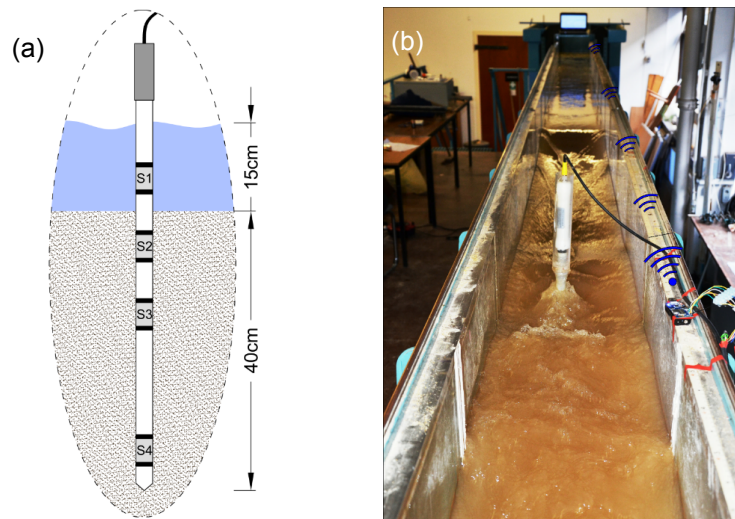
Figure 3.16: (a) Position of sensors in the riverbed segment; **(b)** wireless node location downstream of the scour probe and data transmission to the base station at the entrance of the flume.

The bed was thoroughly levelled before each experiment and the bed level at the probe position was recorded throughout the experiments with a Vernier point gauge at time intervals of 30 mins. An OTT Hydromet current meter (type: 02 '10.150')

connected to NI DAQ (NI USB 6009) interfaced to a computer via LabView recorded the water flow rates in the riverbed segment. A poddymeter instrument located after the valve at the outlet of the downstream tank also provided measurements of the discharge. Prior to initiating flow conditions, the tested section was saturated by allowing water to gently run-off the upstream plywood plate for one hour. Experiments started by allowing the water to flow over the horizontal bed with a defined flow rate of 0.40 m/s. During the flume tests the velocity varied from 0.40 m/s to 1.30 m/s and the corresponding water depth at steady state ranged from 0.5 cm to 15 cm respectively. Deposition was simulated by adding 500 g of sediment at intervals of 30 sec on the upstream ramp from where the sediment was transported by flow conditions and deposited in the scoured riverbed segment.

Low flow rates generated clear water scour conditions that evolved to live bed and/or general scour in the test section when flow velocity was increased. The duration of each flume experiment was seven hours and the results were collected and analysed.

3.4 Experimental results

3.4.1 Feasibility study on the use of dielectric sensor to monitor scour and re-deposition under different environmental conditions

The long-term bed level degradation effect using fresh and saline water of 35 ppt at various temperature conditions is presented in Figures 3.17 and 3.18 respectively. The signal response of the sensor during this test is controlled by the permittivity of the sediment when the electric field that is generated between the two electrodes penetrates the medium surrounding the sensor. Figure 3.17 (a), 3.17 (b) and 3.17 (c) shows that the exhibited amplitude of the sensor embedded into the sediment (100 % soil total weight) rose gradually as the conditions around the sensor changed from soil to fresh water with suspended sediments (i.e. close to 0 % soil total weight).

Similar behaviour of the sensor is observed in saline environment, namely, as saturated sediment is gradually replaced by saline water around the sensor location (i.e. the percentage soil total weight in the tank decreases), an increase in the sensor response is recorded [see Figure 3.18 (a), 3.18 (b) and 3.18 (c)]. A rise of the sensor values is also observed in saline water compared to the findings in fresh water due to high conductivity caused by the presence of salinity in water.
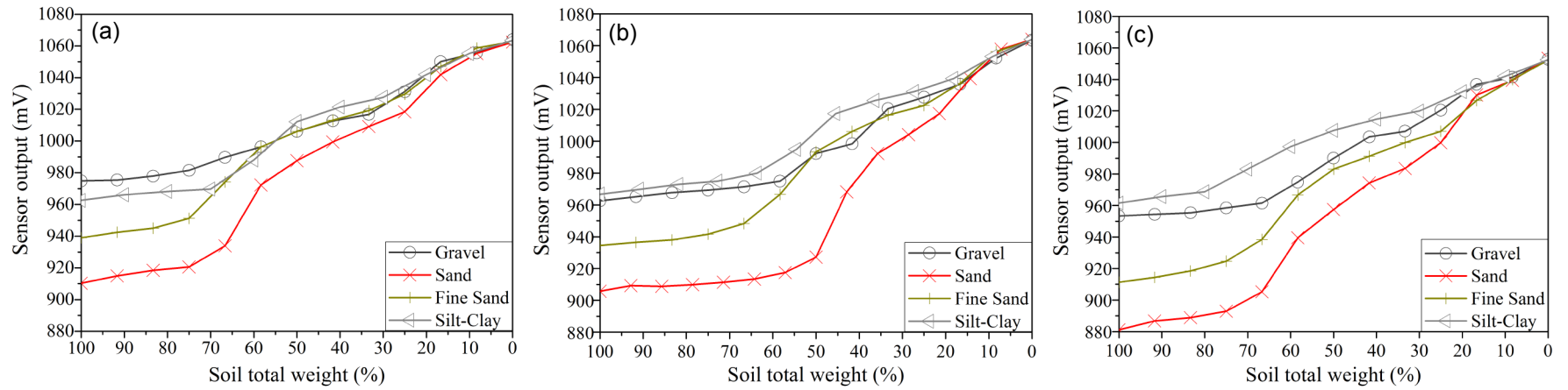
Figure 3.17: Sensor amplitude during long-term bed level degradation tests using fresh water at temperature of **(a)** 2 ºC, **(b)** 11 ºC and **(c)** 21 ºC.
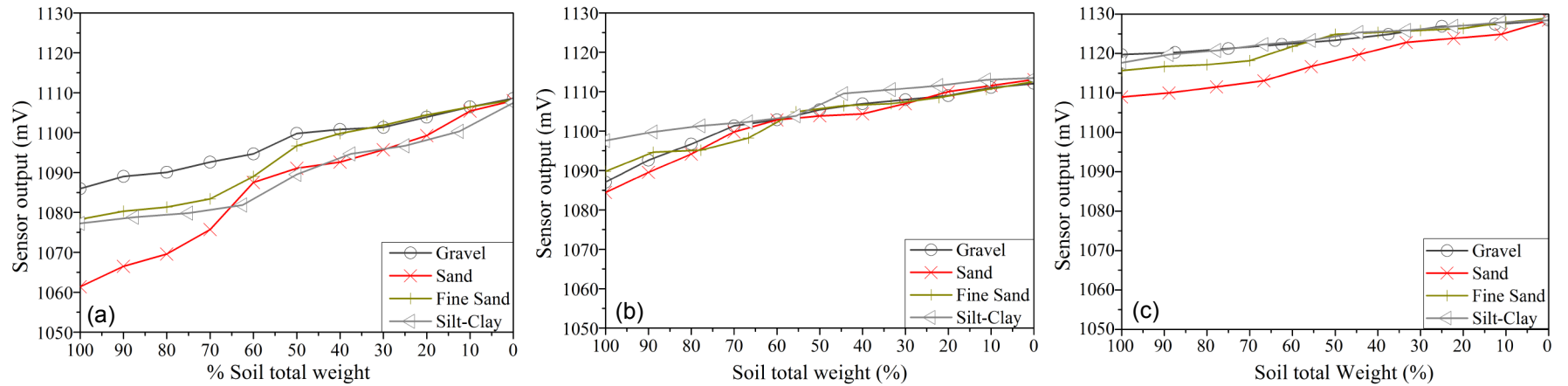
Figure 3.18: Sensor amplitude during long-term bed level degradation tests using saline water of 35 ppt at temperature of **(a)** 2 ºC, **(b)** 11 ºC and **(c)** 21 ºC.

Figures 3.19 and 3.20 present the sensor responses when the probe was subjected to scour and sedimentation simulations at different water temperatures using fresh and saline water respectively. As shown in Figures 3.19 (a), 3.19 (b) and 3.19 (c), before scour conditions, the voltage amplitude of the embedded into the sediment sensor was recorded at a much lower level compared to the sensor exposed in fresh water. During scouring, the voltage output was increased sharply for all tested temperature conditions, because of the change in the medium surrounding the electromagnetic sensor. After scour simulation, the sensor responses rose and reached a value close to the water immersed sensor. Thereafter, the signals of all the tested soil media remained constant, until dropping rapidly when the re-sedimentation process was initiated (see Figure 3.19). Finally, the sensor outputs decreased to a value close but slightly above its original level prior to any scour activity.

Similar behaviour of the sensor response was observed for all of the tested temperature conditions in saline environment as shown in Figures 3.20 (a), 3.20 (b) and 3.20 (c). Based on the obtained results, it is indicated that the sensor outputs in saline environment are reduced from non-scour to scour conditions compared to those obtained in fresh water conditions (see Figures 3.19 and 3.20).
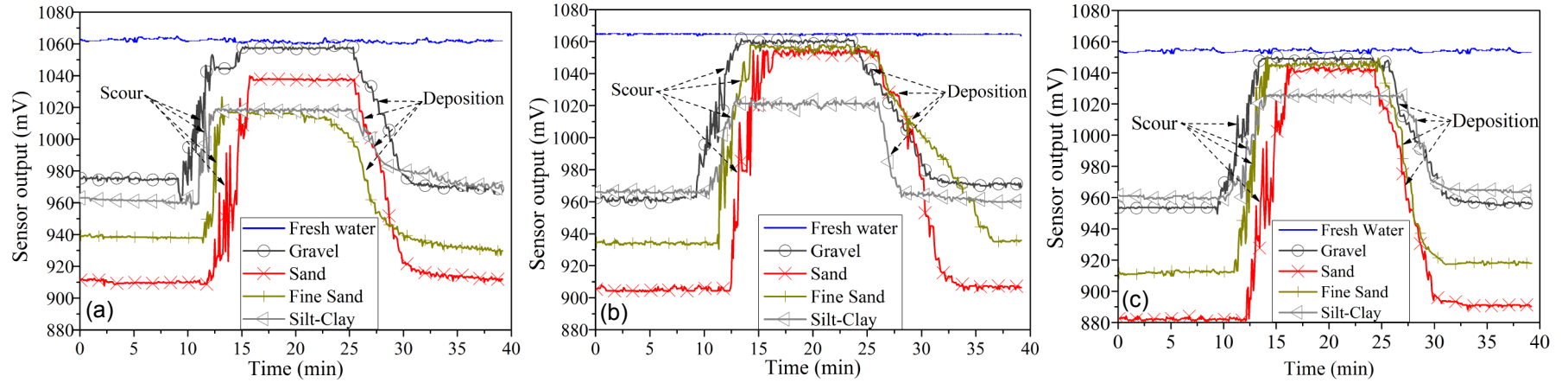
Figure 3.19: Sensor amplitude during scour and sedimentation tests using fresh water at temperature of **(a)** 2 ᵒC, **(b)** 11 ᵒC and **(c)** 21 ᵒC.
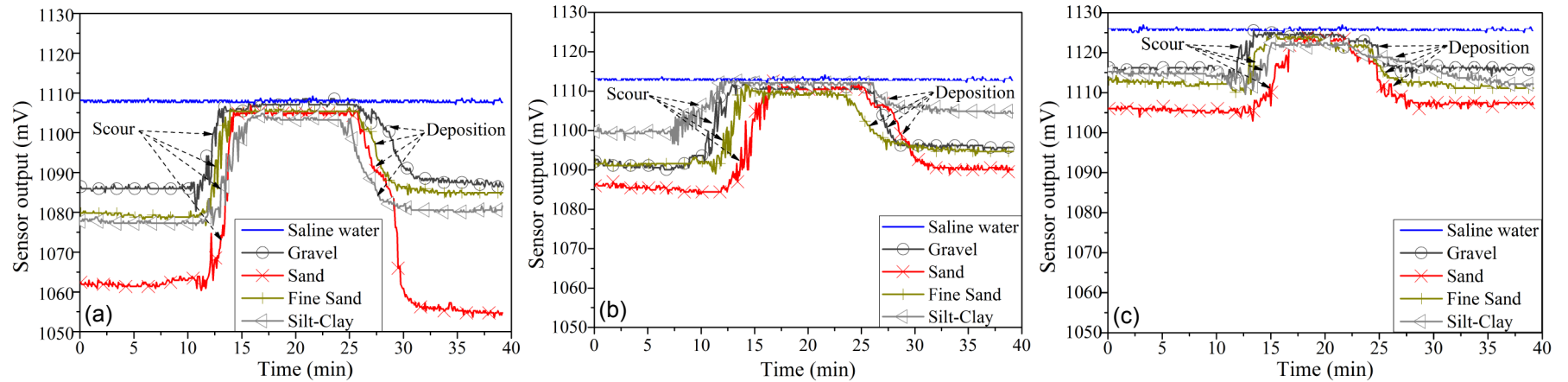
Figure 3.20: Sensor amplitude during scour and sedimentation tests using saline water of 35 ppt at temperature of **(a)** 2 ᵒC, **(b)** 11 ᵒC and **(c)** 21 ᵒC.

The temperature influence on the probe output is presented in Figure 3.21. Statistical analysis was performed with Origin Lab software and the data is presented as mean values ($n = 8$). When tested in fresh water, a slight drop of the sensor signals is observed for the gravel, sand and fine sand materials as the temperature increases, as shown in Figure 3.21 (a). The same does not apply for the signals relating to the silt-clay soil type. When temperature increased from 2 ºC to 11 ºC, the sensor value rose slightly. However, at 21 ºC, the signal dropped to a value below its original recorded at 11 ºC. As Figure 3.21 (b) indicates, the directions of the temperature trends are divergent for different environmental conditions tested as a result of the conductivity effect. Increased temperature in saline water over 2 ºC, 11 ºC and 21 ºC resulted to a corresponding rise of the sensor exhibited amplitudes, which appears linear for silt-clay and sand soil sediments.
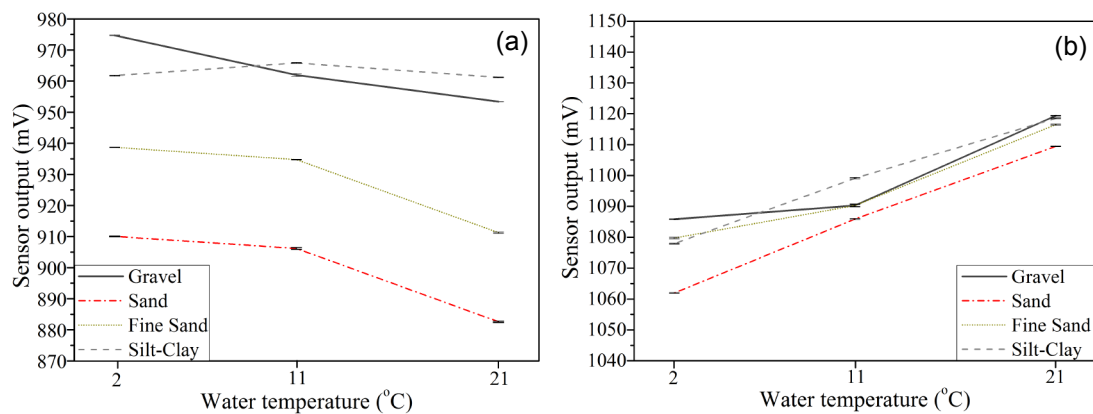
Figure 3.21: Temperature influence on the sensor embedded into different sediments using **(a)** fresh and **(b)** saline water of 35 ppt.

This set of preliminary tests was very encouraging showing that the probe was capable of monitoring bed level variations under different environmental conditions. In the light of this feasibility study, a more systematic series of experimental tests was carried out as detailed below investigating the salinity effect and impact of various sediment conditions on the sensor signals.

3.4.2 Sensor calibration and sensitivity to water salinity and temperature

The calibration curve provided by the manufacturer relates the sensor output to permittivity (see equation 3.5). This relationship was validated by immersing the sensor in different media with known permittivity in the range of square root between 1 (air) and 8.97 (water) at 20°C. As presented in Figure 3.22, an excellent match was obtained between the predicted and measured values (region i).
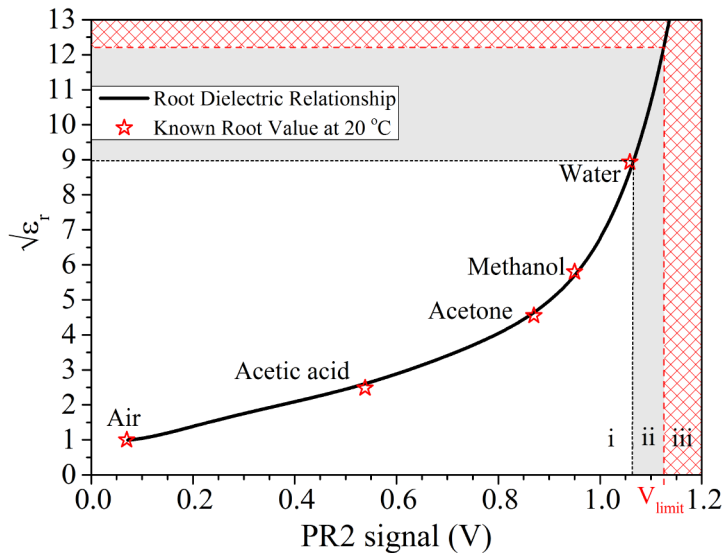
Figure 3.22: Measured and predicted voltage output in solvents with known dielectric constant values.

Regions (ii) and (iii) in the calibration curve arise from additional experiments that were carried out to evaluate the sensor behaviour in greater permittivity values which are described as follows. In particular, to investigate the effects of salinity on the sensor output, the probe was tested in aqueous solutions with various concentrations at the temperature of 18 °C. Figure 3.23 presents the response of the sensor in terms of permittivity compared to the values obtained using the equation proposed by Stogryn (1971). At fresh water (0 ppt) and 5 ppt salinity conditions, there is a satisfactory agreement between the predicted and measured values. For concentrations of 15 ppt, 25 ppt and 35 ppt, an almost linear increase of the calculated permittivity is expected using Stogryn's equation, while the measured permittivity remained essentially constant. The sensor output voltage saturates and is unable to detect permittivity values higher than 150 indicating that its dynamic range is limited. This is therefore the reason for the large difference that was obtained between measured and predicted values in the salinity range 15-35 ppt.
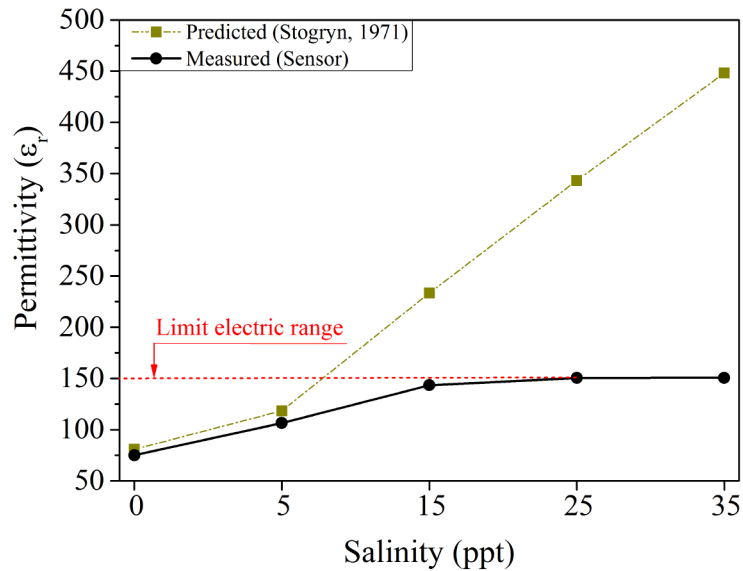
Figure 3.23: Sensor response in various salinity conditions.

In view of the results in Figure 3.23, two further regions can be identified in the calibration plot shown in Figure 3.22. For square root values between 8.97 and 12.25 (region ii), the instrument is able to measure the permittivity. However, the calibration curve should be considered with care because it has not been validated in this range. Region (iii) exceeds the range of the sensor, as the instrument is not able to output a voltage greater than 1.125 Volts, which corresponds to a root permittivity value of 12.25 (see Figure 3.22).

Figure 3.24 (a) shows that permittivity in fresh water decreased with temperature in the range of 2 ºC, 11 ºC and 21 ºC. This trend is in reasonable agreement with the permittivity calculated according to Stogryn (1971). On the other hand, increased temperature in saline water of 35 ppt resulted in a small increase of the sensor output compared to the large increase of values calculated according to Stogryn (1971), as shown in Figure 3.24 (b). Again, this discrepancy is associated with the attainment of the upper limit of the electrical range of the probe.
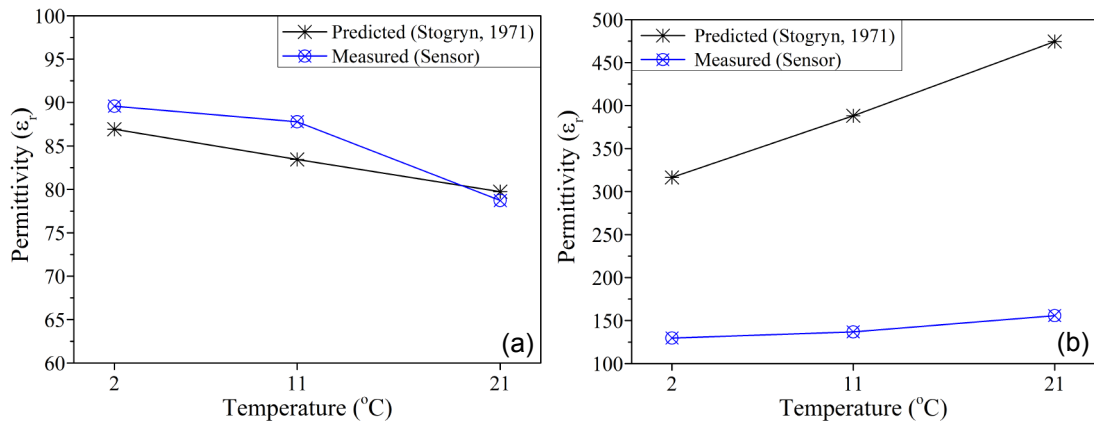
Figure 3.24: Temperature influence on the sensor output when immersed in **(a)** fresh water and **(b)** saline water of 35 ppt.

In conclusion, the sensor appears to measure accurately the dielectric permittivity in the range $\varepsilon_r = 1\text{-}150$ ($\sqrt{\varepsilon_r} = 1\text{-}12.25$) regardless of the source of medium (nature of the liquid, temperature, or salt concentration).

3.4.3 Calibration of the soil mixing model

The effect of soil water content on the sensor response was validated and found to agree with the calibration curve provided by the manufacturer. However, no information was available regarding the influence of soil density on the sensor output. This study estimates this influence using equations 3.3 and 3.4, which then enables discrimination between in-situ and deposited soil conditions.

Figure 3.25 (a) presents the sensor response in four samples having a nominal water content of 10 % (10.03 %, 11.20 %, 9.98 % and 10.59 %) and prepared at different density values of 1.06 g/cm^3, 1.30 g/cm^3, 1.41 g/cm^3 and 1.44 g/cm^3 respectively. As shown in Figure 3.25 (a), soil density has noticeable effect on the permittivity output obtained from the sensor. This is due to the decreased volume of voids of the three phase sample due to increased soil density, and to the larger apparent permittivity of the solids ($\varepsilon_s = 4\text{-}5$) when compared to air ($\varepsilon_a = 1$).

The experimental data in Figure 3.25 (a) then allowed the determination of the optimum parameter α for the soil mixing model (see equation 3.1) using a non-linear least square error regression. Figures 3.25 (a) and 3.25 (b) show the values predicted by equation 3.1 based on the best fit value of $\alpha = 0.478$ together with the values determined experimentally.
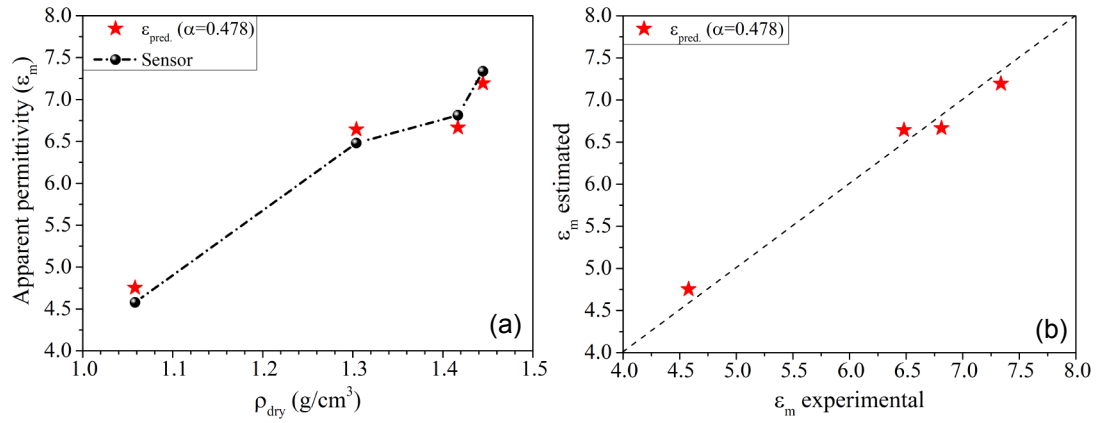
Figure 3.25: (a) Density effect on the sensor output and **(b)** optimum factor α for estimated and experimental permittivity values obtained with non-linear least square error analysis.

Note that the best-fitting parameter α of 0.478 is consistent with the values reported in the literature which found to be in the range from 0.46 to 0.50 (Birchak et al., 1974; Roth et al., 1990; Weitz et al., 1997; and Yu et al., 1997). These experimental results, allowed calibrating the mixing model and enabling equation 3.3 to be used to infer soil porosity from dielectric permittivity readings.

3.4.4 'Static' scour test results

The sensor response when embedded into gravel, coarse sand and medium sand soil types mixed with fresh water, is shown in Figure 3.26 (a). After removal of the sediment (scour conditions), a sharp increase of the obtained apparent permittivity value occurs due to a change of the surrounding medium at the location of the sensor. Note also that, for gravel soil type, the obtained permittivity when the sensor was embedded into the sediment is greater by approximately 7 when compared to the other tested mediums. This permittivity difference between the gravel and sand sediments is associated with changes in the porosity value in the local region around the sensor location which is influenced by the soil particle shape and orientation in the surrounding area of the two electrodes. From equation 3.3, the porosity for $\alpha = 0.478$ was then calculated for each tested soil type, as presented in Figure 3.26 (b).
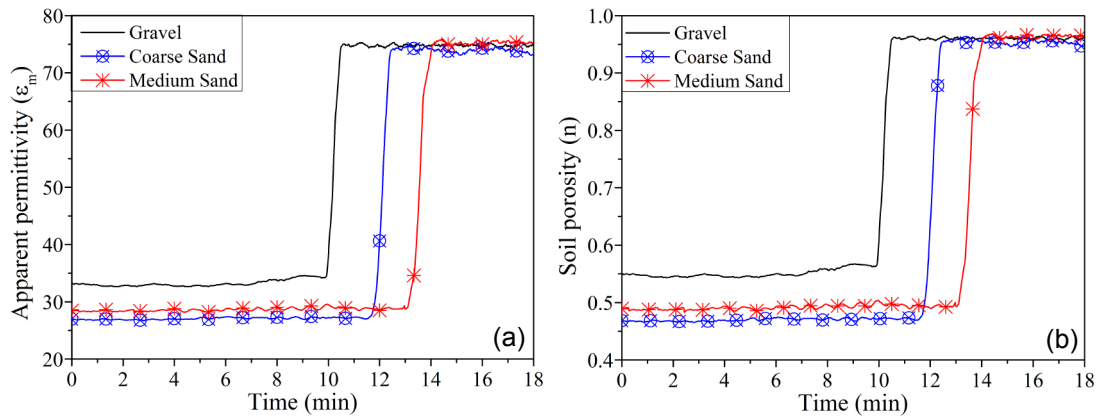
Figure 3.26: (a) Sensor permittivity outputs and **(b)** estimated soil porosity (*n*) values obtained for the optimum factor *α* during 'static' scour tests.

The probe was subsequently tested in saline water of 35 ppt using the aforementioned soil types. The experimental results obtained during these tests using saline water were then compared to the permittivity values predicted using the equation of Debye form as proposed by Stogryn (1971). Assuming that the porosity of each tested medium remains the same between the experiments carried out in fresh and saline water, the only variable in equation 3.2 is the permittivity of the saline water. The permittivity of the saline aqueous solution of 35 ppt at temperature of 11 °C was calculated from Stogryn (1971) as $\varepsilon_{ws} = 388.1$, and then equation 3.2 was used to infer the overall apparent permittivity. The estimated apparent permittivity value was then compared to the experimentally obtained output for each soil type as presented in Figure 3.27. Before scour conditions the sensor output in gravel soil type remained below the estimated permittivity values, as shown in Figure 3.27 (a). A satisfactory agreement is detected between estimated and experimental permittivity values for coarse sand and medium sand soil types, as presented in Figures 3.27 (b) and 3.27 (c) respectively.

The slight difference between the predicted and measured output in the tests using gravel soil type suggests that re-calibration of the parameter *α* is required for sediments with dissimilar characteristics compared to sand mediums. In particular, this discrepancy is caused by the overall greater permittivity value that was detectable in gravel sediments when compared to sand mediums. However, the study focused on the optimum *α* obtained in sand sediments (0.478) as this is the most common medium found in both river and offshore environments.

After scouring, for all the tested soil types in saline water a large difference between estimated and measured outputs is observed. This phenomenon is mainly attributed to the limitation of the instrument with regard to voltage output range, as was presented in section 3.4.2 and Figures 3.22, 3.23 and 3.24.
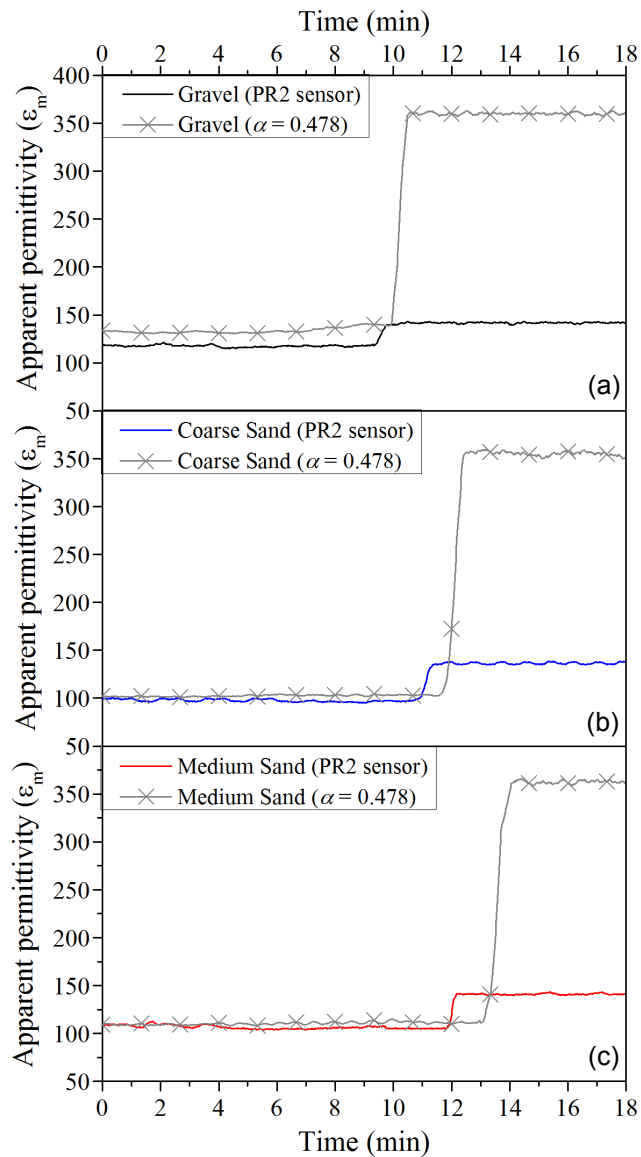
Figure 3.27: Measured and estimated permittivity values for the sensor embedded in **(a)** gravel **(b)** coarse sand and **(c)** medium sand sediments using saline water of 35 ppt.

Based on the porosity values obtained in fresh water, the dielectric permittivity was satisfactorily estimated in saline water for sand sediments. Despite also the inability of the probe to measure properly the greater permittivity in saline water of 35 ppt of NaCl, a significant change in sensor output is still observed, which would permit monitoring of bed level variations in water with high salinity concentrations.

3.4.5 Real-time flume experiments

Saturation process of the riverbed segment

Figure 3.28 presents the apparent permittivity values derived from equation 3.5 during the saturation of the flume riverbed segment that consisted of coarse sand mixture and medium sand soil types each time. Prior to the saturation process, sensors S2, S3 and S4 were embedded into the dry sediment and the corresponding permittivity values ranged from 3 to 4 (see Figure 3.28). When the saturation process is initiated, the permittivity value for sensor S2 increases sharply followed by S3 and S4 responses. Once saturation of the riverbed segment is complete, the permittivity values for the three sensors settle between 23 and 32 for both sediment types. For the duration of the experiment, the permittivity observed by sensor S1 remains constant and equal to 1, as it was located outside the tested section in an air environment.
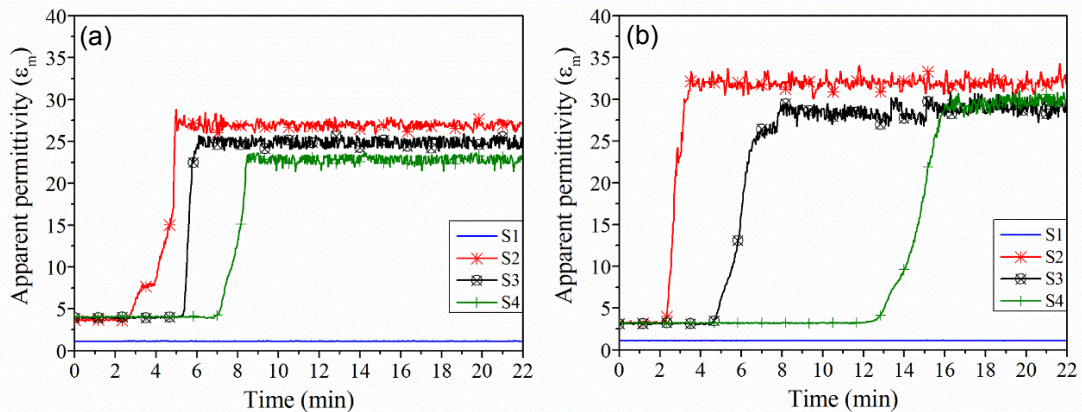
Figure 3.28: Permittivity values obtained in **(a)** coarse sand and **(b)** medium sand sediments during the saturation process of the riverbed segment.

The saturation tests using the flume indicated that water infiltration of the riverbed segment had a significant increasing effect on the apparent permittivity values obtained by the sensor signals.

Flume test results

Figure 3.29 (a) shows the scour probe response, the location of the sensors in the tested section and the measured scour depth obtained in coarse sand mixture sediment. Initially, the measured apparent permittivity of the water-immersed sensor (S1) was at the range of 78. At the same time, sensors (S2, S3 and S4), embedded into the sediment, exhibited permittivity values below 27. As Figure 3.29 (a) indicates, after a

period of 1 hour the scour depth increased to 7.2 cm. At the same period of time, it was observed that the ouput of S2 increased to 75 and thereafter remained almost constant. This change in the S2 is due to the different permittivity which reveals that the sediment around the sensor location is scoured, i.e. the soil is replaced by water.

During the same time period, the S3 output increased only marginally, which indicates that the scouring on S2 insignificantly influenced the S3 output. The scour depth continued to rise and at the period of 2.5 hours was recorded at 15.7 cm. At the same time the S3 output was increased sharply and reached permittivity in the range of 75. Thereafter, the signals of the scoured S2 and S3 sensors remained steady whereas scour reached its equilibrium at depth of 17.5 cm. The sediment deposition process started after a period of 5 hours and the S3 permittivity output dropped to 37 as the area around the sensor level was re-filled with sediment and scour depth was reduced to 12.7 cm. After 6 hours, the S2 permittivity also declined to 34 while S3 continued to decrease further to 33. As shown in Figure 3.29 (a), at the same time measured scour depth was 2 cm indicating that the sediment around both S2 and S3 corresponded to re-deposited saturated sediment. Finally, scour depth did not reach the location of S4 so it exhibited steady permittivity values of 23 throughout the experiment. Figure 3.29 (a) demonstrates that different measured permittivity values were obtained for conditions that corresponded to pre-scour and post-sediment deposition.

Figure 3.29 (b) presents the sensor outputs and scour depth recorded for medium sand soil type. S1 remained submerged in water and exhibited permittivity values at the range of 77. S2 and S3 sensors were embedded into the riverbed segment and their outputs at the beginning of the flume test were recorded around 30 and 29 respectively. Thereafter, a rise of the S2 output was observed reaching values between 68 and 81 while a parallel increase of the scour depth to 7.2 cm occurred.

As shown in Figure 3.29 (b), almost 4.5 hours after the experiment was initiated, the S3 permittivity value increased from 30 to 49. For the same time period, scouring also increased and reached its maximum depth of 12.9 cm. Then, after 6 hours, scour depth decreased to 8 cm while the value of S3 also reduced to 32. The slight variation of the S3 output reveals that scour depth reached but did not fully expose this sensor in water conditions. The decrease of the measured scour depth and S3 values that

occurred after the maximum recorded scour depth corresponds to the physical process of sediment transportation in the flume and deposition in the riverbed segment around the location of S3. An equivalent decrease in both the measured scour depth and the signals of S2 and S3 was observed when the simulation of sediment deposition was initiated after the period of 6 hours [see Figure 3.29 (b)]. Finally, the recorded permittivity output of S2 and S3 after the sediment deposition simulation reached values similar to as pre-scour conditions (31 mV and 29 mV respectively) while scour depth decreased to 1.5 cm. During this test the permittivity output of S4 was almost constant at the range of 29, which indicates that it was not affected by scour and remained embedded in the sediment.
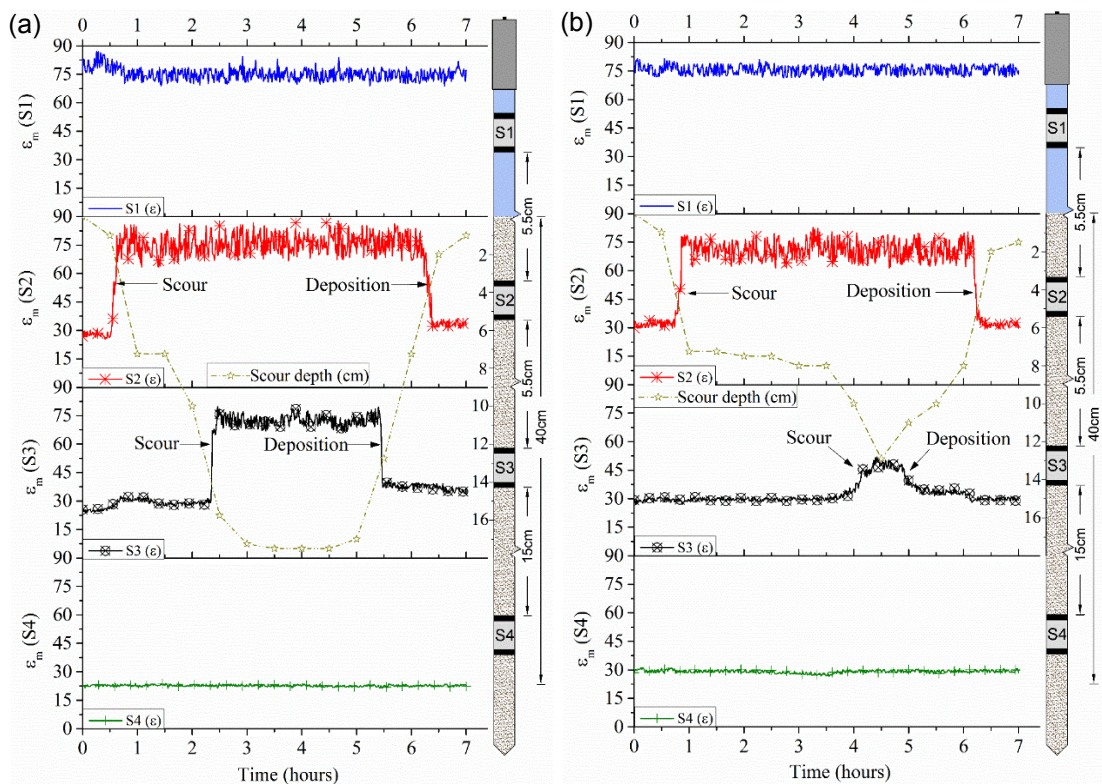
Figure 3.29: Measured permittivity values and scour depth during flume experiments in **(a)** coarse sand mixture and **(b)** medium sand sediments. The measured scour depth and the location of each sensor along the probe length are also presented for each flume test.

The dry density for $\alpha = 0.478$ was then estimated from equations 3.3 and 3.4 in order to obtain the soil density at the location of each sensor for both experiments. Figure 3.30 (a) shows the predicted soil density obtained in coarse sand mixture sediment, which at the start of the experiment varied between 1.5 gr/cm^3 (S2), 1.6 gr/cm^3 (S3) and 1.7 gr/cm^3 (S4). After sediment re-deposition, the density values for S2, S3 were recorded at the range of 1.2 gr/cm^3 and 1.3 gr/cm^3 respectively, while the

S4 was not affected by scour processes during the experiment. Figure 3.30 (a) demonstrates that different soil density conditions occurred when the sensor was embedded to in-situ soil compared to re-deposited sediment.

As Figure 3.30 (b) shows, for medium sand sediment type the obtained soil density based on the output of sensors S2 and S3 exhibited similar levels for pre-scour and post-sediment deposition conditions of 1.3 gr/cm^3 to 1.4 gr/cm^3 respectively. The water-immersed (S1) and the permanently soil-embedded sensor (S4) were unaffected by the aforementioned processes during the experiment and exhibited density values at the range of 0.0 gr/cm^3 and 1.4 gr/cm^3 respectively [see Figure 3.30 (b)].
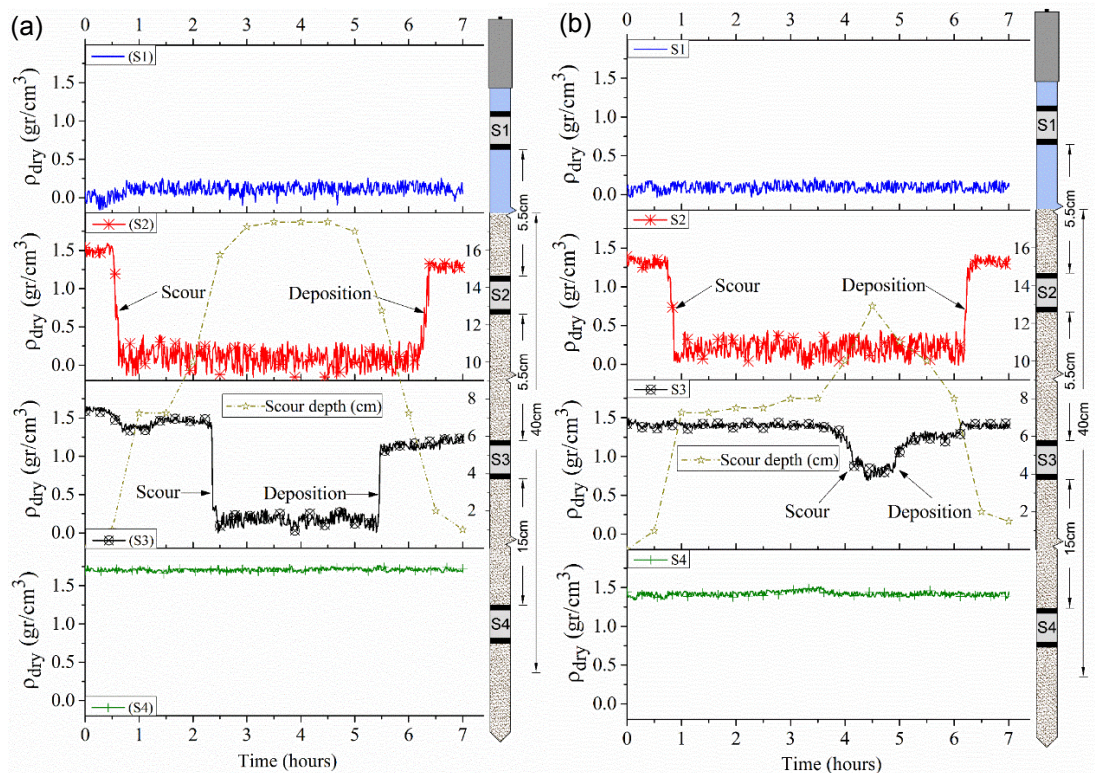
Figure 3.30: Estimated density values and scour depth during flume experiments in **(a)** coarse sand mixture and **(b)** medium sand sediments. The measured scour depth and the location of each sensor along the probe length are also presented for each flume test.

The results obtained in separate open channel flume experiments using coarse and medium sand sediments clearly demonstrate that the sensors accurately tracked the evolution of both scour and sediment deposition. A sharp increase of the sensors' output was recorded when scour occurred at the sensor location. Re-deposited sediment was found to be associated with higher apparent permittivity, reflecting the lower soil density conditions. The sensor is therefore potentially capable of detecting re-deposited sediments characterised by lower density than the original in-situ soil.

3.5 Conclusions

This study has presented a new monitoring technique that can be deployed and allows the continuous monitoring of scour depth variations and sediment re-deposition processes at foundation elements. The sensing principle employs the Amplitude Domain Reflectometry (ADR) technique that utilises the reflection characteristics of electromagnetic waves and was evaluated using an off-the-shelf small-scale probe. The ADR instrument was connected to a wireless interface that could allow the real-time remote monitoring of the obtained data.

Preliminary tests conducted in the laboratory simulating different underwater conditions around the sensor location indicated that the technique successfully measured the long-term degradation effect. The instrument was also found capable of detecting 'static' scour and re-deposited sediment processes despite the inevitable influences of saline water and temperature induced electrical conductivity changes on the sensor signals.

A systematic series of experimental tests was then carried out evaluating the calibration of the instrument and its sensitivity to salinity and temperature effects. A large discrepancy observed between predicted and measured sensor output in saline water was attributed to the limit capability of the instrument's dynamic range. The calibration curve provided by the manufacturer was found to be accurate for permittivity values up to 80. Based on the obtained results three areas were identified on the sensor's calibration curve indicating the accurate (i), the uncertain accuracy (ii) and the out of range (iii) regions.

The use of the sensor signals to discriminate between in-situ and re-deposited soil was also addressed in this investigation. Experimental data obtained at various soil density conditions were employed to calibrate a three phase mixing model with the determination of the optimum geometric parameter α, which was found to be consistent with values reported in the literature. The overall apparent permittivity value was then adequately estimated for sediments with similar characteristics. It was then demonstrated that the soil porosity around each sensor location could also be estimated based on the sensor outputs for sediments with similar characteristics.

This study also thoroughly validated the ADR sensor platform in real-time flume experiments which exhibited high sensitivity to scour and sedimentation processes.

Re-deposited sediment was found to be associated with higher permittivity attributed to lower soil density that was successfully estimated. Analysis of the sensor signals demonstrated the ability of the proposed system to differentiate between pre-scour and post-sediment deposition conditions.

The proposed sensing technique can provide a more economical, accurate and real-time alternative to existing scour inspection methods. The results presented in this investigation provide an important guide and can be used as a benchmark for the field application of the ADR sensor which can be integrated into a structural health monitoring system, delivering key information regarding bed level conditions at foundation elements.

The main limitation of the ADR probe lie in the fact that the instrument can only provide bed level measurements in the local region around each sensor location. The ADR instrument does not therefore allow for continuous monitoring of scour or sediment deposition processes along the probe length but only when the medium around the electrodes of each sensor is altered. For more detailed information of bed level variations along the length of the instrument, further sensors need to be added on the probe which is likely to increase the total cost of the instrument. The study was therefore focused on the design and development of a new sensor that can provide a low-cost solution and enables continuous monitoring of scour and sediment deposition processes along the length of the instrument.

References

Birchak, J.R., Gardner, C.G., Hipp, J.E., and Victor, J.M. (1974). High dielectric constant microwave probes for sensing soil moisture. *Proceedings of the IEEE*, 62(1), pp. 93–98.

Delta-T Devices Limited. (2006). *Moisture content sensor and related methods*. International Patent Publication WO 2006/064266 A1.

Delta-T Devices Limited. (2008). *User Manual for the Profile Probe: type PR2*. Cambridge, UK.

Dobson, M.C., Ulaby, F.T., Hallikainen, M.T., and El-Rayes, M.A. (1985). Microwave dielectric behavior of wet soil part II: Dielectric mixing models. *IEEE Transactions on Geoscience and Remote Sensing*, GE-23(1), pp. 35-46.

Maryott, A.A., and Smith, E.R. (1951). *Table of dielectric constants of pure liquids*. Circular 514, Washington, USA Government Printing Office.

Michalis, P., Saafi, M., and Judd, D.M. (2012). Wireless Sensor Networks for Surveillance and Monitoring of Bridge Scour. *Proceedings of the 11th International conference of Protection and Restoration of the Environment* (Katsifarakis, K. L., Theodossiou, N., Christodoulatos, C. Koutsospyros, A. and Mallios, Z. (eds)). Thessaloniki, Greece, pp. 1345 -1354.

Michalis, P., Saafi, M., and Judd, D.M. (2013). Capacitive Sensors for Offshore Scour Monitoring. *Proceedings of the ICE – Energy*, 166(4), pp. 189–196.

Roth, K.R., Schulin, R., Fluhler, H., and Attinger, W. (1990). Calibration of Time Domain Reflectometry for Water Content Measurement using a Composite Dielectric Approach. *Water Resources Research,* 26(10), pp. 2267-2273.

Stogryn, A. (1971). Equations for Calculating the Dielectric Constant of Saline Water. *IEEE Transactions on Microwave Theory and Techniques,* 19(8), pp. 733-736.

Weitz, A.M., Grauel, W.T., Keller M., and Veldkamp, E. (1997). Calibration of TDR technique using undisturbed soil samples from humid tropical soils of volcanic origin. *Water Resources Research,* 33(6), pp. 1241-1249.

Whalley, W.R., Dean, T.J., and Izzard P. (1992). Evaluation of the Capacitance Technique as a Method for Dynamically Measuring Soil Water Content. *Journal of Agricultural Engineering Research,* 52, pp. 147-155.

Yu, C., Warrick, A.W., Conklin, M.H., Young, M.H., and Zreda, M. (1997). Two- and three-parameter calibrations of time domain reflectometry for soil moisture measurement. *Water Resources Research*, 33, pp. 2417-2421.

Chapter 4

Design and Optimisation of a New Impedance-based Sensor for Monitoring Bed Level Variations at Foundations

*Sections of this chapter are an edited version of the published or at preparation/submission stage articles in the following journals and international conference proceedings:

Michalis, P., Judd, D.M. and Tarantino, A. Design and Optimisation of a New Impedance-based Sensor for Scour and Sediment Deposition Monitoring. *IEEE Sensors Journal* [In preparation, to be submitted within 2 months].

Michalis, P., Judd, D.M. and Tarantino, A. Development and Laboratory Characterisation of a New Electromagnetic ADT Sensor for Scour and Sediment Deposition Monitoring at Hydraulic and Marine Structures. *IEEE Transactions on Geoscience & Remote Sensing* [In preparation, to be submitted within 2 months].

Michalis, P., Tarantino, A., and Judd, D.M. (2014). Electromagnetic Sensors for Monitoring of Scour and Deposition Processes at Bridges and Offshore Wind Turbines. In: *European Geosciences Union General Assembly 2014*, Vienna, Geophysical Research Abstracts, Vol. 16, EGU2014-9427-6.

Michalis, P., Judd, D.M., and Tarantino, A. (2014). Real-time Monitoring of Scour and Sedimentation Evolution with a New Developed Prototype Sensor. In: *12th International Conference of Protection and Restoration of the Environment*, Skiathos, Greece, ISBN: 978-960-88490-5-1.

4.1 Introduction

This chapter presents the design and optimisation of the geometric components of a new sensor based on soil electromagnetic properties. The proposed technique exploits the relatively large difference in the permittivity values of saturated sediment compared to water as a means of measuring the scour conditions at hydraulic and marine structures. This approach has also been employed by other instruments (e.g. TDR) but their application for scour monitoring is limited due to issues derived mainly by the high cost, the complexity of equipment and that they are not able to withstand field conditions. This study aims at developing a new low-cost, robust and accurate sensor that can provide information of bed level conditions along the length of the instrument and can be employed for wide spread monitoring of bed level conditions at foundations.

The chapter initially presents the operating principle of an impedance-based method for scour and sedimentation monitoring. Finite Element Modelling (FEM) is performed to optimise the sensor geometry based on the computed capacitance and electric flux density in various simulated media that represent an offshore environment. The set-up of the electrostatic simulations in addition to the analysis and optimisation of the sensor are presented. The investigation firstly focuses on the effect of various inner cross sections of the sensor. The optimum electrode arc length and angular position are also investigated based on the capacitance values and on the magnitude of the electric flux density generated between the sensor electrodes. The proposed optimum geometric components of the final design of the sensor are then defined as those which maximise the magnitude range of the electric field and its penetration distance into the medium. These criteria are expected to result in increased sensitivity of the sensor to scour and sedimentation processes. Finally, the major findings of this study are summarised and presented.

4.2 Impedance-based method for dielectric permittivity measurement: operating principle

Instruments that use soil electromagnetic properties to measure erosion at foundation elements rely on their ability to detect changes in the medium permittivity (ε). The proposed technique to measure scour and sedimentation processes is based on the large contrast in permittivity values of saturated and re-deposited sediment compared to water.

The influence of the sensor characteristics on the input and output signal is proposed to be used in this study in order to provide an indication of underwater bed level variations. As shown in Figure 4.1, the sensor will present an impedance value Z_p that will vary according to the medium surrounding the probe.
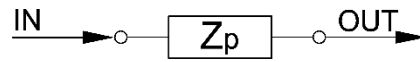
Figure 4.1: Sensor impedance presented between a signal source (input) and a signal detector (output).

The characteristic impedance for a lossless line is given by the following equation (Karmel et al., 1998):

$$Z = \sqrt{\frac{L}{C}}$$

(eq. 4.1)

where L is the inductance per unit length and C is the capacitance per unit length. The C factor describes the energy stored by producing an electric field within a dielectric material and L the energy stored within a magnetic field. The L depends on the sensor geometry and the magnetic permeability. Most materials have a magnetic permeability value equal with the permeability of free space $\mu = \mu_o = 4\pi \times 10^{-7}\ H \cdot m^{-1}$ unless they are magnetic. Soil samples are non-magnetic materials (Roth et al, 1990), hence L is constant for a given sensor geometry, therefore according to equation 4.1 the Z value is dependent only on the C factor.

The sensor capacitance C_s is a function of the area and the distance between the electrodes and the dielectric material of the surrounding medium. The C_s for complex electrode geometries is calculated as follows (Whalley et al., 1992):

$$C_s = g \times \varepsilon$$

(eq. 4.2)

where C_s, is related to the medium permittivity (ε) via the geometrical constant (g). Taking into account that the area of the sensor electrodes and their distance apart are fixed, C_s only varies with changes in the medium permittivity. The sensor impedance is therefore directly related to the permittivity of the medium surrounding the electrodes though the capacitance factor. Figure 4.2 also shows two capacitors combined in series creating an equivalent total capacitance.

Figure 4.2: Two capacitors connected in series.

As presented in equation 4.3 the total capacitance of two capacitors placed in series is always less than the capacitance of any of the individual capacitors and is dominated by the lowest capacitor.

$$\frac{1}{C_{total}} = \frac{1}{C_1} + \frac{1}{C_2} \Rightarrow C_{total} = \frac{C_1 \times C_2}{C_1 + C_2} \qquad \text{(eq. 4.3)}$$

An incident wave generated from a source at the boundary of two media with different permittivity characteristics will be partitioned into a reflected and a transmitted wave. This is due to the mismatch that is produced between the characteristic impedances of the source and the sensor. Increased impedance mismatch results in a greater reflected wave while a closer match enhances the transmission of the signal. As presented in equations 4.1 and 4.2, a high permittivity value (i.e. in water medium) results in increased capacitance and a lower sensor impedance value which will be close to the source impedance (usually 50 Ohms). This will lead to an improved impedance match in favour of the signal transmission.

This study presents the design of the geometric components of a new type of impedance-based sensor, capable of providing continuous monitoring of scour and sediment deposition processes along the length of the instrument. The FEM optimisation is carried out based on the capacitance values generated under various permittivity conditions. The proposed sensor components are presented in Figure 4.3 (a) and consist of a dielectric rod equipped with four separate stainless steel strip electrodes running along its length and inserted into a low permittivity corrosion resistant thin insulating jacket. The electrode strips form the sensor and generate an

electromagnetic field that penetrates the medium outside the access tube with the sediment acting as the dielectric material [see Figure 4.3 (b)]. The total capacitance of the sensor will be a sum of the series connected capacitors that correspond to the dielectric rod, the air, the access tube and the external simulated medium.
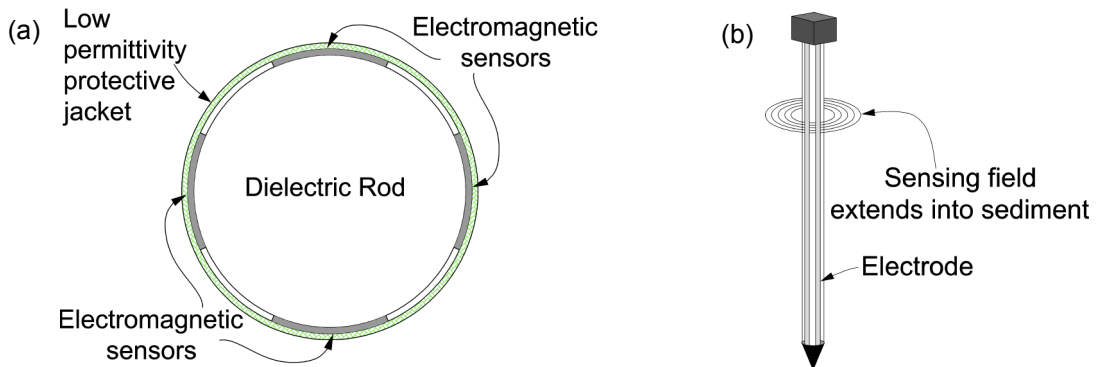
Figure 4.3: (a) Sensor components and **(b)** sensing field generated between electrodes.

As depicted in Figure 4.4, during scouring the sediment around the sensor location will be replaced by water leading to a decrease in the embedded length (L) and an increase in the exposed length (d). This will also indicate a change in the average permittivity of the surrounding medium from saturated sediment (ε_s) to water (ε_w), which will alter the amplitude and phase of the transmission signal.
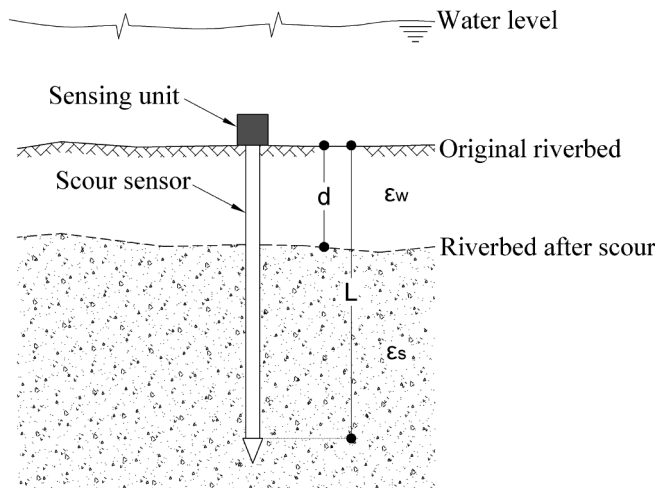
Figure 4.4: Exposed and embedded length of the scour probe embedded into the riverbed.

The change in the amplitude transmission properties of the sensor is proposed in this study to be used in order to provide an indication of scour and sedimentation processes around the probe location.

4.3 Finite element modelling (FEM) set up

4.3.1 Sensor geometry and input parameters

Electrostatic simulations were performed in order to define the optimum geometry of the sensor using the two-dimensional finite element software Maxwell 2D. Various permittivity conditions were simulated that corresponded to vacuum ($\varepsilon_v = 1$), air ($\varepsilon_a = 1.0006$), saturated sediment ($\varepsilon_s = 25$) and water ($\varepsilon_w = 80$). Two strip electrodes were initially simulated in order to define their optimum size and location according to the computed capacitance and the magnitude of the electric flux density (*magD*). The *magD* describes the displacement effects of an electric field on the polarisation or bound charges within a dielectric material.

The model was defined as electrostatic and simulated in XY plane. In two-dimensional (2D) simulation the cross section is extended infinitely in the orthogonal directions, therefore the total capacitance that is generated between the strip electrodes was calculated in picoFarads per meter (pF/m). At the boundary of the simulation area, the condition was set to 'balloon' which models the case where the structure is assumed to be infinitely far away from all other electromagnetic sources. The electric potentials of the two strip electrodes were set to +1 Volt (V) and 0 V respectively. The metallic and the dielectric components were assumed to be ideal conductors and lossless respectively. The investigation carried out included small air gaps between the electrodes and the inner cross section as well as the access tube, as depicted in Figure 4.5. The models did not consider air gaps between the access tube and the external environmental simulated material.
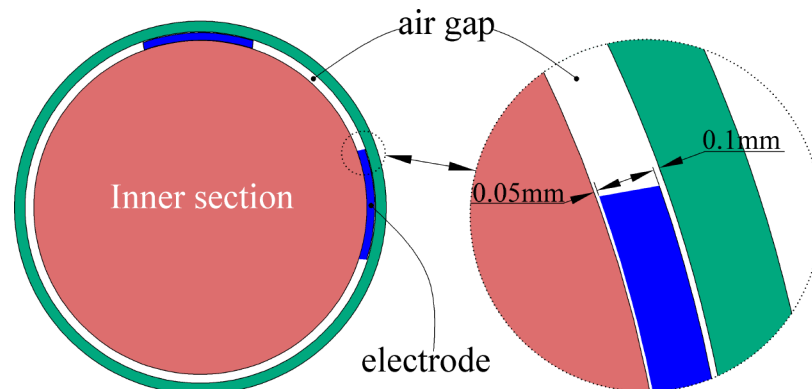
Figure 4.5: Detail of the electrode position between the inner section of the sensor (air gap = 0.05 mm) and the access tube (air gap = 0.01 mm).

With regards to the inner cross section a solid rod would be the obvious simplest choice. However, because the permittivity of the rod is $\varepsilon_r > 1$ the electric flux will be more easily attracted and passed through it. Hence, simulations with a hollow tube were also carried out in order to provide more information of the electric flux properties for the case of the inner air having lower ε_r. The simulated inner cross sections therefore comprised of a solid rod and a hollow tube each time which were attached to two strip electrodes. The permittivity values assigned in the two models are presented in Figure 4.6. The access tube effect on the computed capacitance and its influence on the sensitivity of the sensor were also examined.
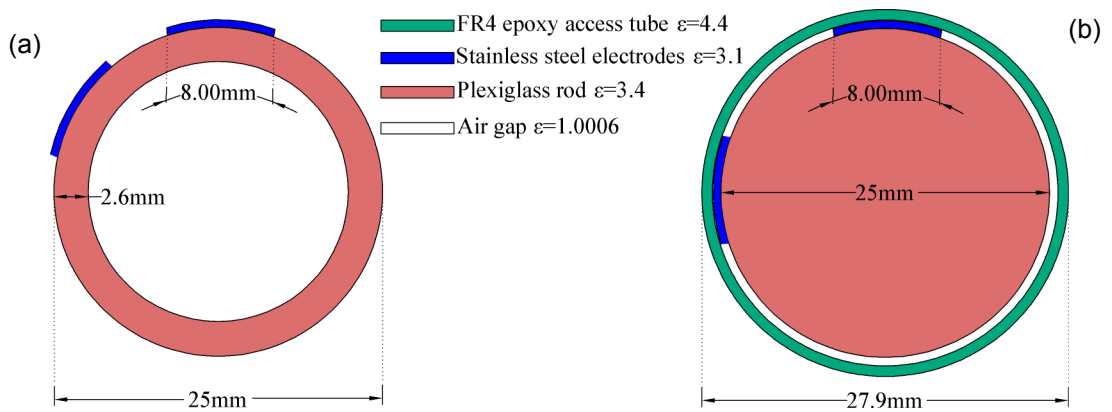
Figure 4.6: Typical models using **(a)** a hollow tube without the presence of access tube and **(b)** a dielectric rod inner cross section enclosed by an access tube.

The analysis was carried out with the electrodes positioned at centre to centre angles of 60°, 90° and 120° respectively in order to define the optimum electrode position (see Figure 4.7).
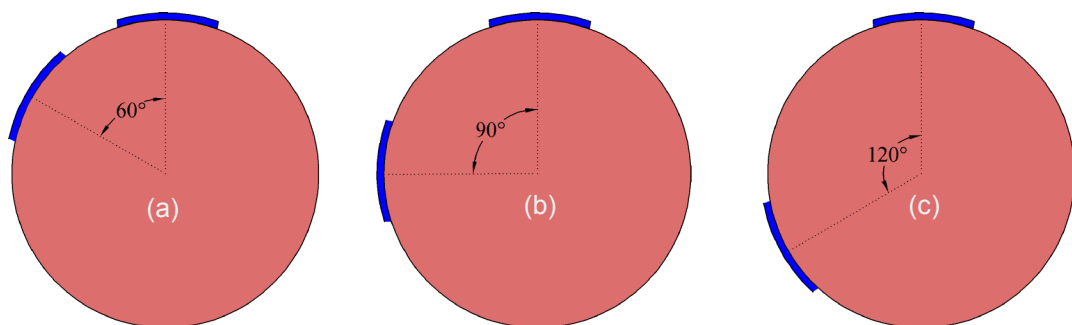
Figure 4.7: Models with the electrodes placed at angle positions of **(a)** 60°, **(b)** 90° and **(c)** 120° respectively.

The effect of the electrode size on the computed capacitance was also investigated by simulating various electrode arc lengths of 8.00 mm, 9.30 mm, 11.85 mm and 13.75 mm each time. Simulations were then carried out for the optimum

geometric characteristics of the sensor with four paired strips that will allow for bed level monitoring around the probe location.

4.3.2 FEM solve set up

The model solve set up was adjusted to 15 % refinement per pass with 10 requested passes while the error was set to 0.01 % (see Figure 4.8). The generated typical mesh for simulated water conditions is shown in Figure 4.9.
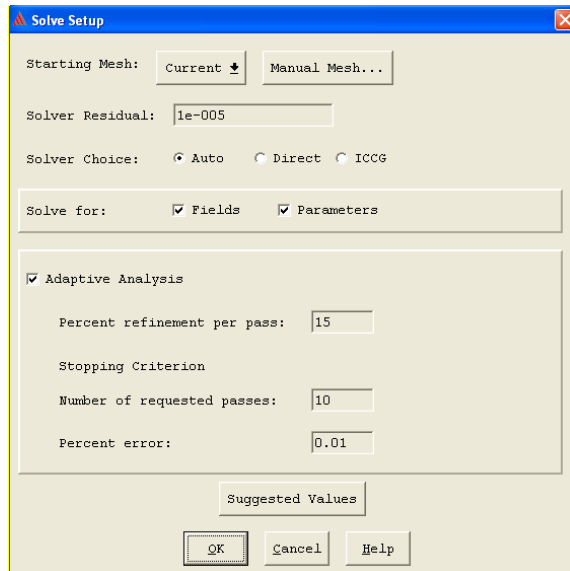
Figure 4.8: Solve set up used for the simulated models.
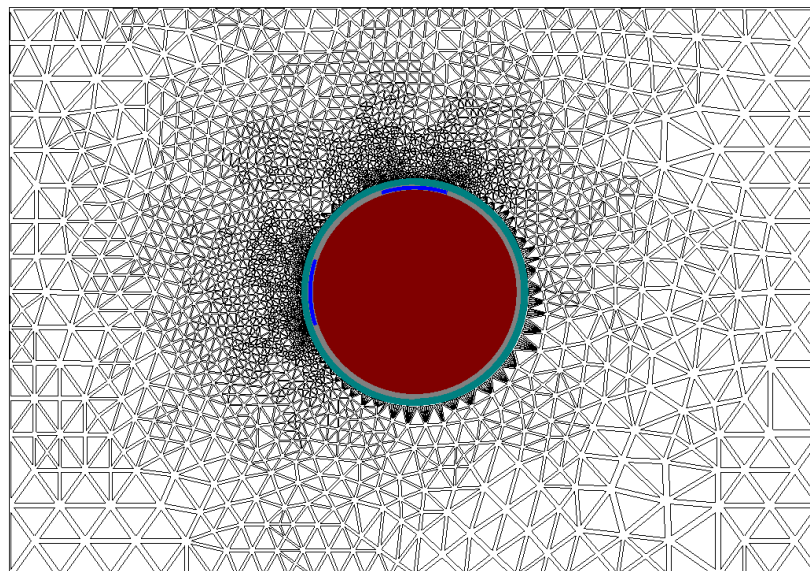
Figure 4.9: Typical mesh generated in simulated water conditions.

4.4 Analysis and optimisation of the sensor using FEM

4.4.1 Inner cross section and assessment of access tube influence

The structure of the inner cross section was investigated using first a solid dielectric rod and then a hollow dielectric tube supporting two electrodes of 8.00 mm arc length. The capacitance was then computed for different electrode spacing angles of 60º, 90º and 120º respectively. Simulations with the same geometric characteristics were also carried out investigating the influence of the access tube on the computed capacitance.

Figure 4.10 presents the computed capacitance for simulations with the electrodes enclosed by an access tube. The maximum capacitance value of 138 pF/m corresponded to water conditions for electrodes placed at an angle of 60º attached to a solid dielectric rod. The capacitance decrease to 129 pF/m and 120 pF/m with increased angle position of the electrodes to 90º and 120º respectively. Greater capacitance values were also recorded when a dielectric solid rod inner section was simulated compared to the models with a hollow tube (see Figure 4.10).
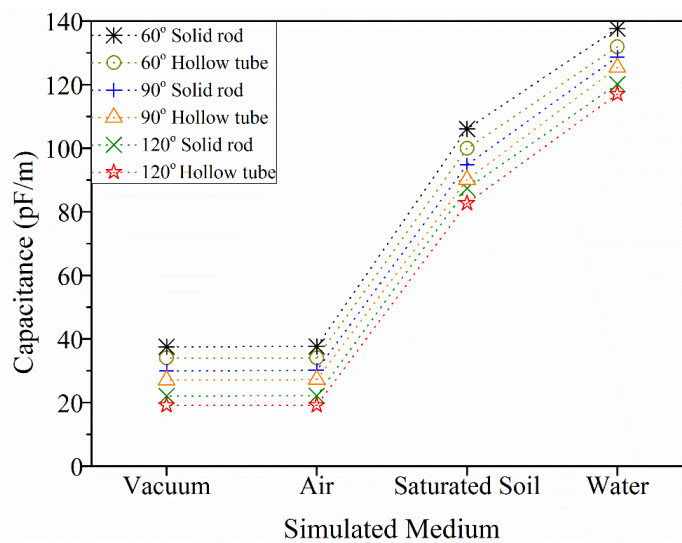
Figure 4.10: Computed capacitance for different inner tube cross sections and electrodes placed at various angle positions enclosed by an access tube.

Figure 4.11 shows the results obtained with the models simulated without the presence of the access tube which led to a significant increase in the computed capacitance values. The maximum capacitance (774 pF/m) also corresponded to water conditions for electrodes placed at 60º and attached to a dielectric rod. Increased electrode angles of 90º and 120º led to a decrease in capacitance to 604 pF/m and 542

pF/m respectively. The capacitance difference between water and saturated soil conditions was recorded at 516 pF/m, 402 pF/m and 361 pF/m for electrodes attached to a dielectric rod and positioned at an angle of 60º, 90º and 120º respectively (see Figure 4.11).
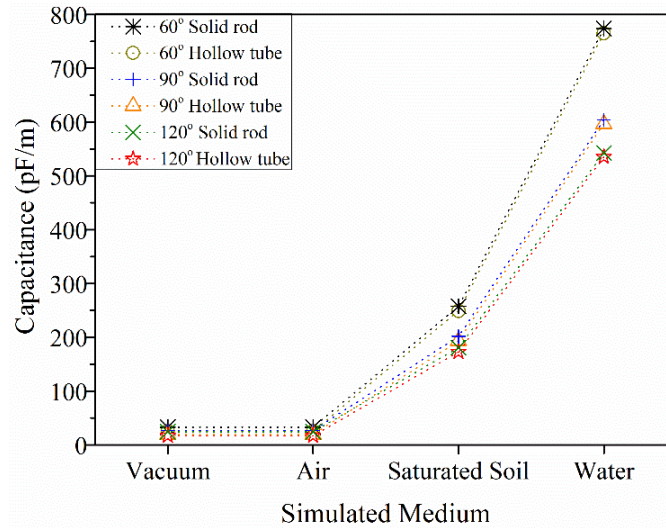
Figure 4.11: Computed capacitance for different inner tube cross sections and electrodes placed at various angle positions without the presence of the access tube.

In conclusion, the two simulated inner cross sections resulted in a capacitance difference at the range of 7 to 8 pF/m between the maximum values obtained for the electrodes attached to a dielectric rod than a hollow tube. The effect of the inner cross section (solid rod or hollow tube) on capacitance was therefore regarded as insignificant compared with changes due to the external medium. The presence of the required access tube also significantly decreased the obtained total capacitance for all tested conditions. This is due to the low permittivity of the access tube that encloses the electrodes and to the air gap that was simulated at the electrode position between the inner cross section and the access tube which dominated the total capacitance. The models presented in the following sections were simulated only with a solid dielectric rod as this inner section will increase the mechanical robustness of the sensor and will be easier to manufacture. The solid rod inner section was simulated to support two electrodes that are enclosed by an access tube.

4.4.2 Optimum electrode angle position

The position of the electrodes was investigated by placing two electrodes with arc length of 8.00 mm at different centre to centre angle positions of 60º, 90º and 120º.

The optimum electrode location was defined according to the magnitude and the spatial distribution of vector D of the electric flux density that was obtained for the different simulated conditions as presented in Figures 4.12, 4.13, 4.14 and 4.15.

As shown in Figure 4.12 (a), the obtained *magD* in saturated sediment conditions is greater with the electrodes placed at an angle of 60°, having a maximum value of 1.23×10^{-8} C/m². The maximum *magD* is reduced to 9.36×10^{-9} C/m² and 8.46×10^{-9} C/m² as the electrode angle is increased to 90° and 120° respectively, as illustrated in Figures 4.12 (b) and 4.12 (c) respectively.
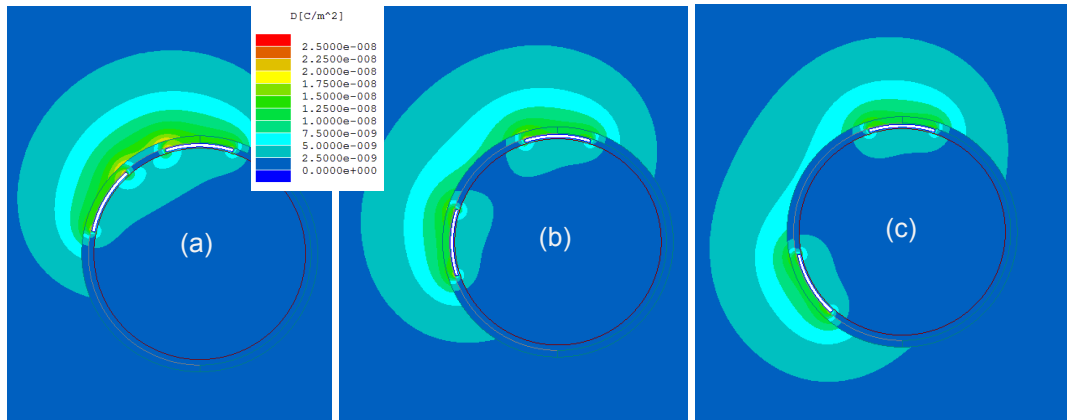
Figure 4.12: *MagD* obtained in saturated sediment conditions with the electrodes placed at angle positions of **(a)** 60°, **(b)** 90° and **(c)** 120°.

The maximum *magD* obtained in water conditions is also recorded for the electrodes placed at an angle of 60° with the value of 1.68×10^{-8} C/m² [see Figure 4.13 (a)]. The magnitude of the electric flux density is reduced to 1.35×10^{-8} C/m² and 1.26×10^{-8} C/m² when the electrodes were modelled at angles of 90° and 120°, as shown in Figures 4.13 (b) and 4.13 (c) respectively.
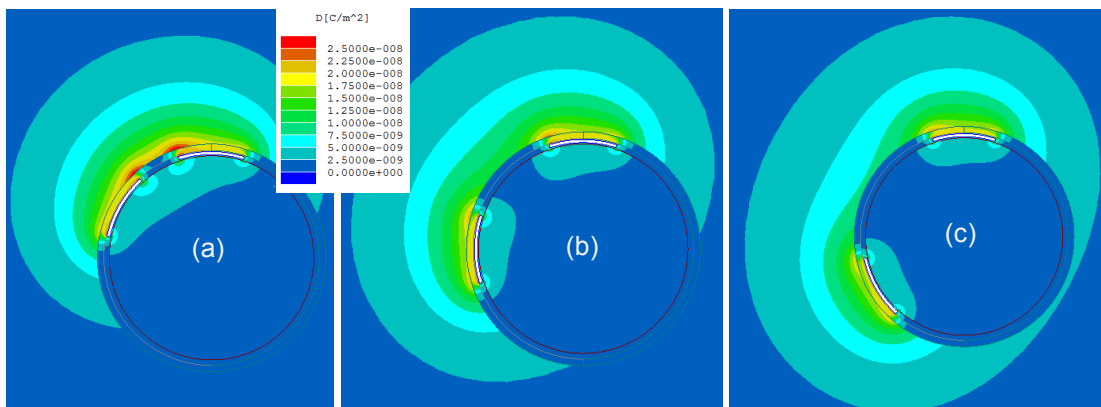
Figure 4.13: *MagD* obtained in water conditions with the electrodes placed at angle positions of **(a)** 60°, **(b)** 90° and **(c)** 120°.
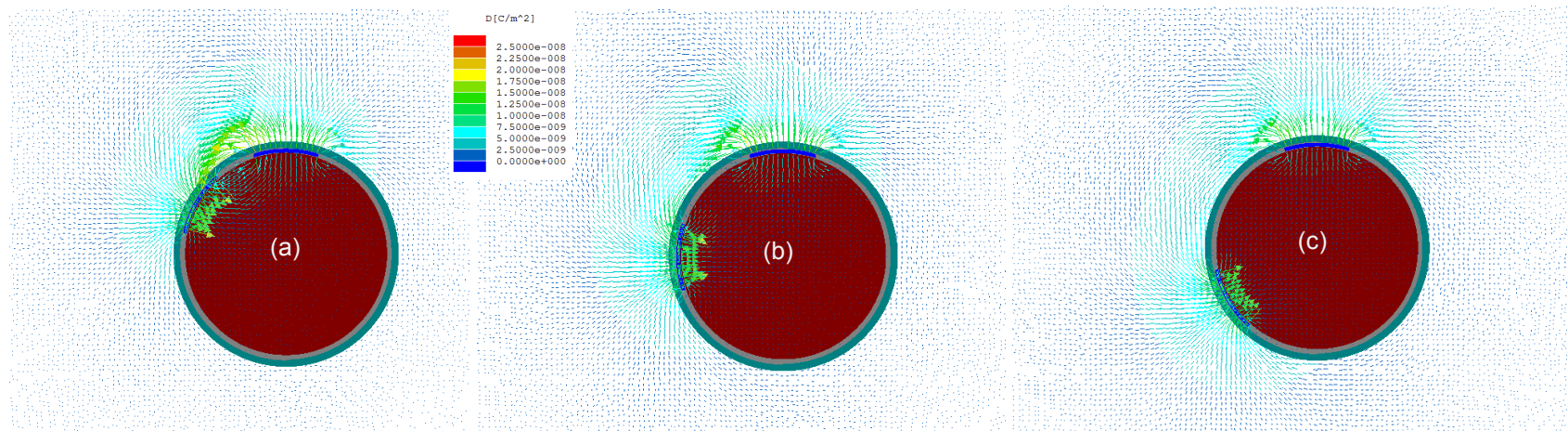
Figure 4.14: Vector electric flux density obtained in saturated sediment conditions with the electrodes placed at angle positions of **(a)** 60º, **(b)** 90º and **(c)** 120º.
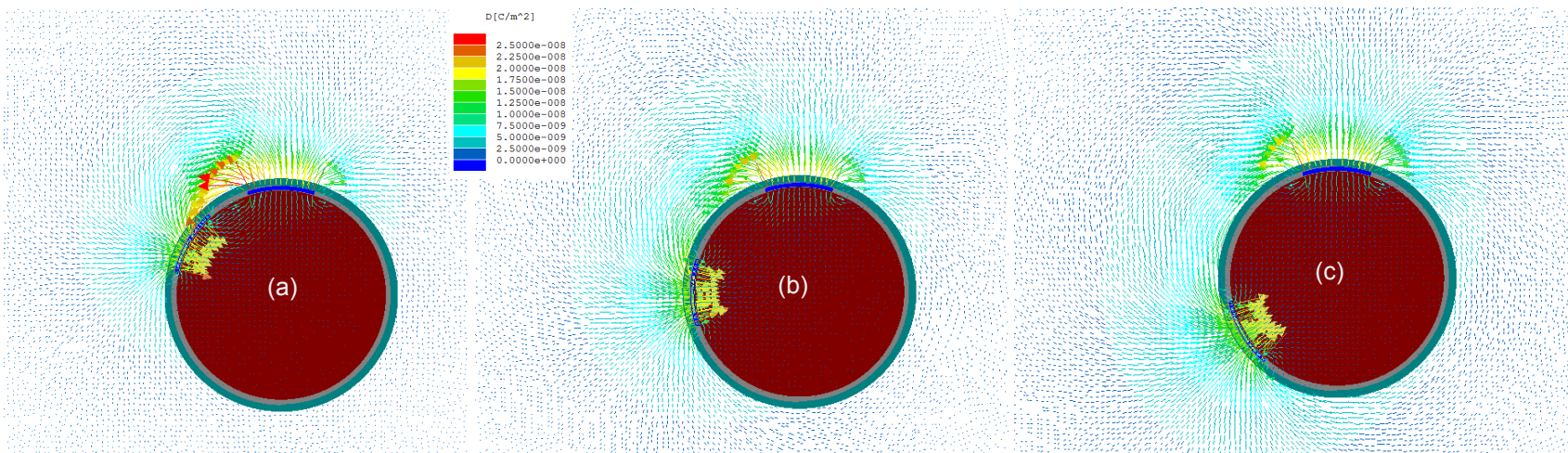
Figure 4.15: Vector electric flux density obtained in water conditions with the electrodes placed at angle positions of **(a)** 60º, **(b)** 90º and **(c)** 120º.

In conclusion, the small distance between the electrodes when placed at an angle of 60° resulted in a greater *magD*, but also led to a weaker field penetration outside the access tube. Conversely, a greater electrode angle of 120° led to a decrease of the *magD* but also to an overall increase of the penetration area outside the access tube. It is concluded that best compromise is achieved for the angular position of 90° where the obtained capacitance, the strength and penetration area of the electric flux density are considered satisfactory. The models presented in the following section were therefore analysed according to the optimum electrode angle of 90°.

4.4.3 Optimum electrode arc length

The effect of increased electrode arc length on the obtained capacitance, the *magD* and the vector *D* of the electric flux density is the focus of this section. The simulations were carried out with the electrodes positioned at an angle of 90° with arc lengths of 8.00 mm, 9.30 mm, 11.85 mm and 13.75 mm. Increased electrode arc length resulted in greater capacitance with the maximum value obtained in simulated water conditions and for electrode length of 13.75 mm (see Figure 4.16).
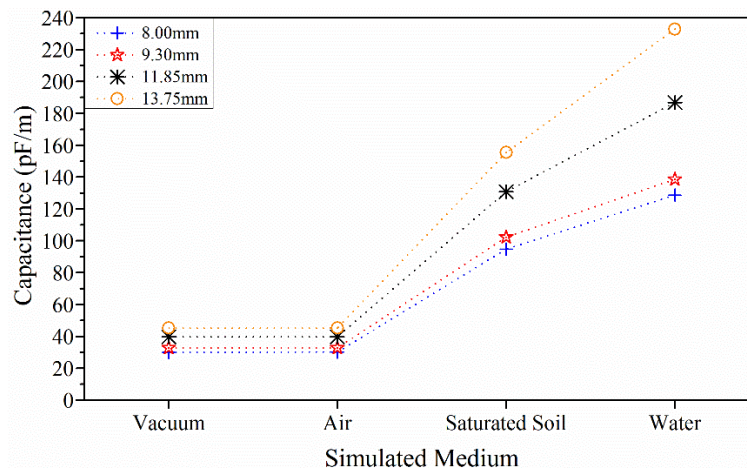
Figure 4.16: Capacitance values obtained for various simulated media and electrode arc lengths.

Figure 4.17 presents the predicted capacitance difference between water and saturated sediment conditions for increased electrode size. The capacitance difference for 8.00 mm electrode arc length is recorded at 33.92 pF/m and further increases by 7 %, 65 % and 128 % for electrode sizes of 9.30 mm, 11.85 mm and 13.75 mm respectively.
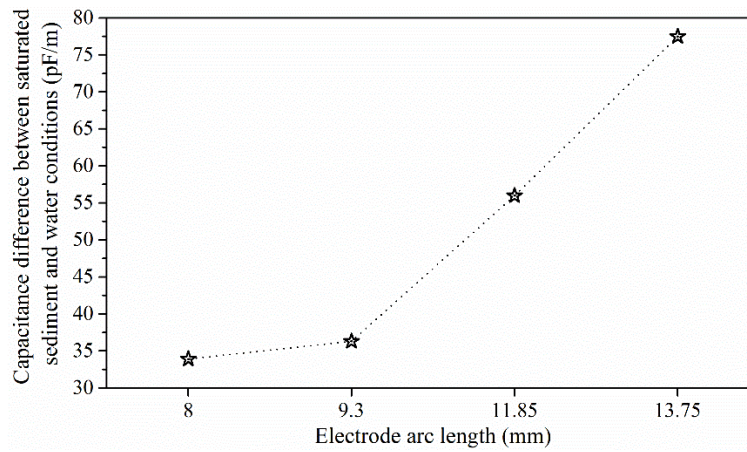
Figure 4.17: Capacitance difference obtained between water and saturated sediment conditions for various electrode arc lengths.

Figures 4.18 and 4.19 show the variation of the *magD* obtained for different simulated electrode lengths in saturated sediment and water conditions respectively. Greater *magD* is obtained for increased electrode size with a maximum value of 1.40×10^{-8} C/m^2 recorded for electrode arc length of 13.75 mm in saturated sediment (see Figure 4.18). The maximum strength of the electric flux density in the simulated water environment is also obtained for the electrode arc length of 13.75 mm, which corresponds to 2.13×10^{-8} C/m^2 (see Figure 4.19).
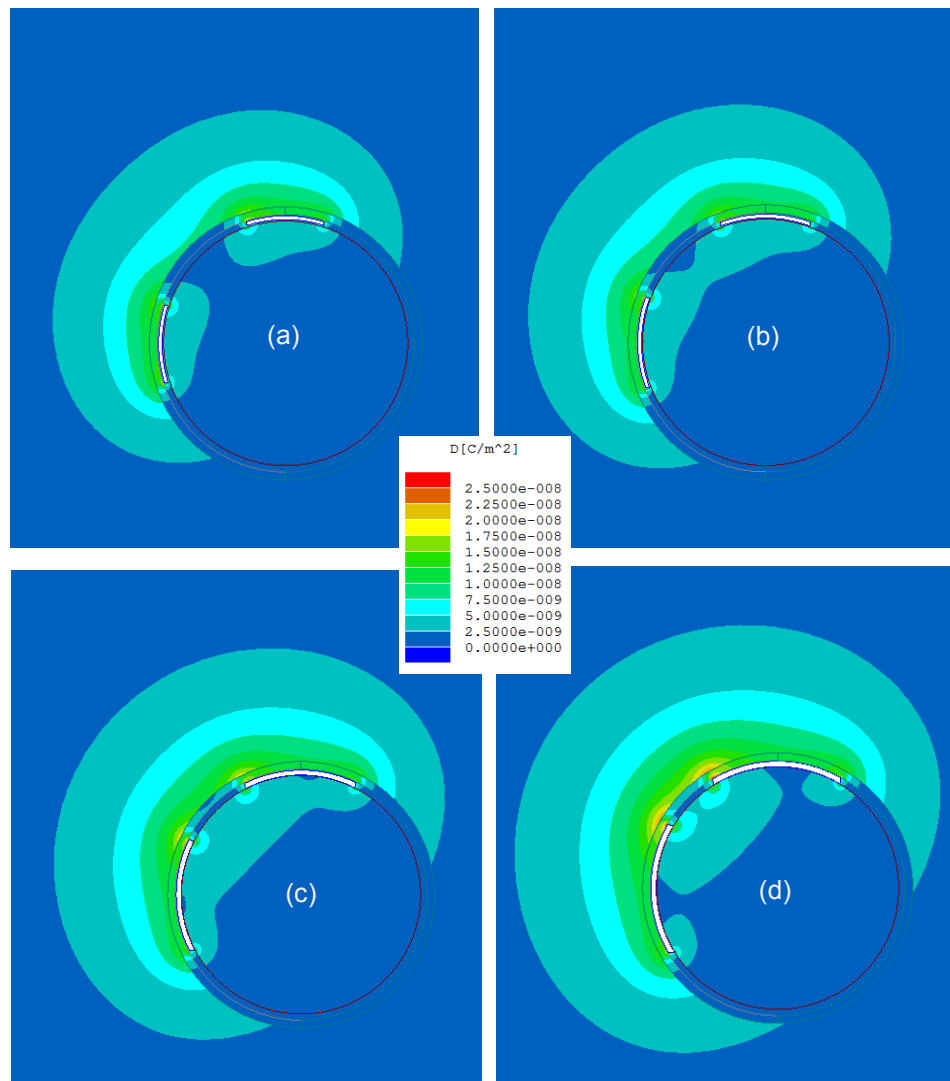
Figure 4.18: *MagD* obtained in saturated sediment conditions for electrode arc lengths of **(a)** 8.00 mm, **(b)** 9.30 mm, **(c)** 11.85 mm and **(d)** 13.75 mm.
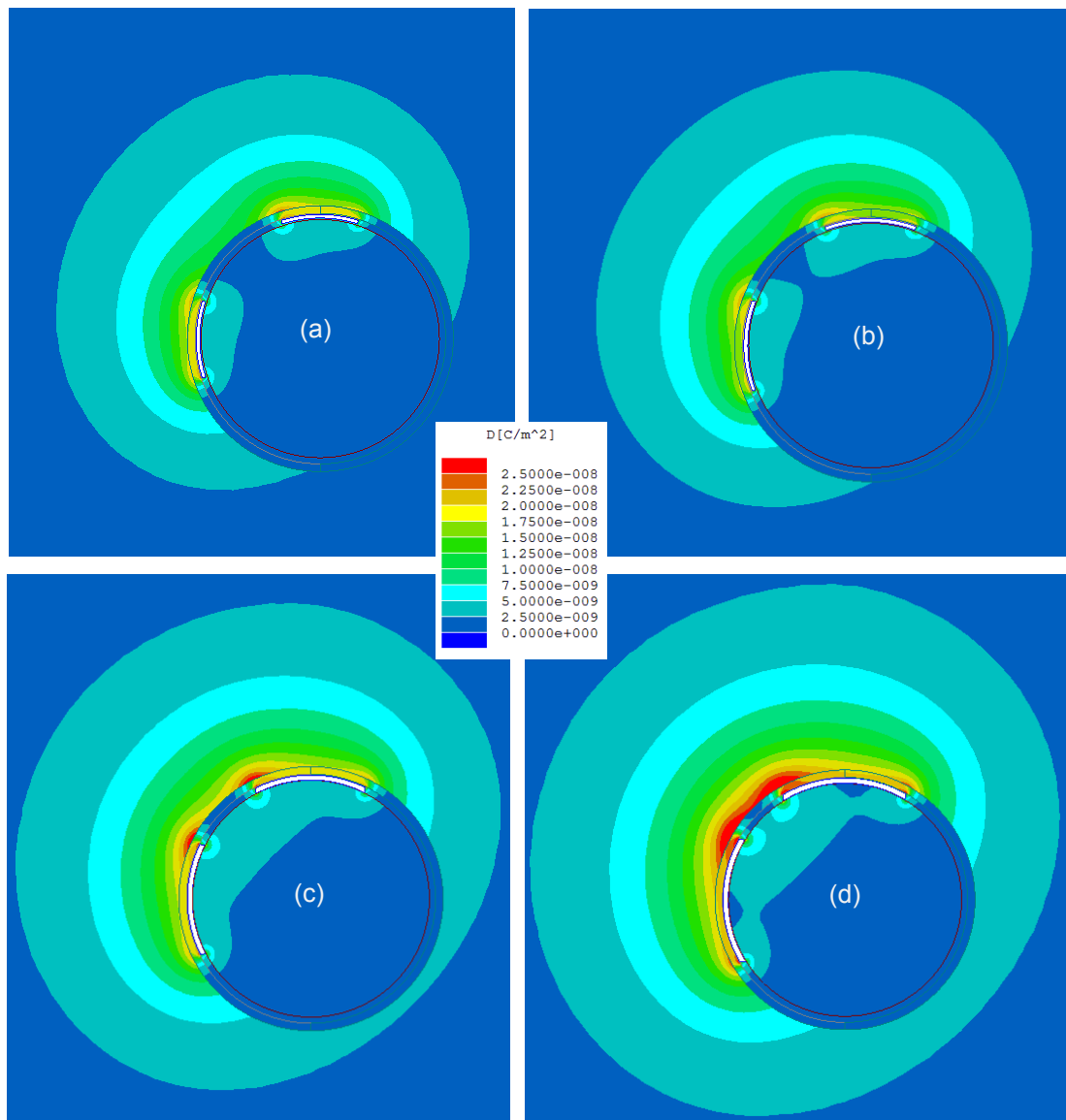
Figure 4.19: *MagD* obtained in water conditions for electrode arc lengths of **(a)** 8.00 mm, **(b)** 9.30 mm, **(c)** 11.85 mm and **(d)** 13.75 mm.

Figure 4.20 and 4.21 present the vector D of the electric flux density obtained in saturated sediment and water environment respectively. The penetration area around the sensor is also observed greater and to be maximised in water conditions for increased electrode arc length (see Figure 4.21).
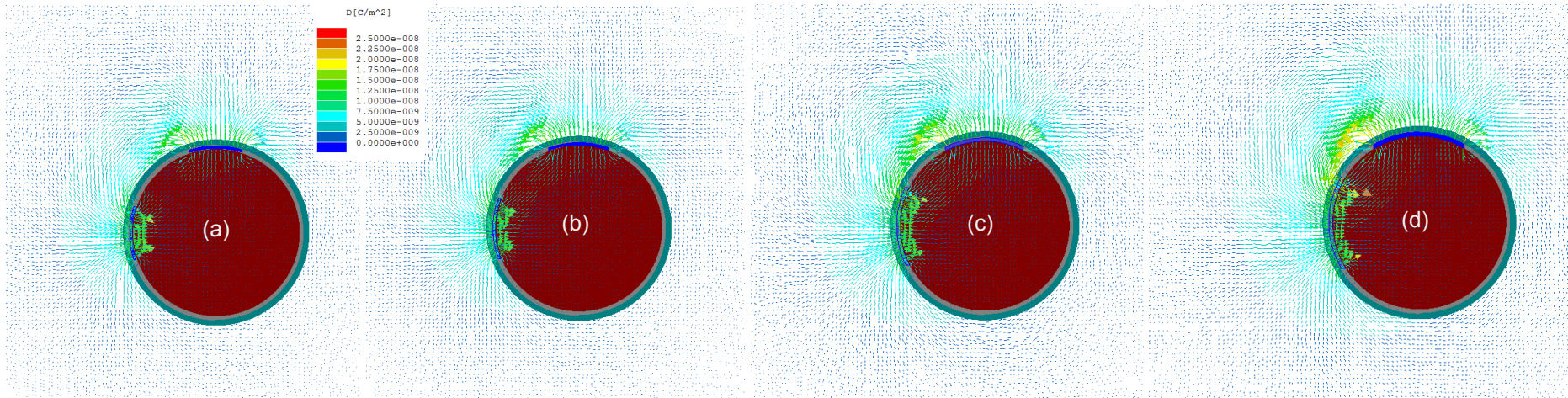
Figure 4.20: Vector D obtained in saturated sediment conditions for electrode arc lengths of **(a)** 8.00 mm, **(b)** 9.30 mm, **(c)** 11.85 mm and **(d)** 13.75 mm.
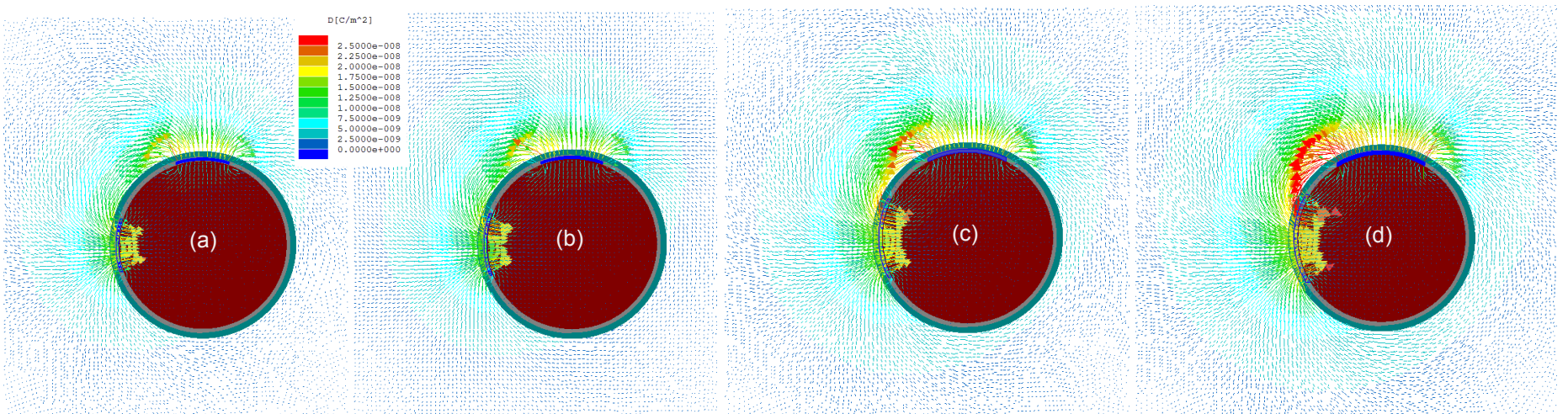
Figure 4.21: Vector D obtained in water conditions for electrode arc lengths of **(a)** 8.00 mm, **(b)** 9.30 mm, **(c)** 11.85 mm and **(d)** 13.75 mm.

The obtained results indicate that greater electrode sizes maximise the sensitivity of the sensor to the various simulated external environmental conditions. For electrode arc length of 13.75 mm, the capacitance, *magD* and field penetration area are increased and appear to be the optimum compared to other simulated electrode sizes. This geometric configuration should provide increased sensitivity of the sensor to changes to medium permittivity, therefore to scour and sediment deposition processes.

4.4.4 Final design of the prototype scour sensor

The proposed design of the prototype scour probe consists of four strips with arc length of 13.75 mm placed at a centre to centre angle of 90º and paired opposite to each other. The electrodes (i.e. each pair of strips) are attached to an insulating solid rod. The electric field generated between the four strips will allow for monitoring of scour and sediment deposition processes around the probe location. The electric potential of the transmitter and receiver electrodes were set to +1 V and 0 V respectively for the purpose of electrostatic simulation.

The *magD* and electric field penetration area obtained in air ($\varepsilon_\alpha = 1.0006$), saturated sediment ($\varepsilon_s = 25$), water ($\varepsilon_w = 80$) and deposited sediment ($\varepsilon_d = 35$) simulated conditions, are presented in Figure 4.22. The sediment deposition condition is simulated with a greater permittivity value compared to the original sediment due to different density conditions that are anticipated to occur between the two environments as presented by Michalis et al. (2014) and in Chapter 3.

As Figure 4.22 (a) indicates, the electrostatic field that is generated in air environment between the sensor electrodes passes more readily through the dielectric material of the inner cross section. It is also observed that is hardly penetrating the medium outside the access tube. This is attributed to the greater permittivity value of the dielectric rod when compared to air environment. The *magD* and penetration area are significantly increased in the other simulated conditions with an electric field that has a good circular symmetry being generated between the sensor electrodes, as illustrated in Figures 4.22 and 4.23. The maximum *magD* is obtained in water environment while greater strength of electric field is also recorded in deposited sediment compared to saturated sediment conditions. For all simulated models the maximum *magD* that is generated between the transmitter and receiver electrodes was

observed for the region that corresponds to the edge of the electrodes (see Figures 4.22 and 4.23).
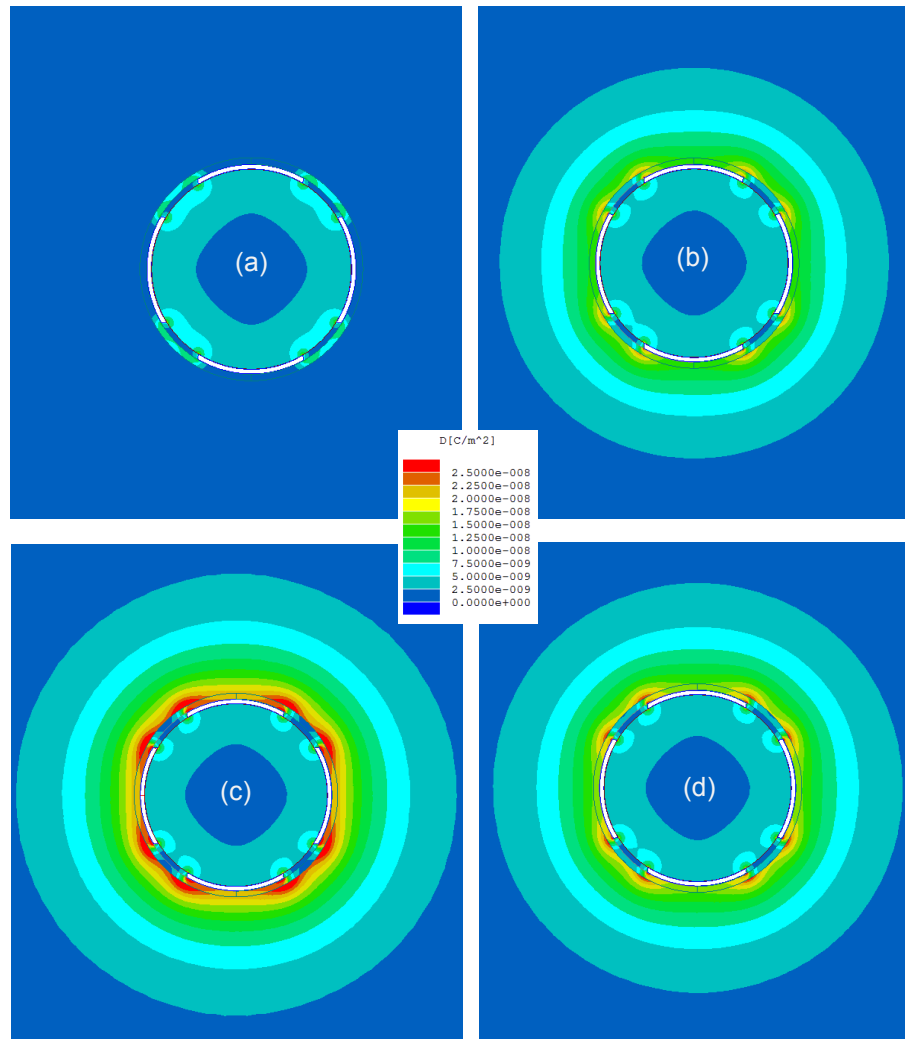
Figure 4.22: *MagD* and penetration of electric field obtained in **(a)** air, **(b)** saturated sediment, **(c)** water and **(d)** deposited sediment simulated conditions for the optimum electrode design.
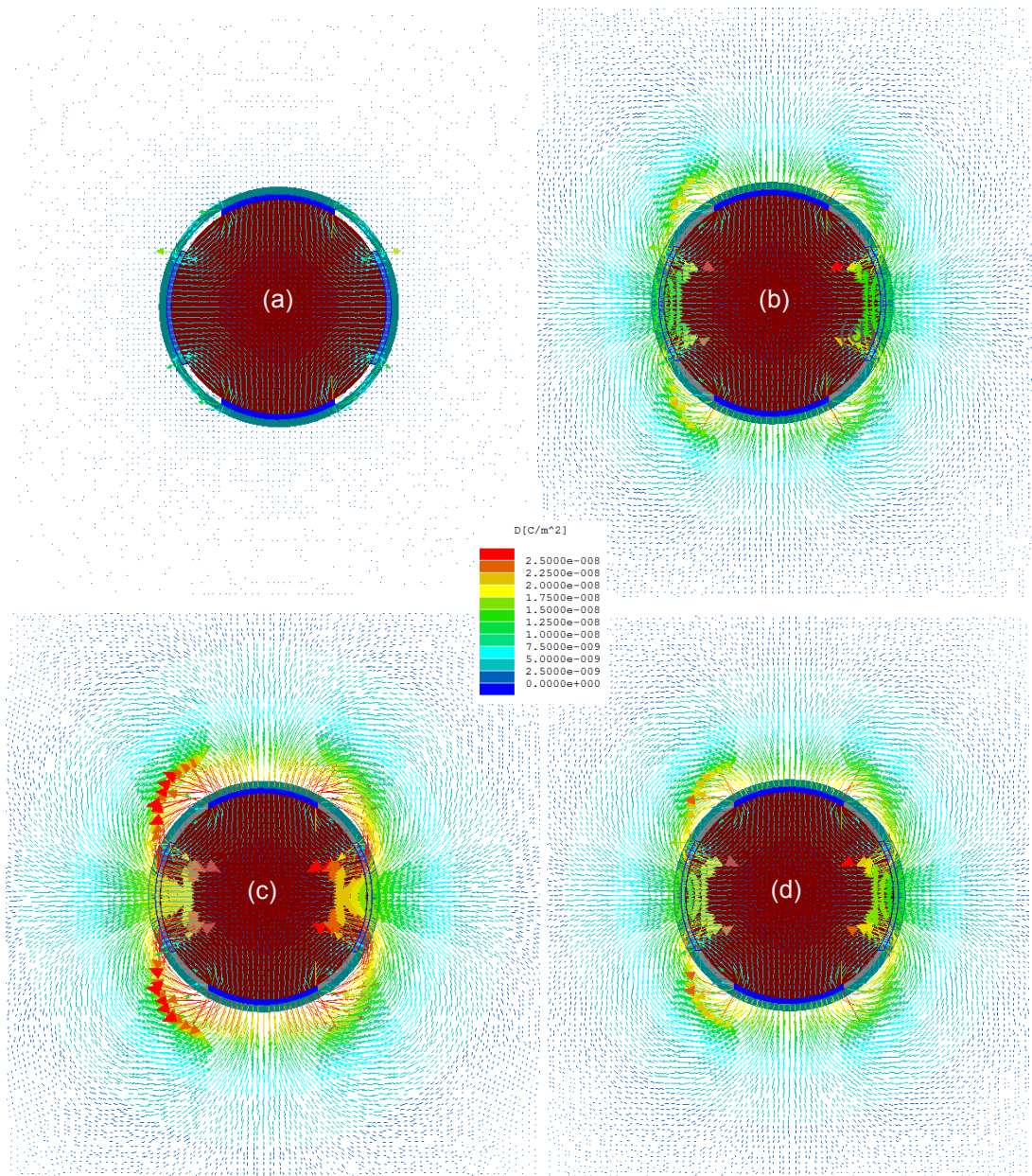
Figure 4.23: Vector *D* and penetration of electric field obtained in **(a)** air, **(b)** saturated sediment, **(c)** water and **(d)** deposited sediment simulated conditions for the optimum electrode design.

In conclusion, the simulations that comprised of four paired strips led to a circular symmetry of the generated electric flux density which extended into the surrounding medium. The *magD* was found to be maximised in water environment due to its higher permittivity value compared to the other simulated environments.

4.4.5 Sampling volume of the sensor

The extent of electric field penetration into the medium and the *magD* are the factors having a significant effect on the sensitivity of the proposed sensor to the external environmental conditions. The penetration distance and strength of the electric field were therefore selected to be recorded at three different sampling positions, as shown in Figure 4.24.
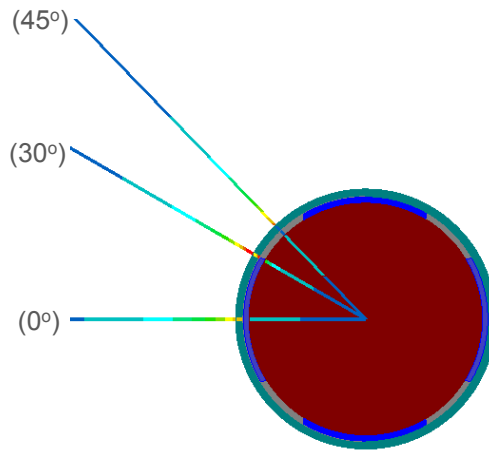
Figure 4.24: Sampling volume of the electric field generated at different positions that correspond to the middle of the electrode with an angle of 0º, at the edge with an angle of 30º and at half distance between the 2 electrodes with an angle of 45º.

As shown in Figure 4.25, the maximum penetration distance of the electric field outside the access tube is achieved in simulated water conditions and corresponds to 53 mm. The penetration distance is decreased to 48.3 mm and 43.7 mm in deposited and saturated sediment environment respectively. As shown in Figures 4.25 (a), 4.25 (b) and 4.25 (c), higher strength electric field is also achieved in water conditions ($2.09 \times 10^{-8}\,\text{C/m}^2$) for the angle position of 30º compared to saturated ($1.36 \times 10^{-8}\,\text{C/m}^2$) and deposited soil conditions ($1.57 \times 10^{-8}\,\text{C/m}^2$) respectively. It is also observed that the strength of electric field that extends into the medium is decaying significantly after the distance of 25 mm for all the different simulated conditions and sampling volume angular positions (see Figure 4.25).
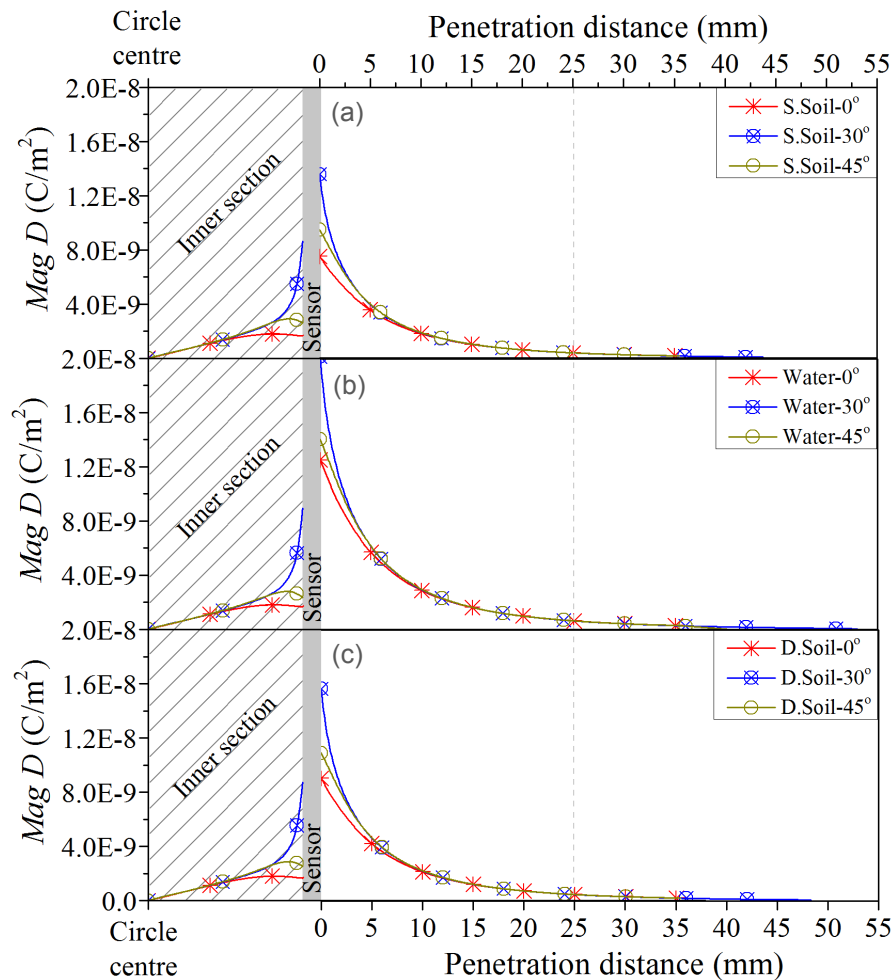
Figure 4.25: Penetration distance and strength of electric field generated in simulated **(a)** saturated soil (s.soil), **(b)** water and **(c)** deposited soil (d.soil) conditions for various sampling locations. The dashed and grey areas correspond to the electric field generated at the inner section and at the electrode location respectively.

The obtained results indicate that the maximum *magD* and penetration distance of the electric field in all simulated environments is achieved for the sampling location of 30°, which corresponds to the horizontal distance recorded to the edge of the sensor electrode. Greater strength of electric field is also observed for the sampling position at the half distance between the 2 electrodes (45°) compared to the middle of the electrode (0°), which exhibits the minimum *magD*.

4.5 Conclusions

This study has presented the development and optimisation via Finite Element Modelling (FEM) of the components of a new impedance-based electromagnetic sensor for measuring scour and re-deposited sediment conditions at foundation elements.

The investigation initially focused on the influence of the various geometric components of a two strip electrode sensor on the computed capacitance, the strength and penetration area of the electric field. The two simulated inner cross sections resulted in a capacitance difference at the range of 7 to 8 pF/m between the maximum values obtained for the electrodes attached to a dielectric rod than a hollow tube. This variation in the capacitance output is mainly due to the internal air gap of the hollow tube which reduces the overall permittivity when compared to that of the solid rod.

The presence of the necessary access tube had a significant decreasing effect on the total capacitance and therefore the sensitivity of the sensor. This is attributed to the low overall capacitance caused by the presence of the access tube and the simulated air gaps. These two parameters dominated and had a major effect on the total capacitance, even though they have a small physical size compared to the external medium.

Increased angular separation of the electrodes around the central dielectric rod had a significant decreasing impact on the computed capacitance and the strength of the electric flux density. The small distance between the electrodes when placed at an angle of 60° resulted in a greater *magD* due to direct coupling between the edges of the electrodes, but also led to a weaker field penetration outside the access tube. Conversely, a greater electrode angle of 120° led to a decrease of the *magD* but also to an overall increase of the penetration area outside the access tube. The obtained results indicated that the optimum geometric configuration corresponds to the electrodes placed at an angle of 90°. This angular position is considered to fulfil the criteria compared to the other electrode positions as the obtained capacitance, the strength and penetration area of the electric flux density are considered satisfactory.

The overall electric flux density was observed to be increased in water when compared to saturated sediment conditions for all simulated electrode angular positions. This is due to the large difference of the relative permittivity of water as

compared to saturated sediment, which results in a greater magnitude of electric field and in increased capacitance values in simulated water environment.

The investigation was then continued by simulating various electrode sizes. Greater capacitance values were recorded for the maximum electrode arc length of 13.75 mm. The same electrode arrangement also gave the maximum difference between saturated sediment and water conditions. This is due to the increased electrode area and the near proximity of the two electrodes that increased the overall capacitance. Greater electrode length also led to a significant rise of the strength and penetration area of the electric flux density. The electrode length of 13.75 mm is expected to provide increased sensitivity of the sensor to changes in medium permittivity therefore to scour and sediment deposition processes.

The final design of the proposed sensor comprises of four paired strips generating a circular symmetrical electric field which enables good penetration into the medium outside the access tube. The *magD* was found to maximise in water environment compared to the other simulated environments. Due to the proximity of the electrodes, the maximum strength and penetration area into the external medium was obtained for the sampling location of 30° which corresponds to the horizontal distance recorded to the edge of the sensor electrode. For all the sampling angular positions the strength of the electric field extending into the medium was found to be significantly decreased after the penetration distance of 25 mm.

The optimum sensor components that were defined in this study will allow for monitoring of bed level conditions around the probe location and therefore provide improved accuracy to scour and sedimentation processes. The investigation continued with the fabrication and laboratory evaluation of a sensor based on the aforementioned optimum electrode arrangements.

References

Karmel, P.R., Colef, G.D., & Camisa, R.L. (1998). *Introduction to electromagnetic and microwave engineering*. New York, Wiley.

Michalis, P., Tarantino, A., and Judd, D.M. (2014). Electromagnetic Sensors for Monitoring of Scour and Deposition Processes at Bridges and Offshore Wind Turbines. *European Geosciences Union General Assembly 2014*, Vienna, Geophysical Research Abstracts, Vol. 16.

Roth, K.R., Schulin, R., Fluhler, H., and Attinger, W. (1990). Calibration of Time Domain Reflectometry for Water Content Measurement using a Composite Dielectric Approach. *Water Resources Research,* 26(10), pp. 2267-2273.

Whalley, W.R., Dean, T.J. and Izzard P. (1992). Evaluation of the Capacitance Technique as a Method for Dynamically Measuring Soil Water Content. *Journal of Agricultural Engineering Research*, 52, pp. 147-155.

Chapter 5

A New Electromagnetic ADT Sensor for Monitoring Scour and Sediment Deposition Evolution

*Sections of this chapter are an edited version of the published or at preparation/submission stage articles in the following journals and international conference proceedings:

Michalis, P., Judd, D.M. and Tarantino, A. Design and Optimisation of a New Impedance-based Sensor for Scour and Sediment Deposition Monitoring. *IEEE Sensors Journal* [In preparation, to be submitted within 2 months].

Michalis, P., Judd, D.M. and Tarantino, A. Development and Laboratory Characterisation of a New Electromagnetic ADT Sensor for Scour and Sediment Deposition Monitoring at Hydraulic and Marine Structures. *IEEE Transactions on Geoscience & Remote Sensing* [In preparation, to be submitted within 2 months].

Michalis, P., Tarantino, A., and Judd, D.M. (2014). Electromagnetic Sensors for Monitoring of Scour and Deposition Processes at Bridges and Offshore Wind Turbines. In: *European Geosciences Union General Assembly 2014*, Vienna, Geophysical Research Abstracts, Vol. 16, EGU2014-9427-6.

Michalis, P., Judd, D.M., and Tarantino, A. (2014). Real-time Monitoring of Scour and Sedimentation Evolution with a New Developed Prototype Sensor. In: *12th International Conference of Protection and Restoration of the Environment*, Skiathos, Greece, ISBN: 978-960-88490-5-1.

5.1 Introduction

This chapter explores new and cost effective methods for monitoring scour and sediment deposition processes in the vicinity of bridges and offshore wind turbine foundations.

The study initially examines the capability of a prototype sensor to detect bed level variations using a capacitance-based method. Since preliminary tests did not provide satisfactorily results, the electromagnetic response of the prototype sensor is investigated in depth by means of network analyser to explore the features of the transmitted signal in various frequency ranges. This investigation aims to detect the most suitable wave propagation characteristic variable that could be easily measured by a low-cost detector implemented in a prospective commercial sensor to monitor bed level variations. In particular, attention is paid to the characteristics of the transmitted signal because signal processing is simpler and the cost of electronics is reduced compared to reflection wave measurements.

The network analyser investigation revealed that the amplitude of the transmitted signal at given frequency could be an appropriate variable to be associated with scour depth. The electromagnetic sensor was therefore developed based on the Amplitude Domain Transmissometry (ADT) measuring principle which appears to be the first application for monitoring soil-water mixtures.

The study then focuses on the development of an analogue model to predict and control the optimum frequency (the frequency at which amplitude of transmitted signal should be read). The analogue consisted of stub lines to mimic the frequency response of the prototype sensor.

A series of experiments conducted to evaluate the signal of the prototype sensor and the ADT technique to detect scour and deposited sediment processes. The performance of the new sensor is assessed with special consideration on the identification of its optimum frequency under different environmental conditions (temperature, salinity, soil type). The investigation then focuses on the optimisation of the sensor design to enhance the accuracy of the calibration curve relating the amplitude of the transmitted signal to scour depth.

Scaling procedures based on the theoretical relationship between the transmitted signals with the electrode length are also verified using a small-scale optimised sensor. The capability of the small-scale sensor to accurately measure scour and re-deposited sediment processes is also validated in real-time flume experiments. Finally, the major findings of this chapter are summarised and presented.

5.2 Fundamentals of EM wave propagation

5.2.1 Transmission line applications on soil samples

Numerous studies focused on the interpretation of measurable Electro-Magnetic (EM) variables as functions of frequency and of the soil moisture content in laboratory environment and field conditions. The principle of using EM methods to determine soil properties relies on the large difference between the permittivity of water when compared to dry soil mediums.

Time Domain and associated methods

The majority of reported investigations employ Time Domain (TD) measurements to provide an estimation of soil properties. This is based on the characteristics of reflected and transmitted signals subjected to an impedance mismatch. For example, Time Domain Reflectometry (TDR) has been widely applied in order to provide dielectric permittivity measurements on soil samples (Hoekstra and Delaney, 1974; Davis and Annan 1977; Topp et al., 1980; Topp et al., 1984; Topp and Davis 1985; Ledieu et al., 1986; Zegelin et al., 1989; Persson, 2002; Robinson et al., 2003; Bittelli et al., 2007; and Skierucha et al., 2012). The obtained permittivity value is then used to estimate the volumetric water content through calibration curves as proposed by Topp et al. (1980) and Roth et al. (1990). TDR technology has also been deployed to detect scour measurements at underwater foundation elements (Dowding and Pierce, 1994; Yankielun and Zabilansky, 1999; Yu and Yu, 2009; Yu and Zabilansky, 2006; Yu et al., 2013; and Tao et al., 2014).

In TDR, a transmission line with known length is inserted into the sediment. The soil permittivity is determined based on the propagation velocity, which is a function of the soil dielectric permittivity. However, a solution for scour monitoring with the use of TDR technology has not been realised due to the high cost of these instruments

($\approx$ £9000 per sensor) and because they require specialist personnel due to complicated signal analysis (Lueker et al., 2010). The sensor battery life, the performance in conductive mediums and the cable length that the probe can be attached to without signal attenuation (Blonquist et al., 2005) also limits the application of TDR sensors for scour monitoring.

Time Domain Transmissometry (TDT) has been also investigated in recent times for the estimation of water content (Topp et al., 2001; Harlow et al., 2003; Hook et al., 2004; and Blonquist et al., 2005). In a TDT sensor, the pulse travels one way along the length of the probe and the transmitted signal is then recorded. The pulse of the TDT sensor is less affected by the multiple reflections compared to the TDR sensor which simplifies the signal processing and reduces the cost (Will and Rolfes, 2013). The TDT sensor is also advantageous compared to TDR because the sampling is performed at the sensor location, therefore requires one way signal travel which reduces the signal attenuation. However, the installation of the TDT sensor is more difficult than TDR probes because of the required probe geometry. To date, the TDT technique has not been used for monitoring of scour or sedimentation processes.

Other studies also investigated the transformation of waveforms obtained with TD instruments to the Frequency Domain (FD) via Fast Fourier Transform (FFT) (Heimovaara, 1994; Harlow et al., 2003; Lin, 2003; and Jones and Or, 2004). FFT is used to extract information about the soil permittivity from the reflection waveform, which is obtained in the TD and interpreted in the FD.

A microwave Swept Frequency domain Instrument (SFI) was also developed by Pelletier (2006) and proposed as an alternative to TD methods for higher accuracy of soil moisture measurements. The SFI instrument connected to a network analyser provides a frequency difference measurement which is proportional to the signal's propagation time delay (Pelletier et al., 2012).

Impedance and Amplitude Domain methods

The Impedance and Amplitude Domain (AD) techniques have also been used to obtain information about the soil electrical properties. Early research efforts by Hipp (1974) indicated the ability of a transmission line to measure the permittivity of clay sediments over various frequency ranges. A coaxial line was utilised to provide the

complex impedances of soil samples by using an admittance bridge instrument. Measurements of the Voltage Standing Wave Ratio (VSWR) resulting from the input impedance of a soil-filled transmission line, were also used to estimate the reflection coefficient and hence the impedance of soil samples (Hipp, 1974).

An Amplitude Domain Reflectometry (ADR) instrument was also introduced by Gaskin and Miller (1996). The sensor comprises of a fixed impedance coaxial line connected to stainless steel wires and to a 100 MHz sinusoidal oscillator. The measuring principle of the ADR sensor is based on the reflection characteristics of the signal originated due to an impedance mismatch. The reflected component interferes with the incident signal causing a variation of voltage amplitude along the length of the transmission line. The amplitude difference obtained at two points, between the beginning of the transmission line and at the transmission line-probe junction, is recorded. This measurement is interpreted to assess the relative impedance of the probe and then the volumetric water content of the soil matrix (Gaskin and Miller, 1996). Further development of this invention was the Profile probe PR2 (Delta-T Devices Ltd, 2006) which consisted of stainless steel rings mounted on a plastic rod and inserted into an access tube. This ADR instrument also used an oscillator to transmit the incident wave at the fixed frequency of 100 MHz, through a matched transmission line to each sensor location which monitored soil moisture content up to six depths.

Among the instruments based on the ADR measuring principle, the PR2 sensor has been evaluated for scour and sedimentation monitoring, which was firstly carried out and presented by Michalis et al. (2012) and Michalis et al. (2013). A thorough validation of the same instrument in various density and water conditions using 'static' scour simulations and real-time flume experiments was also presented in Chapter 3.

The AD instruments provide a low-cost and accurate alternative to TD methods due to their lower operating frequency and standard circuity. The DC output signal of AD sensors also make them an attractive solution as they can be connected to conventional data loggers. However, instruments using the reflection coefficient in AD method do not take into account the multiple reflections that occur in mixtures with various interfaces. Due to the complex behaviour of the multiple reflections and for simplicity reasons, the sensors based on the reflection coefficient measurements only consider a single reflection at the transmission line (Gaskin and Miller, 1996). The

first single reflection measurement can provide a satisfactory accuracy with regards to the EM properties of soil when sensor electrodes are used to measure local regions around their location. However, their accuracy is likely to be compromised in samples which are characterised by different regions (e.g. various permittivity conditions that may occur at increased depth intervals below river/sea bed) because of the additional reflections occurring in the various boundaries that they are not taken into account by the instrument.

This study presents the development and laboratory characterisation of a new type of electromagnetic sensor. The prototype sensor with transmission line characteristics exploits the effect of the medium dielectric permittivity on the properties of Transverse Electro-Magnetic (TEM) wave, as a means of measuring scour and sedimentation processes. The developed instrument utilises the Amplitude Domain Transmissometry (ADT) method which appears to be employed for the first time for monitoring bed level variations at the foundation structure. The potential electronics concept of the sensor and the data interpretation is much simpler and less expensive compared to other instruments (e.g. TDR) and that thus is the main motivation of this study which aimed to develop a new, low-cost and accurate monitoring solution. The following sections aim to provide an insight of the fundamentals on the propagation of TEM waves in dielectrics and of the various concepts of transmission lines.

5.2.2 TEM wave propagation in dielectrics

EM methods have been widely used for the estimation of the medium permittivity value which is based on the interaction of EM waves with the electrical properties of the material to be measured. An electromagnetic wave is composed of oscillating electric and magnetic fields arising from varying distributions of electric charges and currents. As shown in Figure 5.1, when both the electric and magnetic fields are perpendicular to the direction of propagation the uniform wave plane is a TEM wave.
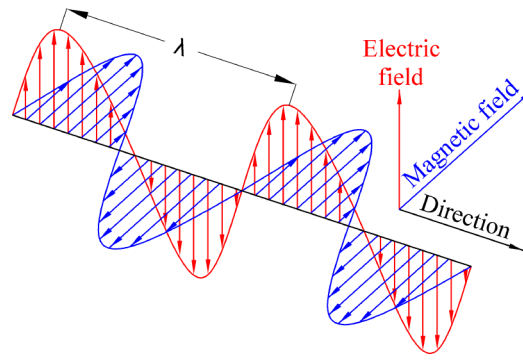
Figure 5.1: Propagation of a sinusoidal varying TEM wave in free space.

The wavelength (λ) is the distance between two adjacent crests or troughs and for the case of propagation in free space is given as follows:

$$\lambda = \frac{v}{f} \tag{5.1}$$

where in free space the phase speed (v) is the speed of light ($c = 3 \times 10^8 \, m/s$) and f (Hz) is the frequency of the light wave. The velocity of electromagnetic waves in free space (c) is a function of the permittivity $\varepsilon_o = 8.85 \times 10^{-12}$ F/m and permeability $\mu_o = 4\pi \times 10^{-7}$ H/m^{-1} of free space and is given by equation 5.2:

$$c = \frac{1}{\sqrt{\mu_o \times \varepsilon_o}} \tag{5.2}$$

The phase velocity (v) in a dielectric medium is defined by the relative permeability μ_r and the relative apparent permittivity of the material ε_r in which the wave propagates within, and is given as follows:

$$v = \frac{c}{\sqrt{\mu_r \times \varepsilon_r}} \tag{5.3}$$

Assuming non-magnetic media ($\mu_r = 1$), the signal propagation velocity is directly related to the relative permittivity (ε_r), by re-arranging equation 5.3 which gives:

$$\varepsilon_r = \left(\frac{c}{v}\right)^2 \tag{5.4}$$

The frequency (*f*) is also proportional to the wavelength and the signal propagation velocity (*v*) by combining equations 5.1 and 5.3:

$$f = \frac{c}{\lambda\sqrt{\mu_r \times \varepsilon_r}} \qquad (5.5)$$

The outcome is therefore dependent on the relative permittivity as a change in the value of the ε_r will alter the wavelength.

An example of the propagation of electromagnetic waves in different regions that are generated by a source is shown in Figure 5.2. The three regions are defined by each impedance (*Z*) value which is dependent on the magnetic permeability (*μ*) and the dielectric permittivity (ε_r) of the medium where the waves are propagating. At the boundary between regions 1 and 2, a portion of the incident wave will be reflected due to the different electrical properties between the two regions. The transmitted wave in region 2 will continue to propagate forward until the interface between regions 2 and 3 where a fraction of the wave is reflected while a net transmitted wave is forward propagating. The backwards travelling waves at the different boundaries will also be partitioned to reflected and transmitted waves, as shown in Figure 5.2. The energy in regions 1 and 2 remains constant at steady state, as the power that leaves the regions to form the reflected and transmitted waves is immediately replenished by the incident wave. The relative magnetic permeability of most soils is equal to 1 (Roth et al., 1990) since they are non-magnetic, therefore the main variable that governs the wave propagation through water and sediment boundaries is the medium dielectric permittivity.
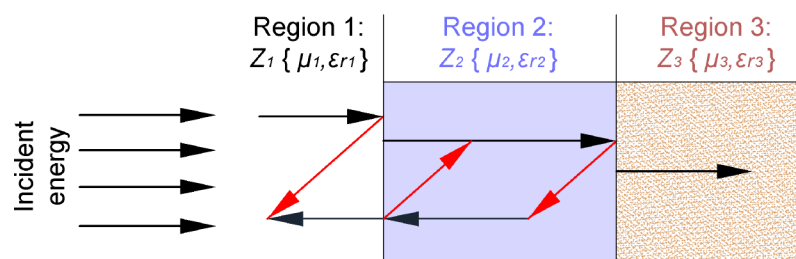
Figure 5.2: Propagation of TEM waves in different dielectric mediums.

Figure 5.3 shows the standing wave that is formed by the superposition between the total reflected backward propagating wave and the incident forward travelling wave. The standing wave oscillates but remains stationary and does not propagate. The nodes on a standing wave are null points with zero displacement, while antinodes are

the points where the maximum displacement is recorded. The distance between two crest antinodes is equal to a wavelength (λ) while between two adjacent nodes as well as between a node and antinode are equal to $\lambda/2$ and $\lambda/4$ respectively, as shown in Figure 5.3.
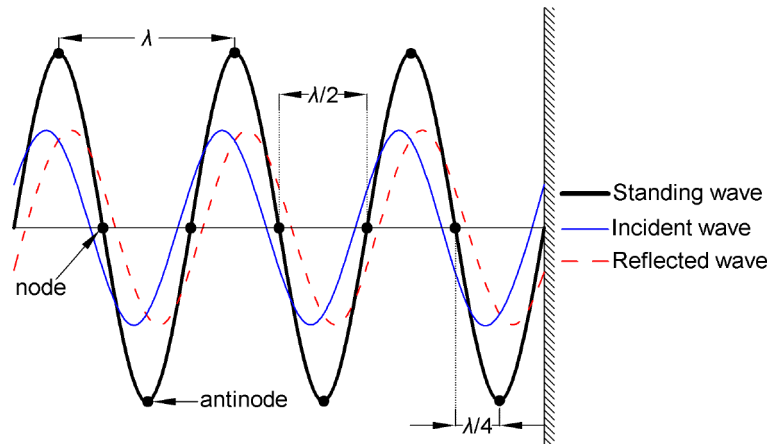
Figure 5.3: Standing wave pattern generated by the superposition of incident and reflected waves.

The characteristics of electromagnetic waves travelling along transmission lines have been employed in order to extract information about medium electrical properties. The transmission line parameters presented in the following section are considered of most importance as they can be utilised to provide an estimation of soil properties, therefore measurements of scour depth variations.

5.2.3 Transmission line concepts

Transmission lines consist of two or more parallel conductors used to transmit electric energy and signals that are generated from a source to a load. A structure is considered a transmission line when its length is greater than the one tenth of the wavelength of the signal it carries. The frequency of a sine wave that propagates into a transmission line remains unchanged but its amplitude will be gradually attenuated. By using the circuit theory concept, a transmission line can be divided in segments with length Δz [see Figure 5.4 (a)]. It can then be described by a series resistance R (Ohms/m), a series inductance L (Henries/m), a shunt conductance G (Siemens/m), and a shunt capacitance C (Farad/m), as shown in Figure 5.4 (b):
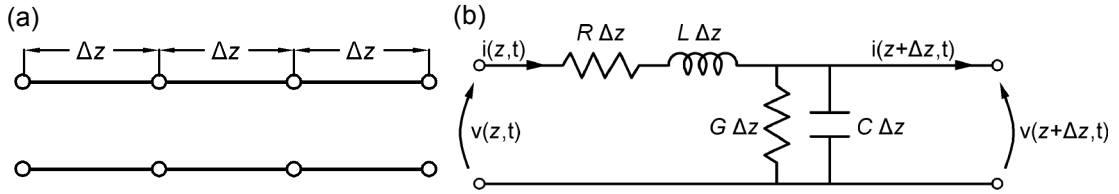
Figure 5.4: (a) Divided transmission line into sections with length Δz and **(b)** distributed circuit element model of a transmission line.

Kirchhoff's voltage and circuit laws are employed to define a relationship between the voltage and the current for the transmission line segment:

$$v(z,t) - R\Delta z i(z,t) - L\Delta z \frac{\partial i(z,t)}{\partial t} - v(z+\Delta z,t) = 0$$

$$i(z,t) - G\Delta z v(z+\Delta z,t) - C\Delta z \frac{\partial v(z+\Delta z,t)}{\partial t} - i(z+\Delta z,t) = 0$$

(eqs. 5.6)

The equations 5.6 are then divided with Δz and by taking the limit for $\Delta z \rightarrow 0$ they are reduced to the coupled transmission line equations:

$$\frac{\partial v(z,t)}{\partial z} + Ri(z,t) + L\frac{\partial i(z,t)}{\partial t} = 0$$

$$\frac{\partial i(z,t)}{\partial z} + Gv(z,t) + C\frac{\partial v(z,t)}{\partial t} = 0$$

(eqs. 5.7)

By using phasor forms for voltage and current respectively and after decoupling the wave equations are derived:

$$\frac{d^2V(z,t)}{dz^2} - \gamma^2 V(z,t) = 0$$

$$\frac{d^2 I(z,t)}{dz^2} - \gamma^2 I(z,t) = 0$$

(eqs. 5.8)

where γ is the complex propagation constant whose real part α (Np/m) and imaginary part β (rad/m) are the attenuation and the phase constants respectively:

$$\gamma = \alpha + j\beta = \sqrt{(R + j\omega L)(G + j\omega C)}$$

(eq. 5.9)

The solution to the differential wave equations is a superposition of forward (V^+, I^+) and backward (V^-, I^-) travelling voltage and current waves respectively:

$$V(z,t) = V^+ e^{(j\omega t - \gamma z)} + V^- e^{(j\omega t + \gamma z)}$$

$$I(z,t) = I^+ e^{(j\omega t - \gamma z)} + I^- e^{(j\omega t + \gamma z)}$$

(eqs. 5.10)

The characteristic impedance Z_o (Ohms) of a transmission line is related to the forward travelling waves and is defined as the ratio of the magnitude of voltage (V) to the magnitude of current (A) respectively:

$$Z_o = \frac{V^+}{I^+} = \sqrt{\frac{R + j\omega L}{G + j\omega C}} \qquad \text{(eq. 5.11)}$$

The characteristic impedance for an ideal lossless line ($R = G = 0$) is given by the following equation:

$$Z_o = \sqrt{\frac{L}{C}} \qquad \text{(eq. 5.12)}$$

The load impedance (Z_L) equals the ratio of the superposition between forward and backward travelling voltage to current respectively and combined with equation 5.11 can also be expressed as a function of the Z_o:

$$Z_L = \frac{V^+ + V^-}{I^+ - I^-} = Z_O \frac{V^+ + V^-}{V^+ - V^-} \qquad \text{(eq. 5.13)}$$

The input impedance Z_{in} is dependent on the transmission line length (l) and is given by:

$$Z_{in} = Z_o \frac{Z_L + jZ_o \tan \beta l}{Z_o + jZ_l \tan \beta l} \qquad \text{(eq. 5.14)}$$

where βl is the electrical length of the transmission line.

Termination of transmission lines

For the case of a short-circuited line where $Z_L = 0$, equation 5.14 becomes as follows (Sadiku, 2001):

$$Z_{in}^{SC}\Big|_{Z_L=0} = jZ_o \tan \beta l \qquad \text{(eq. 5.15)}$$

where Z_{in} could be capacitive or reactive depending on the value of the transmission line length (l) and on the signal frequency (through β). When the termination is open-circuited then $Z_L = \infty$ and the equation 5.14 is transformed to:

$$Z_{in}^{OC} = \lim_{Z_L \to \infty} Z_{in} = \frac{Z_o}{j \tan \beta l} = -jZ_o \cot \beta l \qquad \text{(eq. 5.16)}$$

which indicates that the open-circuited line has a purely imaginary input impedance. From equations 5.15 and 5.16 the characteristic impedance (Z_o) can also be derived as follows:

$$Z_o = \sqrt{Z_{oc} Z_{sc}} \qquad \text{(eq. 5.17)}$$

The short-circuit transmission line appears to be an open-circuit and vice versa when the electrical length (l) is equal to odd integrals of quarter-wave lengths ($\lambda/4$) (Hipp, 1974). This condition is satisfied when $\beta l = \pi/2$ and equation 5.14 reduces to:

$$Z_{in} = \frac{Z_o^2}{Z_L}$$

(eq. 5.18)

When the electrical length is equal to half-wave length ($l=\lambda/2$), then $\beta l = \pi$ and the input impedance is not transformed regardless of the characteristic impedance but is equal to the load impedance:

$$Z_{in} = Z_L$$

(eq. 5.19)

The next section focuses on common transmission lines and presents examples of impedance calculations based on their geometric characteristics.

Parameters of common transmission lines

Typical transmission lines with different geometries that are used to deliver the power generated by source to a load are presented in Figure 5.5.
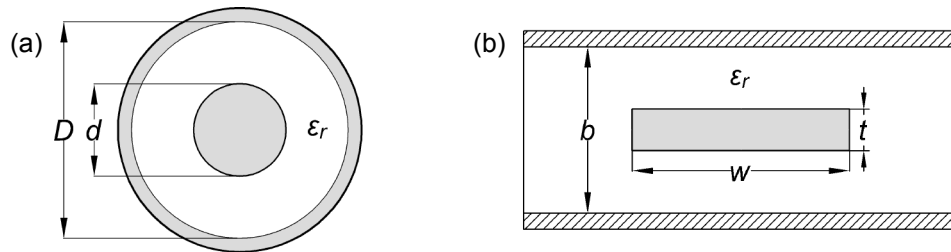
Figure 5.5: Common transmission lines and their geometric characteristics for **(a)** coaxial cable and **(b)** shielded stripline.

The most common transmission line is the coaxial cable which has a circular cross section and is composed of an inner and outer conductors separated by a dielectric, as shown in Figure 5.5 (a). The characteristic impedance of the coaxial line is given by (Rosenstark, 1994):

$$Z_o = \frac{60}{\sqrt{\varepsilon_r}} \ln\left[\frac{D}{d}\right]$$

(eq. 5.20)

Let us assume that the relative dielectric constant of the insulating material (ε_r) of a coaxial cable is equal to 1.4 and the diameters of the inner (d) and outer conductors (D) are 4.76 mm and 12.76 mm respectively. The Z_o is then calculated by equation

5.20 equal to 50 Ohms which corresponds to the characteristic impedance of coaxial cables that are widely used for industrial and commercial radio frequency applications.

The stripline consists of a rectangular conductor placed inside a dielectric surrounding by two infinite ground plates, as shown in Figure 5.5 (b). The Z_o for the stripline depends on the width and the thickness of the strip as well as the relative permittivity of the substrate and is given by (Cohn, 1955):

$$Z_o = \frac{94.15}{\sqrt{\varepsilon_r}\left(\dfrac{w/b}{1-t/b} + \dfrac{C'_f}{0.0885\ \varepsilon_r}\right)} \qquad \text{(eq. 5.21)}$$

where C'_f is the fringing capacitance in micro-microFarads per centimetre (μμF/cm) of a semi-infinite plate between two infinite ground planes:

$$C'_f = \frac{0.0885\ \varepsilon_r}{\pi}\left\{\frac{2}{1-t/b}\log_e\left[\frac{1}{1-t/b}+1\right] - \left[\frac{1}{1-t/b}-1\right]\log_e\left[\frac{1}{(1-t/b)^2}-1\right]\right\} \qquad \text{(eq.5.22)}$$

For example, if the relative dielectric constant between two conductors is $\varepsilon_r = 3$ with substrate height of $b = 1.5$ cm, plate width of $w = 0.3$ cm and plate thickness of $t = 0.5$ cm, then from equation 5.22 the fringing capacitance is $C'_f = 0.82$ and by using equation 5.21 the characteristic impedance is calculated as $Z_o = 48.53$ Ohms.

The voltage and current of a signal propagating along a transmission line are dependent on its characteristic impedance Z_o. The impedance is a function of frequency which at a low frequency is dominated by the resistive components. Conversely at a high frequency the inductive and capacitive parameters mainly influence the impedance value. Impedance matching is important because in the case of equal source, characteristic and load impedances then maximum power transfer over a transmission line is achieved to the load. Impedance mismatch will cause a decreased transmission and increased reflection of the signal.

Impedance mismatch

An electromagnetic wave travelling along a transmission line will encounter an impedance change at boundaries between materials with different electrical properties. The incident signal will then be partitioned into reflected and transmitted signals (as described in section 5.2.2). The reflection coefficient is defined as the ratio of the reflected voltage amplitude to the forward voltage amplitude:

$$\Gamma = \frac{V^-}{V^+} = \frac{Z_L - Z_O}{Z_L + Z_O} \qquad \text{(eq. 5.23)}$$

while the transmission coefficient for a lossless line is obtained from the following equation:

$$T = 1 + \Gamma = 1 + \frac{Z_L - Z_o}{Z_L + Z_o} = \frac{2Z_L}{Z_L + Z_o} \qquad \text{(eq. 5.24)}$$

The standing wave ratio is also a function of the load impedance and is defined as the ratio between the maximum and minimum voltage amplitudes detected at various positions along the transmission line:

$$SWR = \frac{V_{max}}{V_{min}} = \frac{1 + |\Gamma|}{1 - |\Gamma|} \qquad \text{(eq. 5.25)}$$

Various terminations of transmission lines and their effect on the obtained incident, reflected, transmitted and standing waves are shown in Table 5.1.

Table 5.1: Load impedance, reflection coefficient and standing wave ratios for various terminations.

Termination	Z_L	Γ	SWR
Shorted-circuit	0	-1	∞
Open-circuit	∞	1	∞
Impedance match	Z_o	0	1

The generated voltage patterns of the incident wave ($V_{inc.}$), the reflected wave ($V_{refl.}$), the transmitted wave ($V_{trans.}$) and standing wave ratio (V_{SWR}) for different terminations are presented in Figures 5.6, 5.7, 5.8 and 5.9. When the termination of a transmission line is short-circuited ($Z_L = 0$) the incident and reflected waves are equal in amplitude resulting in zero transmitted wave, as shown in Figure 5.6. The standing wave originates by the superposition of the incident and reflected waves. The antinodes of SWR are recorded at odd multiples of quarter wave lengths ($\lambda/4$) and the nodes at even multiples of half wave lengths ($\lambda/2$).
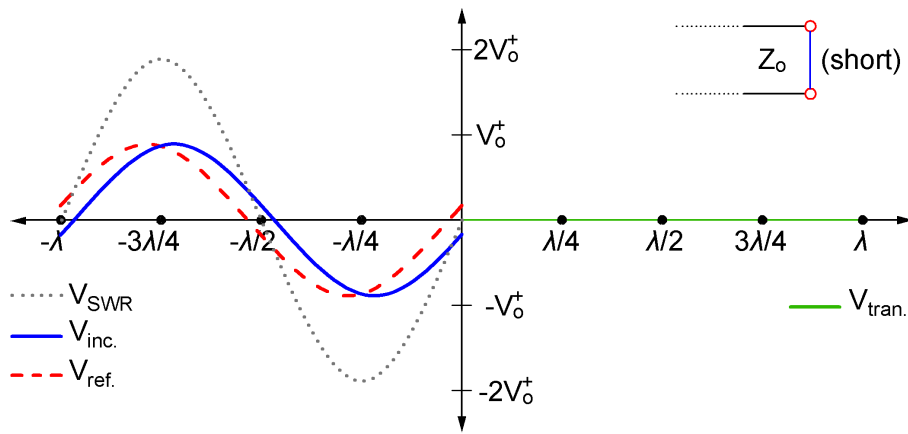
Figure 5.6: TEM wave characteristics for short-circuited termination of a transmission line.

Figure 5.7 presents the case of the open-circuited line where the incident and reflected waves are equal and in phase (0°). The antinode and node points are interchanged with respect to the short-circuited line, occurring at even and odd multiples of $\lambda/4$ respectively.
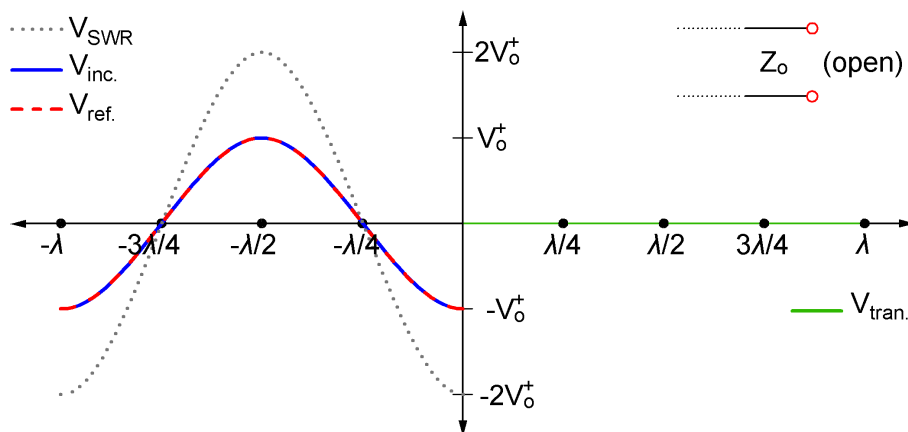
Figure 5.7: TEM wave characteristics for open-circuited termination of a transmission line.

The cases of impedance match and impedance mismatch at an instant in time are presented in Figures 5.8 and 5.9 respectively. When $Z_o = Z_L$ all the power generated by the source is absorbed by the load resulting in zero reflection while the standing wave is a unity, as shown in Figure 5.8.
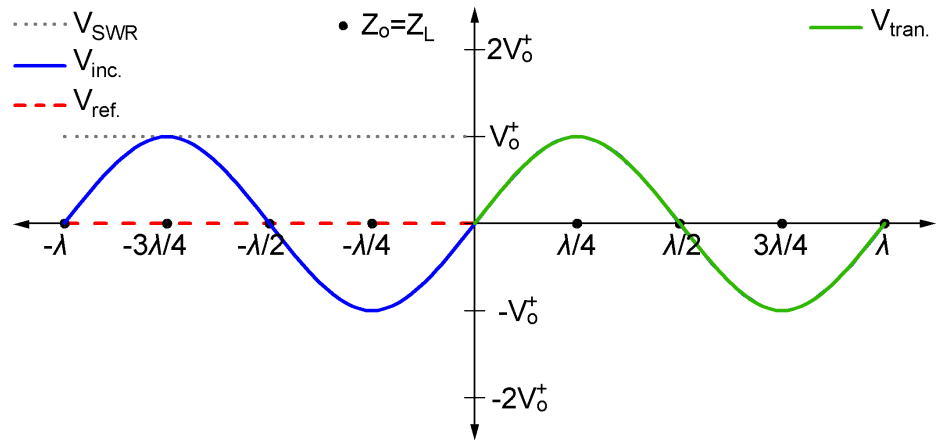
Figure 5.8: TEM wave characteristics of a transmission line at an instant time for impedance match.

In the case of an impedance mismatch the incident wave is partitioned to transmitted and reflected signals, as presented in Figure 5.9. As a result, a standing wave is formed in the incident transmission line while the transmitted wave amplitude is reduced.
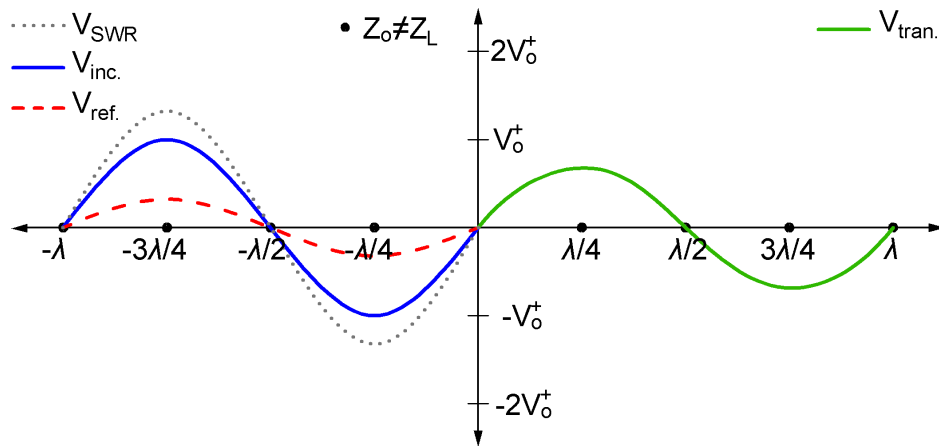
Figure 5.9: TEM wave characteristics of a transmission line at an instant time for impedance mismatch.

By measuring the reflection and transmission parameters of a device it is possible to characterise a transmission line which is inserted into a medium. Transmission line parameters are employed to extract important information about the medium electrical properties such as measurements of the permittivity as discussed in section 5.2.1.

This investigation aimed to develop and validate a new type of transmission line which employs the transmission characteristics of the signal to provide a measurement of scour and sediment deposition processes. A series of experiments was conducted to evaluate and understand the electrical behaviour of the prototype sensor.

5.3 Design concept no.1: investigating a capacitance-based measurement

The study aimed to investigate the capability of capacitance-based measurements to detect position of soil-water interfaces and therefore scour depth variations. The concept lies on the principle that the overall permittivity of the medium surrounding the probe will increase during scouring due to the higher dielectric permittivity of water compared to saturated sediment. The 'average' dielectric permittivity directly affects the capacitance of the probe which would be expected to increase when scour conditions occur.

5.3.1 Experimental set up of concept no.1

A prototype probe of 100 cm length was fabricated based on the optimum geometry defined in FEM study presented in section 4.4.3 of Chapter 4. The sensor was composed of two strip electrodes with arc length of 13.75 mm placed at an angular position of 90° and was inserted into a fibre glass access tube with external diameter of 28 mm. Two different types of measurements were recorded which consisted of a direct and an indirect capacitance measurement by connecting the sensor electrodes to a capacitance meter and to a monostable circuit respectively.

The probe was placed into a clear acrylic tank with diameter of 300 mm and height of 1000 mm, as shown in Figure 5.10 (a). Experiments were initially conducted with the two sensor electrodes connected to a capacitance meter (model U1701B) to record the capacitance values at various locations of the soil-water interfaces [see Figure 5.10 (b)].

Tests were then carried out with the sensor electrodes linked to the monostable multi-vibrator which has one state of the output stable and the other quasi-stable. The monostable circuits are triggered at a constant frequency creating a pulse of fixed amplitude which causes the system to enter the quasi-stable state and produces a characteristic rectangular waveform. The pulse width varies with the timing of the external capacitance and the smoothed average output voltage depends on the 'average' permittivity of the medium surrounding the probe. The two electrodes were linked via BNC cables with the monostable circuit, placed into a plastic container and

connected to a measuring system which consisted of a power supply, a pulse generator and a multi-meter instrument [see Figure 5.10 (c) and 5.10 (d)]. The measuring system was configured to operate at a pulse frequency of 2 MHz.
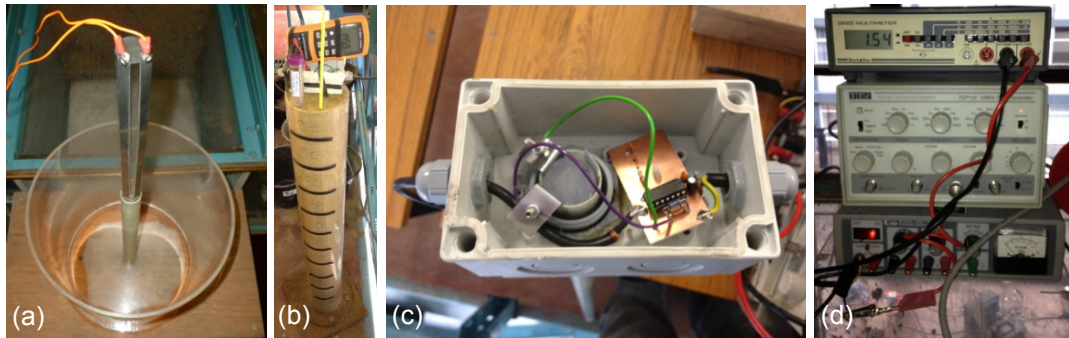
Figure 5.10: (a) Sensor electrodes inserted into the tank, **(b)** 100 cm length prototype sensor connected to a capacitance meter and **(b)** to a monostable circuit linked to **(c)** the measuring system.

The experiments were initially carried out by substituting the air with water medium inside the tank (i.e. saturating from the bottom) and measurements were recorded at depth intervals of 10 cm. Similar tests were then conducted investigating the capacitance response of the sensor under the different interfaces of dry coarse sand-air and saturated coarse sand-water.

5.3.2 Capacitance meter and monostable circuit results

Figure 5.11 presents the results obtained with the sensor electrodes connected to the handheld capacitance meter. A gradual linear increase in the capacitance values was recorded when the tank was filled with fresh water (i.e. water replaced air in the pore space) at depth intervals of 10 cm. This is due to the higher permittivity of water when compared to air. Similarly the sensor capacitance values detected increased height of dry sand column (see Figure 5.11). However, when the capability to detect variation of the fresh water-saturated sand interface was tested, the recorded capacitance was always greater than the one obtained when only water was present in the tank despite that water permittivity is greater than sand permittivity. This indicates that the capacitance meter is not capable of measuring the variation of the water-saturated sand interface and therefore scour depth variations.
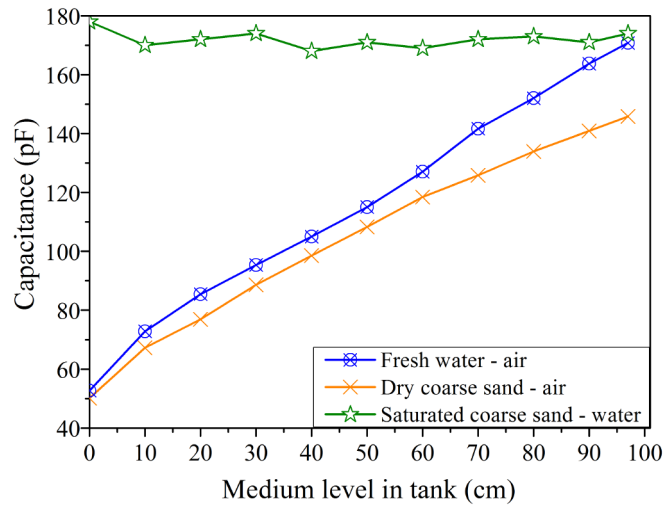
Figure 5.11: Capacitance obtained for various medium interfaces with the sensor electrodes connected to the capacitance meter.

Similar response was observed when the sensor electrodes were connected to the monostable circuit (Figure 5.12). The results indicate that at the operating frequency of 2 MHz the measuring system successfully detected variations in the air-fresh water and air-dry coarse sand interfaces with a strong linear relationship. However, the monostable circuit did not measure satisfactorily variations of the fresh water-saturated soil interface, as the voltage output in saturated coarse sand was always greater than values obtained in water medium.
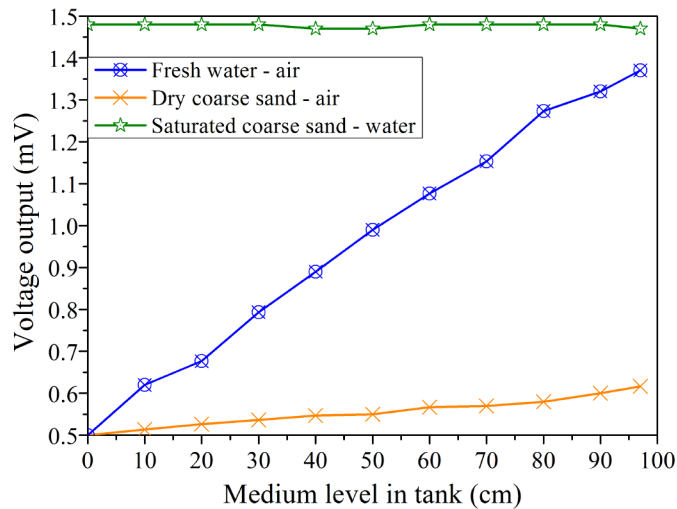
Figure 5.12: Voltage output obtained for various medium interfaces with the sensor electrodes connected to the monostable circuit at the frequency of 2 MHz.

The investigation with the handheld capacitance meter and monostable circuit indicated that both measuring systems were not capable of detecting scour or sediment deposition processes as they did not respond successfully to saturated sand-water level

variations. This is likely to be associated with the pulse width limitation and/or the low operating frequency of 2 MHz of the monostable circuit. Other studies also highlighted that at frequencies < 30 MHz the signal of sensors based on capacitive principle is highly sensitive to the electrical conductivity effect and suggested higher operating frequencies to ensure that the output is primarily dependant on the permittivity value (Thomas et al., 1991; Watson et al., 1995; Robinson et al., 1998; and Delta-T Devices Limited, 2006). The investigation was therefore continued with sensor connected to a network analyser to assess the sensor performance in higher frequencies and identify variables associated with electromagnetic wave transmission that are sensitive to bed level processes.

5.4 Design concept no.2: investigating the response of the EM sensor as a transmission line in various frequency bands

As the preliminary study examining the capacitance-based measurement indicated that the sensor did not respond successfully when tested at low frequencies, there was scope for further investigation using a Radio Frequency (RF) Vector Network Analyser (VNA) (model HP8712C) to assess the sensor response at higher frequencies.

The investigation with the VNA aimed to detect wave propagation variables associated with the transmitted signal suitable for detecting scour and deposited sediment processes. The transmitted characteristics of the signal in the AD are employed in this study as they are likely to simplify the signal processing and reduce the cost of the electronics concept when compared to the reflection measurements used in particular in TD method. The transmission measurements may therefore support the development of a new low-cost sensor that will generate an output signal that can be easily interpreted for the detection of bed level variations in the vicinity of the foundation structure.

5.4.1 Coupling of the EM sensor with the Vector Network Analyser

The transmission coefficient of the VNA depends on the match between the characteristic and sensor impedance (as described in section 5.2.3). It is defined as the

transmitted voltage divided by the incident voltage and is the portion of RF transmitted power that reaches the receiver port of the VNA:

$$T = \frac{V_{Trans}}{V_{Inc}} \qquad \text{(eq. 5.26)}$$

In the case of $|V_{Trans}| > |V_{Inc}|$ then the Device Under Testing (DUT) has gain while when $|V_{Trans}| < |V_{Inc}|$ the DUT exhibits attenuation or loss. The reflection coefficient is the ratio of the reflected and incident voltage and is given as follows:

$$\Gamma = \frac{V_{Refl}}{V_{Inc}} \qquad \text{(eq. 5.27)}$$

The operating frequency of the VNA was set for a swept frequency ranging from 0.3 MHz to 1 GHz. The linear behaviour of the VNA imposes magnitude and phase changes through the DUT that are linear with the frequency. The VNA output power level was adjusted to 10 mW with the sweep time set to auto mode and the number of recorded frequency points to 201. The 10 mW incident AC power delivered to the DUT through a 50 Ohm impedance cable is equivalent to 0.707 Volts (root mean square) AC voltage. The transmitted voltage is then calculated as follows:

$$V_{Trans} = 0.707 \times T \qquad \text{(eq. 5.28)}$$

The two strip electrode sensor (same as the one tested in experiments described in section 5.3.1) was also used in this investigation [see Figure 5.13 (a)]. Each strip electrode of the probe was connected with the inner conductors of two 50 Ohm coaxial cables, as shown in Figure 5.13 (b), which were linked to the transmitter and reflection ports of the VNA.
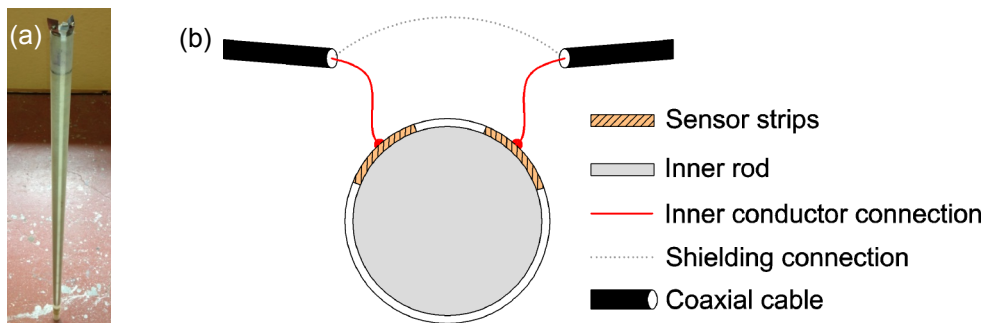
Figure 5.13: (a) Complete assembly of a two strip sensor inserted into a fibre-glass access tube and **(b)** schematic diagram of electrode connection of the sensor with the coaxial cables.

The sensor arrangement corresponded to the case of the impedance placed in series with the measuring system, as depicted in Figure 5.14.
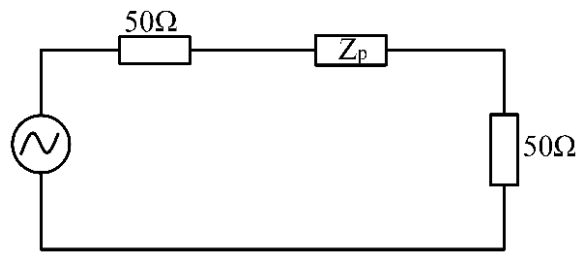
Figure 5.14: Sensor arrangement with the measuring system with the impedance (Z_p) placed in series.

The probe was placed in a cylindrical tank with diameter and height of 250 mm and 1250 mm respectively. The study initially evaluated the sensor response in air and fresh water environment. Afterwards, the tank was filled with fresh water and coarse sand was added progressively. Measurements of the transmission ratio were recorded and analysed at soil increments of 10 cm until the probe was fully covered by the uncompacted saturated sediment.

5.4.2 Preliminary results and tentative working principle of the sensor

Figures 5.15, 5.16, 5.17 and 5.18 present the sensor response in a series of tests where the air-fresh water and the fresh water-saturated sediment interfaces were varied. The sensor output in air at the frequency range from 0.3 MHz to 300 MHz is shown in Figure 5.15. It is observed that at specific frequencies much of the incident energy is transmitted (resonance crests) but at other frequency points there is poor signal transmission (troughs) resulting in high reflection ratio. A periodicity of the frequency points at intervals of 105 MHz where the troughs occurs is also pointed out in the highlighted grey areas (i) and (ii) of Figure 5.15. A similar repetitive pattern of the frequency points which correspond to the resonance crests is also detected.
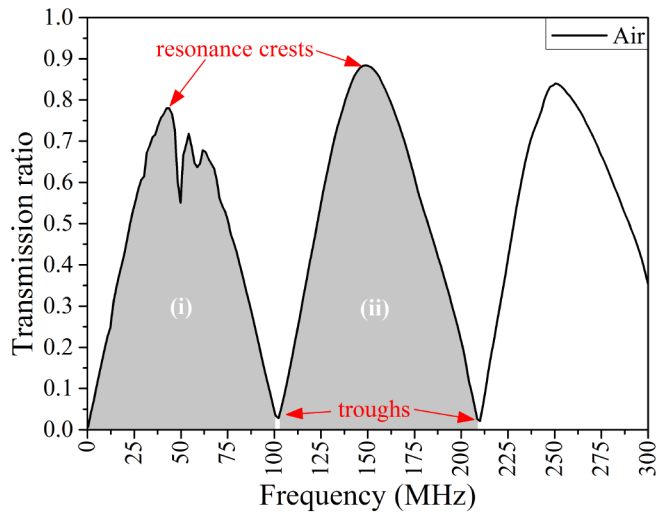
Figure 5.15: Obtained transmission ratio with the sensor placed in air environment at the frequency range from 0.3 MHz to 300 MHz. A repetitive pattern of the frequency points which correspond to the transmission crests and troughs is detected in the highlighted areas (i) and (ii).

The same frequency periodicity of the transmission crest and troughs is also obtained when the sensor was tested in different air and fresh water interfaces, as shown in Figure 5.16. When the tank was filled gradually with fresh water, the frequency point which corresponds to the first transmission troughs is decreased from 102 MHz (air) to 76 MHZ (air-water interface) and 56 MHz (water). This due to the higher permittivity of water with respect to air, which results in an increased electrical length and decreased wavelength as explained later in this chapter.
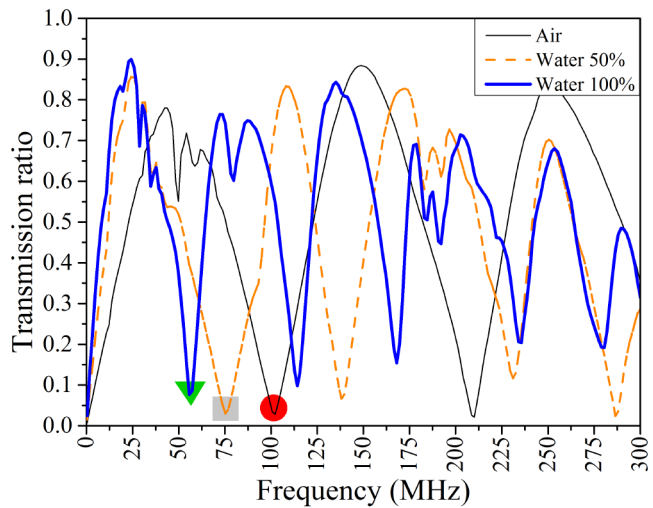
Figure 5.16: Obtained frequency response with the sensor placed in air and fresh water environments at the frequency range from 0.3 MHz to 300 MHz. The frequency point of the first transmission trough is decreased for higher permittivity conditions which corresponded to air (circular mark), air-water interface (square mark) and water medium (triangle mark).

The transmission ratio recorded during experiments with various depths of fresh water-saturated sand interfaces at frequency ranging from 0.3 MHz to 1 GHz and 0.3 MHz to 300 MHz is shown in Figures 5.17 and 5.18 respectively. The examined boundaries between water and sediment mediums correspond to bed level variations and are presented as different scour depths throughout the investigations presented in this chapter. The grey highlighted region of Figure 5.17 indicates that at frequencies higher than 300 MHz, the resonance crests and troughs diminish due to radiation and conduction losses. The investigation was therefore continued at the frequency range from 0.3 MHz to 300 MHz where resonance phenomena are occurring (see Figure 5.18).
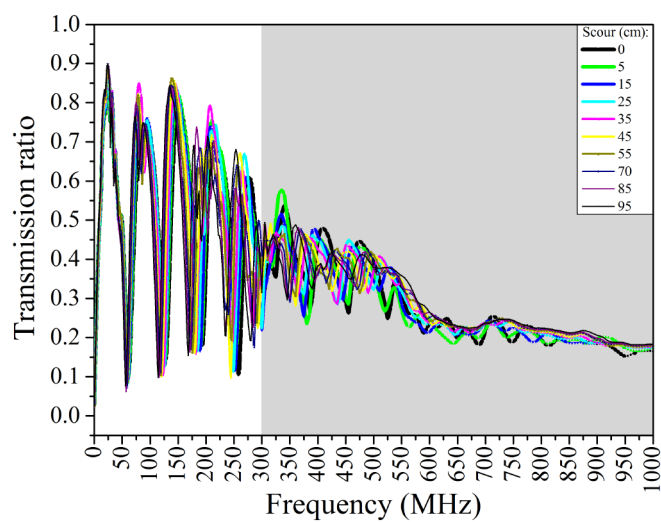
Figure 5.17: Transmission ratio obtained during 'static' scour simulations at the frequency range from 0.3 MHz to 1 GHz. The grey area highlights the frequency region where a significant reduction in the amplitude of the crests and troughs is observed.
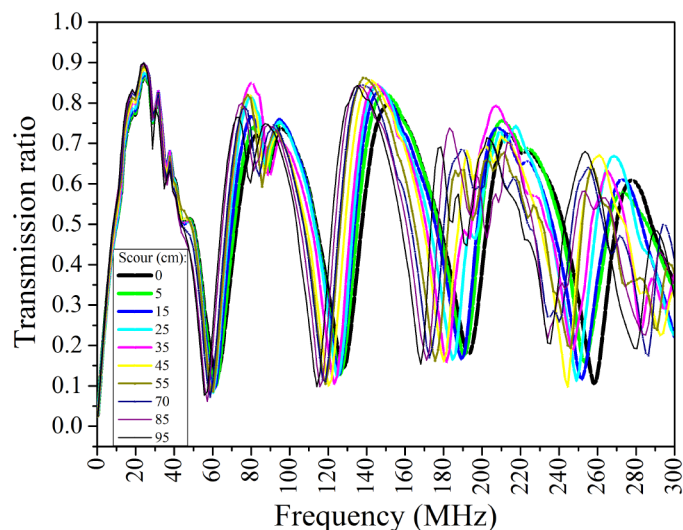
Figure 5.18: Transmission ratio obtained during 'static' scour simulations focusing at the frequency range from 0.3 MHz to 300 MHz where the resonance phenomena occur.

The analysis was then focused on specific frequency bands to identify transmission variables sensitive to scour depth variations. As shown in the highlighted grey area of Figure 5.19, the transmission ratio at the selected frequency range (64 MHz to 70 MHz) progressively increases as scour increases. A decrease of the frequency points where the resonance troughs occur is also detected, which is associated with the gradual increase of the simulated scour processes, as pointed out in grey highlighted areas of Figure 5.20.
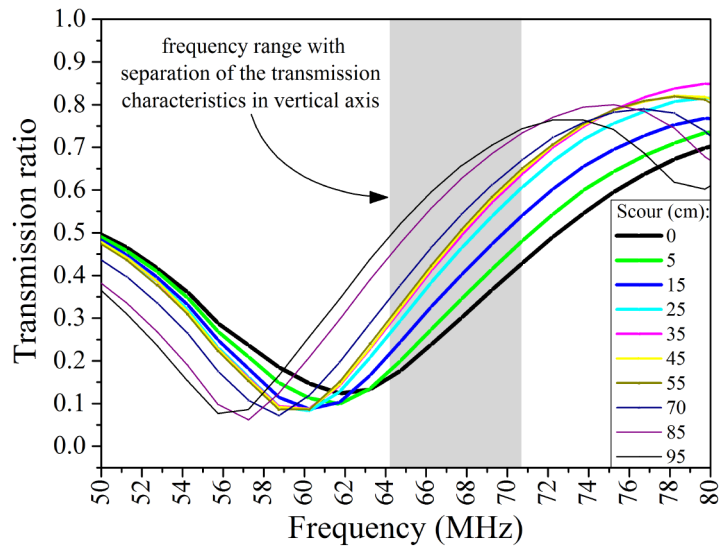
Figure 5.19: Transmission characteristics at the frequency band from 50 MHz to 80 MHz.
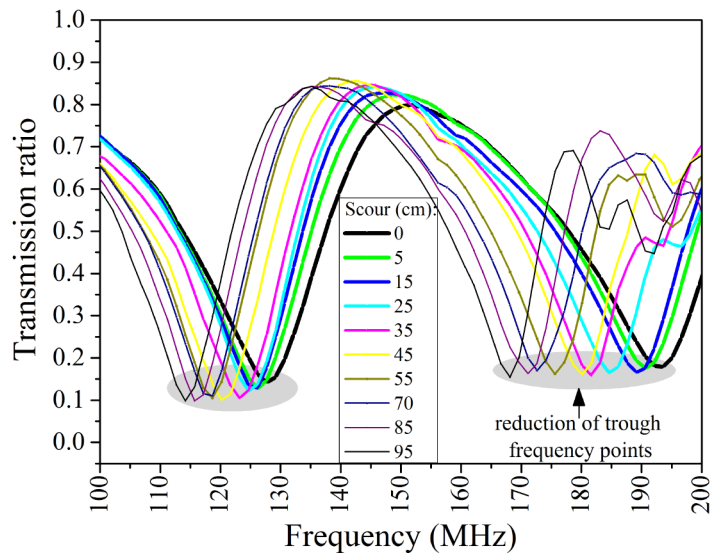
Figure 5.20: Transmission characteristics at the frequency band from 100 MHz to 200 MHz.

As shown in Figure 5.21, the simulated 'static' scour depths can be obtained by the decrease of the frequency points which correspond to the transmission troughs that occur in the frequency band from 114 MHz to 127 MHz. Bed level variations inside

the tank can also be measured from the transmission ratio by using a single frequency (see Figure 5.22).
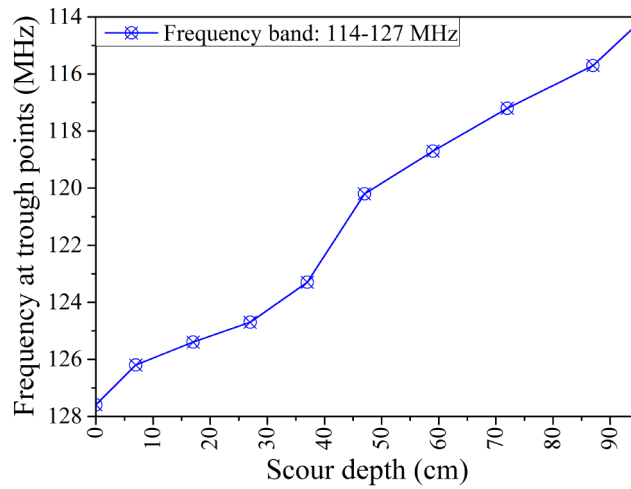
Figure 5.21: Scour depth measurement based on frequency change occurring at transmission trough points at the band from 114 MHz to 127 MHZ.
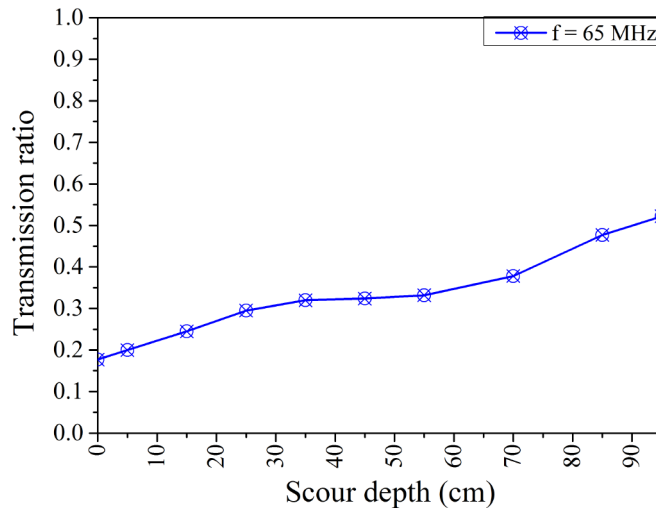
Figure 5.22: Scour depth measurement based on the transmission ratio obtained at the single frequency of 65 MHz.

From equation 5.28 the transmitted voltage signal is calculated from the transmission ratio obtained at the frequency of 65 MHz as presented in Figure 5.23 (a). The relative voltage change of the transmitted signal of the sensor at the same frequency is also calculated and shown in Figure 5.23 (b). Increased scour depth had a cumulative effect on the sensor transmission signal and on the relative voltage change. However, the signal is not following a linear increasing trend creating a plateau that is detected in the region that corresponds to the middle of the prototype sensor (see Figure 5.23).
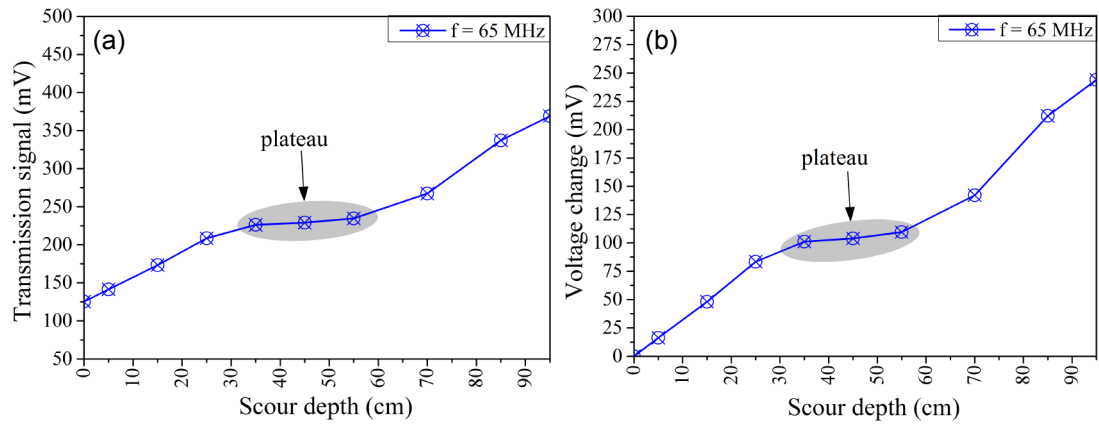
Figure 5.23: Scour depth measurement based on **(a)** the transmitted voltage signal and **(b)** the transmitted voltage relative change at the single frequency of 65 MHz.

The study identified two variables on the transmission characteristics of the sensor that responded successfully to bed level variations, i.e. (i) transmission signal at a single frequency and (ii) frequency at resonance troughs. However, frequency measurement of the resonance points would require more complicated data interpretation and expensive electronics, which will need to operate in various frequency bands rather than a single frequency. As a result, voltage measurements (amplitude of the transmitted signal) at a single frequency is the simple obvious option as it can be implemented more effectively within commercial multichannel loggers reducing the cost of the sensor/system and enabling the real-time monitoring of scour action. The investigation therefore focused on option (i) and, in particular, on the optimum frequency at which transmitted voltage variations can effectively be used to monitor bed level processes.

The optimum frequency of the sensor is also unlikely to match the operational frequency of the commercial detector. A study was therefore undertaken to develop a tool to enable controlling the optimum frequency based on the sensor geometry. This would allow using commercial oscillators operating at specific frequencies reducing the total cost and ease the development of the sensor's electronics.

The investigation continued with the development of an analogue based on stub line to better understand, qualitatively and quantitatively, the frequency response of open-circuited transmission lines. The objective was to enable prediction and/or control of the optimum frequency of the sensor where amplitude of the transmitted signal should be read.

5.5 An analogue for the EM sensor: stub line experiments

The preliminary analysis carried out with the sensor electrodes connected to the VNA revealed a repetitive pattern of the crests and troughs of the transmission signal as a function of frequency. The purpose of the tests described in this section was to assess and explain the transmitted properties of the signal that were observed over specific frequency ranges by employing the stub line characteristics. The study also used stub line experiments to mimic various water-saturated soil interfaces aiming to identify similarities with the behaviour of the frequency response of the sensor observed during 'static' scour tests.

A stub line is terminated in an open-circuit and is used as a transformer to produce a required input impedance at a certain frequency. In stub line experiments, permittivity (ε) remains constant but the electrical length is changing due to a change in the physical length of the cable.

The quarter wavelength ($\lambda/4$) transmission line theory was utilised to explain the periodicity of the frequency points. At a signal frequency where the electrical length of a system is equal to even or odd multiples of $\lambda/4$, the source presents the exact opposite of the termination impedance (Hipp, 1974). Therefore, if a $\lambda/4$ transmission line is terminated in an open-circuit, the stub will present a short-circuit at the point where it connects to the line; while if the line is short-circuited at its output, the stub will present an open-circuit.

5.5.1 Signal characteristics dependency on stub line length

A straight connector was used to link two 50 Ohm BNC cables to the transmitter and receiver ports of the network analyser, as shown in Figure 5.24 (a). The frequency range of the VNA was set to sweep from 0.3 MHz to 300 MHz. Ideally, all the incident energy produced by the network analyser is being transmitted through the connector and BNC cables to its match receiver port resulting in zero reflection energy portion. Any minor losses apparent in the frequency response were therefore removed at the start of each experiment by normalising the transmission ratio to 1.

The straight connector was then replaced by a T-piece (stub) which was connected each time with different cable lengths of 52 cm, 104 cm, 156 cm and 207

cm [see Figures 5.24 (b) and 5.24 (c)]. The other end of each cable represented an open-circuit resulting to an opposite current that is reflected when the incident wave reached the end of the line.
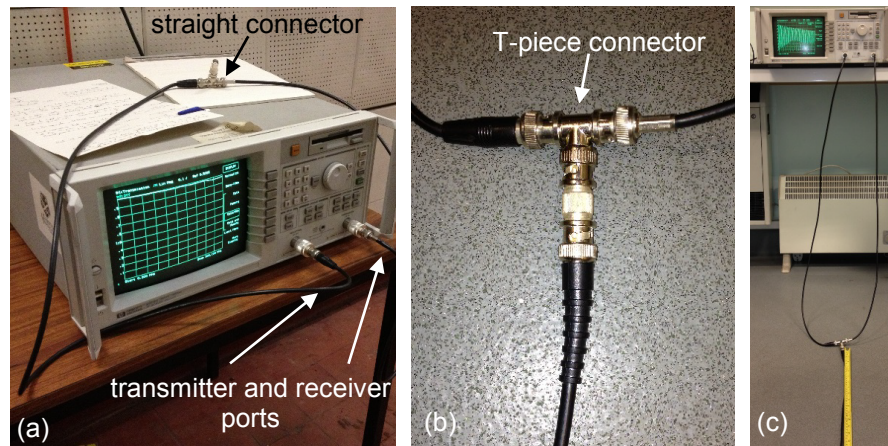
Figure 5.24: (a) Straight connector linking two 50 Ohm BNC cables to the transmitter and receiver ports of the VNA and **(b)** T-piece connector linked to **(c)** a section of an open-ended cable.

The aforementioned stub arrangements corresponded to the case when the impedance is placed in parallel with the measuring system (see Figure 5.25).
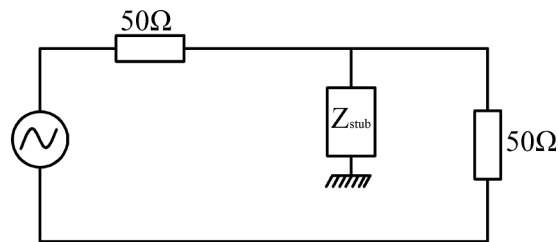
Figure 5.25: Stub arrangement with the measuring system with the impedance (Z_{stub}) placed in parallel.

Figure 5.26 presents the results obtained using a stub connection linking to BNC cables of different length each time. When the cable length is almost doubled from 104 to 207cm, the frequency that corresponds to the first resonance crest point on the transmission graph is reduced by half, as shown in Figure 5.26 (a). Comparable behaviour is observed on the reflection ratio, presented in Figure 5.26 (b), as the frequency points where reflection crest and trough points are occurring are also a function of the length ratio between the two tested cable sizes.
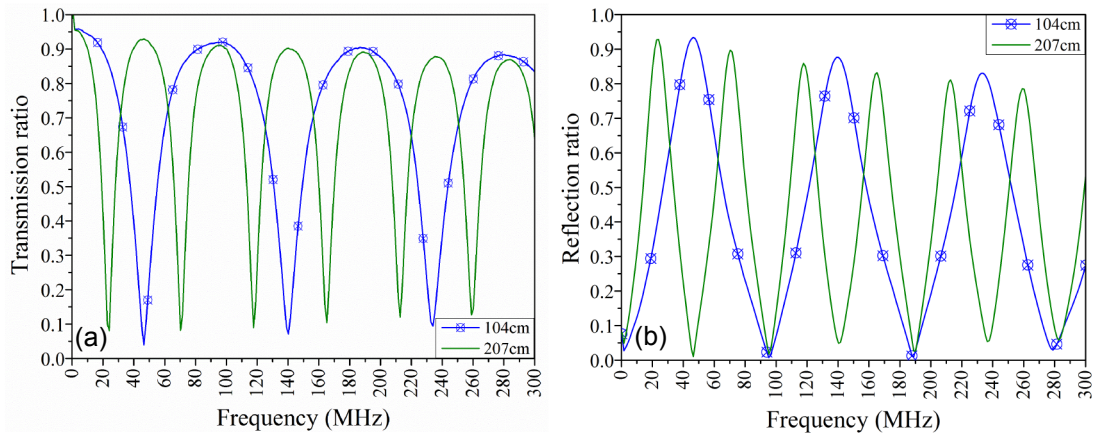
Figure 5.26: (a) Transmission and **(b)** reflection ratios obtained for stub cables with length of 104 cm and 207 cm indicating that the frequency response is a function of the cable length ratio.

Similar findings were detected for different cable lengths of 52 cm, 104 cm and 156 cm, as shown in Figure 5.27. Greater cable lengths increase the electrical length while the resonance crests and null points appear to be a function of the length ratio between the stub lines. Figures 5.26 and 5.27 also show a repetition of the obtained frequency response with equal spacing troughs and crests for all the tested cable lengths. Comparable behaviour was observed for the recorded transmission characteristics of the prototype sensor as presented in section 5.4.2. This is due to the fact that the open-circuit is being transformed to a short-circuit whenever the electrical length becomes equal to odd multiples of a quarter wavelength ($\lambda/4$). In the case of the stub line tests the impedance is placed in parallel, therefore the short-circuit causes a high reflection ratio of the incident signal.

As shown in Figure 5.27, the reflection ratio reaches its maximum values at frequency points where the electrical length is equal to odd multiples of $\lambda/4$ and the open-circuit is being transformed to a short-circuit. At even multiples of $\lambda/4$ the open-circuit is being transformed back to an open-circuit and therefore minimising the reflection signal as the stub impedance then has a little influence on the main through line.
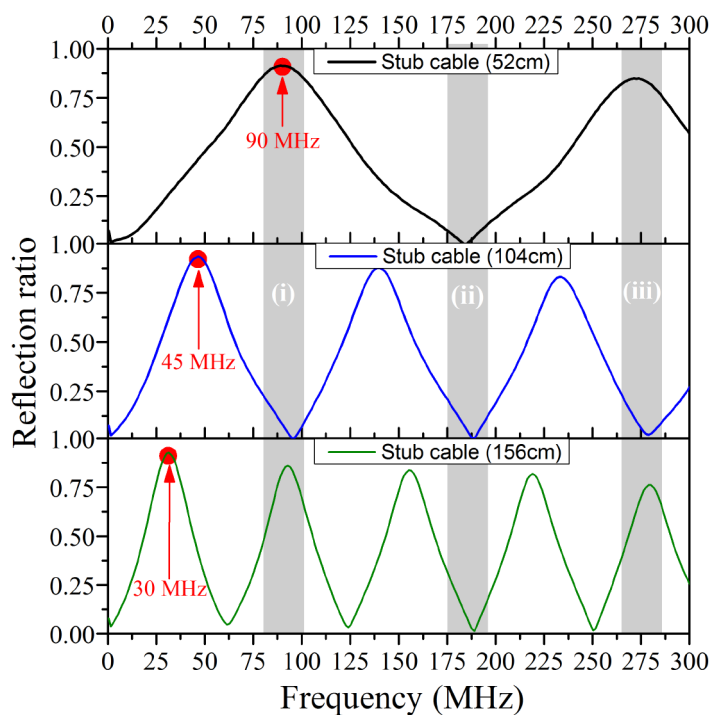
Figure 5.27: Reflection ratio obtained for stub lines with length of 52 cm, 104 cm and 156 cm for the frequency range from 0.3 MHz to 300 MHz. The reflection characteristics are a function of the stub cable length; the grey bands (i), (ii), and (ii) indicate that greater cable lengths increase the electrical length of the stub and also results in a repetition of the crests and troughs at odd and even multiples of $\lambda/4$ respectively. The frequency point which corresponds to first crest is also reduced from 90 MHz to 45 MHz and 30 MHz for increased cable length of 52 cm, 104 cm and 156 cm respectively.

The obtained results indicated that the transmission and reflection signals are a function of the stub's electrical length. Equal spacing crests and troughs are occurring which corresponded to frequencies where the electrical length is becoming equal to odd and even multiples of $\lambda/4$ respectively. These findings help with predicting the frequency points where these resonances occur.

5.5.2 Prediction of resonance frequency of stub lines

The experiments carried out with the prototype sensor revealed that the system is more sensitive to changes in conditions at certain frequencies where a periodicity of crest and trough points is observed. This section presents the prediction of the frequencies where the repetition of the resonance crests and troughs occur. This is based on the length of the open-circuited stub lines, which causes a greater refection of the incident energy at odd multiples of quarter wavelengths where a null point is expected in the transmission ratio.

The measured by the VNA and predicted frequency points which correspond to reflection crests are presented in Table 5.2 and Figure 5.28. Five different cable lengths were tested in this investigation and the frequencies were recorded where the transformation from open to short-circuit occurs, in turn resulting in increased reflection ratio (i.e. decreased transmission signal). By using the length ratio between the tested BNC cables and one reference frequency point (i.e. 90.27 MHz), the frequencies where the odd multiples of $\lambda/4$ occur are predicted.

Table 5.2: Measured and predicted frequency points of reflection crests occurring at even multiples of $\lambda/4$ for various stub line lengths. By using the reference frequency of 90.27 MHz, the other frequency points are satisfactorily predicted based on the stub cable length ratio.

Cable length (cm)	Length ratio	Frequency (MHz)							
		$\lambda/4$		$3\lambda/4$		$5\lambda/4$		$7\lambda/4$	
		P^*	M^{**}	P^*	M^{**}	P^*	M^{**}	P^*	M^{**}
52	1.00	90.27	90.27	270.82	272.72	451.37	455.16	631.91	636.36
104	0.50	45.14	46.54	135.41	139.01	225.68	232.73	315.96	326.45
156	0.33	30.09	31.54	90.27	92.77	150.46	155.25	210.64	218.98
207	0.25	22.68	24.04	68.03	70.28	113.39	117.77	158.74	165.25
300	0.17	15.65	16.55	46.94	49.04	78.24	81.53	109.53	114.02

P^* = predicted, M^{**} = measured.
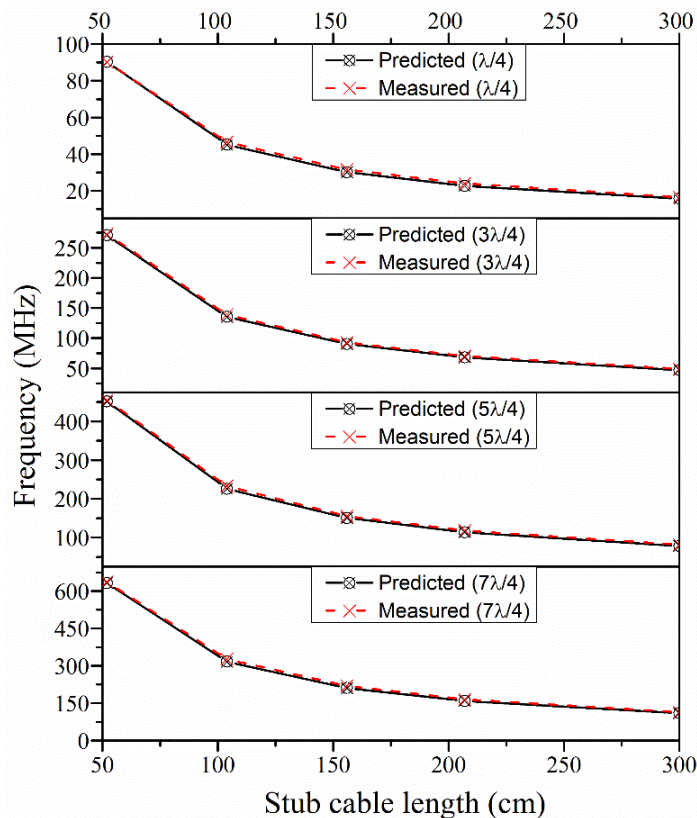
Figure 5.28: Comparison between measured and predicted frequency points of reflection crests for various stub line lengths at the frequency band from 0.3 MHz and 300 MHz. An excellent agreement is obtained between the predicted and measured frequency points corresponding to resonance crests.

The obtained results indicated that the frequency points where the reflection crests and troughs occur, corresponded to odd and even multiples of $\lambda/4$ that were successfully predicted. These findings were useful as they can be implemented for the prediction of the optimum frequency of sensors with different lengths. The investigation was continued with the simulation of the fresh water-saturated soil interface using stub cables of different impedance values.

5.5.3 Stub lines to simulate variations of water-soil interfaces

In the preliminary tests carried out with the prototype sensor to simulate 'static' scour processes, a decrease of the frequency points where the transmission nulls occur was observed as water substituted saturated sediment inside the tank. At the same time, a separation in the vertical direction (transmission ratio) was detected, suggesting that amplitude of transmitted signal could be used for scour depth measurements. The objective of this investigation was to model the electrical response of the probe for various location of the fresh water-saturated soil interface using stub lines with lengths representing the different impedances generated by different levels of the fresh water-saturated soil interface.

50 Ohm coaxial cables connected to the VNA were used in these experiments as shown in Figure 5.29 (a). The impedance representing the saturated soil is expected to be greater compared to the one which corresponds to water. This is due to the fact that water has a higher permittivity which leads to increased capacitance and hence to reduced impedance (see equation 5.12). In these tests, in order to reduce the impedance value the water medium ($Z1$) was simulated by placing in parallel coaxial cables of 50 cm length. The saturated soil ($Z2$) was represented by a single cable of equal length. A decrease of the impedance of the first coaxial cable section ($Z1$) mimics the case of higher permittivity in turn associated with increased scour (greater water to saturated soil ratio). The inner conductors and the shield parts of each coaxial cable segment were connected each other and plugged to the T-section between the transmitter and receiver ports of the VNA [see Figure 5.29 (a)]. Different impedance configurations representing various water – saturated soil interfaces were simulated, as shown in Table 5.3 and Figure 5.29 (b). The transmission and reflection response in a range of frequencies was recorded and analysed.

Table 5.3: Experiments with models representing different water (*Z1*) saturated soil (*Z2*) interfaces.

Test	*Z1* (Ohms)	*Z2* (Ohms)
1	50	50
2	25	50
3	16.66	50
4	8.33	50
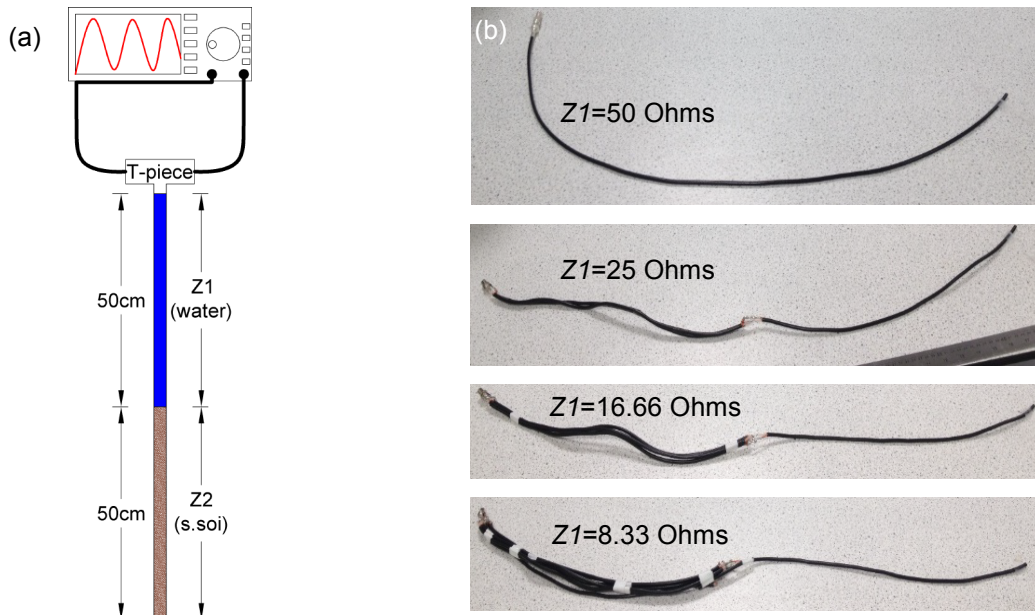
Figure 5.29: (a) Experimental set up used for the stub line tests and **(b)** stub lines composed of two sections of 50 cm length respectively representing various water-saturated soil boundaries.

During the preliminary tests of 'static' scour simulations with the prototype sensor of 100 cm length (presented in section 5.4.2) a frequency band was identified with greatest sensitivity to scour depth variations. This frequency range was detected from 60 MHz and 70 MHz, which lies between the first null point in transmission and the subsequent resonance crest. The first null point in air environment was obtained at 100 MHz but is reduced to 62 MHz in water conditions due to the higher permittivity that causes an increase in the electrical length and a decrease in the wavelength.

Figures 5.30 and 5.31 focus on a frequency band similar to the one detected with the prototype sensor in air. In the frequency range from 80 MHz to 150 MHz, when *Z1* is set to 50 Ohms, 25 Ohms, 16.66 Ohms and 8.33 Ohms, a corresponding decrease in frequency of the first null point in the signal is observed. A separation of the obtained transmission and reflection ratios in the vertical axis is also detected, as shown in Figures 5.30 and 5.31. A similar behaviour of the frequency response is

obtained during the scour tests with the prototype sensor (presented in Figures 5.19 and 5.20) which is in qualitative agreement with the results obtained in this section.
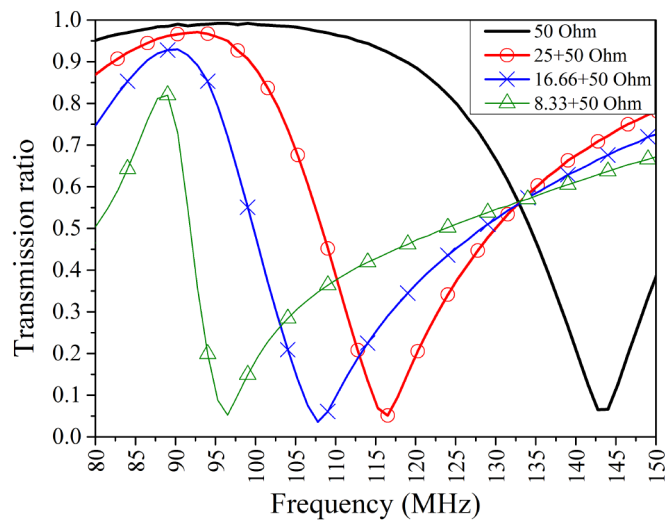
Figure 5.30: Transmission ratio obtained for the two sections of equal length coaxial cables that represented different impedance values for the frequency range of 80-150 MHz. A decrease of the frequency of the first null point is observed for increased impedance mismatch along the stub cable.
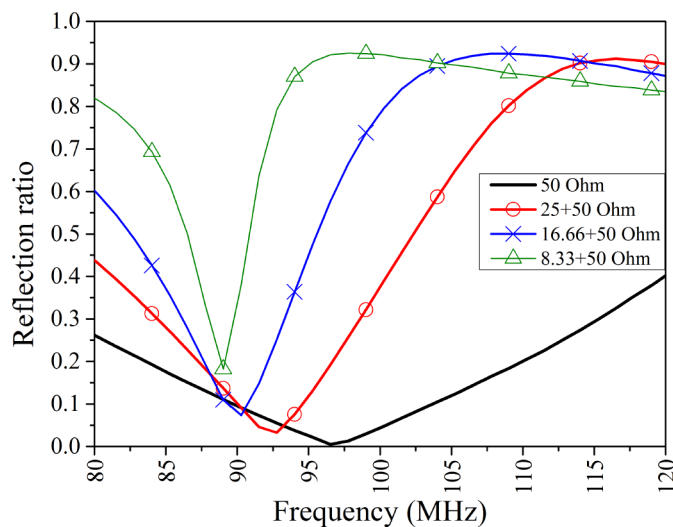
Figure 5.31: Reflection ratio obtained for the two sections of equal length coaxial cables that represented different impedance values for the frequency range of 80-120 MHz. It is pointed out a decrease of the frequency of the first null point for increased impedance mismatch and a separation of the recorded reflection ratio in the vertical direction.

This investigation demonstrated that the observed effects on the frequency characteristics of the impedance representation of various medium interfaces are similar to the behaviour of the prototype sensor in scour conditions. A leftward shift of the trough frequency point was detected, as observed in the prototype sensor response when the water-saturated soil interface was lowered, which is associated with the change of two impedances in series. Namely, the response is comparable with the

case when the wavelength is becoming shorter or the electrical length is increased which is associated with the prototype sensor transmission characteristics in scour conditions. The study continued with the comparison of the frequency response obtained from prototype sensor and stub lines. This will later be used as a guide for the electrical characterisation of the developed instrument.

5.6 Investigating the sensor frequency response via stub line

This investigation aimed at understanding the sensor transmission characteristics in various frequency ranges where a repetitive pattern of the crest and troughs was obtained (as presented in section 5.4.2). A similar periodicity of the frequency points where the transmission resonances occur was also detected in the stub line experiments (see section 5.5.1). A successful comparison of the electrical response between the sensor and the stub line will enable the prediction of the optimum frequency for sensors with different electrode lengths. It will also allow to complement and control the required operating frequency of the sensor based on the electrode geometry.

5.6.1 Resonances as a function of sensor physical length

The similarity of the prototype sensor with the stub line models lies in the fact that both are described as open-circuited transmission lines. In the scour probe tests, the physical length of the prototype sensor remains the same and the electrical length is changing due to permittivity effects originated by a change in the ratio of the segments exposed to water and saturated soil. On the contrary, during the stub line measurements, permittivity remains the same but the electrical length is changing due to a change in the physical length of the cable.

Two sensors with electrode lengths of 50 cm and 100 cm where fabricated and tested in air. Each sensor consisted of four paired strips and inserted into a fibre glass access tube. The geometric components of the sensor were based on the findings of the FEM study as presented in section 4.4.4 of Chapter 4. The inner conductors of the coaxial cables were then connected to each pair of strips as shown in Figure 5.32.
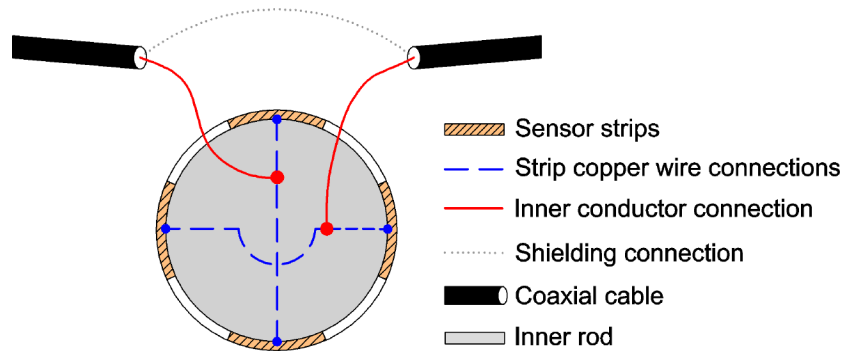
Figure 5.32: Schematic diagram presenting the sensor electrode connections with the inner conductors of the coaxial cables linking to the transmission and reflection ports of the VNA.

The system consisted of a signal source (i.e. VNA) transmitting the incident energy through a 50 Ohm coaxial cable. The connection arrangement of the prototype sensor with the measurement system comprises of the sensor impedance (Z_p) positioned in series with the impedances that correspond to the coaxial cables as presented in Figure 5.33 (a). Conversely, the cable impedance in the stub line experiments (Z_s) is placed in parallel with the characteristic impedance of the BNC cables [see Figure 5.33 (b)].
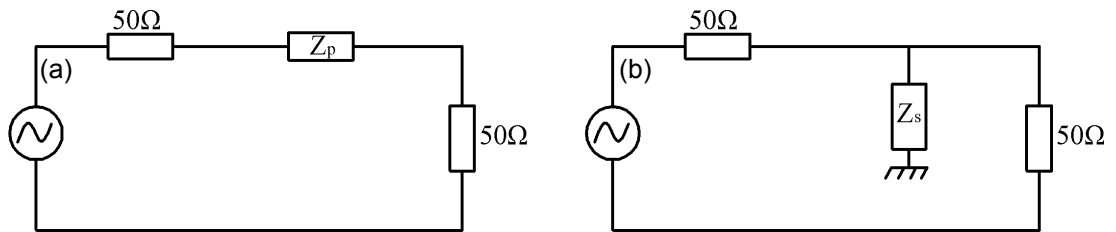
Figure 5.33: Measuring system **(a)** with the sensor impedance (Z_p) placed in series and **(b)** the stub impedance (Z_s) placed in parallel.

The different impedance connections with the measuring system, in series (prototype sensor) or in parallel (stub lines), is expected to have an opposite effect on the incident signal in each case. A low sensor impedance value for Z_p when it is connected in series is expected to result in an improved match of the sensor impedance with the characteristic one (i.e. 50 Ohms) in favour of the signal transmission. Conversely, when the Z_s is connected in parallel with the measuring system most of the incident signal will be reflected when the stub impedance has a low value. Due to these impedance arrangements, the reflection ratio obtained from stub line tests corresponds with and was compared to the transmission ratio recorded from the prototype sensor.

The sensors with equal electrode lengths of 50 cm and 100 cm were compared with the results obtained from stub line lengths of 52 cm and 101 cm respectively. As shown in Figure 5.34, a reasonable agreement is recorded between the prototype sensor and stub cable frequency responses. The variations in Figure 5.34 (a) can be attributed to slight differences between the cable (52 cm) and the sensor (50 cm) lengths but mainly to the 'open' rather than the enclosed coaxial line in the case of the BNC cables. A similar behaviour of the transmitted and reflected ratios is apparent in Figure 5.34 (b) which reach their maximum values at frequencies where the transformation from open (even multiples of $\lambda/4$) to short (odd multiples of $\lambda/4$) circuit occurs. When the nominal length of both the sensor and the stub cable is increased to 100 cm, the electrical length is also increased which results in more resonance points as presented in Figure 5.34 (b).
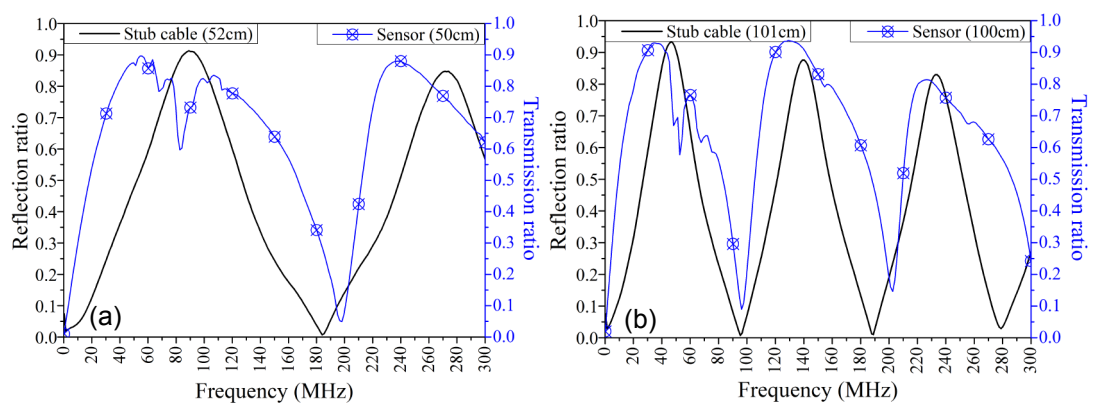
Figure 5.34: Comparison between reflection (stub line) and transmission (prototype sensor placed in air environment) ratios for nominal lengths of **(a)** 50 cm and **(b)** 100 cm. A reasonable agreement is obtained in both cases with more resonances occurring for the length of 100 cm due to increased electrical length.

Figure 5.35 compares the transmission ratio recorded for 50 cm and 100 cm sensor lengths respectively. A similar relationship with the stub cable experiments is identified with the prototype sensor, i.e. the obtained frequency response is a function of the electrode length ratio. When the sensor length is doubled, the frequency that corresponds to the first null point (at an even multiple of $\lambda/4$) is practically reduced by half from 198 MHz to 98 MHz, as shown in Figure 5.35. Minor differences can be attributed to the fabrication procedure of the sensor and the laboratory conditions.
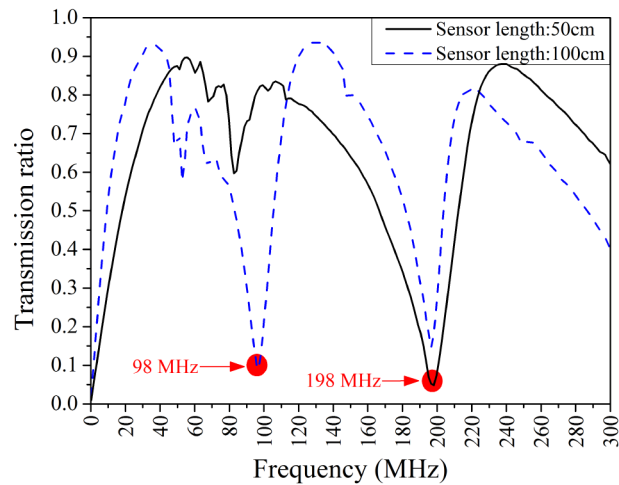
Figure 5.35: Transmission characteristics obtained in air environment for sensor lengths of 50 cm and 100 cm for the frequency range from 0.3 MHz to 300 MHz. The comparison indicates that resonance points are a function of the sensor electrical length.

In conclusion, the similarities between the prototype sensor and the stub line have been demonstrated. By comparing the behaviour of stub lines and the scour sensor having different lengths, it was shown that the location of crests and troughs in the transmitted or reflected signal spectrum are directly associated with the physical length of the sensor. The investigation also indicates that the optimum frequency of the sensor is anticipated to vary and be a function of the physical length of its electrodes.

The results of this study can therefore be used to predict the characteristic frequency points for sensors of various electrode lengths. The sensor geometry is also proposed to be used as a tool to fine-tune the optimum frequency to be matched with commercial available oscillators, which is advantageous for the development of the electronics concept. The investigation presented in the next sections aimed to identify the optimum frequency of the prototype sensor for measuring 'static' scour depth variations under different environmental conditions.

5.7 Preliminary sensor evaluation in 'static' scour tests and various environmental conditions

The study validated the sensor response under environmental conditions commonly encountered in the field. The experiments were carried out in the laboratory and were intended to detect the optimum frequency and validate the calibration curves of the sensor for different soil types, using fresh and saline water at different temperatures.

5.7.1 Experimental procedures

Two different sensors were fabricated having length of 50 cm and 100 cm respectively with electrodes formed by two pairs of strips. The probe assembly was then inserted into a fibre glass protective tube (see Figure 5.36).
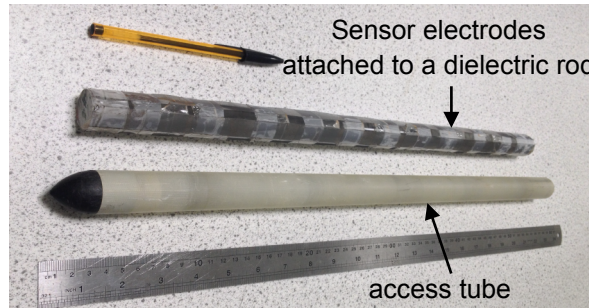
Figure 5.36: Sensor with electrodes length of 50 cm and access tube.

As shown in Figure 5.37, the upper parts of the two facing strips were connected together using a thick copper wire and the inner conductors of the coaxial cables were then attached to each copper wire (a schematic diagram of the strip connections was also presented in Figure 5.32). The shield parts of the coaxial cables were connected together for continuity of the transmission line. The other end of the sensor represented an open-circuit as the electrodes were all electrically isolated.
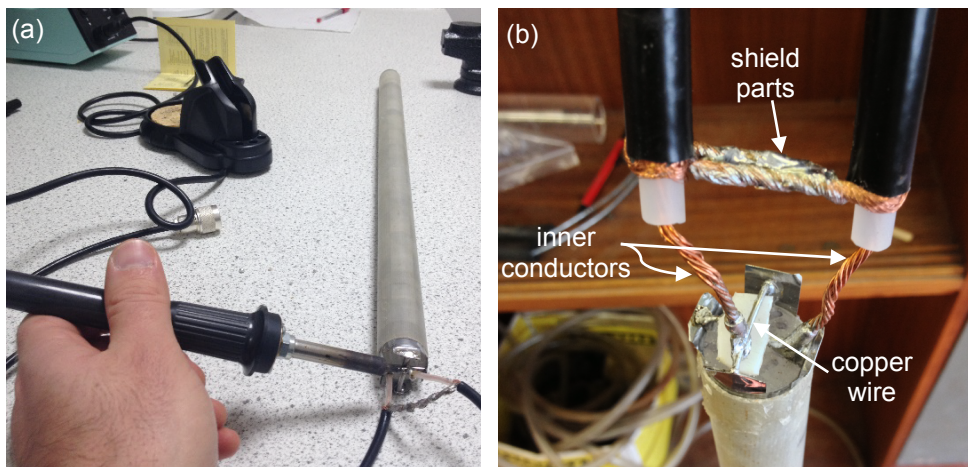
Figure 5.37: (a) Shielding of the two facing electrodes with the coaxial cable and **(b)** connection of each sensing part composed of two electrodes (which each one consisted of two paired facing strips) connected with the inner conductors of the coaxial cables.

The probe was connected to two coaxial cables linked to the VNA, as presented in Figure 5.38 (a). A waterproof housing was used which consisted of a polycarbonate enclosure and a cable gland to seal and protect the upper section of the probe from getting in contact with the damp materials used in the experiments [see Figure 5.38

(b)]. The probe was inserted into a clear acrylic tank with diameter and height of 250 mm and 1250 mm respectively, as shown in Figure 5.38 (c).
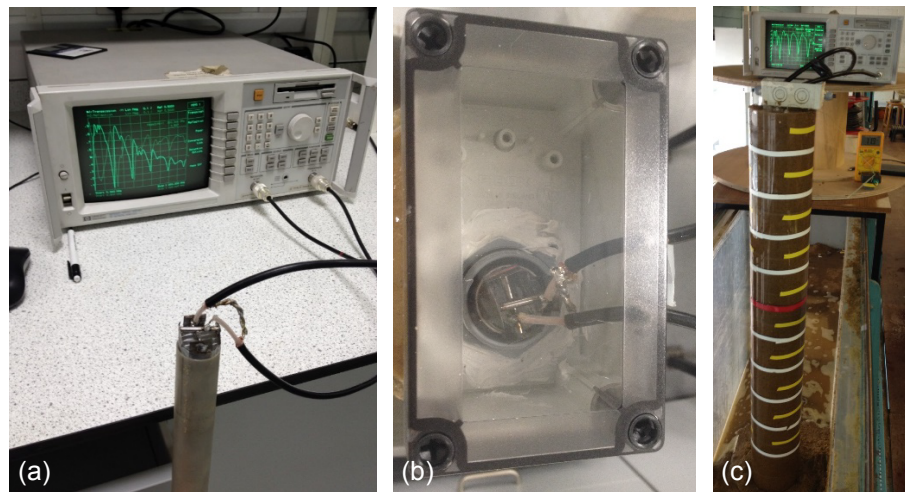
Figure 5.38: (a) Prototype sensor connected to the network analyser, **(b)** waterproof housing used to protect the sensing part during experiments and **(c)** assembly of experimental set up.

The investigated soil types consisted of medium gravel, coarse sand, medium sand and a mixture of silt-clay with median grain sizes D_{50} of 13.8 mm, 1.05 mm, 0.375 mm and 0.0313 mm respectively, which were determined according to ASTM D6913 - 04(2009) standard. The salinity effect was also evaluated with saline aqueous solutions of 35 parts per thousands (ppt) of NaCl that were prepared by dissolving in fresh water 0.598 moles (mol) of NaCl per litre (L).

A feasibility study was initially carried out testing the 50 cm sensor in air, fresh and saline water of 35 ppt of NaCl while bed level variations were mimicked with coarse sand sediment. The influence of the variation of water-saturated soil interface on the transmission signal of the 100 cm sensor was then validated in fresh and saline water of 35 ppt for gravel, coarse sand, medium sand and a mixture of silt-clay. Measurements were recorded at depth intervals of 10 cm as this resolution was considered acceptable for scour monitoring at a real foundation structure. A subsequent set of experiments using the same sediments evaluated the temperature influence on the transmission characteristics of the sensor at 4 ºC and 12 ºC.

5.7.2 Feasibility study using a 50 cm sensor

Figure 5.39 presents the response of a four strip sensor with electrodes of equal length of 50 cm when tested in air, fresh water and water with salinity of 35 ppt of NaCl at the temperature of 15 °C. When the probe was inserted into fresh water environment it is observed an increase of the electrical length due to the higher permittivity of water when compared to air. The frequency of the first trough point where the transmission ratio reaches a value close to zero is also reduced from 199 MHz in air environment to 121 MHz in fresh water conditions. The frequency of the first trough point when the sensor was tested in saline water was also recorded at 117 MHz which is close to the one obtained in fresh water. However, the presence of salinity in water had a significant impact on the amplitude as the resonances are reduced compared to the other tested mediums.
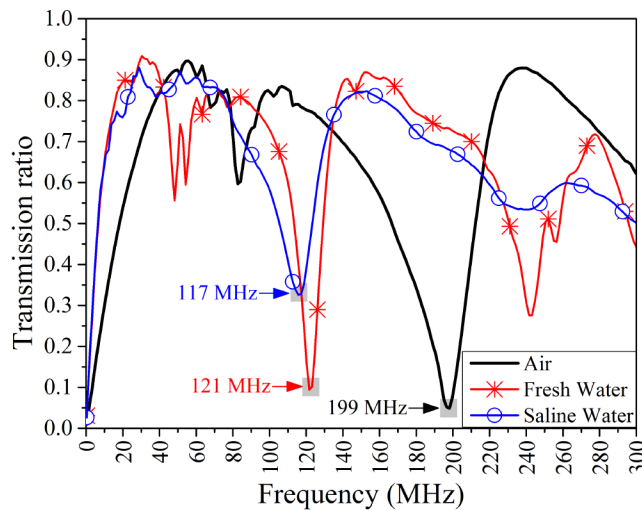
Figure 5.39: Evaluation of 50 cm sensor in air, fresh and saline water for the frequency range from 0.3 MHz to 300 MHz. The presence of fresh water led to an increase of the electrical length compared to air environment while salinity in water decreased the amplitude of the resonance points.

Figures 5.40 and 5.41 present the sensor output when it was subjected to various water – saturated coarse sand interfaces that simulated 'static' scour processes using fresh and saline water respectively. The resonance points of the various frequency responses correspond to scour depth steps of 5 cm. As shown in Figure 5.40, two resonance troughs are obtained in fresh water. It is also observed that increased scour depth led to a decrease of the frequency points that correspond to crests and troughs, which is particularly evident at the frequency band between 100 MHz and 270 MHz.
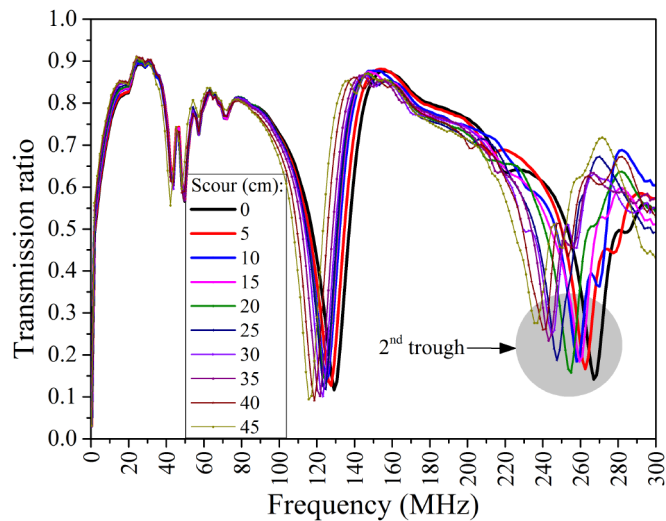
Figure 5.40: Results obtained in 'static' scour experiments with a 50 cm prototype sensor in coarse sand sediment using fresh water. Two resonance troughs are obtained while the electrical length is increased for greater scour depths which results in a decrease of the frequency points where transmission troughs occur.

The amplitude of the resonance transmission ratio appears to be reduced in the tests carried out in saline water for the frequency range from 0.3 MHz to 300 MHz (see Figure 5.41). The trough resonance frequencies are almost insensitive to bed level variations compared to the response observed in fresh water. A decrease in the amplitude between the first transmission crest - trough is also observed. The amplitude of the second transmission trough, which occurred in fresh water in the frequency range from 230 MHz to 270 MHz (see Figure 5.40), is also significantly reduced in saline water as depicted in Figure 5.41.
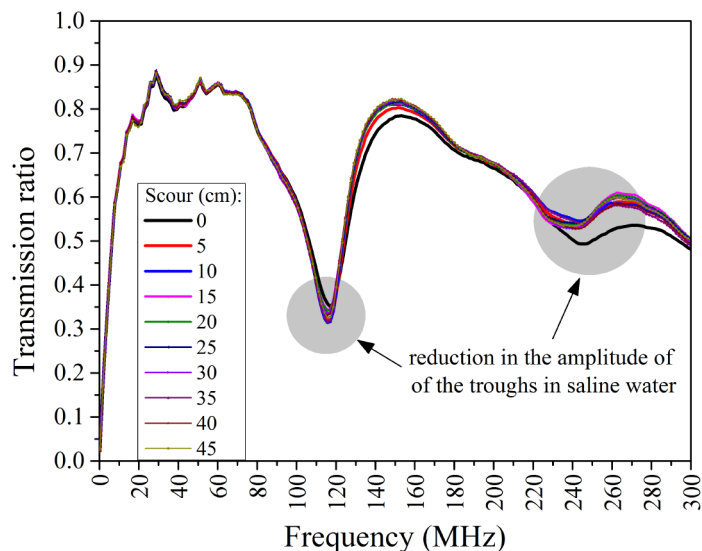
Figure 5.41: Results obtained in 'static' scour experiments with a 50 cm prototype sensor in coarse sand sediment using water with salinity of 35 ppt of NaCl. A significant reduction in the amplitude of the crests and troughs is observed compared to the results obtained in fresh water.

The study then intended to identify the optimum frequency which can provide an accurate indication of scour measurement. Figure 5.42 (a) focuses on the frequency range that corresponds to the transition from the first trough to the next crest which are occurring at even and odd multiples of $\lambda/4$ respectively. It is observed that increased scour depth in fresh water resulted in a decrease of the frequency of the null point and also to an increase in the transmission ratio at the frequency of 130 MHz. A different frequency of 151 MHz was identified for the case of saline water where the sensor sensitivity appears to be reduced due to the bunching of the curves at higher levels of scour, as depicted in Figure 5.42 (b).
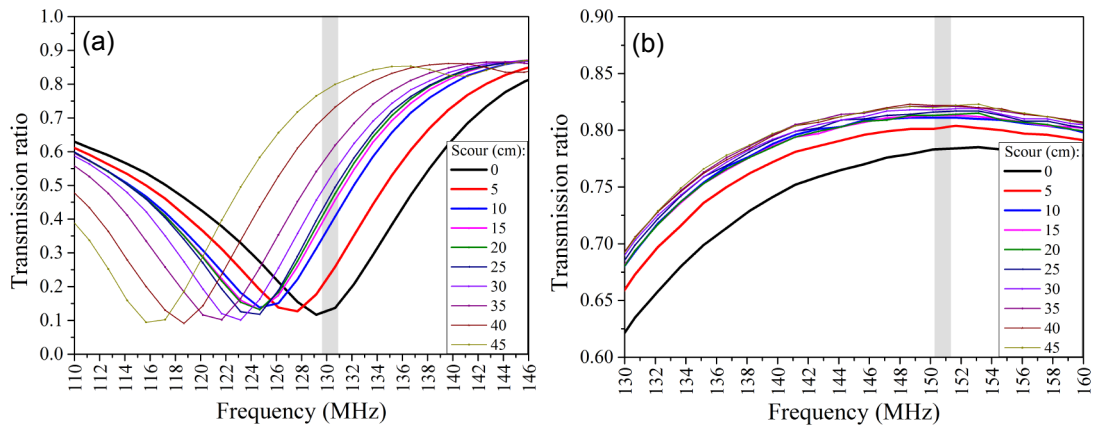
Figure 5.42: Behaviour of transmission characteristics in **(a)** fresh and **(b)** saline water focusing on frequency ranges of 110-146 MHz and 130-160 MHz respectively. The grey highlighted areas correspond to the frequencies that were selected for further analysis.

The frequencies of 130 MHz and 151 MHz were selected to be analysed further and presented in Figure 5.43. The sensor in fresh water satisfactorily responded to scour depth variations. The calibration curve exhibits a plateau at mid-length of the sensor which indicates a less sensitive region [see Figure 5.43 (a)]. The sensitivity of the scour probe was also found to be reduced significantly when saline water was used in the experiments, as depicted in Figure 5.43 (b). In fresh water the maximum voltage difference between water and saturated sediment conditions is recorded at the range of 450 mV, while in saline water is decreased to almost 20 mV (see Figure 5.43).
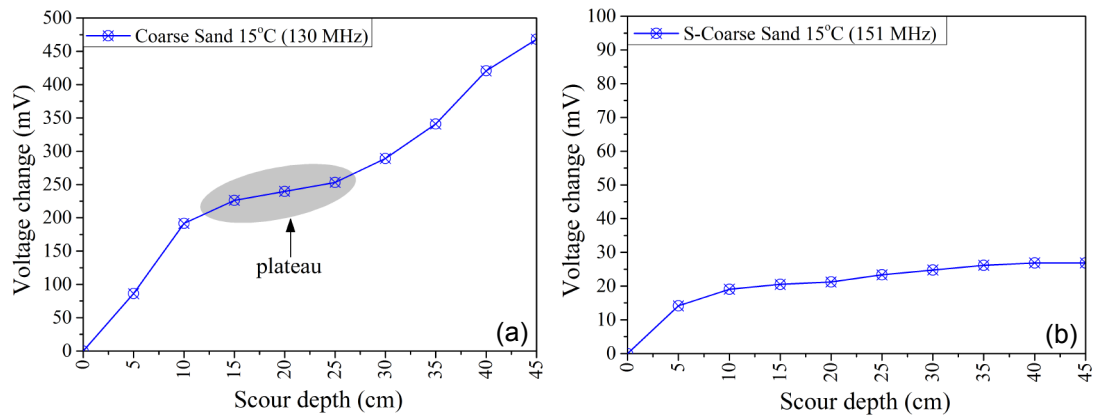
Figure 5.43: Scour depth measurement based on voltage relative change obtained for 50 cm prototype sensor using coarse sand sediment in **(a)** fresh water conditions at the frequency of 130 MHz and in **(b)** water with salinity of 35 ppt of NaCl at the frequency of 151 MHz.

In conclusion, different optimum frequencies in fresh and saline water were identified in order to provide a useful measure of scour conditions. The sensor accurately responded to variations in the water-saturated coarse sand interface, but its sensitivity was significantly reduced in 'static' scour simulations using saline water of 35 ppt of NaCl.

5.7.3 Evaluation of 100 cm sensor in various environmental conditions

Figure 5.44 presents the results obtained in air, fresh water and saline water of 35 ppt of NaCl at the temperature of 12 $^{\circ}$C. Above the frequency of 80 MHz the amplitude of the resonance crests and troughs are observed to be reduced significantly in saline water.
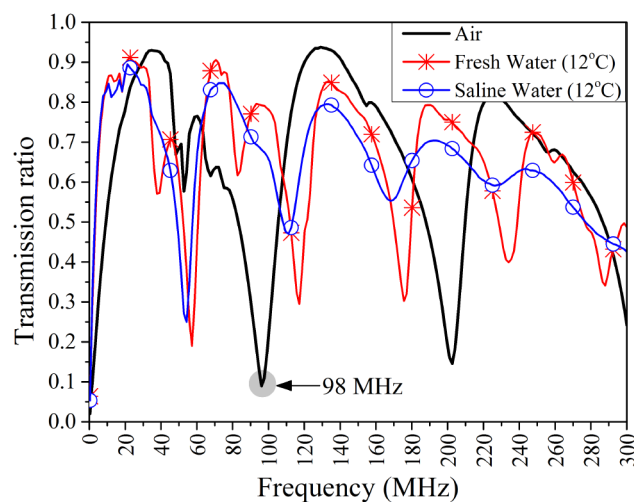
Figure 5.44: Frequency response obtained with 100 cm prototype sensor in air, fresh and saline water of 35 ppt of NaCl conditions at the temperature of 12 $^{\circ}$C at the frequency range 0.3 MHz - 300 MHz.

It is noticeable that the sensor resonances are also a function of the sensor length. When the electrodes length is increased from 50 cm to 100 cm the frequency point of the first trough obtained in air environment is reduced by almost half from 199 MHz to 98 MHz respectively (see Figures 5.39 and 5.44).

Soil type influence

The response of the prototype sensor was tested in different sediments using fresh water. A typical example of the obtained transmission characteristics when scouring process was imitated in gravel soil at temperature of 12 ºC is presented in Figure 5.45. A frequency change of the resonance points and a shift of the transmitted signal amplitude at given frequency is detected as usual as scour proceeds.
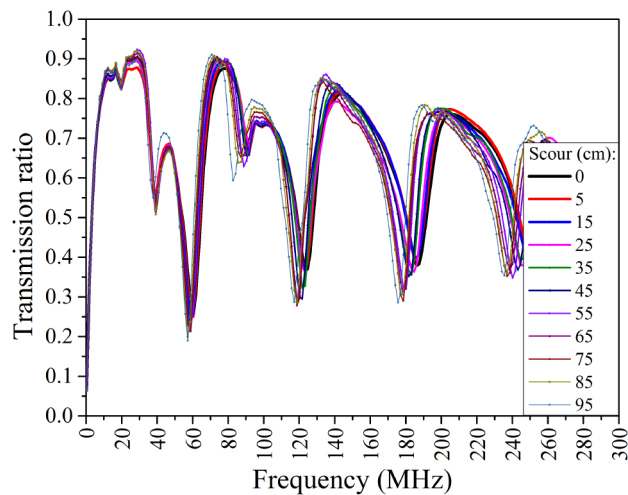
Figure 5.45: Transmission ratio obtained in 'static' scour experiments using a 100 cm sensor in gravel soil type using fresh water at the frequency range from 0.3 MHz to 300 MHz.

Figure 5.46 presents the transmission signal of the sensor obtained in 'static' scour simulations using gravel, coarse sand, medium sand and a silt/clay mixture. In the frequency range from 60 MHz to 70 MHz a satisfactory separation of the frequency responses is obtained in the vertical direction for all the tested sediments. The separation of the transmission characteristics is observed to be decreased in all soil types for scour depths between 35 cm and 75 cm which corresponds to the mid-length of the sensor. The frequency of 64.7 MHz was selected as the optimum one and was further analysed.
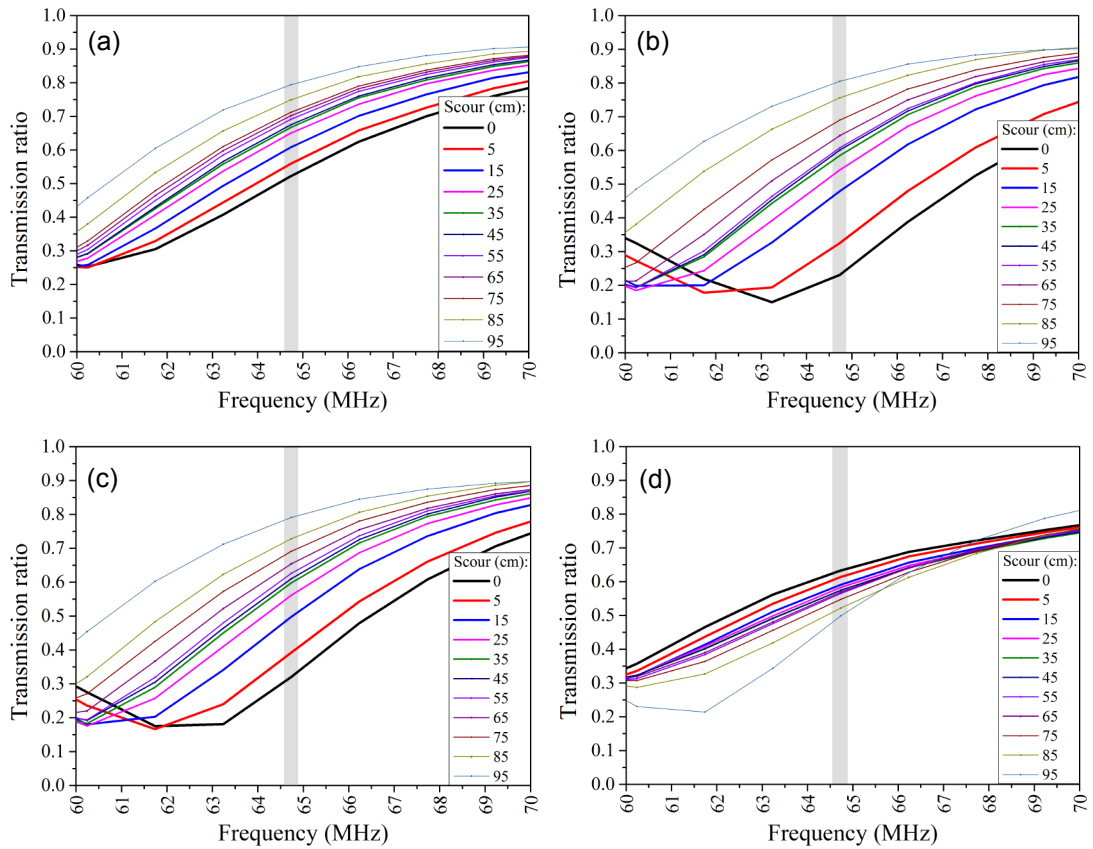
Figure 5.46: Frequency response obtained in 'static' scour experiments with the 100 cm prototype sensor using fresh water at temperature of 12°C in **(a)** gravel, **(b)** coarse sand, **(c)** medium sand and a **(d)** mixture of silt-clay at the frequency range from 60 MHz to 70 MHz. The grey highlighted columns correspond to the frequency that was selected for further analysis (64.7 MHz).

The analysis of the calibration curves obtained for various sediments at the optimum frequency of 64.7 MHz in fresh water is shown in Figure 5.47. Increased scour depth had a cumulative effect on the transmitted voltage change which reached a maximum value of 405 mV for coarse sand soil type and a minimum value of 80 mV for silt-clay sediment. The instrument also appears to be less sensitive in the region that corresponds to the mid-length of the sensor.
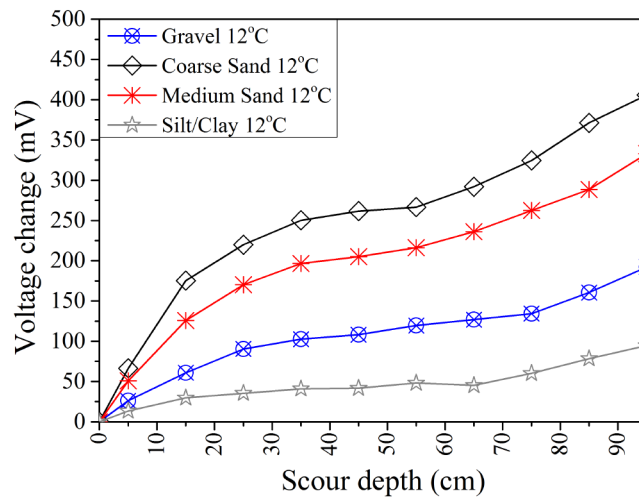
Figure 5.47: Scour depth measurements at intervals of 10 cm based on voltage change obtained with 100 cm prototype sensor in various soil types at optimum single frequency of 64.7 MHz in fresh water conditions at the temperature of 12 °C.

The results indicated that at the optimum frequency the sensor responded satisfactorily to different scour depths. A dependency of the calibration curve on the soil type was also detected while the linearity and sensitivity of each calibration curve is found to be decreased for scour depths between 35 cm and 75 cm which corresponds to the middle length of the sensor. The sensor optimum frequency also appears to be a function of its electrodes length as it is reduced by half (from 130 MHz to 64.7 MHz) when the electrodes length are doubled (from 50 cm to 100 cm), as shown in Figures 5.42 and 5.46.

Salinity influence

The sensor performance in saline water of 35 ppt of NaCl was then investigated at the temperature of 12 °C using the same soil types. Figure 5.48 presents a typical response of the transmission ratio when scour process was mimicked in gravel sediment. It is observed that the obtained frequency response is hardly affected and the sensor signal do not experience a noticeable change for the different bed levels that represented increasing scour depths.
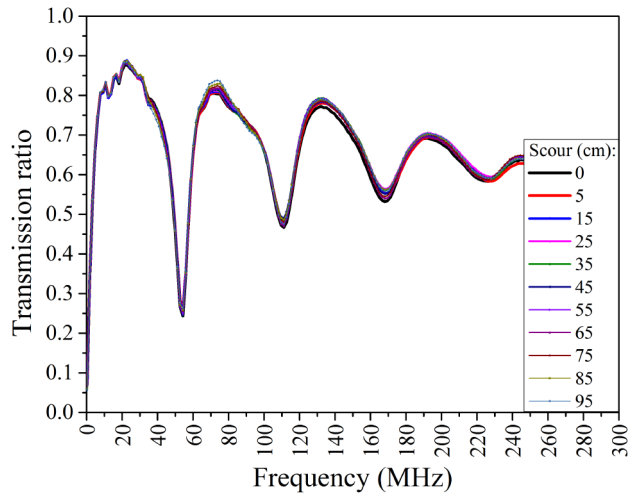
Figure 5.48: Transmission characteristics obtained in 'static' scour simulations using a 100 cm sensor in gravel soil type using saline water at the frequency range from 0.3 MHz to 300 MHz.

The sensitivity of the sensor is observed to be significantly reduced in saline water due to the reduction in the separation of the transmission characteristics in vertical direction (see Figure 5.49). The frequency of 75.2 MHz occurring at the crest of an odd multiple of $\lambda/4$ is selected for further analysis for all the tested soil types.
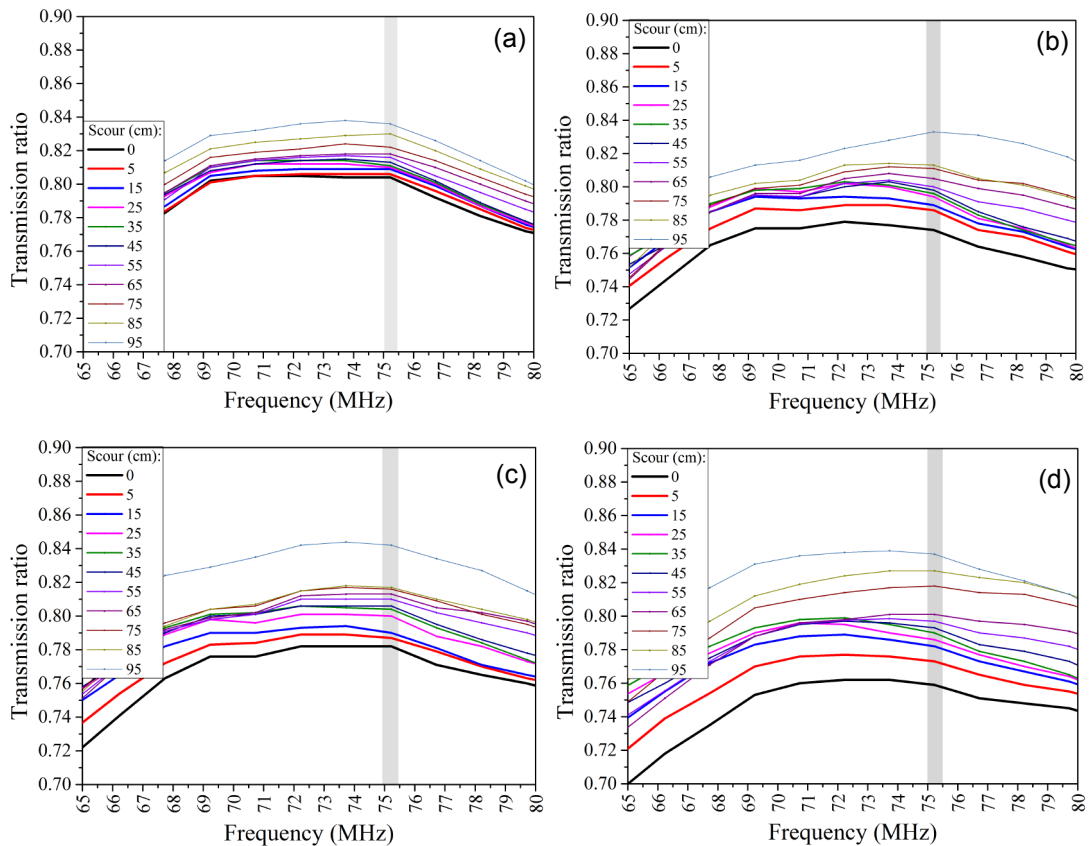
Figure 5.49: Frequency response obtained in 'static' scour experiments with the 100 cm prototype sensor using saline water of 35 ppt of NaCl at temperature of 12°C in **(a)** gravel, **(b)** coarse sand, **(c)** medium sand and a **(d)** mixture of silt/clay at the frequency range 65 MHz - 80 MHz. The grey highlighted columns corresponds to the frequency that was selected for further analysis (75.2 MHz).

The transmitted signal response to increased scour depth at the optimum frequency in saline water of 35 ppt of NaCl at the temperature of 12°C is presented in Figure 5.50. At the selected frequency of 75.2 MHz the sensor recorded scour processes at depth intervals of 10 cm but its sensitivity is significantly reduced. For instance, the maximum voltage change for coarse sand sediment is recorded at 42 mV compared to 405 mV obtained in fresh water which is a reduction by 89.6%. It is also worth noticing that the maximum voltage change is achieved when the sensor was tested in the sediment of silt/clay which is in contrast with the results obtained in fresh water environment (presented in Figure 5.47). However, other studies (Reedy and Scanlon, 2003; and Kelleners et al., 2004) have highlighted that the interaction of elevated salinity levels and high clay contents in sediments can adversely affect and cause large errors in EM sensor measurements. The results obtained in silt/clay soil type might also be associated with errors in the laboratory experimental set up. This phenomenon was not investigated further.
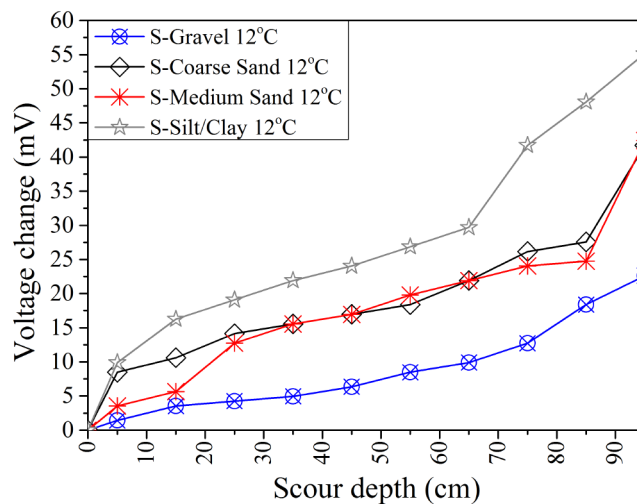
Figure 5.50: Scour depth measurements at intervals of 10 cm based on voltage change obtained with 100 cm prototype sensor in various soil types at optimum single frequency of 75.2 MHz in saline water of 35 ppt of NaCl conditions at the temperature of 12 °C. A significant decrease in the sensitivity of the sensor by 89.6% is pointed out when saline water was used in the experiments.

The findings indicated that salinity in water had a significant adverse effect on sensor readings. A different optimum frequency was selected compared to the tests in fresh water to provide measurements of scour depth levels. It is also worth noticing that the optimum frequency in saline water also depends on the electrodes length of the sensor and is reduced by half (from 151 MHz to 75.2 MHz) when the sensor length is doubled (from 50 cm to 100 cm), as shown in Figures 5.42 and 5.49.

Temperature influence

The temperature influence on the sensor response was evaluated in 'static' scour experiments at the temperature of 4 ℃ as presented in Figure 5.51 and 5.52. The effect of the mixture of silt-clay on the sensor signal was not assessed further in this study as this soil type is more unlikely to be the original soil and/or the refilling material in the case of a riverbed. This is due to its very fine particles which at high flow conditions, usually generated in the middle of a river cross section from the presence of an obstacle (i.e. foundation element), is transported away and not deposited. The tests were therefore carried out using gravel, coarse sand and medium sand in fresh and saline water of 35 ppt of NaCl. Similar behaviour of the frequency response as with the temperature of 12 ℃ is observed for the results obtained at water temperature of 4 ℃. The selected optimum frequencies in fresh and saline water are also the same for both water temperature conditions and corresponded to 64.7 MHz and 75.2 MHz, as shown in Figures 5.51 and 5.52 respectively.
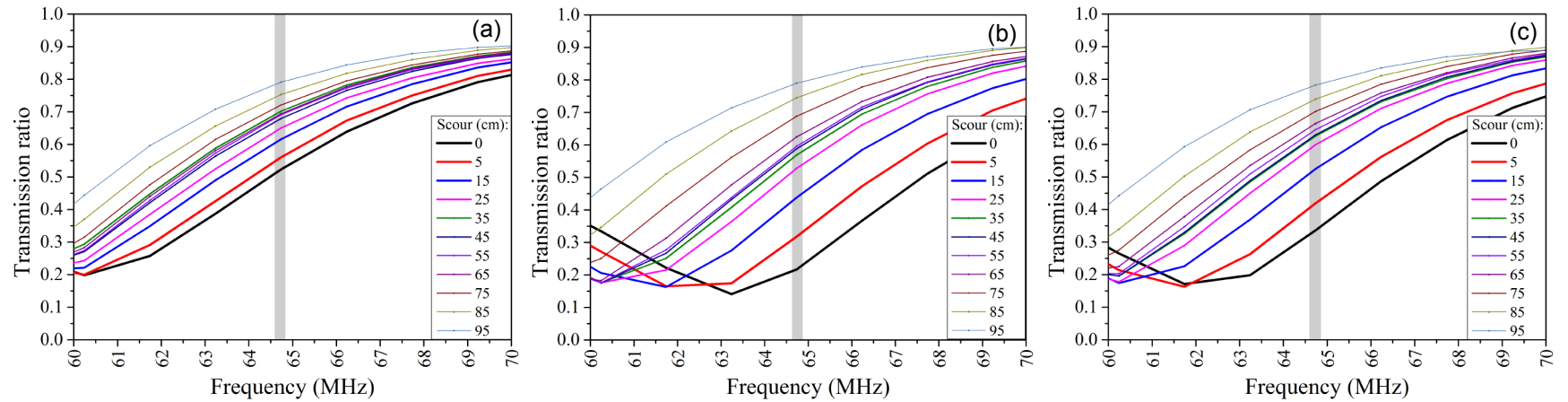
Figure 5.51: Frequency response during 'static' scour tests with the 100 cm sensor using fresh water at temperature of 4°C in **(a)** gravel, **(b)** coarse sand, **(c)** medium sand at the frequency range from 60 MHz to 70 MHz. The grey highlighted columns corresponds to the frequency that was selected for further analysis (64.7 MHz).
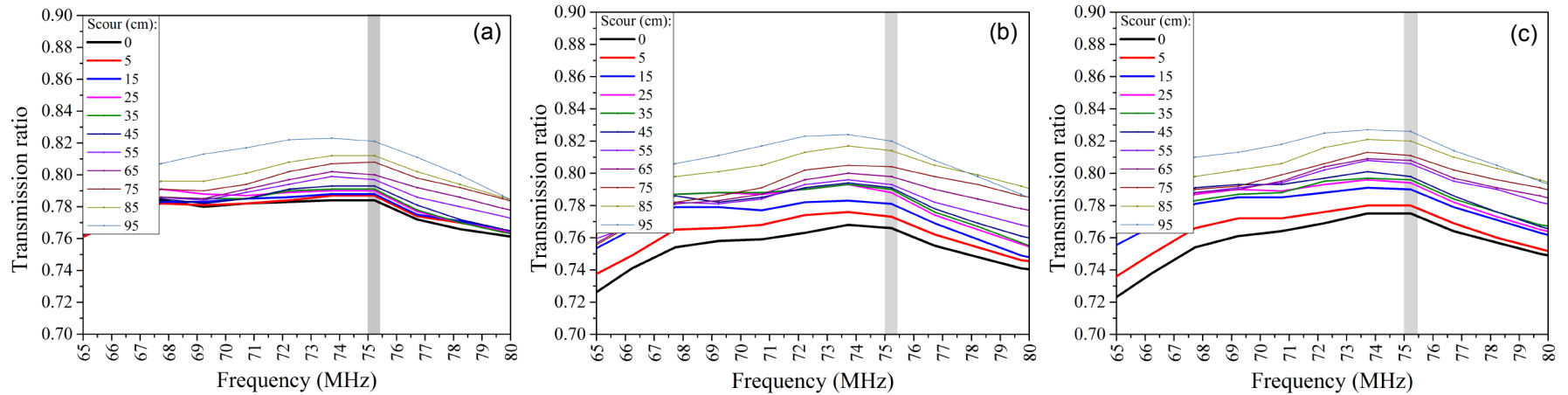
Figure 5.52: Frequency response during 'static' scour tests with the 100 cm sensor using saline water at temperature of 4°C in **(a)** gravel, **(b)** coarse sand, **(c)** medium sand at the frequency range from 65 MHz to 80 MHz. The grey highlighted columns corresponds to the frequency that was selected for further analysis (75.2 MHz).

The results obtained at the temperature of 4°C using fresh and saline water are presented in Figures 5.53 (a) and 5.53 (b) respectively. The maximum transmitted voltage change in fresh and saline water of 35 ppt is recorded in coarse sand sediment at 405 mV and 38 mV respectively which are similar with the values obtained at temperature of 12 °C (as presented in Figures 5.47 and 5.50). The calibration curves are also found to be dependent on the soil type as shown in Figure 5.53. The various water temperatures do not appear to have a significant effect on the sensor readings.
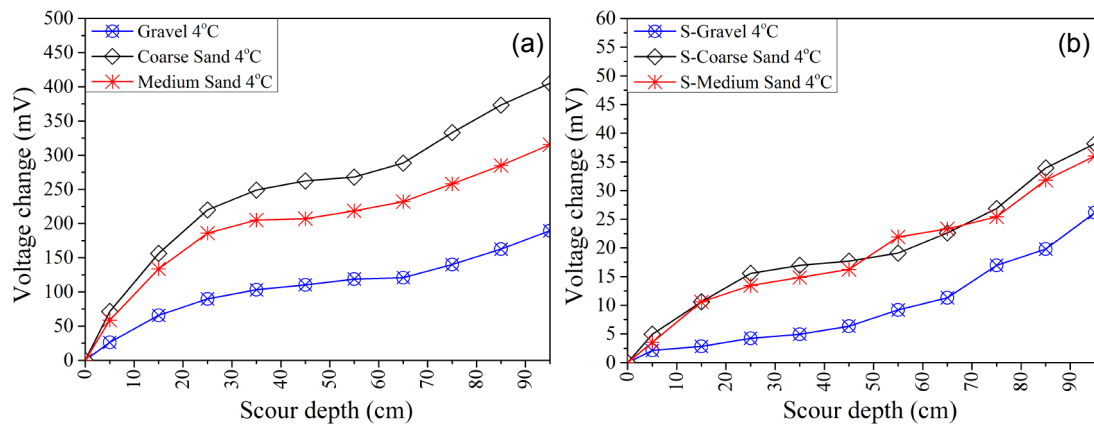

Figure 5.53: Scour depth measurements at intervals of 10 cm based on voltage change obtained with 100 cm prototype sensor in various soil types at optimum single frequencies in **(a)** fresh (64.7 MHz) and **(b)** saline water of 35 ppt of NaCl (75.2 MHz) conditions at the temperature of 4°C. The temperature conditions did not have a major effect on the sensor readings compared to the results obtained at temperature of 12°C.

The results obtained in fresh water indicated that the prototype sensor of 100 cm length successfully measured 'static' scour depth variations. For all the tests carried out in both water conditions a greater voltage change was recorded in coarse sand and medium sand sediments compared to gravel soil type, which highlights that a lower permittivity of the sand sediments was detectable in the experiments. The sensor was also capable of providing scour depth measurements in saline water of 35 ppt despite that the sensitivity of the instrument was significantly reduced compared to the results obtained in fresh water. Different water temperatures at 12 °C and 4 °C did not have a major impact on the frequency response of the sensor. The calibration curves were also dependent on the tested sediments therefore it is underlined that a soil specific calibration is necessary for the accurate determination of scour depth along the probe length. This can be accomplished directly in the field when sliding the probe in the access tube and monitoring the signal when the probe progressively moves downward from the water into the riverbed.

The selected optimum frequencies were also found to be a function of the sensor length and to be doubled when the electrode length is reduced by half. A major limitation of the calibration curve was the decreased sensitivity when scour approaches the centre of the probe length. The study presented in the next sections therefore focused on optimising the electrode geometry of the sensor to achieve uniform sensitivity along the entire probe length.

5.8 Final optimisation of the sensor design and evaluation in various environmental conditions

The experiments carried out with the 100 cm sensor revealed an area that corresponds to the middle of the prototype sensor length where the linearity and sensitivity of the calibration curves were found to be reduced. To optimise the sensor accuracy, an empirical approach was adopted because of complexities in simulating the propagation of electromagnetic waves using three dimensional finite element modelling. The response of the final optimised sensor was then assessed under various environmental conditions that will vary in a practical offshore field.

5.8.1 Enhancing the accuracy of calibration curve

The lack of sensitivity observed at the centre of the probe length is likely to be associated with the formation of a standing wave and the node that is generated at that point. The standing wave node has also a decreasing effect on the sensitivity of the transmission signal to scour depth variation. The sensor optimisation was empirically achieved by progressively reducing the length of one strip from each electrode by 5 cm, 15 cm, 25 cm (see Figure 5.54) and 35 cm. This is anticipated to cause a change from an abrupt impedance discontinuity to a more gradual, distributed one, which is expected to diminish the sharpness of nodes in the standing wave.
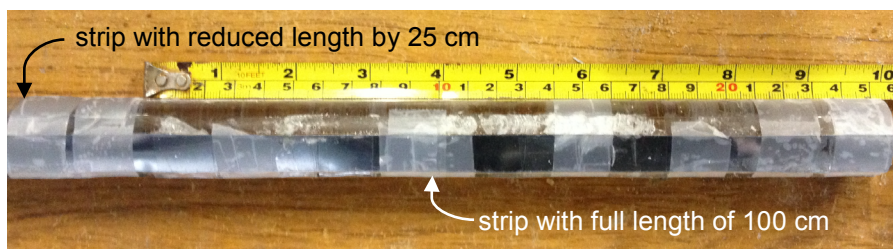
Figure 5.54: Reduction of the strip length from each electrode by 25 cm during the sensor optimisation process.

Tests with each strip length were conducted in coarse sand soil type and fresh water conditions using the same experimental set up and procedures described in section 5.7.1. A comparison between the different sensor electrode models to define the optimal strip length and frequency is presented and discussed as follows.

Figures 5.55 (a) and 5.55 (b) present the behaviour of the transmission characteristics obtained for the frequency band from 0.3 MHz to 300 MHz for different reduced strip lengths in air and water environment respectively. The higher permittivity in water conditions caused the decrease of the wavelength and led to an increase of the electrical length when compared to air environment for all tested electrode lengths.
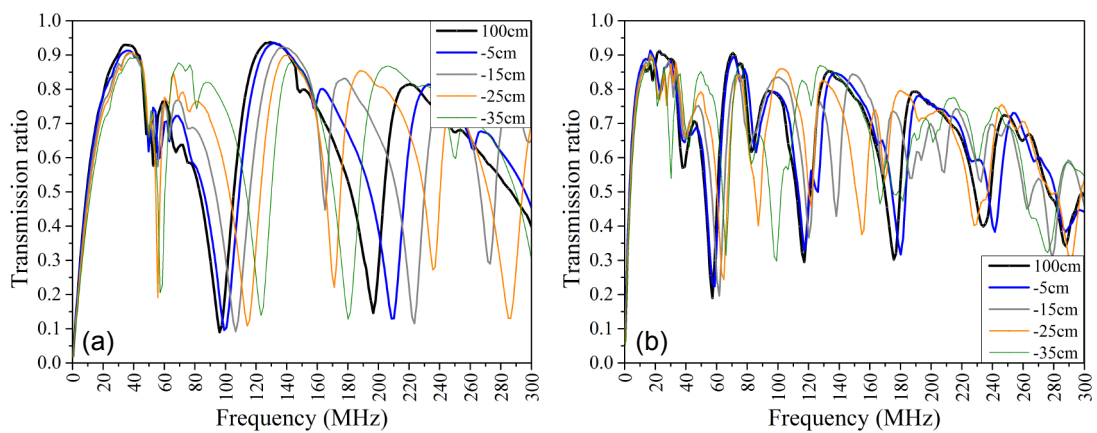
Figure 5.55: Transmission ratio obtained with 100 cm prototype sensor and for reduced strip length from each electrode by 5 cm, 15 cm, 25 cm and 35 cm at the frequency range from 0.3 MHZ to 300 MHz in **(a)** air and **(b)** water environment. The high permittivity of water medium led to the increase of the electrical length and decrease of the wavelength for all different tested electrode lengths.

Figure 5.56 (a) and 5.56 (b) focuses on the frequency range where the first transmission trough is obtained in air and water conditions respectively. The reduction in length of one strip of each electrode by 5 cm, 15 cm, 25 cm and 35 cm caused an increase of the frequency point that corresponds to the first transmission trough in both tested environments.
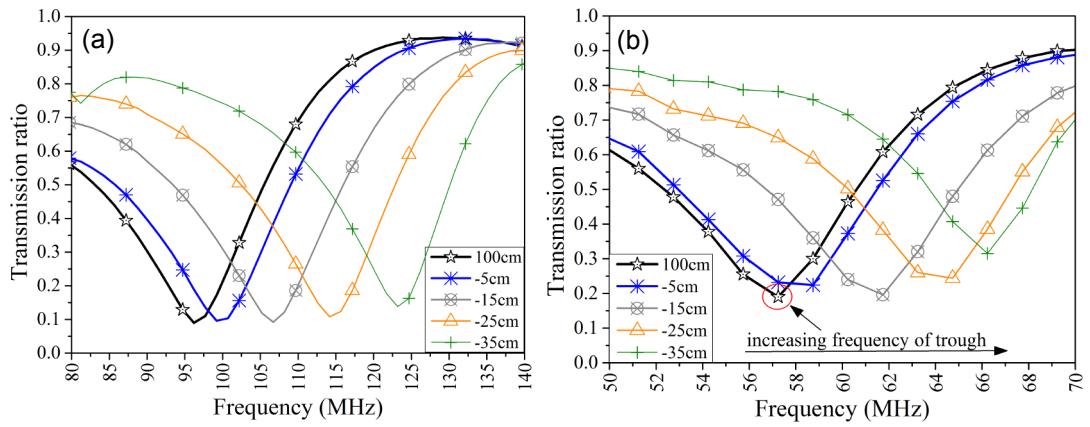
Figure 5.56: Transmission ratio obtained with 100 cm prototype sensor and for reduced strip length by 5 cm, 15 cm, 25 cm and 35 cm in **(a)** air environment focusing at the range from 80 MHz to 140 MHz and in **(b)** water conditions at the frequency band from 50 MHz to 70 MHz. The gradual shortening of the one strip of each electrode caused an increase of the frequency point of the first transmission trough.

'Static' scour simulations in coarse sand sediment were then carried out for each electrode length and the investigation focused on the frequency range from 60 MHz to 70 MHz, as shown in Figure 5.57. The gradual reduction in length of one strip of each electrode caused a progressive increase of the first trough resonance frequency. A better separation of the transmission characteristics along the vertical axis is also detected when the electrode is gradually shortened. This improved separation is particularly evident for scour depths between 35 cm and 55 cm which is achieved for one strip from each electrode decreased in length by 25 cm and 35 cm, as depicted in Figures 5.57 (d) and 5.57 (e). Different frequencies were selected to be analysed further for the various strip lengths due to changing frequency of the trough point occurring at the range 60 MHz to 70 MHz.
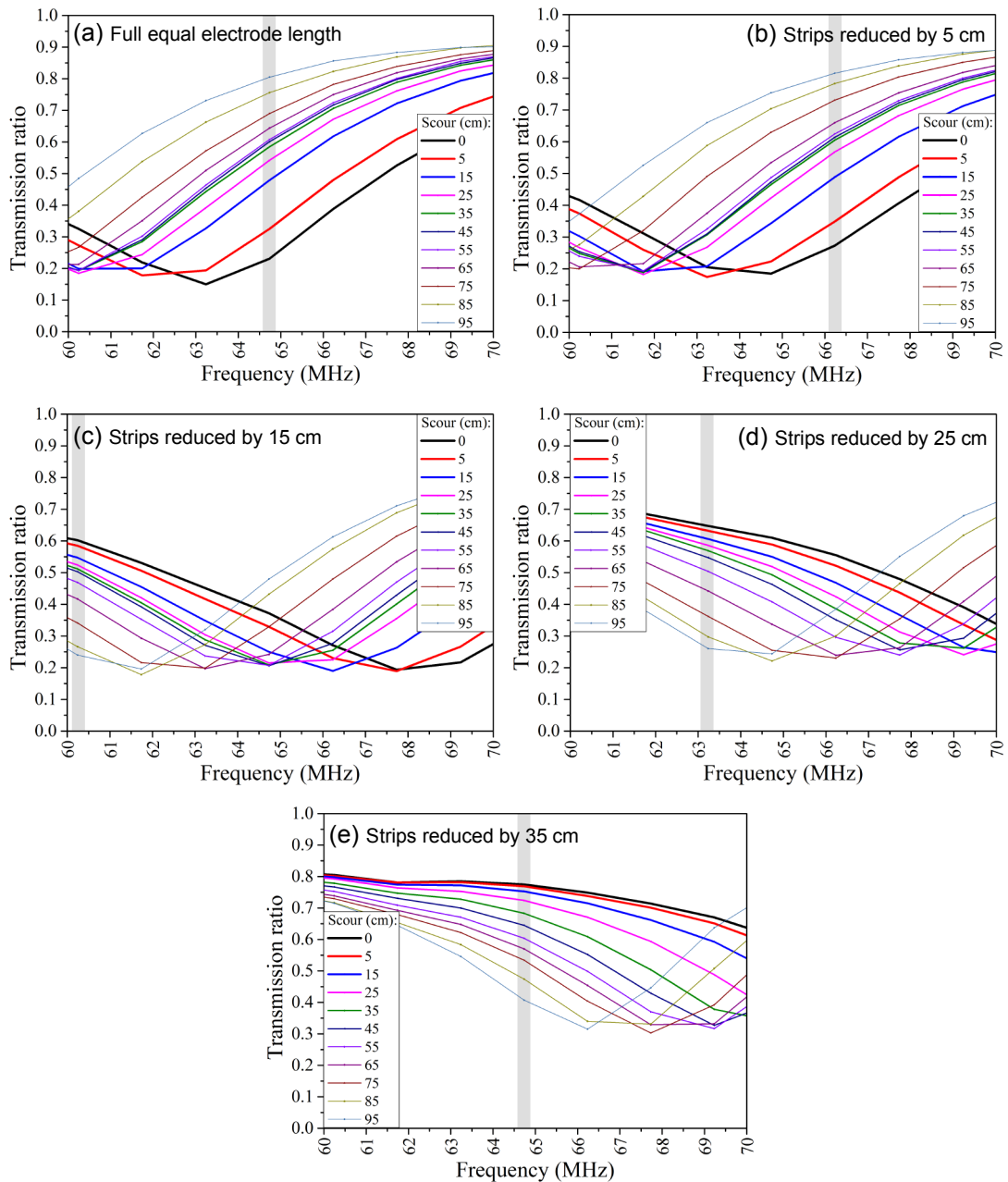
Figure 5.57: Results obtained in 'static' scour simulations in coarse sand sediment investigating the effect on the frequency response of **(a)** a sensor with full equal electrode lengths of 100 cm compared to reduced strip of each electrode by **(b)** 5 cm, **(c)** 15 cm, **(d)** 25 cm and **(e)** 35 cm at the frequency range from 60 MHz to 70 MHz. The gradual shortening of each electrode led to an improved separation of the transmission characteristics in the vertical direction. Various frequencies, highlighted grey columns, were selected for further analysis.

Figure 5.58 presents the transmitted voltage change of the prototype sensor recorded for increased scour depth and the linear fit obtained for each electrode length. A plateau is created in the region that corresponds to the mid-length of the prototype sensor which is evident for the full equal electrode lengths and the cases of the strips reduced by 5 cm and 15 cm. The plateau is also observed to disappear and a more

gradual voltage increase is obtained for the tests carried out with electrode strips reduced by 25 cm and 35 cm.
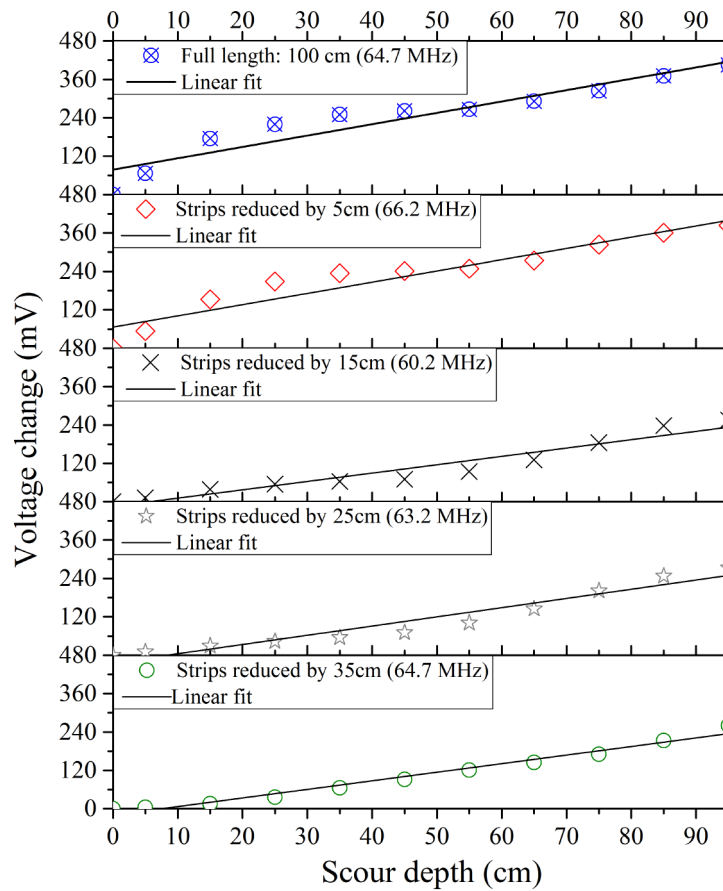
Figure 5.58: Transmitted voltage change obtained in 'static' scour experiments in coarse sand sediment investigating the effect on the frequency response of a sensor with full equal electrode lengths of 100 cm compared to the reduced length of one strip from each electrode by 5 cm, 15 cm, 25 cm and 35 cm at different selected frequencies in the range from 60 MHz to 70 MHz.

The sensitivity and the linearity of the scatter plots obtained for each electrode length (shown in Figure 5.58) are measured by the slope (*m*) and the Pearson's correlation coefficient (*r*) respectively which are summarised in Table 5.4. A very strong positive relationship of the linearity is obtained between the voltage change and scour depth which is optimised for reduced length of one strip of each electrode by 35 cm with a value of 0.989. The sensitivity of the sensor is also found to decrease slightly from 3.551 mV/cm of scour depth (full equal length electrodes: 100 cm) to 2.682 mV/cm scour depth (strips reduced by 35 cm). This small sensitivity reduction does not have a major influence on the ability of the instrument to measure scour depth at intervals of 10 cm or less. The electrode length reduced by 35 cm was therefore

considered as the optimum one based on the linearity of the correlation coefficient which is close to 1.

Table 5.4: Pearson's correlation coefficient (r) and slope (m) obtained for linear fit of the scatter plots between voltage change and scour depth for each electrode length.

Electrode/strip length	r	m
Full equal length electrodes: 100 cm	0.946	3.551
Strips reduced by 5 cm	0.954	3.508
Strips reduced by 15 cm	0.966	2.612
Strips reduced by 25 cm	0.969	2.878
Strips reduced by 35 cm	0.989	2.682

The reduction of each strip from the two sensor electrodes had an effect of the electrical length and led to a gradual increase of the linearity between the recorded voltage change and scour depth. At the frequency of 64.7 MHz the sensor with reduced length of each strip by 35 cm successfully responded to bed level variations during 'static' scour simulation tests with a strong linear relationship. The performance of the final optimised sensor was then validated in experiments conducted under different environmental conditions.

5.8.2 Evaluation of the final optimised sensor in 'static' scour tests

The evaluation of the sensor with the optimised electrode length, shown in Figure 5.59, was then carried out using the experimental set up described in the section 5.7.1. The sediment types used consisted of medium gravel, coarse sand and medium sand soil types with median grain sizes D_{50} of 13.8 mm, 1.05 mm and 0.375 mm. Previous experiments indicated an insignificant temperature effect on the sensor response therefore at this stage the study did not focus on the temperature influence on the performance of the instrument.
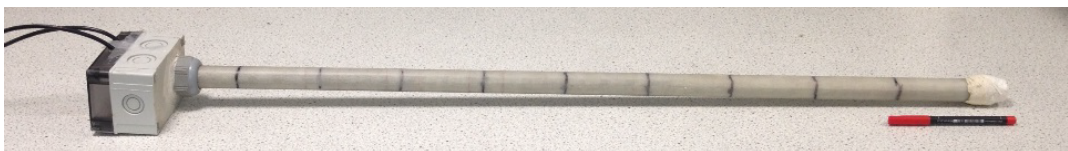
Figure 5.59: Developed prototype sensor of 100 cm length used in the experiments.

The sensor was connected to the VNA and inserted into the tank, shown in Figure 5.60. The experiments firstly evaluated the effect of air and water conditions on the sensor response using fresh and saline water of 35 ppt of NaCl. Afterwards, the

sediment types were added progressively to the water-filled tank and transmission measurements were recorded at depth intervals of 10 cm.
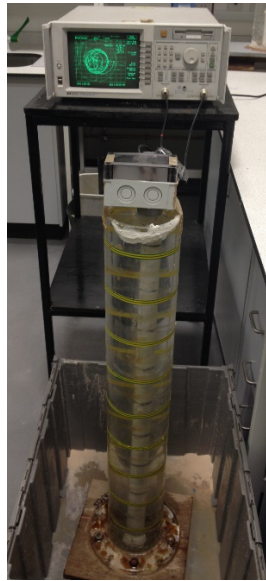
Figure 5.60: Investigation of various air-water interfaces on the sensor response.

The salinity effect on the sensor performance using medium sand sediment was also investigated and presented herein. Various saline aqueous solutions were prepared dissolving in fresh water for each test 0.085 mol NaCl/L, 0.256 mol NaCl/L, 0.427 mol NaCl/L and 0.598 mol NaCl/L that corresponded to 5 ppt, 15 ppt, 25 ppt and 35 ppt of NaCl respectively. These tests aimed at identifying the single optimum frequency of the optimised sensor at each different environmental condition.

Preliminary evaluation of the optimised sensor in various environments

The evaluation of the frequency response of the sensor with the optimised geometry when placed in air, fresh water and saline water of 35 ppt of NaCl is presented in Figure 5.61. The electrical length of the sensor is increased in fresh water conditions compared to air environment, as shown in Figure 5.61 (a). This is due to the higher permittivity of water which results in a frequency reduction of the points where the crests and troughs occur as the velocity of propagation and wavelength decreases. In saline water of 35 ppt of NaCl, the amplitude between the maximum and minimum transmission ratios is reduced compared to fresh water conditions and to air environment. This phenomenon is particularly evident for the frequency range from 100 MHz to 300 MHz, as shown in Figure 5.61 (b).
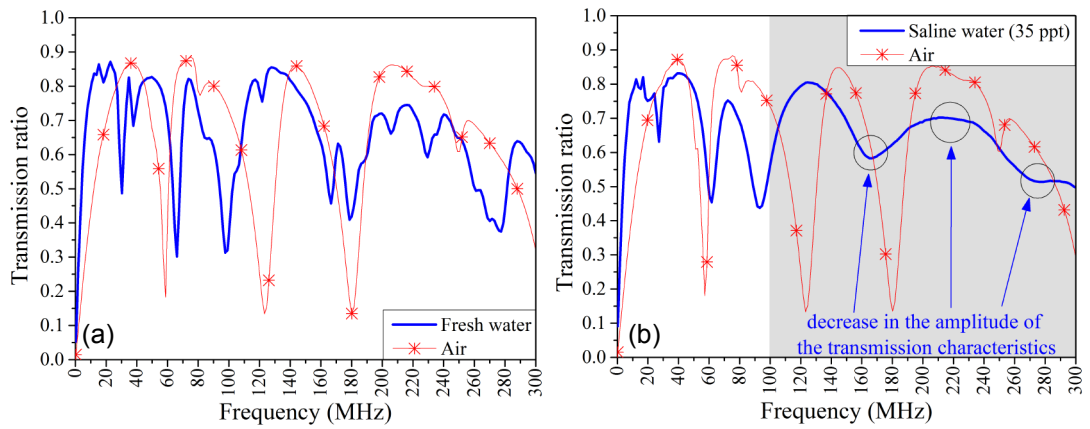
Figure 5.61: Transmission ratio obtained with the optimised sensor of reduced length of two electrodes by 35 cm in **(a)** air - fresh water and **(b)** air - saline water of 35 ppt of NaCl conditions at the frequency range from 0.3 MHz to 300 MHz. A decrease in the amplitude of the transmission characteristics is observed in saline water compared to air environment which is evident at the frequency range 100 MHz – 300 MHz and corresponds to the highlighted grey region.

The frequency response of the sensor was significantly influenced by the different permittivity conditions when was tested in various environments. The investigation was then carried out in 'static' scour simulations using different soil types.

Soil type influence (optimised sensor)

Figures 5.62 present a typical response of the optimised sensor when subjected to scour simulations in medium sand sediment using fresh water. It is observed that different scour depths had an increasing effect on the electrical length and a decreasing influence on the wavelength due to the higher permittivity.
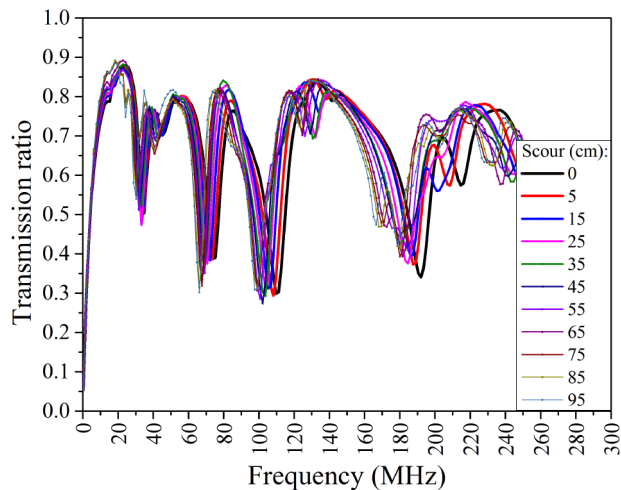
Figure 5.62: Transmission ratio obtained with the optimised sensor of reduced strip length from each electrode by 35 cm in medium sand sediment using fresh water at the frequency range from 0.3 MHz to 300 MHz.

‘Static’ scour tests were then carried out in gravel, coarse sand and medium sand sediments in fresh water as presented in Figure 5.63. A decrease of the frequency point that corresponds to an even multiple of $\lambda/4$ where the transmission trough occurs is detected as water substituted the saturated sediment inside the tank. The high permittivity of water due to increased scour level also caused the decrease of the wavelength of each transmitted signal. At the frequency range from 60 MHz to 70 MHz a satisfactory separation of the transmission characteristics in the vertical direction is also observed for all the tested sediments, as shown in Figure 5.63 (a), 5.63 (b) and 5.63 (c).
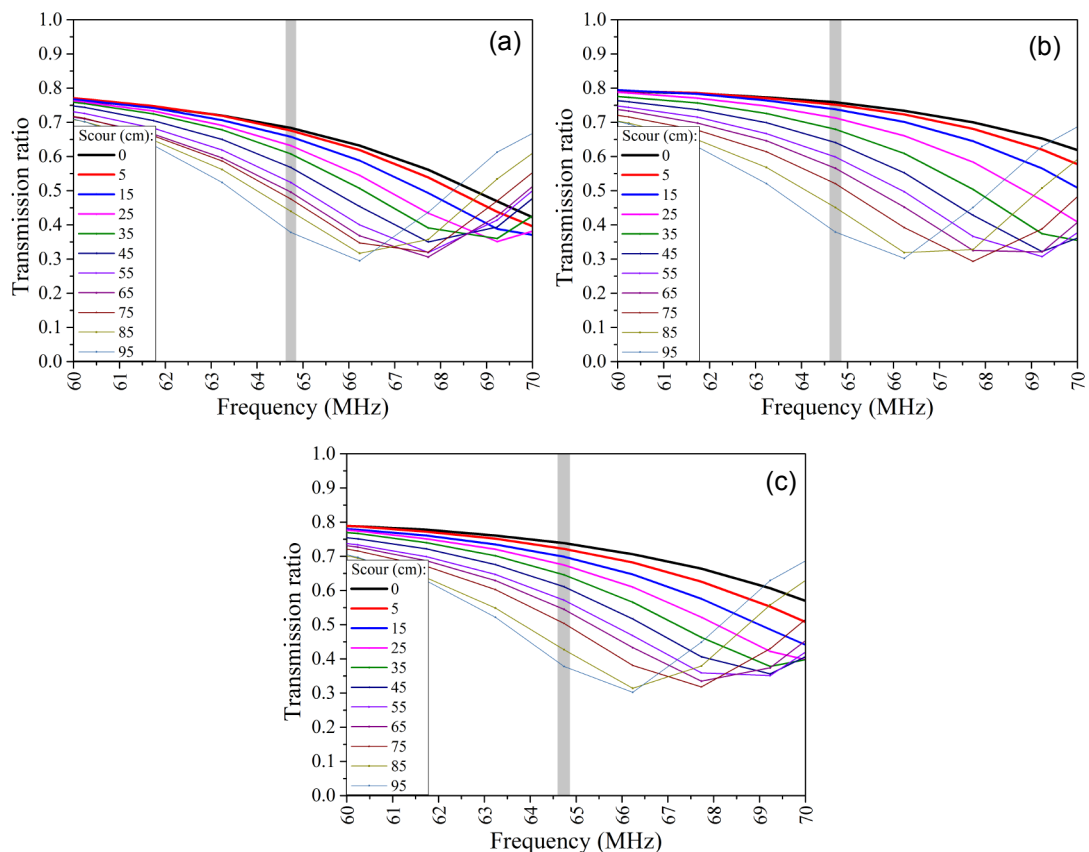
Figure 5.63: Transmission ratio obtained with the optimised sensor of reduced strip length from each electrode by 35 cm in **(a)** gravel, **(b)** coarse sand and **(c)** medium sand sediments using fresh water at the frequency range from 60 MHz to 70 MHz. The grey column in each graph corresponds to the single frequency that was selected to be analysed further (64.7 MHz).

Figure 5.64 presents the transmitted voltage change recorded for various bed levels in tests using different soil types in fresh water conditions. At the frequency of 64.7 MHz it is observed a cumulative effect on the voltage change for increased scour depth. Conversely with the results obtained with the full equal electrode sensor (see

Figure 5.47), it is observed that the calibration curves of the optimised sensor are hardly affected by the soil type.
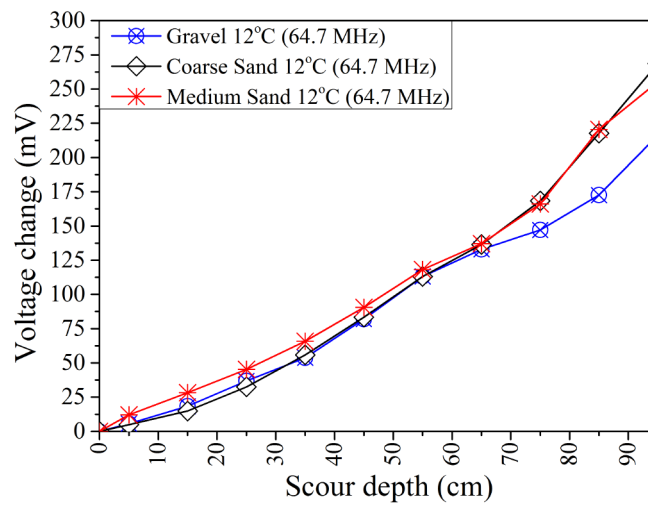
Figure 5.64: Voltage change recorded for increased scour depth at intervals of 10 cm using various soil types in fresh water at the frequency of 64.7 MHz.

The sensitivity and linearity of the transmitted signal for each sediment in fresh water are presented in Table 5.5. A strong linear relationship between the sensor voltage output and increased scour depth is obtained for all the tested soil types as the correlation coefficient (r) is ranged from 0.992 (gravel) to 0.980 (coarse sand). The value of slope (m) of the linear relationship for each sediment in fresh water indicates that the sensitivity of the sensor is slightly reduced in gravel soil type compared to sand sediments.

Table 5.5: Pearson's correlation coefficient (r) and slope (m) obtained for linear fit of the scatter plots between voltage change and scour depth for each sediment type in fresh water.

Sediment	Fresh water	
	r	m
Gravel	0.992	2.226
Coarse sand	0.980	2.727
Medium sand	0.986	2.574

The optimised sensor responded successfully to scour depth variations in different sediments with a strong linear relationship. The results in fresh water also indicated that the optimised sensor does not require soil specific calibration as the obtained calibration curves for various soil types successfully determined scour depth variation along the probe length.

Salinity of 35 ppt influence (optimised sensor)

The salinity effect on the optimised sensor response was assessed using saline water of 35 ppt of NaCl. A typical example of the obtained transmission ratio in medium sand sediment is presented in Figure 5.65. Salinity in water was found to have a major decreasing effect in the amplitude of the recorded transmission characteristics compared to the tests carried out in fresh water. Minor changes in the frequency response are also observed for different simulated scour levels.
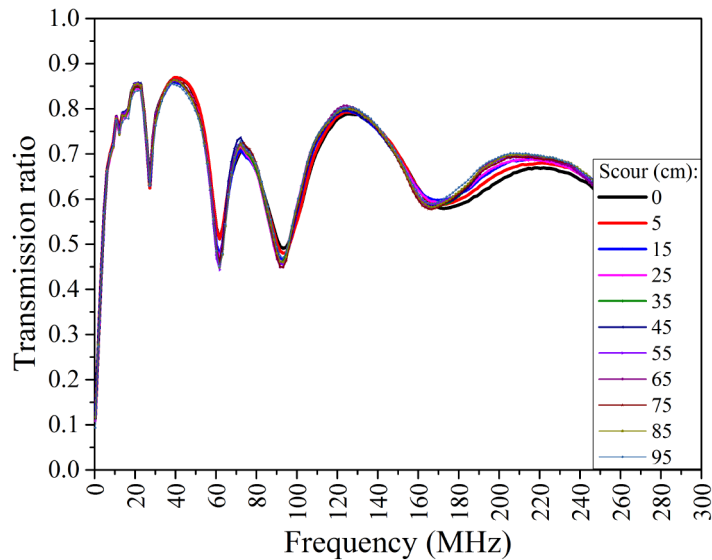
Figure 5.65: Transmission ratio obtained with the optimised sensor of reduced strip length from each electrode by 35 cm in medium sand sediment using saline water of 35 ppt of NaCl at the frequency range from 0.3 MHz to 300 MHz. Increased scour depth had a minor influence on the recorded transmission characteristics.

The evaluation of the sensor to detect 'static' scour processes was then carried out using gravel, coarse sand and medium sand sediments in saline water of 35 ppt of NaCl. The investigation initially focused on assessing different frequency ranges where a separation of the transmission characteristics in the vertical axis is considered satisfactory. The frequency band from 180 MHz to 230 MHz was then considered the optimum and was chosen for further analysis (see Figure 5.66). The obtained frequency response during scour simulations in gravel, coarse sand and medium sand sediments indicate minor changes of the transmission characteristics in the vertical direction.
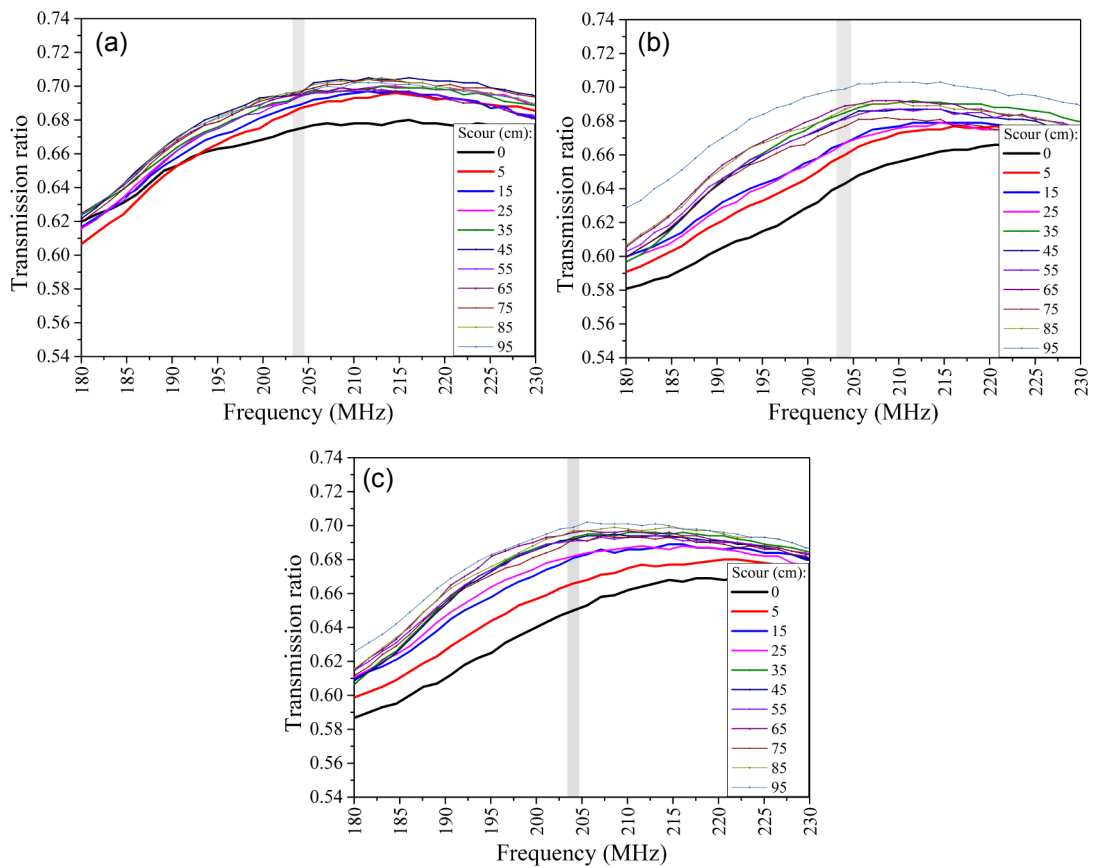
Figure 5.66: Transmission ratio obtained with the optimised sensor of reduced strip length from each electrode by 35 cm in **(a)** gravel, **(b)** coarse sand and **(c)** medium sand sediments using saline water of 35 ppt of NaCl at the frequency range from 180 MHz to 230 MHz. The grey highlighted column indicates the single frequency which was selected to be analysed further (204.1 MHz).

The recorded transmitted voltage change in tests using different sediments in saline water at the frequency of 204.1 MHz indicates that the sensor did not respond satisfactorily to increased scour depth (see Figure 5.67).
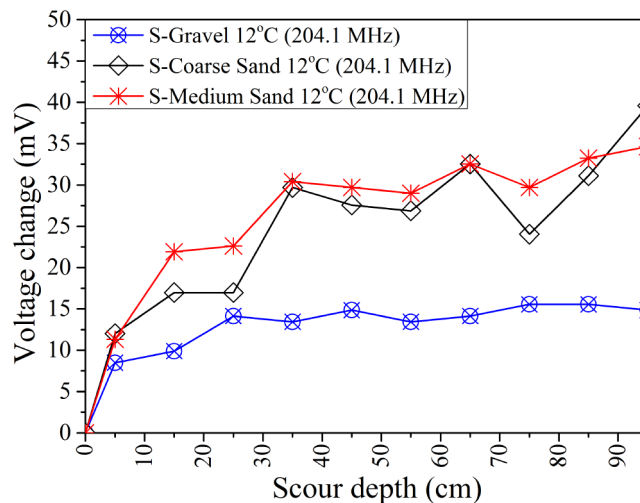
Figure 5.67: Voltage change recorded for increased scour depth at intervals of 10 cm using various soil types in saline water of 35 ppt of NaCl at the frequency of 204.1 MHz.

Table 5.6 shows the linearity (r) and sensitivity (m) of the calibration curves of the sensor obtained for each soil type. In saline water of 35 ppt of NaCl the linearity of each soil type is found to be significantly reduced and varied between 0.754 (gravel) and 0.866 (coarse sand). The value of slope (*m*) of the linear relationship is also substantially decreased compared to the results obtained in fresh water (presented in Table 5.5)

Table 5.6: Pearson's correlation coefficient (*r*) and slope (*m*) obtained for linear fit of the scatter plots between voltage change and scour depth for each sediment type in fresh water and saline water of 35 ppt of NaCl.

Sediment	Saline water	
	r	*m*
Gravel	0.754	0.107
Coarse sand	0.866	0.297
Medium sand	0.839	0.276

Increasing scour depths had an increasing effect on the sensor readings in saline water of 35 ppt of NaCl, but the linearity and sensitivity of the instrument was significantly reduced. The results indicated that the sensor did not satisfactorily measured scour processes along the probe length, therefore its response is not useful in these circumstances. The salinity effect on the transmission characteristics of the sensor was therefore further evaluated in various saline aqueous solutions.

Effect of various salinity concentrations (optimised sensor)

The effect of different salinity concentrations of 5 ppt, 15 ppt, 25 ppt and 35 ppt of NaCl on the sensor response is presented in Figures 5.68 and 5.69. The study focused on the frequency band 50 MHz - 70 MHz where the optimum frequency in fresh water was identified. The salinity in water had a major effect on the obtained frequency response and in particular on the recorded transmission troughs. The tests carried out using saline water of 5 ppt of NaCl show a separation of the transmission characteristics in the vertical axis but also a minor frequency change of the transmission trough that correspond to an even $\lambda/4$, as presented in Figure 5.68 (a). As the salinity concentration in water is increased to 15 ppt, 25 ppt and 35 ppt of NaCl, the separation of the transmission characteristics in the vertical direction and the frequency change of the trough point is significantly decreased, which is particularly evident in Figures 5.68 (b), 5.68 (c) and 5.68 (d) respectively.
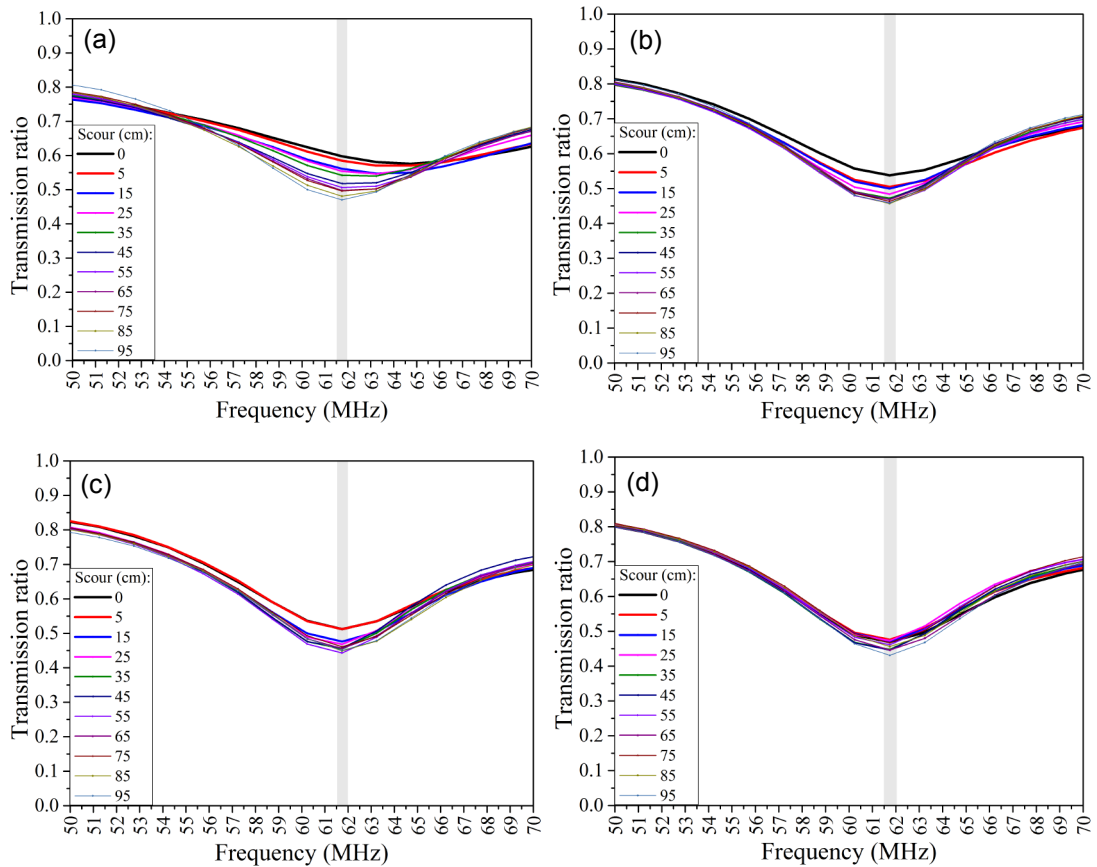
Figure 5.68: Transmission ratio obtained with the optimised sensor of reduced strip length from each electrode by 35 cm in medium sand sediment using saline water of **(a)** 5 ppt of NaCl, **(b)** 15 ppt of NaCl, **(c)** 25 ppt of NaCl and **(d)** 35 ppt of NaCl at the frequency range from 50 MHz to 70 MHz. The grey highlighted column corresponds to the frequency that was selected to be analysed further (61.7 MHz)

The transmission ratio obtained at the frequency of 61.7 MHz was then analysed and presented in Figure 5.69. The sensor satisfactorily responded to scour at depth intervals of 10 cm in saline water of 5 ppt of NaCl. An increasing effect of the voltage output is also obtained in the tests carried out using saline water of 15 ppt of NaCl. The sensor accuracy is found to be significantly reduced with increased salinity concentration to 25 and 35 ppt of NaCl (see Figure 5.69).
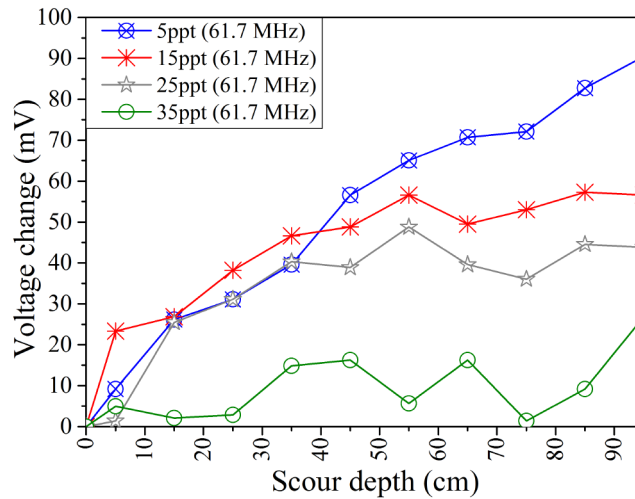
Figure 5.69: Voltage change recorded for increased scour depth at intervals of 10 cm in medium sand sediment at the single frequency of 61.7 MHz in water with different salinity concentrations.

Table 5.7 indicates that as salinity concentration increased from 5 ppt to 15 ppt, 25 ppt and 35 ppt of NaCl, a significant decrease in the linearity (r) and the sensitivity (m) of the sensor response is recorded.

Table 5.7: Pearson's correlation coefficient (r) and slope (m) obtained for linear fit of the scatter plots between voltage change and scour depth for various salinity concentrations in 'static' scour simulations using medium sand sediment.

Salinity concentration	r	m
5 ppt of NaCl	0.986	0.916
15 ppt of NaCl	0.869	0.483
25 ppt of NaCl	0.801	0.411
35 ppt of NaCl	0.593	0.154

The optimised sensor responded satisfactorily to scour depth variations in saline water of 5 ppt of NaCl. However, the transmission signal of the sensor was not useful in the tests carried out for salinity concentrations greater than 5 ppt.

5.9 Scaling procedures and real-time performance assessment of the optimised sensor

The investigation presented in this section initially aimed to validate the relationship of the transmission resonances with the physical length of the electrodes by fabricating and testing a small-scale optimised sensor. Experiments were then carried out to evaluate the frequency response in different permittivity conditions originated from the installation of the sensor in the flume and the saturation procedures carried out in

the riverbed segment. The study then predicted the optimum frequency of the small-scale sensor and validated its capability to detect scour and re-deposited sediment processes in a real-time representative operational environment.

5.9.1 Set up of flume experiment for 'scaled' sensor

A small-scale prototype sensor with length of 39 cm was fabricated and used for the investigation in the flume. Since the accuracy of the optimised sensor with length of 100 cm was improved when one strip from each electrode was reduced in length by 35 cm, one strip from each electrode of the small-scale sensor was therefore also reduced in length by 13.65 cm. This is based on the length ratio (2.56) obtained between the 100 cm optimised sensor and the small-scale sensor of 39 cm.

The experiments were carried out to evaluate the small-scale prototype sensor in the unidirectional current flume (shown in Figure 5.70) of the hydraulics laboratory located at the University of Strathclyde, Glasgow.

Figure 5.70: Unidirectional open channel flume used for the evaluation of the prototype scour sensor.

The flume has bottom and sidewalls made of plexiglas supported by a metal frame with a rectangular cross-section of 0.90 m (height) x 0.40 m (width) and 12.0 m (length) (see Figure 5.71). A circulation system with a sump and a pump supplies water to the horizontally positioned flume and a valve is used to control the flow discharge and hence, the water depth. The riverbed segment consisted of 0.40 m width and 1.50 m length was positioned 6.25 m downstream of the flume entrance and was confined by two smooth plywood plates positioned level with the top surface of the test section (see Figure 5.71). Ramps were used to accommodate the flow to and from the raised bed with slopes of 1/3.75 and 1/2.50 for the upstream and downstream ramps respectively (see Figures 5.70 and 5.71).
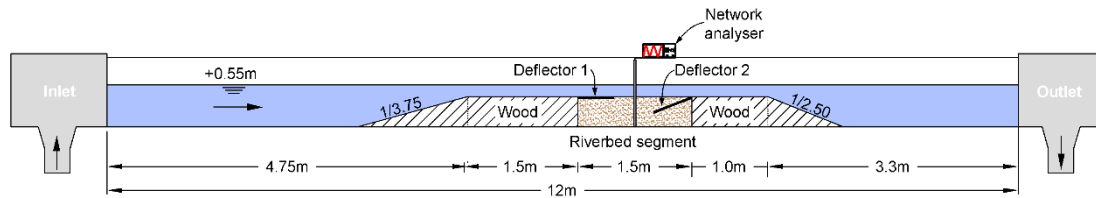
Figure 5.71: Flume experimental set up.

As depicted in Figure 5.71, a plywood plate (deflector 1) was positioned horizontally in the riverbed section, which was located upstream of the prototype sensor. This prevented the initial sediment erosion upstream of the test section and also increased the scouring of the area around the prototype sensor location allowing an in-depth evaluation of the instrument response. Preliminary experiments also indicated scouring at the interface of the sediment and the plywood downstream plate. Therefore a deflector (2) with a slope of 1/2.50 was also positioned within the downstream side of the test section to direct the flow away from the interface (see Figures 5.71 and 5.72). Sediment traps were also installed upstream and downstream of the ramps to decrease sediment transportation and re-deposition in the test section while water was re-circulating in the flume.

Figure 5.72: Deflector (2) with a slope of 1/2.50 installed within the downstream test section.

Each pair of the electrodes of the small-scale optimised sensor, shown in Figure 5.73 (a), was connected to two 50 Ohm coaxial cables and then the sensor was inserted into a fibre glass access tube. The upper part of the probe was fitted with an acrylic cylinder to seal it from water ingress and also lead the electrodes to the VNA. The scour probe of 28 mm external diameter was marked at intervals of 1 cm and was installed in the middle of the riverbed segment and fixed at the bottom of the flume [see Figure 5.73 (b) and 5.73 (c)]. The sensor was connected via coaxial cables to the

VNA which was positioned on the flume frame at a distance of 30 cm downstream of the prototype probe, as shown in Figure 5.73 (d). The optimum frequency was then predicted based on the probe length ratio and the results obtained in the aforementioned investigations presented in sections 5.5.2 and 5.6.1.
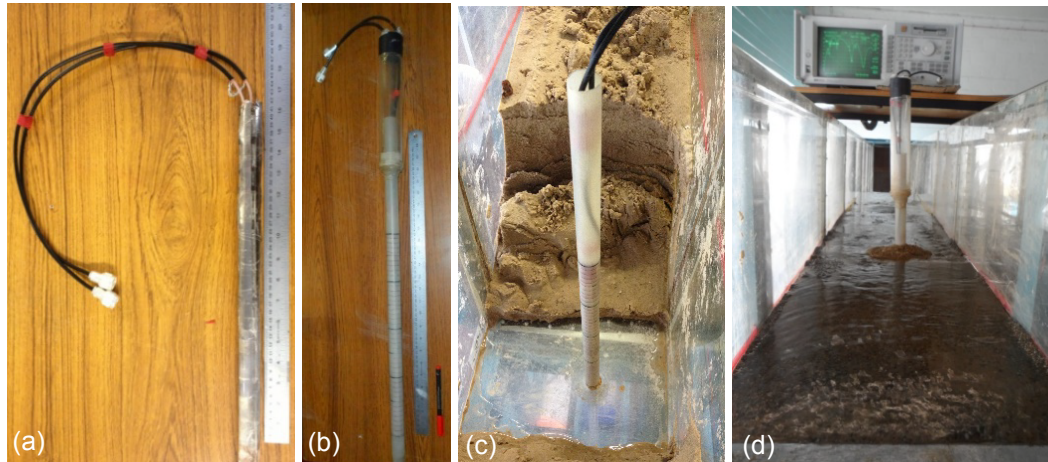
Figure 5.73: (a) Small-scale sensor with length of 39 cm used in flume experiments, **(b)** sensor inserted into a graduated access tube and upper part covered with a cylinder, **(c)** prototype sensor installation into the riverbed segment and **(d)** experimental assembly during flume operation with the network analyser positioned downstream of the test section and connected with the sensor.

Separate flume experiments were conducted using two sand soil types; a mixture of coarse sand sediments (uniformity coefficient: C_u = 4.47) with median grain size D_{50} = 0.781 mm and specific gravity of 2.88 and medium sand soil type (C_u = 2.30) with median grain size D_{50} = 0.375 mm and specific gravity of 2.83. The soil was placed un-compacted to achieve relatively low density values and to accentuate scouring process. As depicted in Figure 5.74 (a) the bed was thoroughly levelled before each test. The bed level at the probe position was recorded throughout the experiments with a Vernier point gauge at time intervals of 30 mins. An OTT current meter (type: 02 '10.150') connected to NI DAQ (NI USB 6009) interfaced to a computer via LabView recorded the water flow rates in the riverbed segment [see Figure 5.74 (b)].
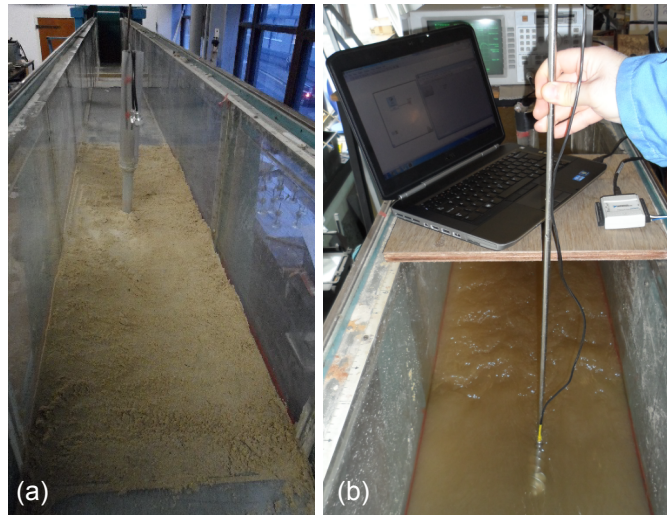
Figure 5.74: (a) Medium sand bed level before the start of the flume experiments and **(b)** OTT current meter interface to a computer via LabView used to record the flow rates.

Discharge measurements were provided by a poddymeter instrument located after the valve at the outlet of the downstream tank. Prior to initiating flow conditions, the tested section was saturated by allowing water to run off the upstream plywood plate for a period of one hour. Four measurements were recorded at time intervals of 5 mins during the saturation process of each flume test to evaluate the sensor response during water infiltration into the sediment.

Experiments started by allowing the water to flow over the horizontal bed with a defined flow rate of 0.30 m/s. During the flume tests the velocity was varied in the range from 0.33 m/s to 1.41 m/s and the corresponding water depth at steady state ranged from 0.5 cm to 13 cm respectively. Deposition was simulated by adding 500 g of sediment at intervals of 30 sec on the ramp located on the upstream side of the tested section. The sediment was subsequently transported by flow conditions and deposited progressively in the eroded riverbed segment.

Clear water scour conditions were generated due to low flow velocity which evolved to live bed and/or general scour in the test section when water flow conditions were increased. Each flume experiment was carried out for a period of seven hours and the results were collected and analysed.

5.9.2 Experimental results for 'scaled' sensor

Scaling and comparison with 100 cm sensor

Figure 5.75 presents the results recorded with the small-scale optimised sensor in air environment compared to those obtained with the 100 cm sensor with one strip from each electrode reduced by 35 cm. A shorter sensor caused a decrease of the electrical length and an increase of the wavelength. The first transmission trough of the 100 cm sensor is occurring at the frequency point of 58 MHz while for the small-scale sensor is at 148 MHz resulting in a ratio of 2.55 which is almost equal with the ratio (2.56) obtained between the sensor lengths.
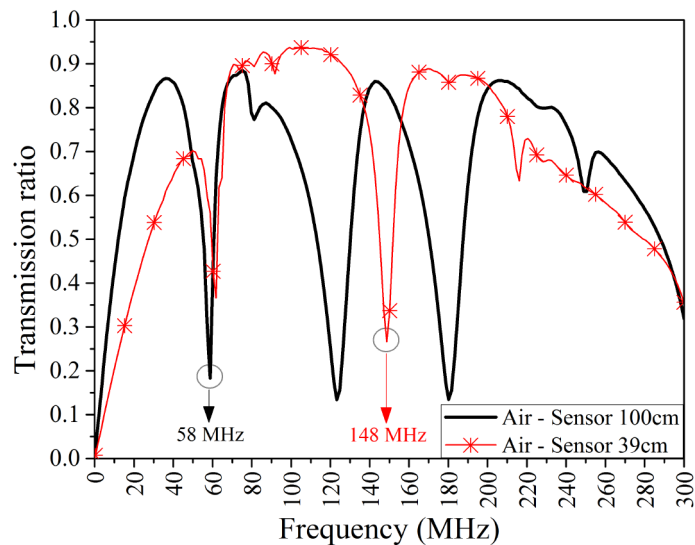
Figure 5.75: Comparison of transmission characteristics obtained for sensor lengths of 39 cm and 100 cm with optimised electrode geometry in air environment for the frequency range from 0.3 MHz and 300 MHz.

These findings indicate that the transmission characteristics of the sensor with the final optimised electrode geometry are also a function of the sensor physical length and can be successfully predicted.

Small-scale sensor installation in the flume and saturation process

The response of the sensor during its installation and the saturation process of the riverbed segment in the flume is presented in this section. Similar behaviour of the sensor is observed in coarse sand and medium sand sediments as presented in Figures 5.76 and 5.77 respectively. When the sensor was covered by 20 cm and then fully covered (40 cm) by dry sediment each time, an increase of the electrical length is

recorded when compared to air environment in both tested soil types. At the frequency range from 0.3 MHz to 300 MHz, the measurements obtained during the saturation process also indicate an increase of the electrical length as water infiltrated the sediment.
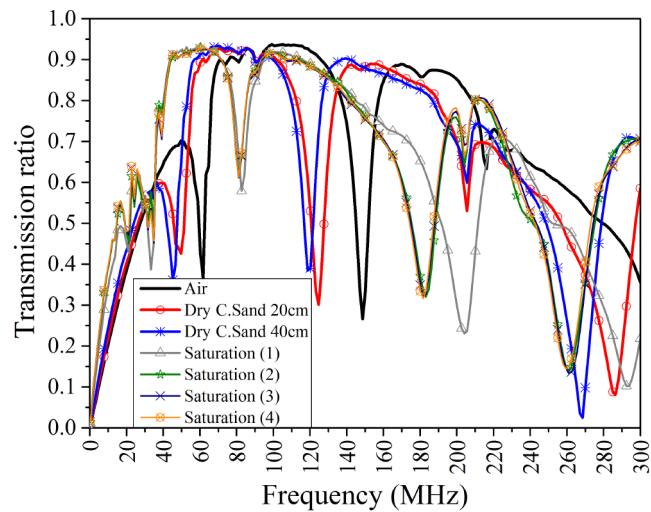
Figure 5.76: Transmission ratio obtained with the optimised small-scale sensor in coarse sand sediment at the frequency range from 0.3 MHz to 300 MHz during the preparation and saturation process of the riverbed segment.
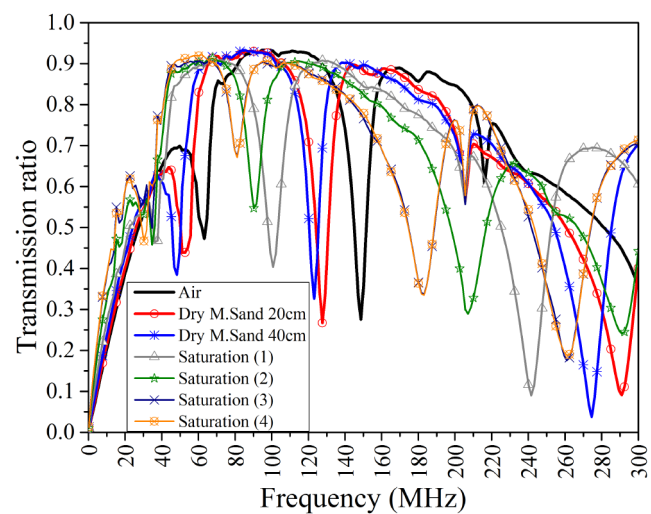
Figure 5.77: Transmission ratio obtained with the optimised small-scale sensor in medium sand sediment at the frequency range from 0.3 MHz to 300 MHz during the preparation and saturation process of the riverbed segment.

The investigation was then focused at the range from 70 MHz to 160 MHz where the first transmission trough is obtained in air environment, as presented in Figures 5.78 and 5.79. The effect of greater permittivity on the sensor measurements is also evident at this frequency range, e.g. the frequency point which corresponds to the transmission trough and occurs at an even $\lambda/4$ is decreased as the dry coarse sand is

added into the riverbed segment. During the saturation process of the flume, a rapid decrease of the trough frequency point is also observed which is more evident in coarse sand compared to medium sand soil type as presented in Figures 5.78 and 5.79 respectively. This also indicates a faster water infiltration rate in coarse sand compared to medium sand soil type. An identical match of the frequency response is detected for the measurements entitled 'saturation 3' and 'saturation 4' in both sand soil types, as presented in Figures 5.78 and 5.79 respectively. Based on this observation it is concluded that both sand sediments have reached a saturation state that is close to 1, therefore their permittivity values remained at a constant value.
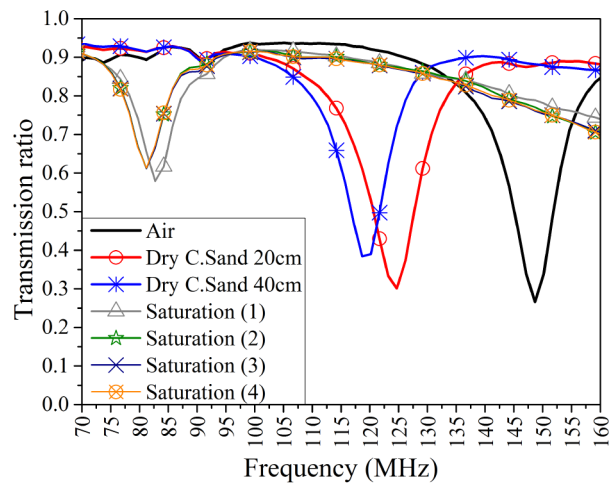
Figure 5.78: Transmission ratio of the optimised small-scale sensor in coarse sand sediment at the frequency range from 60 MHz to 160 MHz during the preparation procedures of the riverbed segment.
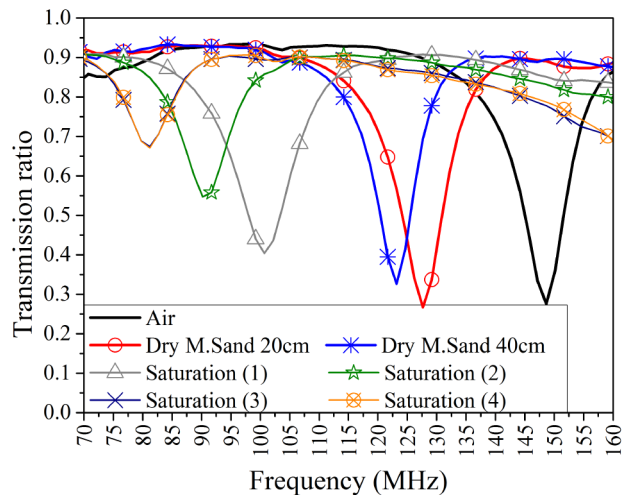
Figure 5.79: Transmission ratio of the optimised small-scale sensor in medium sand sediment at the frequency range from 60 MHz to 160 MHz during the preparation procedures of the riverbed segment.

The sensor was found sensitive to the changing permittivity conditions during its installation and the saturation procedures in the riverbed segment that had a major influence on the frequency response. As water infiltrated the sand sediments the frequency of the trough point that corresponds to an even multiple of $\lambda/4$ was found to be significantly decreased until the soil conditions were fully saturated.

Real-time flume experiments

Figures 5.80 and 5.81 present the transmission ratio recorded during the open channel flume experiments for riverbed segments that consisted of coarse sand and medium sand sediments respectively. The bed level variations appear to have an influence on the obtained frequency response where increased scour and sedimentation levels corresponded to increased and decreased electrical length respectively. The investigation was then focused at the frequency ranges where the transition from odd to even multiples of $\lambda/4$ occur, that is, between the resonance crest and trough in the obtained transmission signal.
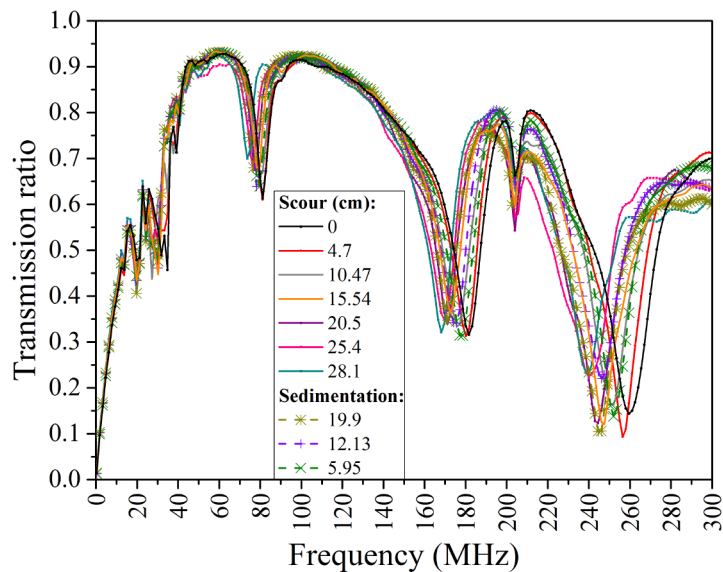
Figure 5.80: Transmission ratio obtained with the optimised small-scale sensor in coarse sand sediment at the frequency range from 0.3 MHz to 300 MHz during scour and sedimentation process in the riverbed segment of the flume.
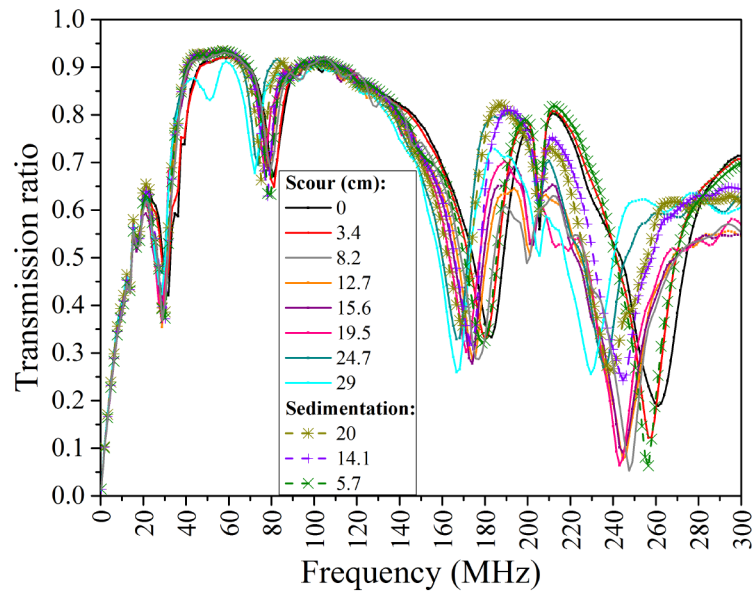
Figure 5.81: Transmission ratio obtained with the optimised small-scale sensor in medium sand sediment at the frequency range from 0.3 MHz to 300 MHz during scour and sedimentation process in the riverbed segment of the flume.

Figures 5.82 and 5.83 present the frequency response of the sensor recorded for various bed level variations at the frequency range from 156 MHz to 176 MHz in coarse sand and medium sand soil types. Increased scour level inside the riverbed segment affected the transmission characteristics as a separation towards the downward direction of the vertical direction is obtained for both sediments (see Figures 5.82 and 5.83). A frequency decrease of the transmission trough is also recorded with increased scouring due to the higher permittivity inside the riverbed segment which increases the electrical length and decreases the wavelength. The re-deposited sediment also caused an upward vertical separation of the transmission characteristics in both sand sediments.

The tests carried out with the optimised 100 cm length sensor (presented in section 5.8.2) showed that scour activity was accurately monitored in fresh water conditions at the frequency of 64.7 MHz. The optimum frequency of the small-scale sensor is then predicted at 166.6 MHz for both sediments based on the length ratio (2.56) obtained between the sensors with lengths of 39 cm and of 100 cm.
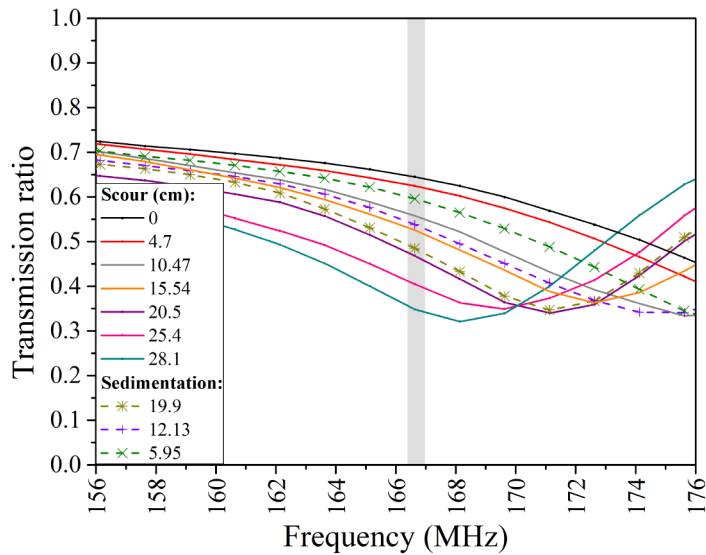
Figure 5.82: Transmission ratio obtained with the small-scale sensor in coarse sand sediment at the frequency range from 156 MHz to 176 MHz in the riverbed segment of the flume. The grey column highlights the single frequency that was predicted and investigated further (166.6 MHz).
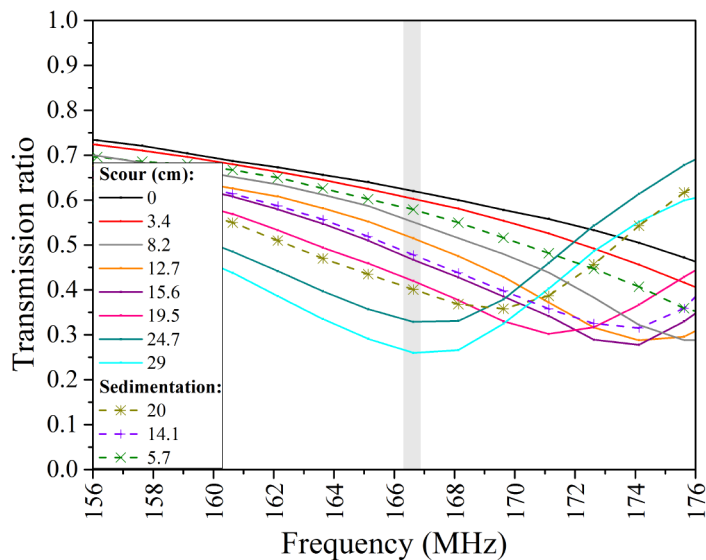
**Figure 5.83:** Transmission ratio obtained with the optimised small-scale sensor in medium sand sediment at the frequency range from 156 MHz to 176 MHz. The grey column highlights the single frequency that was predicted and investigated further (166.6 MHz).

The transmitted voltage change of the sensor during underwater bed level variations in the riverbed segment that consisted of coarse sand and medium sand sediments is presented in Figures 5.84 and 5.85 respectively. At the frequency of 166.6 MHz the sensor responded successfully to scouring and sedimentation processes in both tested soil types. The maximum voltage change in coarse sand sediment is recorded at 210 Volts which corresponded to scour level of 27.1 cm while in medium sand soil type was 254 Volts obtained for scour depth of 29 cm. After sediment

deposition in the riverbed segment the sensor voltage change was decreased to 34.6 mV for bed level of 5.9 cm in coarse sand and to 28.9 mV for bed level of 5.7 cm in medium sand sediment, as depicted in Figures 5.84 and 5.85.
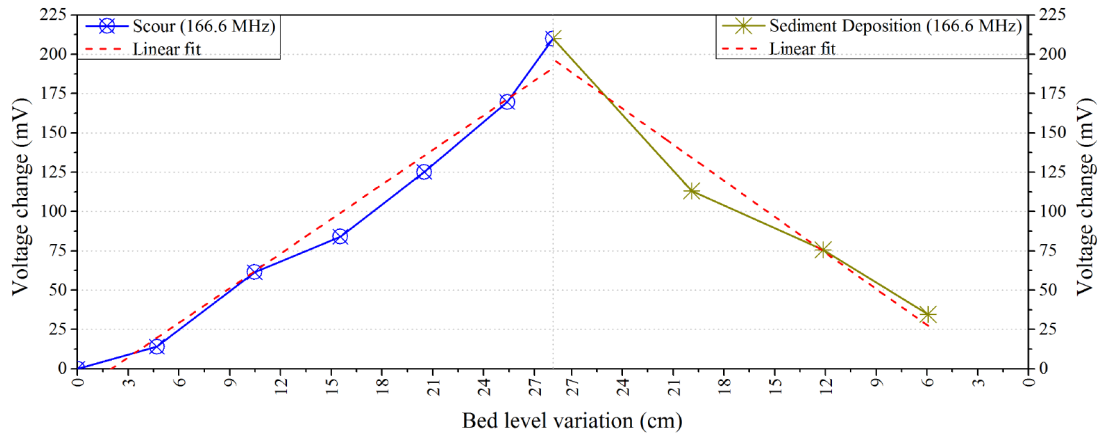
Figure 5.84: Transmitted voltage change of the small-scale sensor recorded for scour and re-deposited sediment processes in the riverbed segment of the flume that consisted of coarse sand sediment.
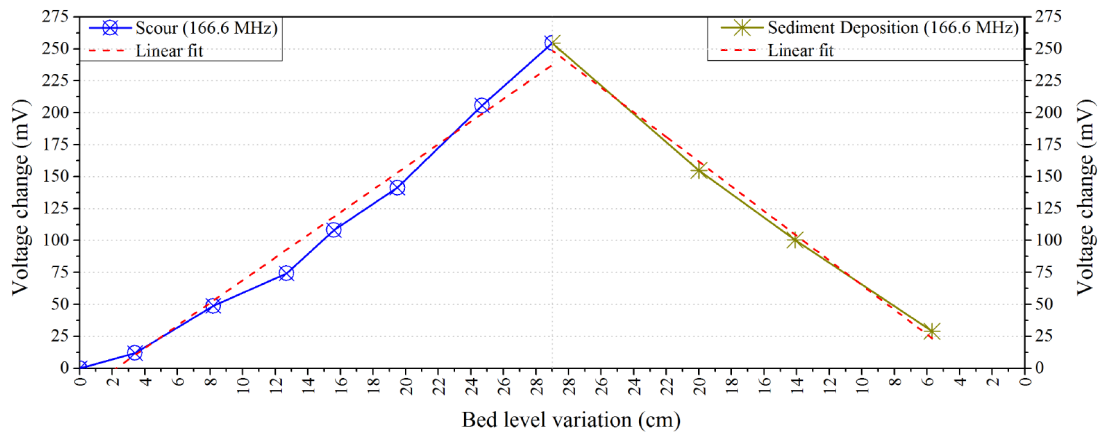
Figure 5.85: Transmitted voltage change of the small-scale sensor recorded for scour and re-deposited sediment processes in the riverbed segment of the flume that consisted of medium sand sediment.

The linearity and sensitivity for each soil type during scouring and re-deposited sediment processes are presented in Table 5.8. A very strong linear relationship between the sensor voltage and the bed level variations in the riverbed segment is obtained for both coarse sand and medium sand sediments. The minimum value of correlation coefficient (r) is recorded at 0.980 obtained during sedimentation process in coarse sand soil type. Similarly, the sensitivity of the small-scale sensor is significantly increased in the flume experiments compared to the 100 cm optimised sensor, as the minimum value of the linear fit slope (m) is recorded at 7.331 mV/cm and corresponds to scouring process in coarse sand sediment.

Table 5.8: Pearson's correlation coefficient (*r*) and slope (*m*) obtained for linear fit of the scatter plots between voltage change, scour and sedimentation depths for coarse sand and medium sand sediments.

Soil type	Scour process		Re-deposited sediment	
	r	*m*	*r*	*m*
Coarse sand	0.987	7.331	0.980	7.651
Medium sand	0.988	8.866	0.997	9.663

The open channel flume experiments indicated that the sensor was highly sensitive and recorded with a strong linear correlation scour and sediment deposition depths. The optimum frequency capable of providing accurate measurements of bed level variations around the probe location was also successfully predicted, based on the length ratio obtained between different sensors sizes.

5.10 Conclusions

This study presented a new type of sensor based on an open electromagnetic transmission line. The measuring principle of the prototype sensor utilised the Amplitude Domain Transmissometry (ADT) technique which appears to be the first application for monitoring soil-water mixtures. The prototype instrument is proposed to be employed for measuring scour and sediment deposition depth variations in the vicinity of the foundation structure.

The initial concept was based on capacitance-based measurements. However, the sensor connected to capacitance-based systems did not respond to saturated sand-water level variation, which is likely to be related with the low operating frequency of the monostable circuit.

The second concept was developed by connecting the sensor to a network analyser and investigating the sensor performance in a higher range of frequencies to identify transmission line variables that are sensitive to scour processes. A series of resonance frequencies and amplitudes were observed, which were found to vary consistently with the variation of the soil-water interfaces simulating scour. The concept was developed around the measurement of the amplitude of transmitted signal at given frequency rather than measurement of resonance frequency, as the former measurements can be easier incorporated within existing monitoring platforms. A single frequency was selected where the simulated scouring conditions had an increasing effect on the voltage output. This optimum frequency was located after the first resonance trough point.

The study then employed the open-circuited stub line to provide an analogue to gain better understanding of the prototype sensor behaviour. A repetition of the resonance frequencies of various stub line lengths was detected with equal spacing between troughs and crests. This is due to the fact that the open-circuit is being transformed to a short-circuit whenever the electrical length becomes equal to odd multiples of a quarter wavelength. In the stub line tests, the impedance was placed in parallel, therefore the short-circuit caused a high reflection ratio of the incident signal. In a parallel mode, the crests and troughs in the transmission signals obtained with the prototype sensor, where the impedance is placed in series, corresponded to frequency

points where the electrical length becomes equal to odd and even multiples of quarter wavelengths respectively.

Experiments carried out with different stub line lengths also demonstrated that the transmitted or reflected signal is directly associated with the cable physical length. The transmission crests and troughs obtained for different lengths of stub lines were then successfully predicted based on the length ratio. Comparable behaviour was detected for sensors of various electrode sizes when compared to different lengths of stub cables. When the physical length of the sensor is shorter the electrical length is decreased and at the same time the frequency point of the transmission trough is increased. This is due to the fact that a higher frequency is required to cause the same quarter wavelength transition from open-circuit to short-circuit (and vice versa). These findings enabled the prediction of the optimum frequency that is required for the successful monitoring of bed level variations using sensors of various electrode lengths. Consequently, the sensor geometry can also be used as a tool to fine-tune the optimum frequency and allow it to match commercial frequency oscillators, therefore reducing the total cost and ease the development of the sensor's electronic concept.

Stub line tests were designed to mimic various locations of the water-saturated soil interfaces. The response of the analogue satisfactorily described the electrical behaviour of the prototype sensor in different media. Namely, higher permittivity associated with greater water interface (i.e. scour conditions) caused the decrease of the wavelength which resulted in lowered frequency of the first resonance trough.

The investigation then evaluated in the laboratory prototype sensors with equal electrode lengths under different soil types, water and temperature conditions that are commonly encountered in offshore environment. At the optimum frequency the sensor was capable of responding to bed level variations at intervals of 10 cm in various sediments using fresh water. A soil-specific calibration was suggested for the accurate determination of scour depth along the probe length, as the calibration curves were found to be dependent on the sediment.

A different optimum frequency was identified in saline water in order to provide a reasonably linear response to scour depth. Although water salinity had a significant attenuating effect on the transmitted signal, the sensor with equal electrode lengths satisfactorily measured scour processes using various sediments in saline water of 35

ppt of NaCl. The optimum frequency in both fresh and saline water conditions was found to be a function of the sensor physical length (according to the stub line analogue), as it was reduced by half when the sensor length was doubled. The obtained results indicated that water temperature at the range of 12 ℃ and 4 ℃ did not have a major influence on the frequency response of the sensor. A plateau was also detected in the tests carried out with fresh water which corresponded to the middle of the probe length thus indicating a decreased sensitivity of the sensor to scour depth in that region.

The sensor design was then optimised for enhanced accuracy of scour processes along the entire probe length. This was achieved empirically with the decrease in length of one strip from each electrode aiming to diminish the sharpness of nodes in the standing wave that will result in improved sensitivity of the transmitted signal at the same point. Tests demonstrated that the gradual reduction of each strip resulted in an improved accuracy of the prototype sensor for bed level monitoring using fresh water during 'static' scour simulations. A very strong positive relationship of the linearity was obtained at the frequency of 64.7 MHz between the voltage change and scour depth which was optimised for reduced length of one strip from each electrode by 35 cm with a value of 0.989.

The optimised sensor response was then thoroughly validated in 'static' scour simulations with different sediment types using fresh water and saline water of various NaCl concentrations. The sensor successfully measured with a strong linear relationship the scour depth at intervals of 10 cm in common soil mediums using fresh water at the frequency of 64.7 MHz while it was also concluded that a soil specific calibration was not necessary. The optimised sensor performance was also tested in saline water of 35 ppt of NaCl where scour simulations had an increasing effect on the sensor readings but the results indicated that the sensor response was not useful in these circumstances. The effect of various salinity concentrations on the sensor readings revealed that the optimised sensor with reduced length of one strip from each electrode by 35% satisfactorily measured bed level variations in saline water of 5 ppt of NaCl. However, measurements of scour depths for salinity concentrations above the range of 5 ppt are proposed to be carried out with a sensor of full equal length of electrodes.

The real-time evaluation of a small-scale optimised sensor with length of 39 cm was then carried out in open channel flume experiments. The measurements obtained in air environment confirmed the relationship between the frequency resonances and the sensor length. The optimum frequency capable of providing measurements of bed level variations around the probe location was also successfully predicted based on the length ratio obtained between different sensors sizes. The flume experiments demonstrated that the small-scale prototype sensor accurately measured scour and re-deposited sediment processes in sand sediments. A very strong linear relationship (correlation coefficient > 0.980) and increased sensitivity (slope of linear fit > 7.331) between the sensor voltage change and the measured bed level variations were obtained at the predicted optimum frequency of 166.6 MHz.

A limitation that arises from the current geometry of the new prototype sensor is that the instrument cannot be used for density evaluation of local regions around the probe location. This is due to the fact that the sensor provides measurements of bed level conditions based on the average permittivity of the area that spans over the length of the probe rather than local information of medium electrical properties at various depth intervals.

It is concluded that the developed prototype ADT sensor presented in this investigation could provide an effective, low-cost alternative compared to existing scour monitoring instruments, as shown in Table 5.9. The validation of the new prototype ADT sensor in operational representative environment also enables the instrument to be classified at Technology Readiness Level (TRL) 6. For the field application of the sensor, the instrument assembly will comprise of an external/internal power supply, an oscillator that operates at the optimum frequency, a specially designed internal transmission line and a measuring circuitry within a waterproof housing providing an analogue signal output. Use of the developed technique for monitoring other types of infrastructure (i.e. dams, embankments, seawalls) is also proposed and this subject is currently under investigation.

Table 5.9: Evaluation of existing scour monitoring methods compared to developed prototype sensor.

Method	Scour/Deposition monitoring	Accuracy	Durability	Applicability	Cost (£)
Diving	X	Low	N/A	Low	700[*]
Sonar	✔	High	Medium	Medium	4,000-9,500[**]
Automatic Sliding Collar	X	Medium	High	Medium	6,500[***]
Ground Penetrating Radar	✔	High	Medium	N/A	2,500-6,500[*]
Global Positioning System	X	High	N/A	Low	3,500-13,000[**]
Float out devices	X	Medium	Low	Low	2,500[***]
Optical sensors	✔	High	Medium	N/A	3,500-6,500[*]
Time Domain Reflectometry	✔	High	Medium	Medium	10,000[***]
Sounding Rods	X	Low	Medium	Low	5,000[***]

*Chen et al (2011)   **Lagasse et al (2009)   ***Lucker et al (2010)

Method	Scour/Deposition monitoring	Accuracy	Durability	Applicability	Cost (£)
Prototype Scour Sensor	✔	**High**	**Work in Progress**	**Work in Progress**	**250**

References

Bittelli, M., Salvatorelli, F., and Pisa, P.R. (2007). Correction of TDR-based soil water content measurements in conductive soils. *Geoderma*, 143(1-2), pp. 133-142.

Blonquist, J.M., Jones, Jr., S.B., and Robinson, D.A. (2005). Standardizing characterization of electromagnetic water content sensors. *Vadose Zone Journal*, 4(4), pp. 1059–1069.

Chen, G., Pommerenke, D., and Zheng, R. (2011). Wireless Smart rocks for Real-Time Scour Monitoring. *International Society for Structural Health Monitoring of Intelligent Infrastructure (ISHMII) Monitor Magazine.* [online] Available at: <http://web.mst.edu/~mhszqd/Short%20Writeup%20for%20ISHMII%20Monitor%20Magazine%20on%20Bridge%20Scour%20Monitoring%20-%20October%2025%202011.docx> [Assessed 26/11/2012].

Cohn, S.B. (1955). Problems in strip transmission lines. *IEEE Transactions on Microwave Theory and Techniques*. 3(2), pp. 119-126.

Davis, J.L., and Annan, A.P. (1977). Electromagnetic detection of soil moisture: Progress report I. Canadian Journal of Remote Sensing, 3(1), pp. 76-86.

Delta-T Devices Limited. (2006). *Moisture content sensor and related methods.* International Patent Publication WO 2006/064266 A1.

Dowding, C.H., and Pierce. C.E. (1994). Use of Time Domain Reflectometry to Detect Bridge Scour and Monitor Pier Movement. *Proceedings of the Symposium on Time Domain Reflectometry in Environmental, Infrastructure, and Mining Applications*, Evanston, Illinois, US Bureau of Mines, Special Publication SP 19-94, pp. 579-587.

Gaskin, G.J., and Miller J.D. (1996). Measurement of soil water content using a simplified impedance measuring technique. *Journal of Agricultural Research*, 63(2), pp. 153–160.

Harlow, R.C., Burke, E.J., Ferre, P.A. (2003). Measuring water content in saline soils using impulse time domain transmission techniques. *Vadose Zone Journal*, 2(3), pp. 433–439.

Heimovaara, T. J. (1994). Frequency domain analysis of time domain reflectometry waveforms: 1. Measurement of the complex dielectric permittivity of soils. *Water Resources Research*, 30(2), pp. 189–199.

Hipp, J.E. (1974). Soil electromagnetic parameters as functions of frequency, soil density, and soil moisture. *Proceedings of the IEEE*, 62(1), pp. 98-103.

Hoekstra, P., and Delaney, A. (1974). Dielectric properties of soils at UHF and microwave frequencies. *Journal of Geophysical Research*, 79(11), pp. 1699-1708.

Hook, W.R., Ferre, T.P.A., Livingston, N.J. (2004). The effects of salinity on the accuracy and uncertainty of water content measurement. *Soil Science Society of America Journal*, 68(1), pp. 47-56.

Jones, B.C., and Or, D. (2004). Frequency Domain Analysis for Extending Time Domain Reflectometry Water Content Measurement in Highly Saline Soils. *Soil Science Society of America Journal*, 68(5), pp. 1568–1577.

Kelleners, T.J, Soppe, R.W.O., Ayars, J.E., and Skaggs, T.H. (2004). Calibration of capacitance probe sensors in a saline silty clay soil. *Soil Science Society of America Journal*, 68(3), pp. 770–778.

Lagasse, P.F., Clopper, P.E., Pagan-Ortiz, J.E., Zevenbergen, L.W., Arneson, L.A., Schall, J.D., Girard. L.D. (2009). *Bridge Scour and Stream Instabil-ity Countermeasures: Experience, Selection and Design Guidance*. Hydraulic Engineering Circular No. 23, Third Edition. Vol. 1. FHWA NHI-09-112, Federal Highway Administration, Washington, D.C.

Ledieu, J., De Ridder, P., De Clerck, P., and Dautrebande, S. (1986). A method of measuring soil moisture by time-domain reflectometry. *Journal of Hydrology*, 88(3-4), pp. 319-328.

Lin, C.-P. (2003). Analysis of non-uniform and dispersive time domain reflectometry measurement systems with application to the dielectric spectroscopy of soils, *Water Resources Research*, 39(1), 1012.

Lueker, M., Marr, J., Ellis, C., Winsted, V., and Akula S.R. (2010). *Bridge Scour Monitoring Technologies: Development of Evaluation and Selection Protocols for Application on River Bridges in Minnesota*. Publication MN/RC 2010-14, Minnesota Department of Transportation, St. Paul, Minnesota.

Michalis, P., Saafi, M., and Judd, D.M. (2012). Integrated Wireless Sensing Technology for Surveillance and Monitoring of Bridge Scour. *Proceedings of the 6th International Conference on Scour and Erosion* (Fry JJ and Chevalier C (eds)), ISSMGE - Societe Hydrotechnique de France, Paris, France, pp. 395-402.

Michalis, P., Saafi, M., and Judd, D.M. (2013). Capacitive Sensors for Offshore Scour Monitoring. *Proceedings of the ICE – Energy*, 166(4), pp. 189–196.

Pelletier, M.G. (2006). *Soil Moisture Sensor*. US Patent 7,135,871.

Pelletier, M.G., Karthikeyan, S., Green, T.R., Schwartz, R.C., Wanjura, J.D., and Holt, G.A. (2012). Soil moisture sensing via swept frequency based microwave sensors. *Sensors*, 12(1), pp. 753-767.

Persson, M. (2002). Evaluating the linear dielectric constant-electrical conductivity model using time-domain reflectometry. *Hydrological Sciences Journal*, 47(2), pp. 269-277.

Reedy, R., and Scanlon, B. (2003). Soil Water Content Monitoring Using Electromagnetic Induction. *Journal of Geotechnical and Geoenvironmental Engineering*, 129(11), pp. 1028–1039.

Robinson, D.A., Gardner, C.M.K., Evans, J., Cooper, J.D., Hodnett, M.G., and Bell, J.P. (1998). The dielectric calibration of capacitance probes for soil hydrology using an oscillation frequency response model. *Hydrology and Earth System Science*, 2, pp. 111–120.

Robinson, D., Jones, S., Wraith, J., Or, D. and Friedman, S. (2003). A review of advances in dielectric and electrical conductivity measurement in soils using time domain reflectometry. *Vadose Zone Journal*. 2(4), pp. 444–475.

Rosenstark, S. (1994). Transmission Lines in Computer Engineering. New York: McGraw-Hill.

Roth, K.R., Schulin, R., Fluhler, H., and Attinger, W. (1990). Calibration of Time Domain Reflectometry for Water Content Measurement using a Composite Dielectric Approach. *Water Resources Research,* 26(10), pp. 2267-2273.

Sadiku N.O.M. (2001). *Elements of Electromagnetics*. 3rd ed. New York: Oxford University Press.

Skierucha, W., Wilczek, A., Szypłowska, A., Sławiński, C., and Lamorski, K. (2012). A TDR-Based Soil Moisture Monitoring System with Simultaneous Measurement of Soil Temperature and Electrical Conductivity. *Sensors*, 12(10), pp. 13545-13566.

Tao, J., Yu, X., and Yu, X.B. (2014). Design and Application of a Field Bridge Scour Monitoring Sensor Based on TDR. *Transportation Research Board 93rd Annual Meeting*, Washington DC, pp. 1-16.

Thomas, A.M. (1966). In situ measurement of moisture in soil and similar substances by `fringe' capacitance. *Journal of Scientific Instruments*, 43(1), pp. 21-27.

Topp, G.C., Davis, J.L., and Annan A.P. (1980). Electromagnetic determination of soil water content: Measurements in coaxial transmission lines. *Water Resources Research*, 16(3), pp. 574–582.

Topp, G.C., Davis, J.L., Baily, W.G., and Zebchuk, W.D. (1984). The measurement of soil water content using a portable TDR hand probe. *Canadian Journal of Soil Science*, 64(3), pp. 313-321.

Topp, G.C., Davis, J.L. (1985). Measurement of soil water content using time domain reflectometry (TDR): A field evaluation. *Soil Science Society of America Journal*, 49(1), pp. 19-24.

Topp, G.C., Lapen, D.R., Young, G.D., Edwards, M., (2001). Evaluation of shaft-mounted TDT readings in disturbed and undisturbed media. *Proceedings of the Second International Symposium and Workshop on Time Domain Reflectometry for Innovative Geotechnical Applications*, Infrastructure Technology Institute, Northwestern University, Evanston, Illinois. Available at: <http://www.iti.northwestern.edu/tdr/tdr2001/proceedings/> [Assessed 11 May 2013].

Watson, K., Gatto, R., Weir, P., and Buss, P. (1995). *Moisture and salinity sensor and method of use.* US Patent US005418466A

Will, B., and Rolfes, I. (2013). Comparative study of moisture measurements by time domain transmissometry. *Proceeding of the IEEE Sensors*, Baltimore, MD, pp. 1-4.

Yankielun, N., and Zabilansky, L. (1999). Laboratory Investigation of Time-Domain Reflectometry System for Monitoring Bridge Scour. *Journal of Hydraulic Engineering,* 125(12), pp. 1279–1284.

Yu, X. and Zabilansky, L. (2006) Time Domain Reflectometry for Automatic Bridge Scour Monitoring. *Site and Geomaterial Characterization*, ASCE Geotechnical Special Publications 149, pp. 152-159.

Yu, X., and Yu, X. (2009). Time Domain Reflectometry Automatic Bridge Scour Measurement System: Principles and Potentials. *Structural Health Monitoring*, 8(6), pp. 463-476.

Yu, X., Zhang, B., Tao, J., and Yu, X. (2013). A New Time Domain Reflectometry Bridge Scour Sensor. *Structural Health Monitoring*. 12(2), pp. 99-113.

Zegelin, S. J., White, I., and Jenkins D. R. (1989). Improved field probes for soil water content and electrical conductivity measurement using time domain reflectometry. *Water Resources Research*, 25(11), pp. 2367–2376.

Chapter 6

Conclusions & Recommendations for Next Stage Developments

6.1 Conclusions

Scour action is a challenge for civil infrastructure systems due to the changing climate bringing more active weather systems. Scour is the leading cause of bridge failures worldwide and it is also considered as a major risk for offshore renewable marine structures. Bed level conditions at underwater foundations are very difficult to monitor, considering that scour holes are often re-filled by deposited loose material that is easily eroded during subsequent smaller-scale events. The evaluation of scour and sediment deposition processes is also becoming more critical taking into account the deterioration of infrastructure and the issues arising from the rehabilitation of hydraulic and marine structures. However, most of the existing monitoring methods cannot provide complete data of both scour and re-deposited sediment evolution due to technical and cost issues.

This study developed a new approach for monitoring underwater bed level variations at the foundations of structural elements based on (i) an off-the-shelf instrument and (ii) a developed prototype sensor utilising a new technique. A synopsis of the various steps followed to achieve the aims and objectives of the investigation is presented in Figure 6.1.
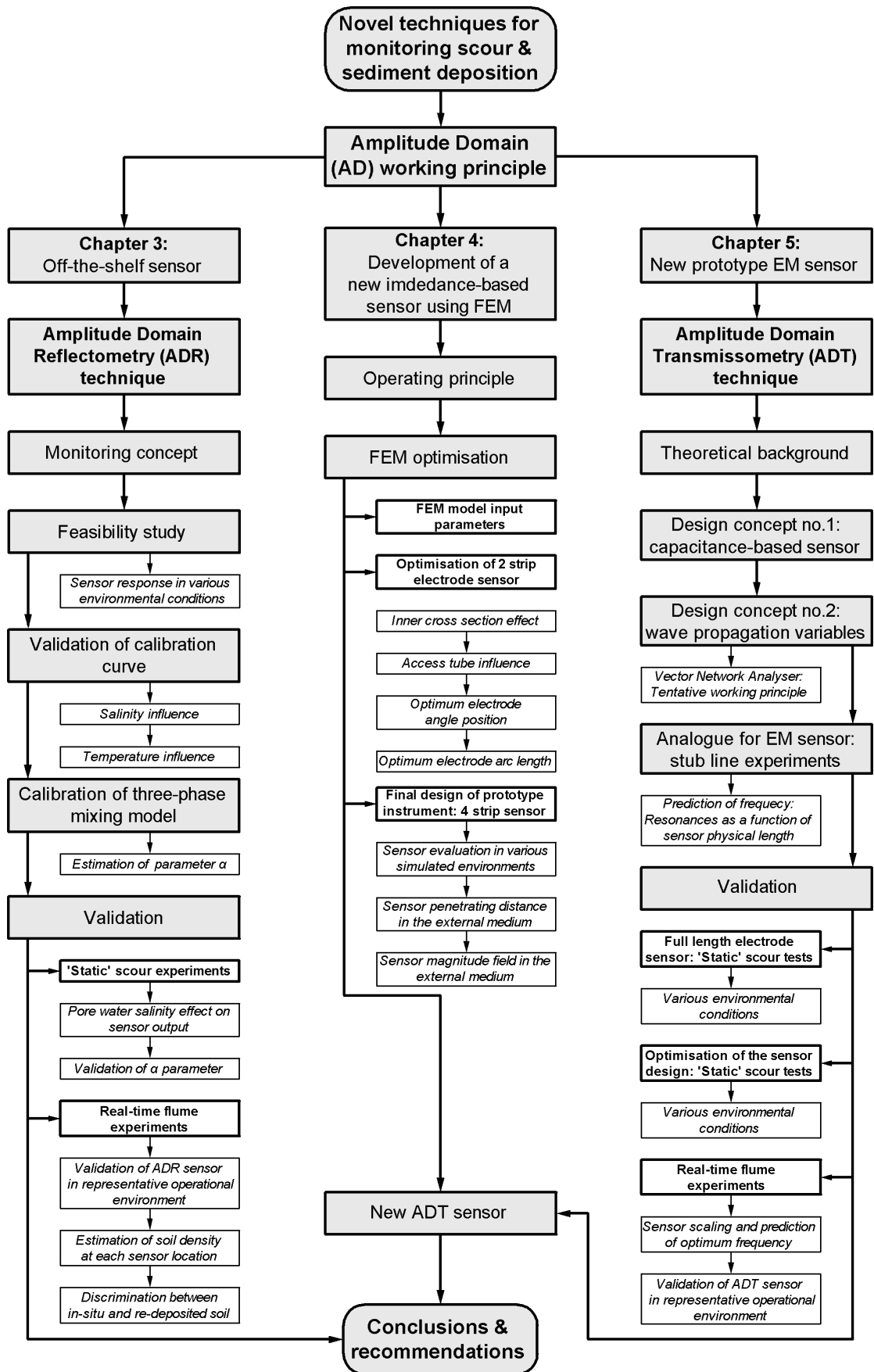
Figure 6.1: Flow-chart presenting the methodology carried out to achieve the objectives of this study.

The capability of the Amplitude Domain Reflectometry (ADR) technique to measure scour and sedimentation processes was demonstrated for the first time in this investigation through series of experiments using an off-the-shelf sensor. Preliminary tests conducted in the laboratory simulating different underwater conditions around the sensor location indicated that the technique successfully measured the long-term degradation effect. The instrument was also found capable of detecting simulated 'static' scour and re-deposited sediment processes despite the inevitable influences of saline water and temperature induced electrical conductivity changes on the sensor signals.

This study also identified the limitations of the ADR sensor by evaluating the calibration of the instrument against liquids with known dielectric permittivity and water of various salinity concentrations. The large discrepancy observed between predicted and measured sensor output in saline water was attributed to the limit capability of the instrument's dynamic range. The calibration curve provided by the manufacturer was found to be accurate for apparent permittivity values up to 80. Based on the obtained results three areas were identified on the sensor's calibration curve indicating the accurate (i), the unknown accuracy (ii) and the out of range (iii) regions.

The use of the sensor signals to discriminate between in-situ and re-deposited soil was also presented in this thesis. Experimental data obtained at various soil density conditions were employed to calibrate a three-phase mixing model with the determination of the optimum geometric parameter α which was found consistent with values reported in the literature. The overall apparent permittivity value was then satisfactorily estimated for sediments with similar characteristics. Based on the sensor readings it was then demonstrated that the soil porosity around each sensor location can be estimated based on the sensor signals.

This study thoroughly evaluated the ADR sensor in real-time flume experiments which was found to be highly dependent on scour and sedimentation processes. The sensor was connected with a wireless interface that allowed the real-time monitoring of bed level variations in the riverbed segment. A tool was also developed for the estimation of the soil density at each sensor location using the relationship between the apparent permittivity and soil porosity. Re-deposited sediment was found to be associated with higher permittivity which in turn was related with lower soil density

that was successfully estimated. The capability of the instrument to differentiate between pre-scour and post-sediment deposition conditions was therefore demonstrated. The results presented in this investigation provide an important guide and can be used as a benchmark for the field application of the ADR sensor for monitoring riverbed level variations.

One of the limitations of the evaluated ADR probe arises from the geometry of the ring-shaped electrodes that are located at different depth intervals (refer to Figures 3.1 and 3.2). This is due to the fact that the instrument can only detect scour or sediment deposition depths based on the medium of the local region around each sensor. The off-the-shelf ADR probe cannot therefore monitor sediment level when is located between the two sensors but only when bed level surpasses the sensor location. For the field application of the instrument multiple sensors need to be added in the probe which will increase the total cost of the instrument.

The second part of research therefore focused on the development of a new low-cost impedance-based sensor that allows continuous monitoring of scour and sediment deposition monitoring along the length of the instrument. The optimisation of the components of the sensor was performed via Finite Element Modelling (FEM). Based on the computed capacitance, strength and penetration area of the electric field, it was concluded that the sensitivity of the sensor was significantly decreased by the presence of the access tube. This was attributed to the effect of the simulated air gaps and the low permittivity of the access tube which dominated the total capacitance value. The simulations also confirmed the sensor sensitivity that responded differently to water and sediment permittivity conditions.

The FEM study was then focused on the optimisation of the electrode angle position and arc length. Increased angular separation of the electrodes around the central dielectric rod led to the reduction of the computed capacitance and of the strength of the electric field displacement. It was concluded that the optimum sensor geometry was obtained for electrodes placed at an angle position of 90º and with strip arc length of 13.75 mm. This geometric electrode configuration was found to provide the greatest capacitance difference between water and saturated soil conditions and therefore increased sensitivity to scour processes. The final design of the proposed sensor comprises of four paired electrode strips generating a fringing field which

enables a good penetration of the electric field into the external medium outside the access tube. The proposed electrode models exhibited high sensitivity to the different assigned permittivity conditions which was recorded greater for the regions around the edges of the sensor. The FEM investigation concluded that the circular symmetrical electric field generated for the optimum electrode arrangement will enhance the sensitivity of the sensor to scour and sedimentation processes around the probe location.

A prototype sensor was then fabricated according to the optimum geometric components defined by the FEM study and tested in laboratory environment connected to a network analyser. The Amplitude Domain Transmissometry (ADT) technique utilised by the developed instrument appears to be the first application for monitoring soil-water mixtures and also for the purpose of measuring scour and sediment deposition processes.

The study initially investigated probes of various electrode lengths that were tested in different environmental conditions. The permittivity factor was found to have an influence on the obtained frequency response. The sensor impedance arrangement (in series or in parallel) with the measuring system was also directly related with the obtained transmission and reflection coefficients. The prototype instrument was described as an open-circuited transmission line with the sensor impedance placed in series with the measuring system.

The design was accompanied by a theoretical analysis to complement and provide an understanding of the electrical behaviour of the instrument. The study employed open-circuited stub line experiments as an analogue in order to gain adequate insight into the signal characteristics of the sensor in a range of frequencies. The frequency response of the sensor was satisfactorily described and was comparable with the results obtained with the stub line tests. The experiments carried out with various stub line and sensor lengths also revealed that the resonances on the obtained frequency response are a function of the physical length of the instrument. It was then demonstrated that crests and troughs in the transmission ratio spectrum can be successfully predicted. These resonances correspond to frequency points where the electrical length becomes equal to odd multiples of $\lambda/4$ (transformation to short-circuit) and even multiples of $\lambda/4$ (transformation to open-circuit) respectively. Frequency

regions between resonance frequencies were investigated to detect wave propagation variables for measuring bed level conditions. A single frequency was identified where the simulated scour processes had an increasing effect on the voltage output (associated with transmitted signal amplitude). Based on the approach developed for resonance frequency prediction, it was also suggested that electrode length can be fine-tuned to modify the optimum frequency so as to match the operational frequency of commercial oscillators and, hence, reduce the total cost and ease the development of the sensor electronics concept.

In laboratory environment the prototype sensor with equal electrode lengths successfully measured 'static' bed level variations at depth intervals of 10 cm from the transmission characteristics at a single optimum frequency and/or from frequency changes occurring at the resonance troughs. The sensitivity of the sensor was found to be significantly reduced by almost 90 % in saline water of 35 ppt of NaCl compared to the results obtained in fresh water conditions. The sensor readings were also not influenced by various water temperatures at the range of 12 ºC and 4 ºC. Different optimum frequencies were identified in fresh and saline water in order to provide a reasonably linear response to scour depth for the case where the sensor is calibrated with respect to the amplitude of the transmitted signal at a single frequency. A plateau was detected in the voltage response of the sensor in the tests carried out using fresh water, which corresponded to the mid-length of the probe and indicated decreased sensitivity to scour depth in that region.

The design process of the sensor was finalised by progressively shortening one strip from each electrode with objective to disturb the null nodes of the standing wave generated at odd multiples of quarter wavelengths. A very strong linear relationship was eventually obtained between the voltage response of the sensor and scour depth in different sediments for reduced length of one strip from each electrode by 35 cm. The salinity effect on the sensor signals was also investigated and it was concluded that bed level measurements for water salinity concentrations above the range of 5 ppt are proposed to be carried out with a sensor of full equal electrode lengths.

Finally, a small-scale prototype sensor was fabricated and tested in the open channel flume in a series of experiments using different sand sediments. At a single frequency the optimised sensor measured scour depth and sediment deposition

processes with satisfactorily sensitivity and a strong linear relationship. This optimum frequency was also successfully predicted based on the sensor length ratio relationship.

The new sensor with the current geometry of strip electrodes provides measurements of bed level conditions based on the average permittivity of the area that spans over the length of the probe (refer to Figures 4.3 and 4.4). The sensor signals cannot therefore be used for density estimation of local regions around the probe location.

The prototype ADT sensor that was developed in this study can provide an accurate and low-cost alternative to existing scour monitoring instruments. The integration of the components of the prototype sensor and the validation of the ADT technique in representative operational environment enables the instrument to be classified at Technology Readiness Level (TRL) 6.

6.2 Recommendations for next stage developments

The off-the-shelf ADR instrument and the new ADT sensor presented in this investigation could fulfil a useful role in cost-effective monitoring and managing scour susceptible structures. The ADT sensor with the current geometry of strip electrodes is proposed to be employed for continuous monitoring of scour and sediment deposition processes along the probe length. To complement the monitoring system, the ADR probe using ring-shaped electrodes could also be used to provide information about soil density conditions around the foundation structure. Both instruments could be transformed into a commercial product although further steps are needed for the integration of the instrument into an early warning system. This will require, in parallel, the development of an engineering model to predict the time-evolution of scouring based on real-time processing of data.

This study developed a methodology and demonstrated its ability to detect in-situ and deposited sediments in fresh water conditions based on the signals of the off-the-shelf ADR sensor. Soil density fluctuations in saline environment could also be potentially estimated and this task is proposed to be carried out for the future development of the ADR sensor. This would be based on the assumption that the medium porosity around the sensor location will remain at the same range in both fresh water and saline water conditions. A trained model could therefore be employed using

the porosity values derived from the overall permittivity obtained in fresh water (as presented in section 3.4.4). However, further investigation is required as the reliability of these measurements is likely to be compromised due to complexities that arise from the interaction of many factors concerning the evolution of bed level processes in offshore environment.

The new ADT sensor was tested in the laboratory in different sediment conditions and successfully measured bed level changes in the order of 10 cm. This range of accuracy was considered satisfactory for the obtained scour information at the foundations of structures. The flume experiments also indicated that a better accuracy of less than 10 cm is viable and for that reason the refinement of the technology is proposed. Additional work will also involve the investigation of different sensor geometries using the same developed technique that can lead to better accuracy, enable density evaluation based on sensor signals and also improve the field implementation of the instrument.

To improve understanding of the electrical response of the sensor during the optimisation process of its design, further simulations may be carried out using three-dimensional (3D) FEM. The results presented in this work also indicated that the temperature did not have a major influence on the sensor response. 3D FEM simulations and laboratory experiments are suggested to be performed evaluating further the temperature effect in controlled environment using a smaller scale prototype. Measurements and analysis of other properties (i.e. phase, reflection coefficients and standing wave ratio) will also provide a further insight of the sensor electrical characteristics in various dielectric permittivity conditions and water salinity concentrations.

A full scale prototype sensor is proposed to be designed, fabricated and then installed to a scour critical structure. For the successful field implementation of the developed instrument, a suitable installation technique needs to be selected. Therefore, a review of existing techniques such as driving, jetting and/or augering should be carried out to select the most appropriate installation technique to be utilised depending on site conditions. These aforementioned techniques have been widely used for the installation of other monitoring systems (i.e. TDR systems, magnetic collars) mainly for bridge foundations but also, very recently, for offshore structures. The durability

of the sensor to offshore environment needs also to be investigated with FEM simulations and then in field conditions.

The scour monitoring system is proposed to be incorporated into an effective communication system issuing automatic warning messages when scour/deposition is detected. Technologies already available in the market (e.g. GSM antennas, satellite telemetry) can be employed for real-time safety surveillance and effective transfer of data obtained from the sensor. The use of underwater wireless communication technologies needs also to be investigated with potential application to the proposed system. The integration of monitoring systems to existing GIS-based platforms for real-time continuous assessment of civil infrastructure could be explored. Finally the application of the ADT technique and of the prototype sensor may be extended to other types of critical infrastructure, this issue being currently under investigation.